CHARACTERISING THE DYNAMIC RESPONSE OF ULTRASONIC CUTTING DEVICES

by

Andrea Cardoni

UNIVERSITY
of
GLASGOW

THESIS SUBMITTED IN FULFILLMENT OF THE REQUIREMENTS
FOR THE DEGREE OF DOCTOR IN PHILOSOPHY
TO THE FACULTY OF ENGINEERING
DEPARTMENT OF MECHANICAL ENGINEERING
UNIVERSITY OF GLASGOW

December 2003

This thesis is produced under the accordance of British Standards BS 4821:1990

Dedication:

To my mother Teresa Maria

To my father Pietro

COPYRIGHT

ABSTRACT

There are many proven benefits in applying high power ultrasonics to manufacturing processes and research demonstrating significant cost savings and process improvements has been underway for around 50 years. Despite this effort, there are still a large number of high power ultrasonic technologies that are not in widespread use and many applications that have never been successfully exploited. Often the reason for this is the lack of knowledge of the fundamental mechanics of the ultrasonic systems and, consequently, the difficulties in designing reliable systems.

The research presented in this thesis has attempted to gain some fundamental insights into the nature of the dynamics of high power ultrasonic systems and, consequently, to address the system design issues that have hampered progress in this technology, particularly for systems with multiple components and complex geometries. The research is enabled by the available modelling and experimental facilities, which are now sufficient to characterise these complex systems. This study uses the results of the fundamental understanding of the dynamic responses, and the measurement and modelling techniques offered by 3D laser Doppler vibrometer (LDV) measurements and finite element analysis, to design tuned multiple-component ultrasonic cutting tools capable of delivering the required energy to the work surface in an efficient and controlled manner.

The current work begins by considering a range of common high power ultrasonic components in order to establish a standardised approach to tool design for optimum performance. The vibration behaviour of tuned components resonating longitudinally at ultrasonic frequencies around 35 kHz is modelled via finite element analysis and measured by experimental modal analysis. Significant improvements in experimental validation of the models are achieved by the use of a 3D LDV, which allows modal analysis from both in-plane and out-of-plane measurements, which is critical in proposing alternative designs.

The vibration characteristics of complex multiple-component systems used in ultrasonic cutting of food products are also investigated. Commonly, the design approach for ultrasonic systems neglects to account for the mutual effects of

physically-coupled components in the system vibration. The design of systems also neglects the nonlinear dynamics effects, which are inherent in high power systems due to the nonlinearities of piezoelectric transducers. The first issue is tackled by considering the vibration behaviour of the whole system and the influence of individual components and, particularly, offers design improvements via modification of block horns and cutting blade components, which are modelled and validated. The issue of nonlinearity is addresses by identifying the mechanisms of energy leakage into audible frequencies and characterising the common multimodal responses. For this study, design modifications focused on reducing the number of system modes occurring at frequencies below the tuned system frequency. As a consequence of these approaches, insights for the design of multiple-component systems in general are provided.

ACKNOWLEDGEMENTS

I would like to express my sincere gratitude and appreciation to my supervisor Dr. Margaret Lucas. Her invaluable knowledge, resourcefulness and support were indispensable for this work. Her encouragement, thoughtfulness, and supervision are deeply acknowledged.

Acknowledgments are extended to Professor Matthew Phillip Cartmell who has been a great advisor. His ingeniousness, devotion as well as his manners are greatly admired. Also to Dr. Fannon Lim who has been a great friend and colleague, and to whom I owe much of my computing knowledge.

Thanks are given to the Engineering and Physical Sciences Research Council (EPSRC) and Nestle' UK, who provided the funding for this research, and to the person of Mr Martin Harrop of Nestle' PTC York, UK for his kind collaboration.

Special thanks are expressed to the people of the wonderful city of Glasgow and to all Scottish people for their friendliness, tolerance and generosity. International students in Scotland are assured of a fulfilling and unforgettable experience.

Finally I would like to express my deep gratitude and sincere appreciation to my parents and my sister. This work would not have come to existence without their patience, sacrifice, and insistence that I acquire higher education. I am forever grateful to my family for their love, kindness, and belief in me.

LIST OF FIGURES

LIST OF TABLES

TABLE OF CONTENTS

CHAPTER 1

INTRODUCTION

1.1 Background

The definition of ultrasound is energy generated by sound waves travelling through fluids or solids at 20,000 or more cycles per second. The lowest ultrasonic frequency (20 kHz) is chosen so that the vibrations are not audible to humans, whereas the highest frequency (in order of Gigahertz) is limited only by the ability to generate the signals.

Ultrasound at frequencies above 100 kHz is exploited for operations where the propagation of waves does not have any significant effects on the subject of the scan, and these include medical imaging and non-destructive testing. The power at which these sound waves are generated is relatively low with intensities in the range of 0.1 to 0.5 W/cm^2 (low power applications).

Ultrasound in the frequency range between 20 kHz and 100 kHz is utilised in those processes requiring large amounts of energy such as manufacturing operations (high power applications). The intensities normally used in high power ultrasound are above 10 W/cm^2. In these applications the required energy is transmitted to the materials to be worked through one or more tuned components screwed into a piezoelectric transducer, converting an electrical signal into mechanical vibrations. The tuned ultrasonic components are designed to respond in a particular mode of vibration, usually longitudinal but sometimes radial or torsional, at the required excitation frequency. Component profiles depend on the specific application, but common shapes are stepped, conical and catenoidal horns for longitudinal-mode systems, cylindrical dies for radial-mode systems and circular bars for torsional-mode systems. Typical amplitude ranges for high power processes are from about 5 to 100 microns.

Since the 1960s, applications of high power ultrasonics have created many novel technologies, such as plastic and metal welding, surface cleaning and cutting, and have demonstrated performance improvements in a range of existing manufacturing processes such as cutting, wire drawing and die forming. Although many of these benefits are well known (e.g. reduced process forces, friction reduction, localised heating, increased process speed) the technology is still under-utilised and slow in being adapted to manufacturing processes. This has often been due to the mainly empirical approach to ultrasonic tool design and the lack of a mechanistic understanding of the linear and nonlinear behaviour of ultrasonically vibrating systems.

In particular, the adverse effects of nonlinear vibrations on ultrasonic devices for high power industrial applications are well known in the ultrasonics community, but these effects have not been characterised previously or researched to pursue possible design solutions. Therefore, advancing high power ultrasonic technology any further is reliant on research that addresses this problem.

1.2 Ultrasonic systems

In general, ultrasonic systems for high power applications comprise the key components shown in Figure 1.1. The common constitutive units are the power supply (or generator), the converter/booster/horn stack, the part fixture, and a means of providing horn contact with the part (usually an actuator). A 50/60 Hz current is converted to 20 kHz to 100 kHz electrical energy in a solid-state power supply. This high frequency electrical energy is supplied to a transducer (or converter) that transforms it to mechanical motion at ultrasonic frequencies. The mechanical motion is then transmitted through an amplitude-modifying booster to the horn. The horn (or sonotrode) transfers this vibratory energy directly to the parts or materials to be ultrasonically treated.

The main purpose of the present work is to propose strategies for the design of ultrasonic tools through an understanding of the dynamics of high power ultrasonic devices. This is achieved by concentrating the research on dynamically complex devices used for cutting food products, which are designed to operate in a longitudinal mode of vibration. The majority of ultrasonically aided manufacturing processes

incorporate longitudinal mode tuned systems, and therefore this research has a wider scope in providing design insights that can be applied to a range of high power ultrasonic applications. In order to emphasise some of the common features of such applications, the basic principles of three ultrasonic operations exploiting the mechanical energy produced by longitudinally vibrating horns, are now described.

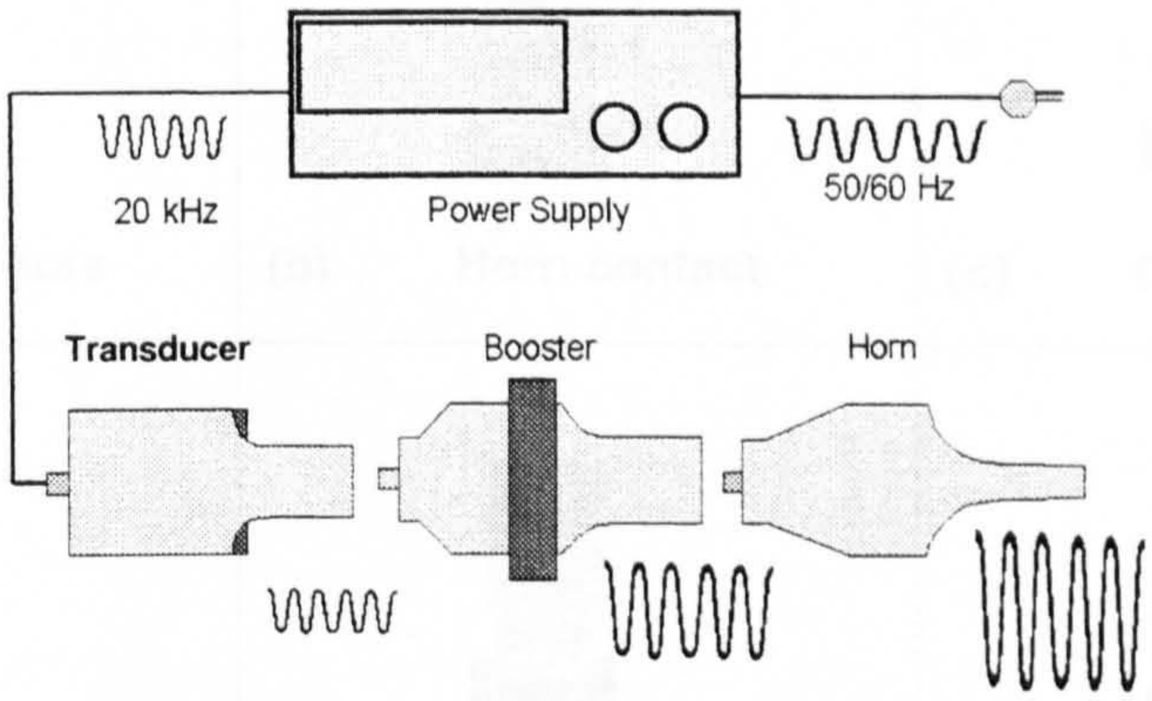

Figure 1.1. Schematic of ultrasonic system [Branson Ultrasonics Corp., Danbury, CT (USA)]

1.2.1 Ultrasonic plastic welding

Ultrasonic plastic welding is the process of joining or reforming thermoplastics through the use of heat generated from high-frequency mechanical motion. As with other ultrasonic operations, it is accomplished by converting high-frequency electrical energy into high-frequency mechanical motion. The mechanical motion of the horn, tuned in a longitudinal mode, along with the applied force, creates frictional heat at the plastic components' mating surfaces so the plastic material will melt and form a molecular bond between the parts. The use of ultrasonic vibrations allows plastic welding to be a fast, clean, efficient, and repeatable process that consumes very little energy. In addition, no solvents, adhesives, mechanical fasteners or other consumables are required, and finished assemblies are strong and clean.

The basic principles of ultrasonic plastic welding are illustrated in Figure 1.2. Initially, the two thermoplastic parts to be welded are placed one on top of the other, in a supportive nest called a fixture as shown in Figure 1.2 (a). A titanium or aluminum tuned horn is brought into contact with the upper plastic part (Figure 1.2 (b)), and a controlled pressure is applied to the parts, clamping them together against the fixture as illustrated in Figure 1.2 (c). Subsequently, the horn is excited in its

tuned (longitudinal) mode, usually at a frequency in the range 20 kHz to 40 kHz depending on the thermoplastics, at amplitudes in the order of microns, for a predetermined weld time.

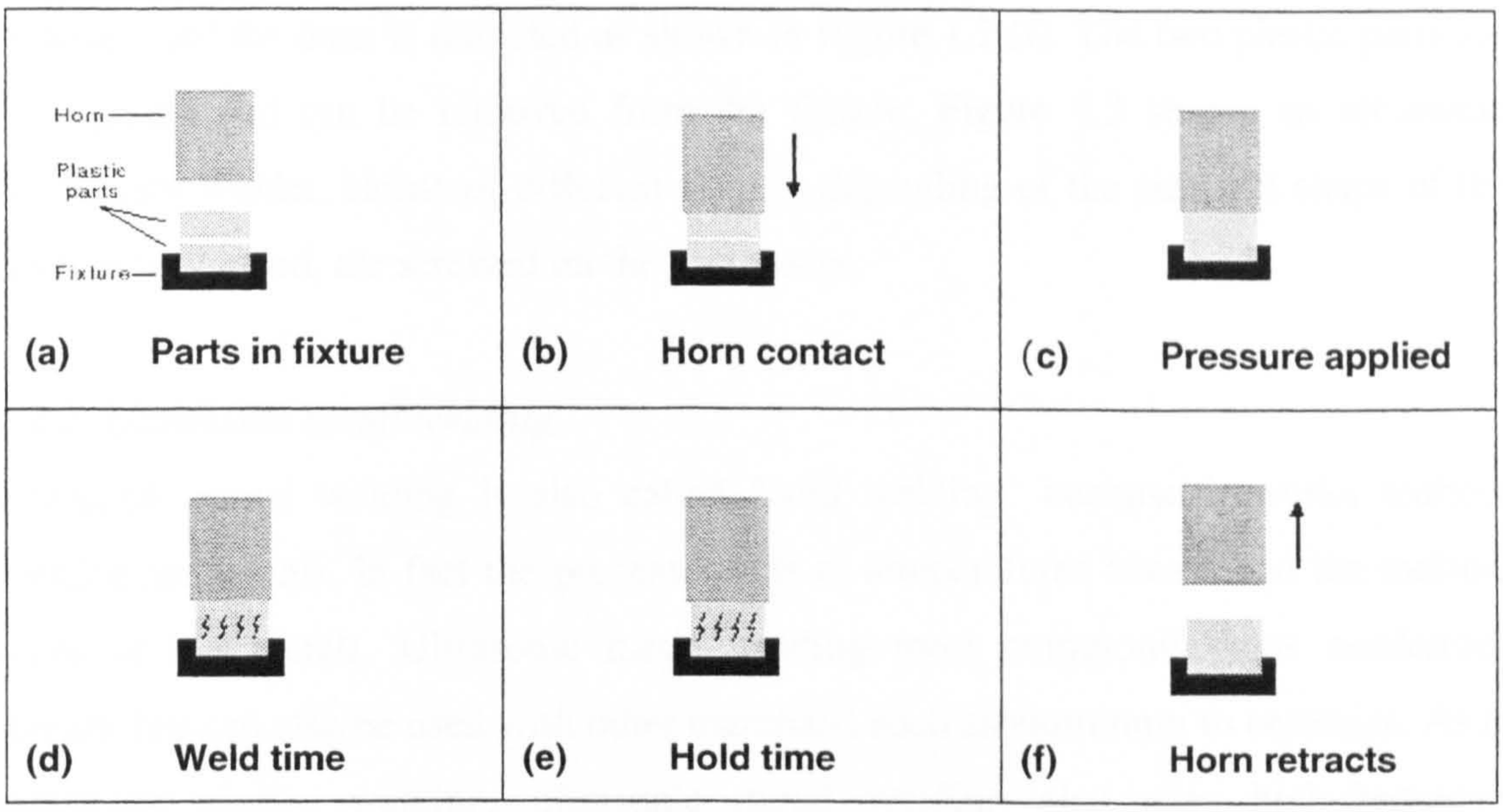

Figure 1.2. Procedure for ultrasonic plastic welding [Dukane Corp., St. Charles, IL (USA)]

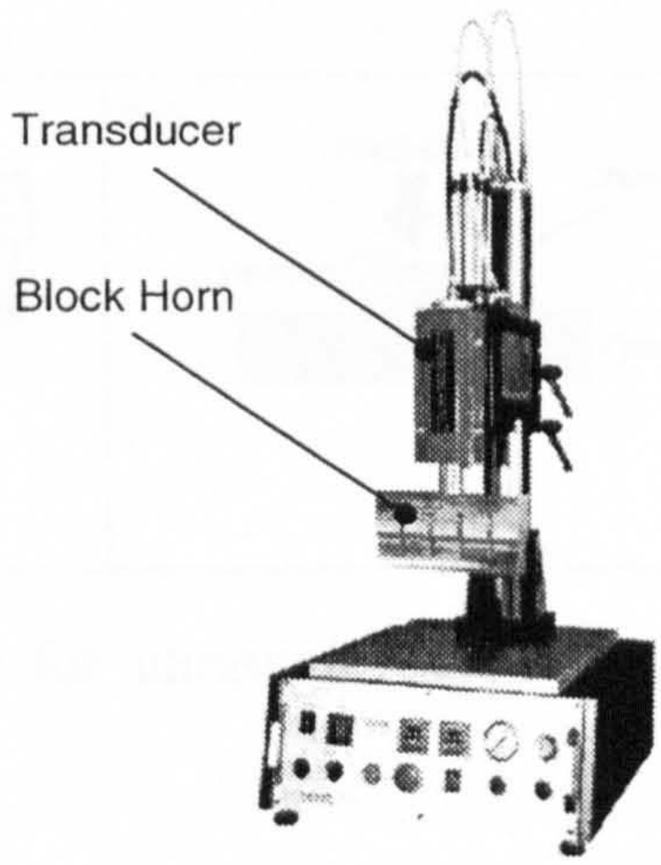

Figure 1.3. Model of an ultrasonic workbench welder [Sonic Italia S.R.L, Milan (ITA)]

Through careful part design, the vibratory mechanical energy is directed to limited points of contact between the two thermoplastic materials. The mechanical vibrations are transmitted through the thermoplastics to the joint interface to create frictional heat. When the temperature at the joint interface reaches the melting point, plastic

melts and flows, and the vibration is stopped in order to allow the melted plastic to cool (Figure 1.2 (d)). The clamping force is maintained for a programmed amount of time (hold time) to allow the parts to fuse as the melted plastic cools and solidifies (Figure 1.2 (e)). Finally, once the melted plastic has solidified, the clamping force is removed and the horn is retracted as shown in Figure 1.2 (f). The two plastic parts are now joined and can be removed from the fixture. Figure 1.3 shows an ultrasonic workbench welder. Horns of different shapes, depending of the size and shape of the parts to be welded, are screwed on the transducer.

1.2.2. Ultrasonic metal welding

Ultrasonic metal welding is also called "cold welding" because it works without melting the metals. In fact the process welds at temperatures lower than the melting point of the metals. Ultrasonic metal welding most commonly joins nonferrous metals, but can also be used with other materials, such as aluminum to ceramics. As in ultrasonic plastic welding, ultrasonic metal welding also uses high-frequency vibrations in a tuned horn excited in resonance. Figure 1.4 shows the main steps of an ultrasonic metal welding process.

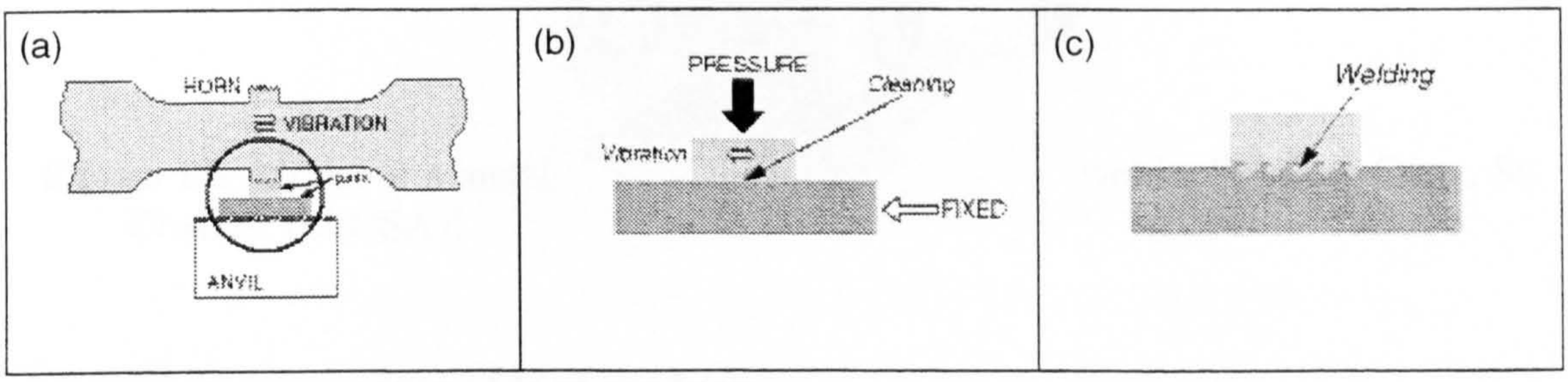

Figure 1.4. Procedure for ultrasonic metal welding [Dukane Corp., St. Charles, IL (USA)]

Initially, the parts to be welded are both placed on the anvil as illustrated in Figure 1.4 (a). Next, a clamping force is applied to the parts (Figure 1.4 (b)). Then the upper part is vibrated by the ultrasonic horn. This causes the parts to rub together. The ultrasonic energy cleans the surface dispersing oxide film layers, and results in the mixing of metal atoms without melting the metals. The activated metal atoms join each other, causing a true metallurgical bond (Figure 1.4 (c)). Figure 1.5 shows a support system where a one-wavelength horn held between two solid boosters vibrates longitudinally

(second longitudinal mode) assuring weld stability and consistency. Vibration is not transferred to the support as the boosters are held at the longitudinal nodes. Two boosters are used instead of one so that horizontal horn deflection is eliminated. A picture of a metal welder is shown in Figure 1.6.

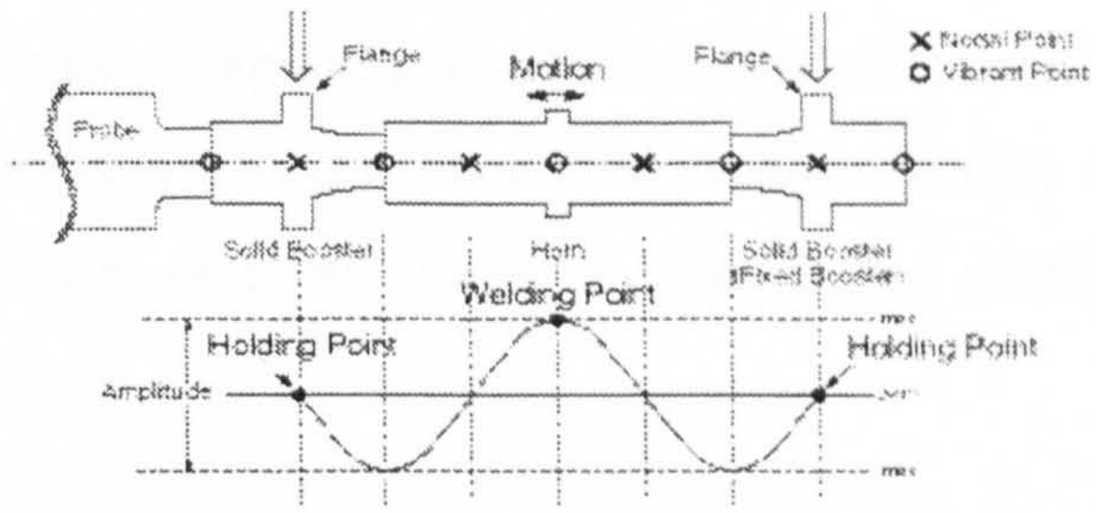

Figure 1.5. Dual Support System [Dukane Corp., St. Charles, IL (USA)]

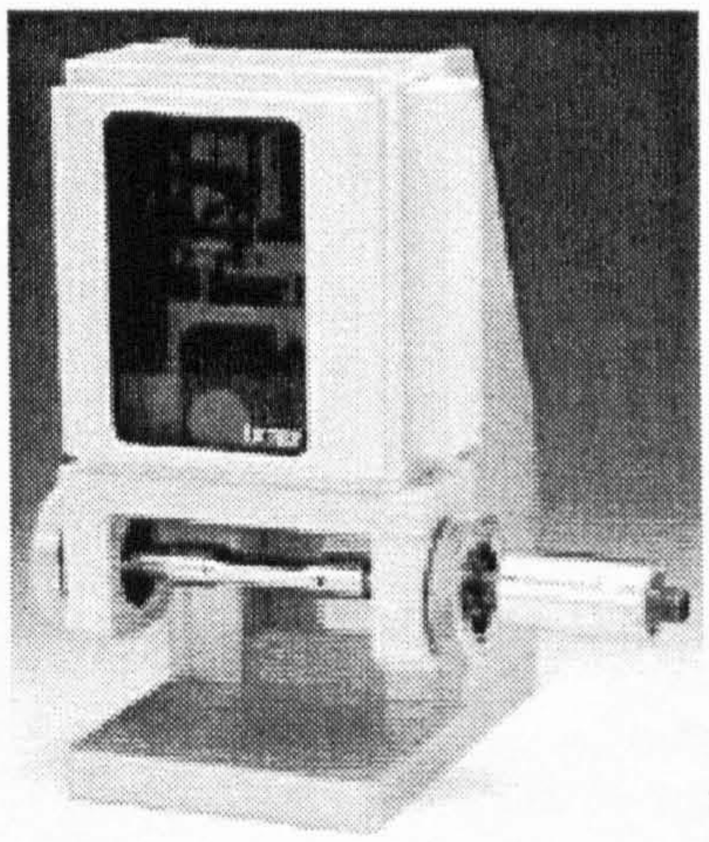

Figure 1.6. Model of a metal welder [Dukane Corp., St. Charles, IL (USA)]

1.2.3 Ultrasonic cutting of food products

Ultrasonic cutting of food products relies on the longitudinal vibrations of tuned knifes providing frictionless surfaces to which food products do not stick or deform. Ultrasonic cutting has demonstrated significant benefits in catering effectively for materials which are traditionally difficult to cut in a controlled manner and which would otherwise generate large amounts of non-recoverable waste using conventional cutting techniques. Some food products which can be cut with ultrasound are:

- bakery and snack foods
- candy and confectionery bars
- cheese

- fish
- prepared meats
- frozen flaked foods
- vegetable
- health bars.

Ultrasonic knives vibrating longitudinally at a frequency between 20 kHz and 60 kHz, depending on the process, are used to slice food products as they come out of an oven or down a conveyor belt, or to slit them into bar-shaped portions in a continuous operation.

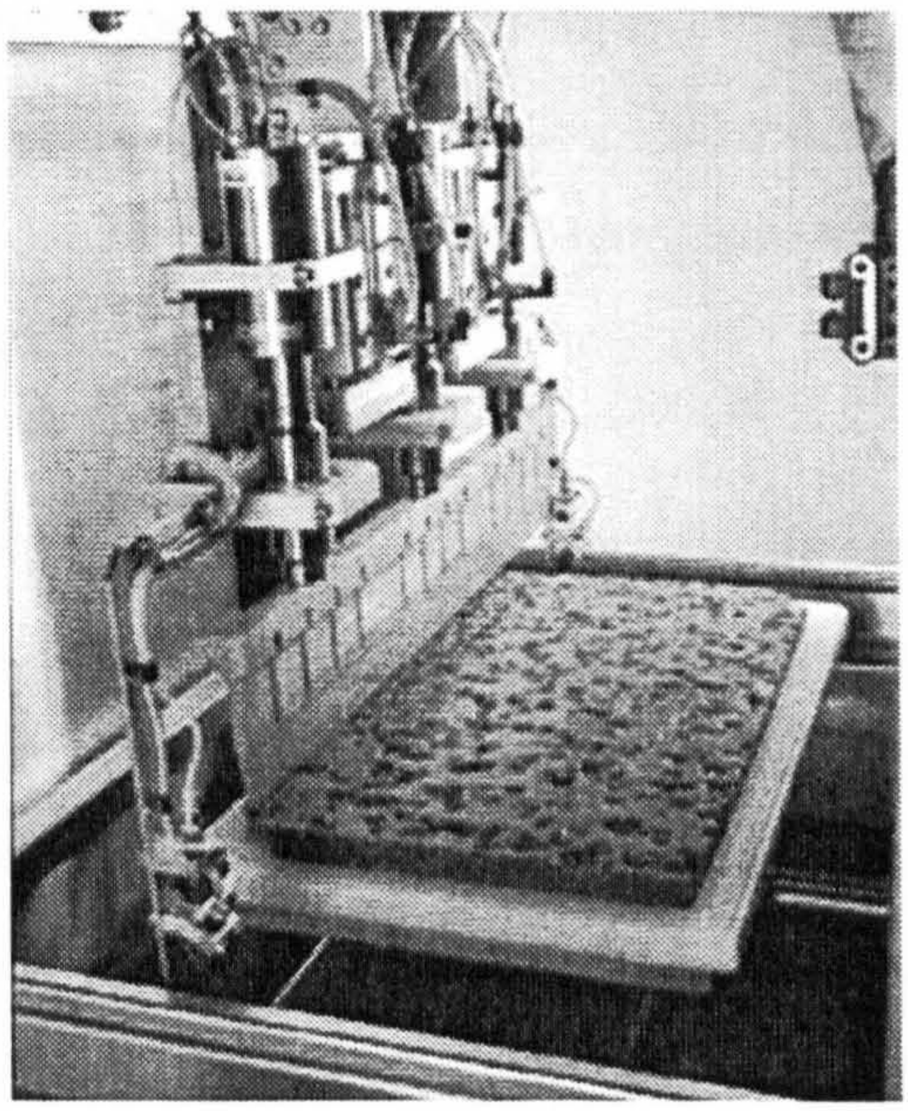

Figure 1.7. Model of an ultrasonic cutting system [Branson Ultrasonics Corp., Danbury, CT (USA)]

Ultrasonic cutting offers numerous advantages, reported in the following list:

- cleaner, repeatable and more consistent slits and cuts
- greatly reduced normal down time for clean up
- does not smear the cut surface
- wider cutting temperature range
- cuts cleanly through various densities and consistencies of products with filler materials
- cuts edges cleanly without pinching or feathering for higher yield in packaging

- cutting speeds can be increased substantially
- ease of use - uncomplicated and user friendly.

Finally, the procedures necessary with conventional cutting, such as pre-cooling or heating the product before the cutting operations, or realigning the product after cutting prior to the packaging operation, can be totally eliminated. An example of an automated cutting system is illustrated in Figure 1.7. The three block horns tapered in the form of sharp knifes are mounted side by side to slice the cake.

1.3 Scope of the work

The successful application of high power ultrasonics relies largely on design of tools for very specific vibration performance parameters, such as frequency, spectral response, amplitude, mode shape, and operating deflection mode. Hence, finding a general design strategy which meets all the requirements for optimum ultrasonic performance is not straightforward.

Recent research has progressed the understanding of ultrasonics applied to cutting of food products [1]. An area of this work has developed a fundamental understanding of the mechanisms of ultrasonic cutting by examining the interaction of the blade and the material through a combination of vibration analysis and fracture analysis [2]. Identification of the dynamic loading requirements for enhanced cutting performance, through the controlled propagation of material fracture, allowed cutting edge modal data to be fed back into the design of the cutting tool.

Although the use of high power ultrasonics has achieved success in cutting of food products, there still exist various unsolved reliability issues which hinder the development of the technology. In particular, the performance of cost effective multiple component tuned systems, driven by a single ultrasonic generator and transducer set, is often plagued by uncontrolled energy transmission through the components. In this research alternative ways forward in the design of cutting systems, based on a fundamental understanding of the vibration characteristics of tuned components and assemblies, are proposed.

Successful performance of ultrasonic cutting systems depends on the excitation of a single mode of vibration (usually longitudinal) at a frequency and amplitude suitable for the operation. In systems consisting of multiple components, the avoidance of modal participation by non-tuned modes occurring at frequencies close to the tuned mode frequency (linear modal coupling) is not easy to achieve. Previous researchers have provided useful design criteria to avoid modal coupling in various single-component ultrasonic systems [3-7], however there exists a lack of published work on this issue applied to complex ultrasonic systems. It is one of the aims of this research to deliver design insights to meet this need.

Recent developments in measurement instrumentation have also enabled measurements to illustrate how transmission of vibration to the cutting blades is adversely affected by nonlinearities [8,9]. It has been shown that such nonlinear behaviour is responsible of at least two detrimental effects, which can be interrelated.

The first one is associated with saturation of the vibration amplitude, occurring when ultrasonic systems are driven at voltage levels above 50 V. The nonlinear relationship between driving frequency and vibration amplitude of piezoelectric stack transducers has been discussed in the published literature [10]. Although transducer models, based on nonlinear piezoelectric constitutive equations, have led to an interpretation of the amplitude saturation phenomenon, the effects of the interfaces and geometry of the attached horns on such a behaviour is not understood and needs further investigation [9].

The second nonlinear phenomenon is also characteristic of systems driven at high power and is exhibited by the simultaneous excitation of one or more modes of vibration distinct from the driven tuned mode (nonlinear modal coupling). This energy leakage mechanism can be observed in single-component ultrasonic systems, but it appears almost systematically in ultrasonic assemblies composed of component stacks. The issue of energy leaks is now posing considerable problems in the use of multiple-blade cutting systems, as the manifestations of this unsolved problem are unacceptable audible frequency noise levels, low efficiency and poor reliability during operation. The consequences of this behaviour on the performance of high power ultrasonic components have not been reported and the findings have not previously

been linked to reliability problems in ultrasonic tooling devices. It is therefore an aim of this work to discuss and address this problematic vibration behaviour.

Therefore this research investigates the vibration characteristics of ultrasonic cutting devices whose performance is hampered by inefficient transmission of vibration energy via linear and nonlinear mechanisms. Since most ultrasonic processes are affected by common reliability problems, advances in the design of cutting systems can be applied to many alternative manufacturing applications.

1.4 Summary of research findings

Initially, the design principles of customised resonators, including bar horns, block horns and cutting blades resonating in the first longitudinal mode at frequencies near 35 kHz, are studied. The vibration behaviour of these tuned units is modelled via finite element analysis and validated via experimental modal analysis using 1D and 3D laser Doppler vibrometers (LDVs). Redesign strategies to enhance system performance by reducing the effects of modal coupling and controlling stress levels, are investigated through component modifications. Since frequent fatigue failures have limited the exploitation of high gain cutting blades, alternative blade shapes providing the required amplitude gain under reduced stress condition have been designed. A design criterion to achieve isolation of the tuned mode and uniformity of amplitude of block horns with slotted profiles is also presented.

Further, the vibration characteristics of a category of multi-component cutting devices, where a single transducer drives three tuned blades via a tuned block horn, are studied. These assemblies operate in the second longitudinal mode at 35 kHz and are designed for cutting food products. A combination of numerical simulations and LDV measurements has revealed that coupling of untuned modes with the operating mode, high stresses and bending vibration responses of the blades, are factors responsible for poor performance of these systems. Hence, the issues of modal coupling and responses of the cutting blades are improved through alterations of the intermediate block horns. In particular, the introduction of geometric modifications such as castellations in the block horn has proved to eliminate participation of bending motion in longitudinal-mode tuned cutting blades. Frequency separation at the driving frequency is achieved through opportune selection of block horn

dimensions via a sensitivity analysis. Finally, stress reductions in the cutting blades are achieved by detuning of the longitudinal-mode frequency of the components (block horn and blades) of the system while maintaining the system tuned frequency.

Evidence suggests that multiple-component ultrasonic systems often leak energy into untuned modes, whose frequencies can be well separated from the operating frequency, with the result that the tuned longitudinal-mode response includes detrimental bending and torsional contributions. Hence, experimental characterisations of the vibration behaviour of several multi-blade ultrasonic cutting systems are carried out. Experiments demonstrate that unwanted responses are particularly difficult to control in systems exhibiting a large number of modal frequencies. In addition, measurements performed over large frequency ranges highlight, for the first time, that ultrasonic devices can exhibit dynamic responses that are qualitatively similar to theoretical models of simple autoparametric systems. The understanding of this type of nonlinearity has suggested that intermodal exchanges are highly favoured in systems with numerous modes at frequencies below the tuned frequency. Consequently, alternative design strategies focused on reducing the number of modes of complex assemblies are discussed and proposed. The introduction of intermediate block horns with a reduced number of slots or solid geometries are proved to help in the control of nonlinear responses. Furthermore, a novel configuration based on tuning multiple-component cutting systems to the first longitudinal mode, instead of the second, has proved to decrease the risk of nonlinear modal coupling.

Finally, the nonlinear relationship between amplitude and power level in ultrasonic systems, previously attributed to piezoelectric transducers [10] and recently associated with the effect of the attached components [9], is further discussed. An empirical strategy for influencing the nonlinear behaviour of the transducer, by attaching tuned components of different geometry and interface configurations, is proposed. It is shown that specifically profiled components connected to the transducer can reduce the saturation effect of the vibration amplitude, which also depends on joint configurations.

CHAPTER 2

REVIEW OF LITERATURE

2.1 Historical aspects of ultrasound

The history of ultrasound is a part of the history of acoustics. The first testimony is attributed to Pythagoras, who in the 6th century discovered the diversities of sound emitted from different lengths of ropes of musical instruments. In 1638 Galileo contributed with his own studies of the science of acoustics. He elevated the study of vibrations, and the correlation between pitch and frequency of the sound source, to scientific standards. Contributions from many physicists and mathematicians during the 17th and 18th century formed the first bases for the development of diverse fields of acoustics. During the 19th century there were two significant developments in the methods for the generation of ultrasounds. The first one was discovered by Joule and called the magnetostrictive effect, which is the phenomenon a means by which it is possible to convert magnetic energy into mechanical vibrations. Length variations in a bar of ferromagnetic material can be obtained by immersing it in a variable magnetic field. The second was discovered by Pierre and Jacques Curie in 1880 and is called the piezoelectric effect, a means by which it is possible to convert electric power into mechanical energy, through exploitation of the property of certain crystals (piezoelectric crystals) of exhibiting dimensional variations when electrically charged. These two important discoveries lifted remarkable interests in researchers who, with the development of electronics and more and more refined piezo-ceramic materials, have designed through the years more and more sophisticated ultrasonic systems for domestic, medical, industrial and military use.

It can be asserted that the era of modern ultrasonics started about 1917, with Langevin's invention of the quartz sandwiched transducer for underwater sound transmission in submarine detection (sonar). The requirement for the development of systems of underwater detection took place after the Titanic tragedy, which collided with an iceberg in 1912, and submarine navigation during World War I. In the late

1920s, as a result of the discoveries of Langevin, many French ocean liners were equipped with systems of underwater echo-sonorous devices. The World War II saw further developments such as naval and military radars that enormously contributed to the design of sonar and systems for propagation of ultrasonic waves. An application in the field of ultrasound, developed in late 1920s and during the 1930s, was the development of analyzers of metal defects using pulsed ultrasounds. The basic concept of such devices, which were mainly used in inspection of the hulls of ships and tanks, had been elaborated from the Soviet scientist Sergei Y. Sokolov in 1928 at the Electrotechnical Institute of Lenin. In the reflection technique, a pulsed sound wave is transmitted from one side of the sample, reflected at the far side, and returned to a receiver located at the source. As a consequence of impinging on a flaw or crack in the material, the signal is reflected and its traveling time altered. The delay becomes a measure of the flaw's location.

The destructive ability of high power ultrasound had been recognised since the 1920s from the time of Langevin when he noted the destruction of fish in the sea and pain induced in the hand when placed in a water tank insonated with high intensity ultrasound [11]. The spectacular effects of high-power ultrasonics on various processes were first described in New York by Robert Wood and Alfred Loomis in 1927. Loomis was a Wall Street tycoon, a famous scientist, a lawyer and a true legend in the history of the United States. Loomis renewed his wartime acquaintance with Professor Wood and offered to collaborate and underwrite several joint research activities. In 1926, Wood told Loomis of Langevin's experiments and suggested the subject offered a wide field for research in physics, chemistry, and biology. It was their group that had allegedly introduced ultrasound to chemistry. When a liquid is exposed to ultrasonic waves, bubble growth is created which is known as cavitation. Sound waves stress these bubbles, causing them to grow, contract and eventually to implode. With implosion, immense heat and pressure are produced that speed reactions. Every imploding bubble is a micro reactor in itself. This is due to the extreme heat released upon implosion that creates a local hot spot. Temperatures can reach 5000°C with pressures of several hundred atmospheres. These effects promoted the advent of sonochemistry which has in recent times become a useful tool for the synthesis of chemicals, pharmaceuticals and the production of new materials with unusual properties.

In the 1950s the development of efficient transducers and the design of tapered half-wavelength horns for the amplification of vibrations [12-14] lead to a burst of activity in high power ultrasonics in solids. Industrial processes such as, metal forming, cleaning and welding, and destructive testing were now performed using ultrasonically resonating components. A review paper covering the numerous applications of high power ultrasonics from this period was presented by Neppiras [15] in 1960. In his work Neppiras advised on the choice of the transducer and velocity transformer to be used depending on the power use. He also described the nonlinear effects of materials investigated in destructive testing.

Despite the many proven benefits of applying high power ultrasonics to manufacturing processes, a low interest in ultrasonics is perceptible after the 1960s'. This was due to a lack of knowledge of the fundamental mechanics of ultrasonic systems and the difficulties in designing reliable systems. However in the 1970s and 1980s, with the advent of finite element techniques capable of simulating the vibration behaviour of fluids and solids, research in ultrasonics found new impetus. A comparison between theoretical and finite element predictions of the vibration performance of large resonators used for ultrasonic welding was given in 1984 by Derks [16]. In the same work the need for a more basic understanding of the processes of ultrasonic equipment in order to fulfil the enormous potential of high power ultrasonics, is discussed. The 1980s and 1990s have been characterised by numerous contributions to the design of ultrasonic tools for manufacturing processes, due to significant advances in the experimental capabilities. With the advent of non-contact measurement devices, the identification of the vibration characteristics of ultrasonic devices, which previously could only be predicted, has been achieved. Hence, the development of new applications, not only in industrial processes but also in other fields such as chemical and medical, have flourished [17,18].

Another factor which has hampered the development of ultrasonic applications, is related to the nonlinear nature of the media (fluids and solids) which ultrasonic waves travel through. Leif Bjorno [19], editor of the journal *Ultrasonics*, has published in 2002 a paper reviewing the progress of research in nonlinear ultrasound in the last four decades. He asserts that while the theoretical and numerical tools giving descriptions of nonlinear ultrasound are available after more than 40 years of intense

research, the exploitation of the theoretical/numerical achievements in practical methods and devices are lagging somewhat behind. Hence, important challenges in nonlinear ultrasonic processes still exist.

2.2 High power ultrasonic applications

The main applications of high power ultrasonic in manufacturing include machining and welding. The advent of these technologies commenced in the 1950s and 1960s with advances in the design of transducers and resonators [15,20,21]. Neppiras [22-28] covered the main aspects of ultrasonic machining through a series of papers released in 1956. In these publications, operating variables such as vibration amplitude, operating frequency, tool area, static load and resistive amplitude are discussed in detail together with their impact on tool design and choice of transducer. The main prerequisites for high operating accuracy and surface finish were achieved through analysis of extensive experimental data. It resulted that ultrasonic machining offered the possibility of cutting slots and holes of any shape with a high degree of accuracy in materials such as ruby, tungsten carbide and glass. However, the thickness of the materials was very small.

A new machining method was published in 1964, which used diamond impregnated probes to cut deep holes through rotating workpieces [29]. This work derived from the experiments carried out at the Atomic Energy Research Estabilishment of Harwell (UK) in the early 1960s. In conventional ultrasonic machining technologies the cutting edge of the working tool vibrated lengthwise onto the material being bored and, since neither tool nor workpiece were rotating, the tool could be oval or triangular, or any shape, in cross-section. Abrasive slurry flowed through the hollow centre of the tool into the workpiece facilitating the cutting operation. A necessary condition was that the amplitude of the longitudinal movement of the tool had to be large enough to allow the abrasive particles to flow underneath it, but of course not so large as to subject the tool to accelerations which would break it. However, after a certain cut depth the abrasive slurry could not escape quickly enough from the tool face, hence the slurry damped the tool motion causing the operation to stall. To overcome these limitations, engineers at the A.E.R.E. used diamond-impregnated probes on a workpiece held in a 4-jaw chuck. The chuck rotated while the hole was machined with the result that the complicated shapes which could be machined with a

non-rotating workpiece were impossible. However, deep holes without any fall in the rate of penetration without use of abrasive slurry and with very high accuracy, were achieved through this method.

In the same year an article was published [30] giving an idea of the developments in ultrasonic machining taking place in the USSR. In this work three ultrasonic machines used for ultrasonic cutting were described. Through embodiment of new principals they were able to remove material at a rate almost three times as fast as their predecessors and cut impressively large holes with remarkable accuracy. The achievement of such precise and fast operations stemmed from the control systems of these machines which automatically took account of the tool wear.

Another important contribution to ultrasonic machining was provided by Kazantsev and Rosenberg, who published a paper in 1965 describing the mechanism of ultrasonic cutting [31]. This work contained the theoretical and experimental investigations of ultrasonic cutting which were carried out in the Acoustics Institute of the USSR Academy of Science. The interactions between working tool, workpiece and slurry, were studied meticulously in order to provide a fundamental understanding of ultrasonic machining.

In 1966 Legge, one of the A.E.R.E. researchers who conducted experiments on ultrasonic cutting with diamond impregnated probes, published a work where the advantages of ultrasonic machining without the use of abrasive slurry were presented [32]. In particular, he showed the dramatic benefits for cutting holes in standard materials such as glass and ceramics by means of rotating transducers. With this technological innovation only the length of the cutting tool limited the possibility of drilling deep holes. Of course, rotating transducers sacrificed some of the special features of ultrasonic machining such as the ability to drill star-shaped holes, but the limitations were slight.

Until the late 1960s the use of ultrasonics for machining was limited to small-scale production or development work with precious stones, semiconductors and glass. In order to prove a more universal applicability of the method, in 1971 Smith [33] carried out an investigation, the main objective being the determination of a standard

procedure for assessing the machinability of any new material. It resulted that for all materials, without exception, the amplitude at the resonant frequency was to two three times more influential than other variables considered, such as static force and grain size.

In 1979 Devine [34] published a paper describing a range of metal working processes which used ultrasonic energy, the object of intensive study in industrial laboratories. This work focused on the technical and operational problems relating to all metal removal processes such as turning, boring, twist drilling, trepanning and tapping. As a result of the investigation, several ultrasonic devices readily and economically adapted to shop machines were presented. Ten years later Moreland and Moore [35] published a similar work where several ultrasonic machining processes were described paying particular attention to the ultrasonic apparatus and the design requirements for the transducer and tool holder.

In recent years Astashev and Babitsky identified an influential factor which hampers the performance of ultrasonic machining systems [36,37]. They showed that the difficulties in maintaining the required amplitude during the cutting of material, largely stem from the inherent nonlinearity of these processes. Therefore, the nonlinear amplitude response of the vibrating tool was obtained theoretically and experimentally. Hence, a novel method of stabilization of the resonant ultrasonic excitation was described.

The exploitation of high power ultrasound for welding operations began in the late 1960s, but the main contributions to this technology were published in the 1970s. Shoh [38], published a review paper in 1976 focused on the industrial applications of power ultrasound to thermoplastics. He described the process of heat generation in plastic materials caused by high frequency oscillations. The advantages of using ultrasound derived from the local melting effect at the interface of the materials being welded. Hence a range of industrial applications such as ultrasonic staking, insertion, packaging, spot welding and seaming of films, which could benefit from the technology, were listed. In addition, he illustrated the extent to which different materials could be welded and provided a detailed description of the welding equipment.

Until the 1980s, research in high power ultrasonics was mainly focused on the exploitation of the vibrational energy delivered by tuned components resonating in a single mode (longitudinal, radial or torsional). In the last two decades, particular attention has been paid to ultrasonic applications such as ultrasonic motors, ultrasonic plastic soldering, ultrasonic welding and ultrasonic fatigue testing. In these processes complex modes consisting of a transverse (torsional or bending) mode and longitudinal mode tuned at the same frequency, have also been used and sometimes preferred to the traditional longitudinal mode. For instance, in conventional ultrasonic welding systems linear vibrations normal to the welding surface are traditionally used, and therefore the vibration stress induced in the welding specimen is one-dimensional. Using complex vibrations, two-dimensional vibration stress can be induced in the welding specimen, and as a result an improvement in the welding characteristics derives from the temperature rise due to two-dimensional complex vibration stress. The idea of exploiting complex vibrations in industrial applications is actually quite an old one. Rozenberg [39] in 1969 studied a longitudinal-torsional composite mode transducer based on the vibrational mode conversion of a longitudinal mode into a torsional mode. However, the construction of such a transducer proved rather complicated.

Tsujino has contributed to the development of ultrasonic welding technologies. He has designed numerous complex mode ultrasonic devices operating at resonating frequencies in the range of 15 kHz to 1 MHz according to the application requirements [40-47]. Systems resonant at frequencies up to 100 kHz for metal and plastic welding are presented, where vibration amplitudes up to 30 μm peak are required [40-43]. Conversely, high frequency vibration systems resonant at frequencies above 100 kHz are designed for ultrasonic wire-bonding where vibration velocities below 1 m/s are necessary [44-47].

In the plenary lecture given at the Ultrasonic International Conference 2003 Ueha [48] has presented two newly developed ultrasonic actuators (or motors) used for object transportation. The operation principles of both system configurations rely on exploitation of complex vibrations. The first motor type is based on a friction drive

achieved by careful design of tuned resonators excited in a complex mode. Ueha proposed that this category of complex mode actuators will find applications in manufacturing processes where miniaturisation, high efficiency and high speed are required. The second category reproduce a phenomenon called near-field acoustic levitation (NFAL). NFAL is a technique which has been successfully applied to non-contact transportation in air where planar objects of several kilograms are levitated and transported. Ueha presented a way to achieve NFAL both for a piston-like sound source and a flexural vibration source. These actuators are expected to be used in manufacturing of electronic devices where high speed and non-contact transportation are required.

2.3 The design of ultrasonic components

The design of half-wavelength resonating tools with lateral dimensions small compared to the tuned length can be well understood from the literature. Merkulov [12] was the first researcher to derive the equations for computing the resonant dimensions of longitudinally vibrating rods with variable cross-sections for amplitude magnifications. He compared the particle velocity gains of half-wavelength horns with conical, exponential, and catenoidal profiles and showed that catenoidal horns provide the highest gains for the same input/output radii ratio. Two years later, Ensminger [14] presented a paper where formulas for the design of conical resonators were determined in a simpler and more useful form. In addition to the work of Merkulov, Ensminger calculated formula for the distribution of stress generated in conical horns. In a paper published in the same year, Merkulov and Kharitonov [13] investigated theoretically and experimentally the design of more complex concentrators formed by rods of variable and cross section. These tuned units called sectional concentrators were used to obtain larger amplifications in comparison with the resonators of simpler forms. Additionally, Merkulov provided a criterion for the horns' evaluation based on the characteristics of the input impedance near resonance.

The design rules for another class of velocity transformers, capable of delivering vibration amplitudes under contained stress conditions, were discussed by Eisner and Seager [21] in 1965. Until then, the conventional method of horn design started with defining some possible shapes from which the axial amplitude could be calculated from the strain distribution, and then calculating the strain distribution. However,

since only resonators of basic shapes could be solved analytically with this approach, a requirement for another design criterion arose. Hence, Eisner and Seager introduced a design method in which a suitable wave function of the vibration amplitude was chosen and the corresponding profile obtained by integration. From this approach it is shown that the best horn design exhibited a peak strain equal to the maximum permissible strain in the material for as great a part of the length as practicable.

In 1972 Jakubowski [49] published a paper where the importance of including the boundary conditions in the mathematical model for the horn design was demonstrated. After introducing the concept of mechanical impedance as it applied to the formulation of horn boundary conditions, two practical design applications, in which the attachments of a cylindrical bar and an exponential horn were treated as concentrated masses, were described. The results showed that estimation and inclusion of the loading conditions in the calculations enabled a more efficient design of transducer-horn systems. In 1976 Amza and Drimer [50] verified that the measured resonant frequency of transducer-horn assemblies was always lower than that calculated from the horn equations. This resonant frequency variation implied a modification of the vibration distribution and of the position of the nodal points in the horn. Using the deviations of the resonant frequency in systems incorporating conical, exponential, and catenoidal horns, Amza and Drimer introduced an expression for computing the effective lengths which could be adapted to a range of horns.

From the late 1960s, another class of ultrasonic horns became popular in ultrasonic welding and machining operations. These are characterised by having at least one of the lateral dimensions (more specifically the dimensions of the output surface) of the same order as the tuned length. However, before the 1980s the design requisites of longitudinally vibrating horns with wide output cross-sections, in contrast to those with small lateral dimensions, was hardly described in the literature.

Although large resonators were widely used in plastic welding applications, few papers were published discussing their design parameters. In a 1976 review on the joining of thermoplastics Shoh published [38] pictures of wide slotted horns used for plastic welding of large areas of material. However, no specific design guidelines were discussed apart from the requirement of the incorporation of slots to improve

uniformity of amplitude of the horn output face. In his PhD thesis (1984) Derks [6] justified the low academic interest in high power ultrasonics, saying that, at the time, industry was surviving well with the technological status. The contribution of Derks in tool design and in the elaboration of the design principles for the development of ultrasonic processes has been significant. He calculated the resonance conditions for the fundamental longitudinal mode of a variety of differently shaped resonators having at least one lateral dimension exceeding one third of the wave-length. All the calculations were carried out for free boundary conditions of the vibrating resonators, as no realistic model describing the complex situation under load was available. Comparison of finite element models and experiments, validated his theoretical predictions for horn design.

A subsequent contribution to the design of tools with rectangular output faces for plastic welding was provided by Adachi et al. [51] in 1986. In this work modal vibration analysis of several resonators with a different number of slots was carried out using finite element models. The effect of slot dimensions on achieving a flat distribution of longitudinal amplitude at the radiating surface was discussed. Hence, a combination of slot spacing, width and height was predicted to provide an adequate uniformity of amplitude at the radiating face of the modelled horns. However, despite the satisfactory results obtained through the finite element method, the author pointed out the requirement for the identification of a more universal strategy to achieve the flattest amplitude distribution in ultrasonic horns. In 1990, Adachi [3] proposed a novel design approach for improving amplitude uniformity of horns with large output surface called the method of wave-trapped horns. This technique consisted of adding small elastic components to the horn to modify its vibration mode. The added elastic components were two wave-trapped rods attached at the input face of the slotted horn at either side of the driving transducer. By means of adjusting the length of the attached rods the reactive mechanical impedance at the attachment points varied until the amplitude distribution of the radiating surface of the slotted horn became highly uniform. This method produced good results for horns with small radiating surfaces. However, in larger resonators where lateral vibration at the attachment points was not negligible, bending vibration diminished the effectiveness of the method.

In 1991, O'Shea [41] published a paper on the design of ultrasonic block horns using finite element analysis. As in Adachi's publications, the effects of slot number, positioning and size on the uniformity of amplitude of the output face of horns were discussed. In addition, the influence of the same design variables on the frequency isolation of the operating mode from close modes, was considered. Hence, an optimum configuration was achieved based on finite element predictions and experimental validations via amplitude probe measurements. From the O'Shea contribution, it became clear that reliable design of tuned components could only be accomplished through the identification of modal parameters (natural frequencies and mode shapes) in a frequency range of several kHz around the operating frequency. Measurement of vibration response in the ultrasonic range was often not feasible using conventional sensors as high surface accelerations made attachment of accelerometers very difficult and only few non-contacting probes retained linearity at ultrasonic frequencies. However, with developments in laser technology in the 1980s and 1990s, devices for vibration measurement and validation of theoretical and numerical models became available. In particular, 1D LDVs, for measurement of normal to surface velocities, and electronic speckle pattern interferometry (ESPI), for detection of in-plane and out-of-plane motions of surfaces, provided the opportunity for vibration measurements of ultrasonic components.

Shellabear and Tyrer [52] successfully used ESPI to measure wholefield vibration displacement of structures in the low ultrasonic frequency range. Lucas and Chapman [53,54], who, a few years prior to O'Shea, had recognized the identification of the modal parameters in the tuned frequency region as being critical for ultrasonic design, employed ESPI for experimental modal analysis of ultrasonic horns. Hence, redesign strategies based on structural modifications achieved through a combination of ESPI, as a technique complementary to 1D LDV measurements, and finite element models, were proposed for a variety of ultrasonic components [55,1,6]. In these studies, the redesign solutions for ultrasonic components resonating in a longitudinal mode (bar and block horns) proved useful for enhancing ultrasonic cutting operations [2,5,7,56].

Furthermore, Lucas [57,58] presented a design procedure for improved vibration control of ultrasonic dies tuned in a radial mode for metal forming processes. The possibility of exploiting radial vibrations for cold metal working applications was

originally identified by Young and al. in 1970 [59]. The detection and characterisation of the nonlinear vibration behaviour of single- and multi-component ultrasonic tools using ESPI and LDV were also investigated by Lucas and Graham [8,9]. In these publications the importance of identifying in-plane responses via ESPI was demonstrated by the measurement of jump phenomena, frequency shifts, and hysteresis cycles, typical features of nonlinear systems. With the advent of 3D LDVs, further advances in ultrasonic tooling design and nonlinear behaviour characterisation are possible.

The opportunity of exciting two modes (complex vibrations) at the same frequency in order to enhance operation of industrial applications such as ultrasonic welding and machining has been researched since the late 1960s [60]. However, only developments in the design of sandwiched piezoelectric torsional [61] and longitudinal-torsional transducers [62] of the last decade have allowed exploitation of this idea. In 1996 Lin [63] published a paper where the design of an exponential horn for welding applications tuned in a longitudinal-torsional composite modes was achieved by equating the resonant frequency expressions of the two modes. Following Lin's approach Zhou et al. [64] studied theoretically and experimentally the longitudinal-bending and torsional-bending complex modes for an ultrasonic system consisting of a sandwiched transducer and an attached horn.

In the last thirty years, a large number of publications on ultrasonic metal and plastic welding and wire bonding have been published. Tsujino and al. [65-67] have designed systems whose uniqueness stems from the means by which complex vibrations are obtained. A specific component (converter) is introduced, consisting of a longitudinally tuned bar horn with transverse slits originally incorporated at the longitudinal node [65] and subsequently near the antinodes [66,67]. In these slits the longitudinal vibration is partially converted to torsional motion, thus forming elliptical loci which enhance the welding operation. Generating longitudinal-torsional complex modes within the converter element, it is possible to drive the ultrasonic devices using a traditional longitudinal transducer instead of a torsional-longitudinal transducer. The results show improvement in welding and wire-drawing; however, concern remains on the large number of modes and the consequent difficulty of tuning these systems.

CHAPTER 3

METHODOLOGY FOR VIBRATION CHARACTERSATION OF ULTRASONIC DEVICES

3.1 Introduction

The use of high power ultrasonics has demonstrated significant benefits in many industrial applications requiring large amounts of energy to be transmitted in a controlled and precise manner to the working surface. In fact, the exploitation of the harmonic motions produced by resonating tools, which are specifically designed according to the operation requirements, constitutes an efficient approach to providing substantial power at relatively low excitations.

Ultrasonic components are designed to resonate in a certain mode of vibration, depending on the type of application, at a frequency above the upper limit of human hearing (16-20 kHz). It is a common belief that the success of the technology relies on careful design of the ultrasonically excited tools and transmission components.

The design of ultrasonic components based on cut-and-try approaches often results in a waste of time and material. In fact, if prototype components do not satisfy the operation requisites and they cannot be modified to achieve adequate performance, then alternative components have to be machined. Design strategies exclusively based on experience are sometimes suitable for manufacturing simple ultrasonic systems but are inadequate for the fabrication of complex devices.

In recent years, finite element (FE) modelling, with extraction of modal parameters from the FE model, has increasingly been used in order to characterise the dynamic behaviour of vibrating structures. These modelling procedures have led to significant progress in ultrasonic system design [4]. In particular, the opportunity to predict the component performance prior to machining, has enabled the development of

increasingly sophisticated ultrasonic devices. However, in order to assess the accuracy of the FE models, an experimental validation of the predicted data is required.

One of the most popular techniques for measuring the vibration behaviour of vibrating structures is known as experimental modal analysis (EMA). The first experimental modal analyses were performed in the 1940s in order to inspect the vibration characteristics of aircrafts. From the 1960s, with the advent of digital computers and the Fast Fourier Transform (FFT), this measurement technique became standard in numerous engineering fields.

EMA relies on the application of a modal parameter estimation method (curve-fitting) to a set of measurements carried out on the structure under investigation [68-71]. Design of ultrasonic components and assemblies can be achieved through a combination of EMA and finite element analysis (FEA). Figure 3.1 shows the different ways in which modal parameters of a vibrating structure can be obtained both analytically, by FEA, and experimentally, by EMA.

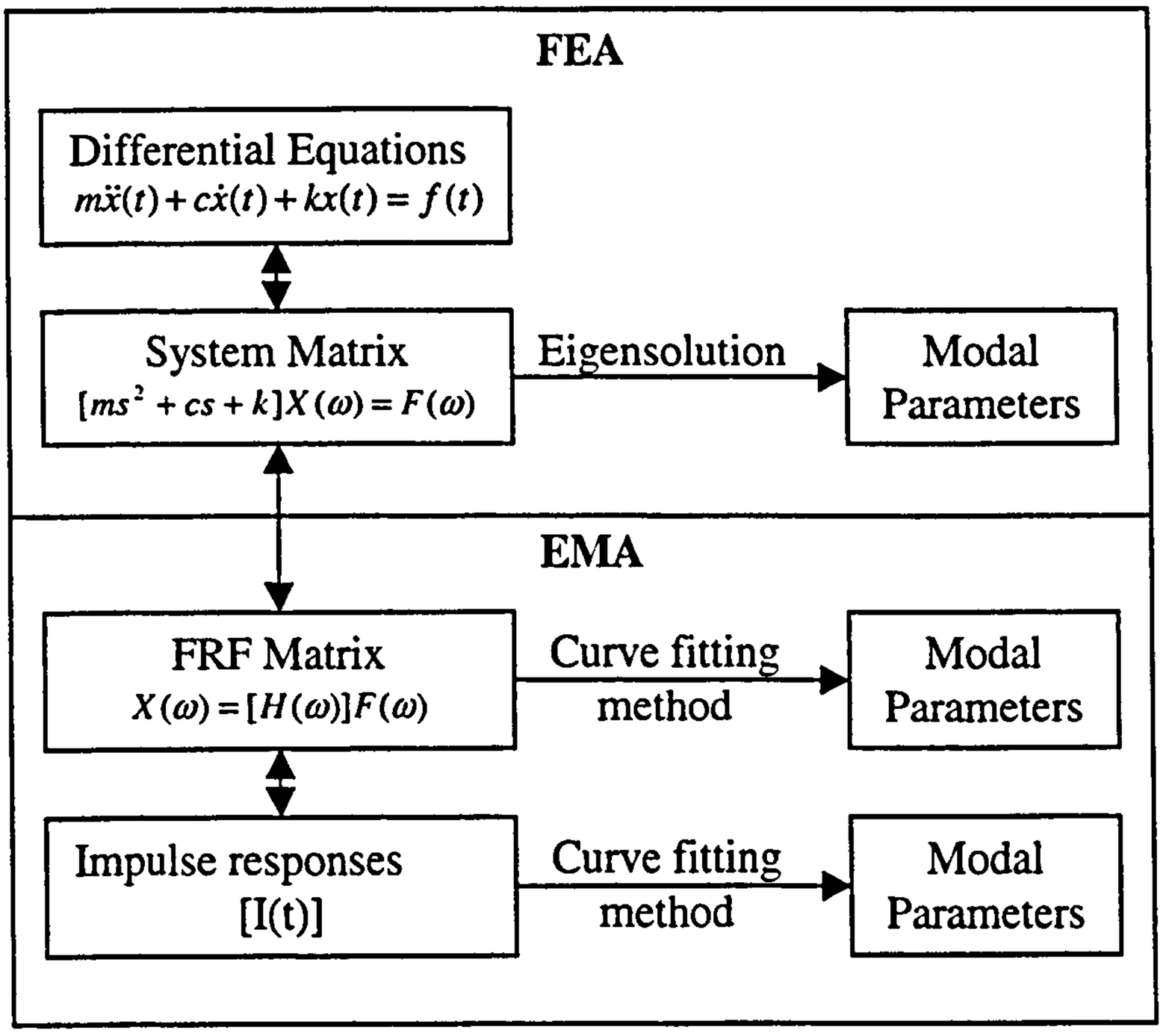

Figure 3.1. Sources of modal parameter extraction

Initially, this chapter deals with an analysis of the basic foundations of vibration theory, as these form the basis of the FEA and EMA estimations. Subsequently, the procedures for conducting EMA are described. Finally, for illustrative purposes of relevance to this study, an investigation of the vibration characteristics of an ultrasonic bar horn is carried out using a combination of FEA and EMA.

3.2 Theoretical basis

A brief introduction to the theory of mechanical vibrations from a simple mathematical perspective is required to understand the process of determining modal parameters. Although real structures are continuous systems, a mathematical description of their modal behaviour can be expressed with the description of the well-known mass, spring and damper elements with one degree-of-freedom. Considering the structure as an assemblage of many of these single degree-of-freedom (SDOF) systems, the mathematical description starts from the differential equation of motion of the damped mass-spring-damper system, illustrated in Figure 3.2.

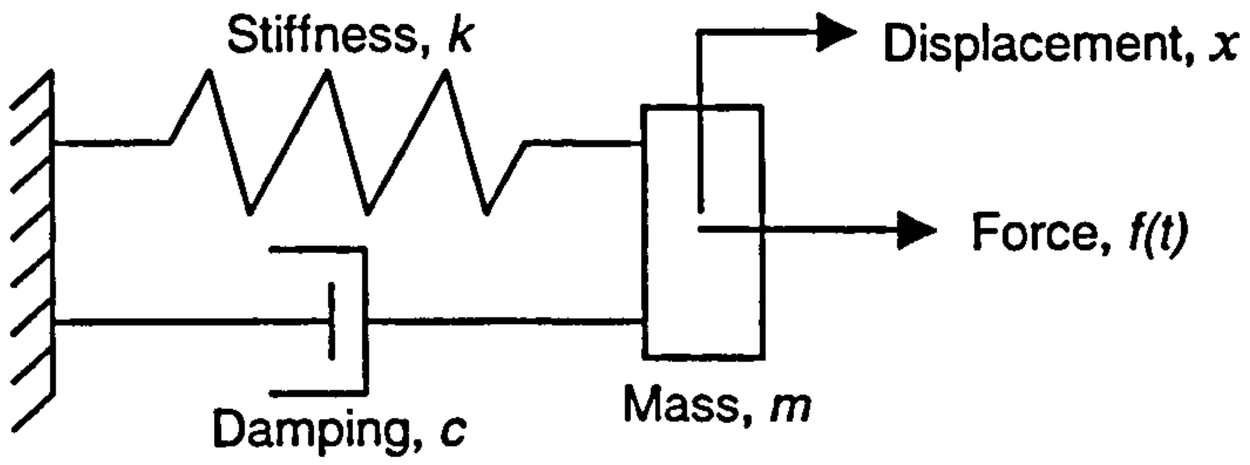

Figure 3.2. Mass-spring-damper system

$$m\ddot{x}(t) + c\dot{x}(t) + kx(t) = f(t) \tag{3.1}$$

where m is the mass of the structure, c the viscous damping and k the stiffness of the spring. For the calculation of the modal model, the properties of the system with no external forcing are considered (i.e. $f(t) = Fe^{j\omega t} = 0$). For this case the governing equation of motion is

$$m\ddot{x}(t) + c\dot{x}(t) + kx(t) = 0 \tag{3.2}$$

A solution of the following form is assumed:

$$x(t) = Xe^{st} \qquad \text{(where } s = j\omega \text{ is complex)}$$

from which the subsequent condition is obtained:

$$(ms^2 + cs + k) = 0 \tag{3.3}$$

This leads to:

$$s_{1,2} = -\frac{c}{2m} \pm \frac{\sqrt{c^2 - 4km}}{2m} = -\bar{\omega}_0\zeta \pm j\bar{\omega}_0\sqrt{1-\zeta^2} \tag{3.4}$$

where $\bar{\omega}_0^2 = (k/m)$; $\zeta = c/c_0 = (c/2\sqrt{km})$. This implies a modal solution of the form:

$$x(t) = eX^{-\bar{\omega}_0\zeta \cdot t} e^{j(\bar{\omega}_0\sqrt{1-\zeta^2})t} = Xe^{-at}e^{j\omega_0 t}$$

which is a single mode of vibration with a complex natural frequency having two parts:

- the imaginary part or oscillatory part: a frequency of ω_0, where $\omega_0 = \bar{\omega}_0\sqrt{1-\zeta^2}$;
- the real or decay part; a damping rate of a, where $a = \bar{\omega}_0\zeta$.

Lastly the forced vibration case is considered (i.e. $f(t) = Fe^{j\omega t} \neq 0$), and the assumed solution is:

$$x(t) = Xe^{st}$$

this yields:

$$(-\omega^2 m + j\omega c + k)Xe^{j\omega t} = Fe^{j\omega t} \tag{3.5}$$

In order to obtain an entity that is independent of the exciting force, the compliance is introduced, which is the displacement per unit harmonic force, α. In terms of the previous equation, the compliance for a SDOF system can be written in the form:

$$\alpha(\omega) = H(\omega) = \frac{X}{F} = \frac{1}{(k - \omega^2 m) + j(\omega c)} \tag{3.6}$$

which is complex, containing both magnitude and phase information.

Note that:

$$|\alpha(\omega)| = \left|\frac{X}{F}\right| = \frac{1}{\sqrt{(k - \omega^2 m)^2 + (\omega c)^2}}$$

$$\angle\alpha(\omega) = \angle X - \angle F = \tan^{-1}(-\omega c/(k - \omega^2 m)) = -\theta_\alpha.$$

Close inspection of the behaviour of real structures suggests that viscous damping is not very representative when applied to multiple-degree-of-freedom (MDOF) systems. There appears to be a frequency-dependence exhibited by real structures, which is not described by standard viscous dashpots. An alternative damping model is provided by hysteretic or structural damping which accounts for the frequency-dependence ($c = d/\omega$), and also facilitates calculations. The compliance for a SDOF system with structural damping becomes:

$$\alpha(\omega) = H(\omega) = \frac{1}{(k - \omega^2 m) + j(d)} \tag{3.7}$$

which can also be written in the form:

$$\alpha(\omega) = H(\omega) = \frac{1/k}{(1 - \omega/\omega_0)^2 + j\eta)} \tag{3.8}$$

where η is the structural damping factor. The same equation applied for a MDOF system, with the excitation force at point k and the response at point i, becomes:

$$\alpha_{ik}(\omega) = h_{ik}(\omega) = \sum_{r=1}^{N} \frac{\psi_{ir}\psi_{kr}}{(\omega_r^2 - \omega^2 + j\eta_r\omega_r^2)} \tag{3.9}$$

where $h_{ik}(\omega)$ is an element of the compliance matrix of the MDOF system, $H(\omega)$. $h_{ik}(\omega)$ is the summation of the SDOF system for each mode with a multiplication factor of $\psi_{ir}\psi_{kr}$ in the numerator. The $\psi_{ir}\psi_{kr}$ terms give the mode shape information. The numerator (as well as the denominator) is complex as a result of the complexity of the mode shapes.

The compliance definition leads to the more general definition of a frequency response function (FRF). An FRF is a function expressing the ratio between a response (output), and a reference (input). An FRF thus always depends on 2 DOFs, the response DOF (numerator) and the reference DOF (denominator). Since both the force and response are vector quantities, they have directions associated with them. Depending on whether the response motion is measured as displacement, velocity, or acceleration, the FRF and its inverse are named as follows:

- Compliance (displacement/force)
- Mobility (velocity/force)
- Inertance (acceleration/force)
- Dynamic stiffness (1/compliance)
- Impedance (1/mobility)
- Dynamic mass (1/inertance)

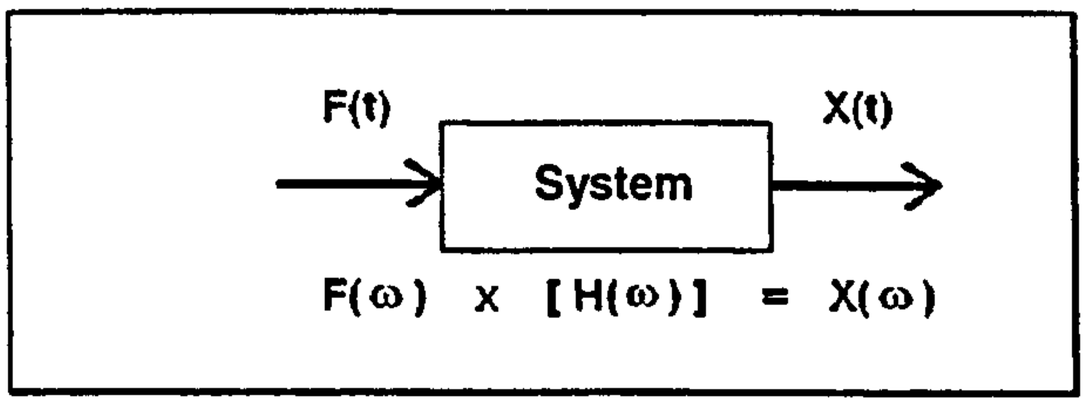

Figure 3.3. Block diagram of an FRF

Alternatively, an FRF can be defined as the Fourier transform of an output response, X(ω), divided by the Fourier transform of the input force, F(ω), as indicated in Figure 3.3.

3.3 Experimental modal Analysis

EMA is the process of determining the modal parameters (natural frequencies, damping factors, modal vectors and modal scaling) of a vibrating component or structure by means of an experimental approach. The understanding and visualisation of modal parameters is crucial in the design stage of structures. The procedure for extracting the modal parameters is set out in Figure 3.4.

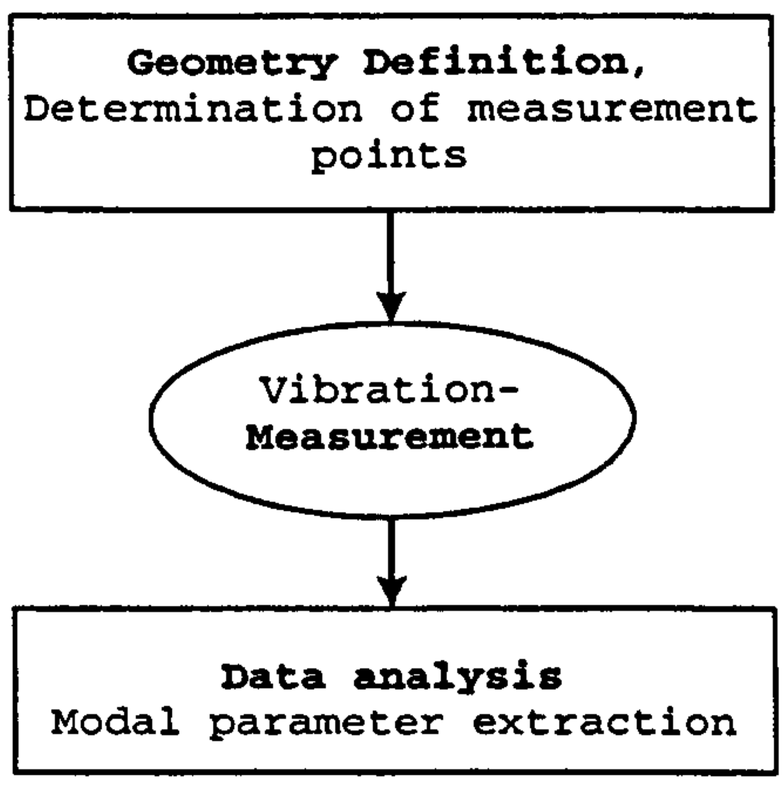

Figure 3.4. EMA procedure

Initially, the number and locations of the measurement points for the structure under test are determined. The structure is excited and responses are measured at the chosen locations in the form of time domain signals. These are transformed into the frequency domain using a fast Fourier transform (FFT) algorithm in the signal processing analyzer. Finally, a curve-fitting routine fits a theoretical expression to the measured FRFs, using a modal analysis software package, from which the modal parameters of natural frequencies, damping and mode shapes can be estimated.

There are four basic assumptions concerning the tested structure [69]. The first assumption is that the studied structure is linear, and therefore its response to any applied force is the sum of the responses to each force acting alone. As a consequence, its behaviour can be characterised by means of a convenient form of excitation, not necessarily similar to the forces that are applied to the structure in its

operating conditions. In practice, real structures are seldom completely linear. In these cases it is hoped that the linear model provides an acceptable approximation of the structure's behaviour. In characterising high power ultrasonic devices, EMA is performed at a low excitation level of the transducer so that the driven tuned components respond in a linear regime. However, the extracted modal parameters do not give a complete picture of the vibration characteristics of a system when it operates under working conditions. In fact, ultrasonic devices at the nominal amplitudes required for industrial processes, exhibit typical signs of nonlinearity, which are undetected at low amplitudes.

The second basic assumption is that the structure's vibration behaviour does not depend on time; therefore modal parameters are constants. For instance, some components are dependent on temperature, which is viewed as a time varying signal, and hence the component has time varying characteristics. If the structure that is investigated changes with time, then measurements made at the end of the test period would determine a different set of modal parameters than measurements made at the beginning of the test period. Ultrasonic systems tend to heat up when they operate, and as a consequence their modal parameters vary with time. Consequently, the only means of attaining information from EMA is by performing the tests at low excitation, so that the temperature remains constant during measurements and the extracted modal parameters are constant. Although natural frequencies detected at low excitations are slightly at variance with those typical at operating excitation levels, clear information about the mode shapes is achieved.

The third basic assumption is that the structure obeys Maxwell's reciprocity, such that a force applied at degree-of-freedom p causes a response at degree-of-freedom q that is the same as the response at degree-of-freedom p caused by the same force applied at degree-of-freedom q. With respect to frequency response function measurements, $Hpq = Hqp$.

The fourth basic assumption is that the structure is observable. The input-output measurements that are made contain enough information to generate an adequate behavioural model of the structure. This assumption is particularly related to the fact that the data normally describe an incomplete model of the structure. This occurs in at

least two different ways. First, the data is normally limited to a minimum and maximum frequency as well as a limited frequency resolution. Secondly, no information relative to the all DOF at the selected points is measurable with the available measurement devices. Other assumptions can be made regarding the system being analysed. Commonly, the modal parameters are assumed to be global. For example, this assumption means that, for a given modal frequency, the frequency and damping information are the same in every measurement.

3.3.1 Geometry definition

Real continuous structures have an infinite number of DOFs, and an infinite number of modes. From a testing point of view, a real structure can be sampled spatially at as many DOFs as wanted. However, because of time constraints, only a limited number FRFs are measured. The selected points must be sufficient in quantity and situated at convenient locations so that the extrapolated modal data can give a full picture of the structure's vibration behaviour.

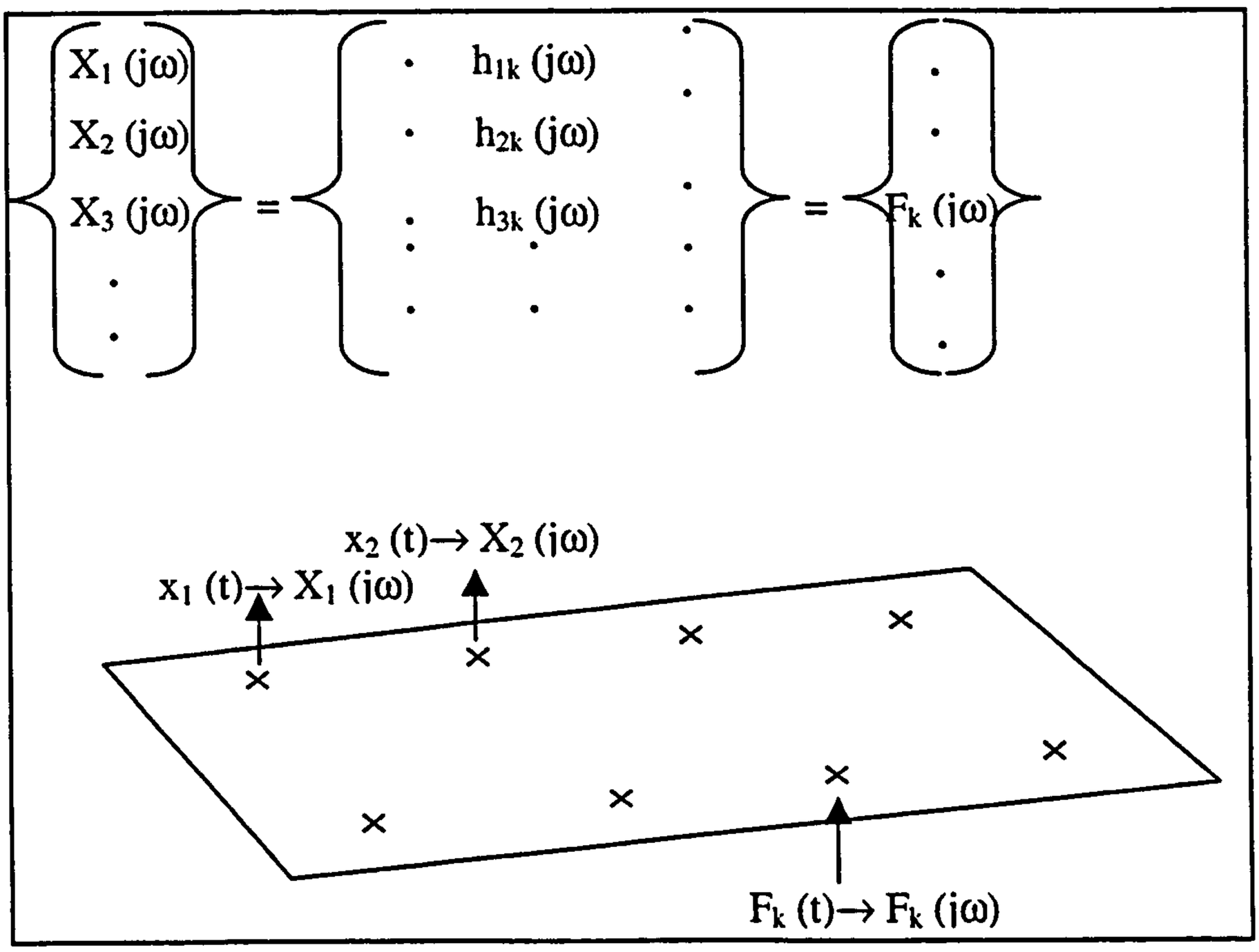

Figure 3.5. Measurement points on a slab [68]

Unquestionably, the more the surface of the structure is spatially sampled by taking more measurements, the more definite are its mode shape results. Figure 3.5 depicts the measurement points selected on a slab.

3.3.2 Vibration measurement

The experimental set-up adopted for FRF measurements is shown in Figure 3.6. The main components are:

- The source of the excitation signal. This will depend on the type of test being undertaken.
- The power amplifier. This item is required to drive the actual device used to vibrate the structure under investigation.
- The exciter. The device used to vibrate the structure. The most commonly used are an attached shaker or a hammer.
- The measurement devices. There are many different types of these devices. Piezoelectric accelerometers, or optical devices (such as laser vibrometers which are used for high power ultrasonics measurements) are used for response measurements. Load cells are used for excitation force measurements.
- The conditioning amplifiers. The choice of amplifiers depends on the used measurement devices. Their function is to strengthen the small signals generated by the measurement devices.
- The analyser. The function of this item is to measure the signals developed from the measurement devices in order to ascertain the magnitudes of the excitation force(s) and responses.
- The controller. This is a common feature in modern measurement chains and can be provided by a computer. As FRF measurements are repetitive a form of automation is highly desirable. The computer also processes the measured data as required for the extraction of modal parameters.

In EMA, FRF measurements are performed either using an impact hammer (impact testing) or a shaker driven by a broadband signal. Multi-channel analysers are used to acquire FRF measurements from input and output DOF pairs on the test structure.

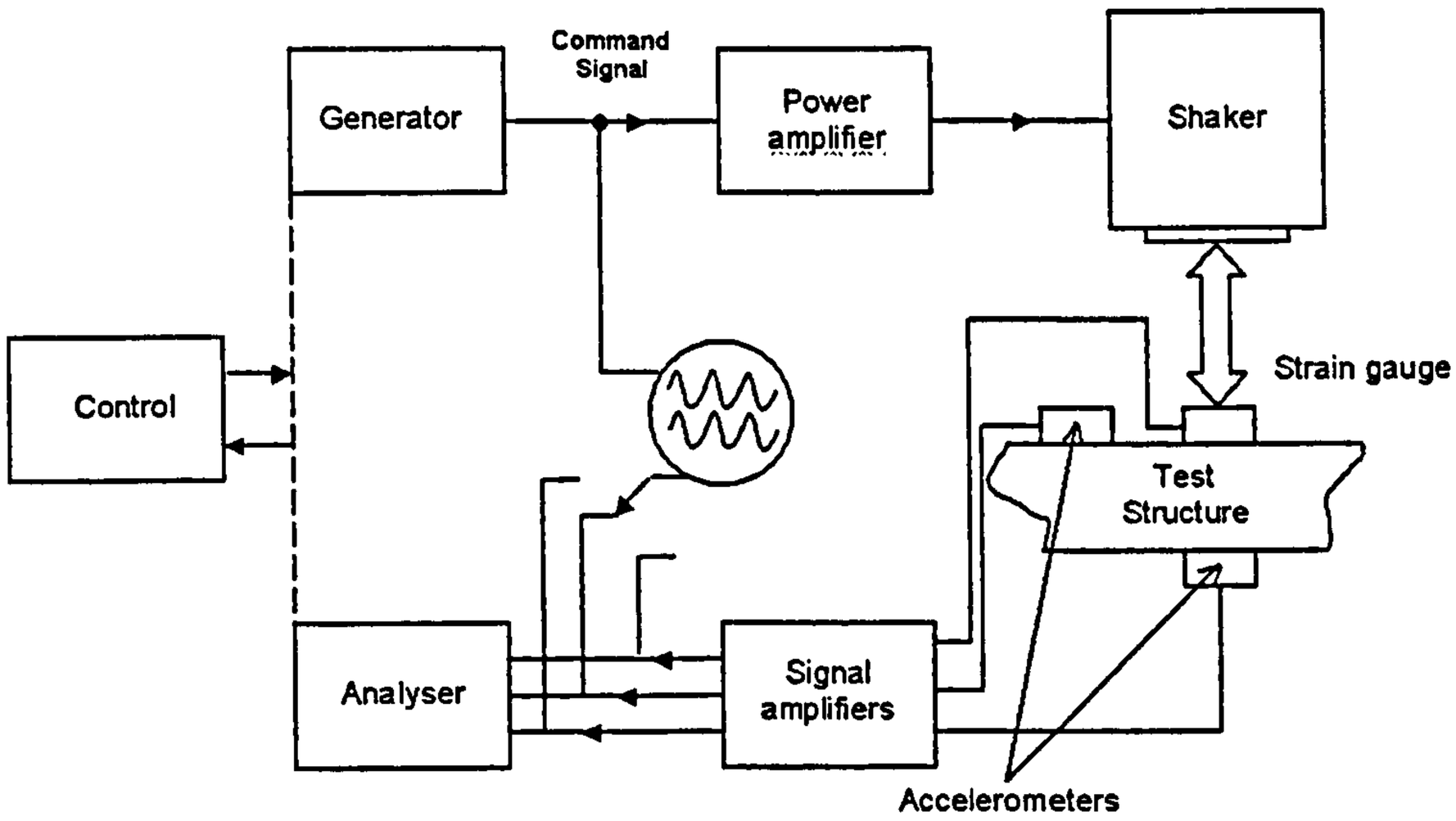

Figure 3.6. Diagram for the measurement system [70]

3.3.2.1 FFT analyser

Although the FRF was previously defined as a ratio of the Fourier transforms of an output and input signal, is it actually computed differently in FFT analysers. This is to remove random noise and distortion from the FRF estimates. The measurement capability of all multi-channel FFT analysers is built around a tri-spectrum averaging loop, as shown in Figure 3.7.

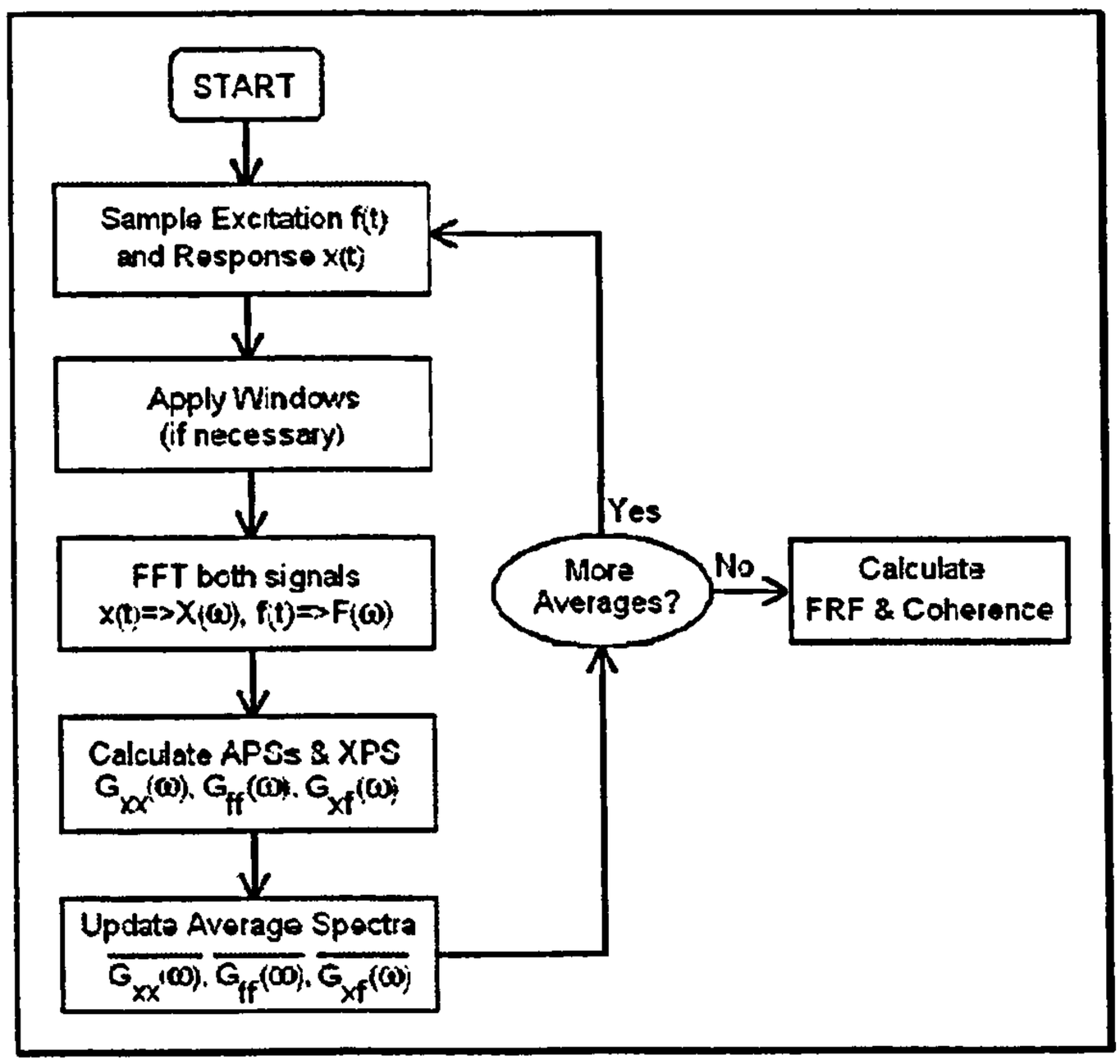

Figure 3.7. Tri-spectrum averaging loop [68]

This loop assumes that two or more time domain signals are sampled simultaneously. Three spectral estimates, an Auto Power Spectrum (APS) for each channel, and the Cross Power Spectrum (XPS) between the two channels, are calculated in the tri-spectrum averaging loop. After the loop is completed, a variety of other cross channel measurements (including the FRF), are calculated from these three basic spectral estimates. In a multi-channel analyser, tri-spectrum averaging can be applied to as many signal pairs as desired. This removes random noise and randomly excited nonlinearities from the XPS of each signal pair. This low noise measurement of the effective linear vibration of a structure is particularly useful for EMA.

FRFs can be calculated in several different ways. One possible FRF estimate is calculated through the assumption that random noise and distortion are summing into the output, but not the input of the structure and measurement system. In this case, the FRF is calculated as:

$$H_1 = \frac{XPS}{Input(APS)}$$

where XPS denotes the cross power spectrum estimate between the input and output signals, and Input APS denotes the auto power spectrum of the input signal. It can be shown that H_1 is a least-squared error estimate of the FRF when extraneous noise and randomly excited nonlinearities are modelled as Gaussian noise added to the output.

An alternative FRF estimate assumes that random noise and distortion are summing into the input, but not the output of the structure and measurement system. For this model, the FRF is calculated as:

$$H_2 = \frac{Input(APS)}{XPS}$$

As for H_1, it can be shown that H_2 is a least-squared error estimate for the FRF when extraneous noise and randomly excited nonlinearities are modelled as Gaussian noise added to the input.

Finally an FRF estimate can assume that random noise and distortion are summing into both the input and output of the system.

3.3.2.2 The FRF matrix model

Structural dynamics measurement involves measuring elements of an FRF matrix model for the structure, as shown in Figure 3.5. This model represents the dynamics of the structure between all pairs of input and output DOFs. The FRF matrix model is a frequency domain representation of a structure's linear dynamics, where linear spectra (FFTs) of multiple inputs are multiplied by elements of the FRF matrix to yield linear spectra (FFTs) of multiple outputs. FRF matrix columns correspond to inputs, and rows correspond to outputs. Each input and output corresponds to a measurement DOF of the test structure. Modal testing requires that FRFs be measured from at least one row or column of the FRF matrix. When the output is fixed and FRFs are measured for multiple inputs, this corresponds to measuring elements from a single row of the FRF matrix (impact testing). Conversely, when the input is fixed and FRFs are measured for multiple outputs, this corresponds to measuring elements from a single column of the matrix (shaker testing).

3.3.2.3 Excitation of the structure

A structure can be excited into vibration in different ways. The two most commonly used are by a hammer blow (impact testing) or by an attached shaker.

With the ability to compute FRF measurements in an FFT analyser, impact testing has become a very popular modal testing method. Impact testing is a fast, convenient, and low cost way of finding the modes of machines and structures. A wide variety of structures and machines can be impact tested. Of course, different sized hammers are required to provide the appropriate impact force, depending on the size of the structure. (Small hammers for small structures, large hammers for large structures).

Not all structures can be impact tested as impacting forces, because of their limited frequency range or low energy density over a wide spectrum, are not sufficient to excite the modes of interest of certain structures such as ultrasonic components. Hence, when impact testing cannot be used, FRF measurements are made by

providing excitation with one or more shakers, attached to the structure. Common types of shakers are electro-dynamic and hydraulic shakers.

In modal testing of ultrasonic systems, the piezoelectric transducer works as a shaker.

3.3.2.4 Excitation signals

A variety of broadband excitation signals have been developed for making shaker measurements with FFT analysers.

These signals include:

- Transient
- True Random
- Pseudo Random
- Burst Random
- Fast Sine Sweep (Chirp)
- Burst Chirp

Random and fast sine sweep signals are typically used for determining modal frequencies of ultrasonic systems.

True random signal is used in combination with spectrum averaging, random, which removes the nonlinearities randomly excited in the structure. Obtaining a set of noise free FRF estimates with no distortion in them is very important for obtaining accurate modal parameters. The main disadvantage of a true random signal is that it is always non-periodic in the sampling window. Therefore, a special time domain window (a Hanning window or similar), is used with true random testing to minimize leakage.

In modal testing performed using a swept sine excitation signal, the sine waves must sweep from the lowest to the highest frequency in the spectrum, over the relatively short sampling window time period, this fast sine sweep often makes the test equipment sound like a bird chirping, hence the name chirp signal.

3.3.3 Modal parameters extraction from curve-fitting

The process of matching a mathematical expression to a set of empirical data points is achieved by minimising the squared error between the analytical function and the measured data. The knowledge of the modal quantities allows a description of the dynamic behaviour.

The majority of the curve-fitting methods operate on the response characteristics in the frequency domain. All curve-fitting methods fall into one of the following categories:

- Local SDOF (or single mode) method
- Local MDOF (or multiple mode) method
- Global method
- Multi-Reference method

In general, the methods are listed in order of increasing complexity. SDOF methods estimate modal parameters one mode at a time. MDOF, Global, and Multi-Reference methods can simultaneously estimate modal parameters for two or more modes at a time. Local methods are applied to one FRF at a time. Global and Multi-Reference methods are applied to an entire set of FRFs at once. Local SDOF methods are the easiest to use, and can be applied to most FRF data sets with light modal density, whereas MDOF methods must be used in cases of high modal density (Figure 3.8). Global methods work better than MDOF methods for cases with local modes. Multi-Reference methods can find repeated roots (very closely coupled modes) where the other methods cannot.

3.3.3.1 Local SDOF methods

A number of local SDOF modal analysis procedures exist. The methods vary as to whether they assume that all response is attributed to a single mode, or whether other modes' contributions are represented by a simple approximation. Using a combination of the simplest local SDOF curve-fitting methods, three procedures to determine the modal parameters of a test structure, are now described. All used methods are based on applying an analytical expression for the FRF to measured data.

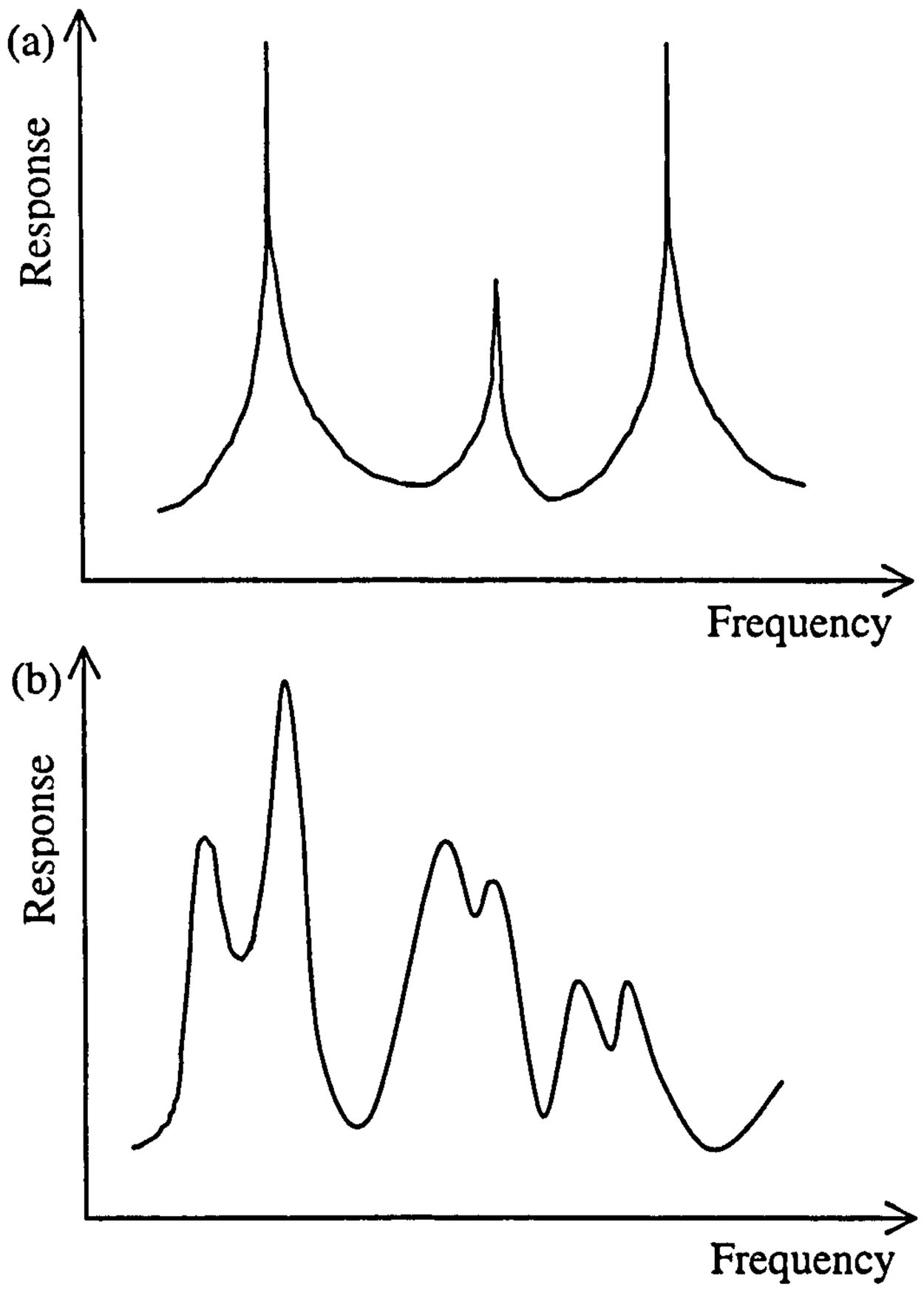

Figure 3.8. (a) Light, (b) high modal density

A simple way to obtain a natural frequency is by using the "Modal Frequency as Peak Frequency" algorithm. Hence, the frequency of a resonance peak in the FRF is used as the modal frequency. This peak frequency, which is also dependent on the frequency resolution of the measurements, is not exactly equal to the modal frequency but is a close approximation, especially for lightly damped structures. If the measurements have been performed correctly, the resonance peak appears at the same frequency in every FRF measurement. Of course, it will not appear in those measurements corresponding to nodal lines (zero magnitude) of the mode shape.

The modal damping information can be easily achieved by looking at the width of the resonance peak. The resonance peak width should also be the same for all FRF measurements, meaning that modal damping is the same in every FRF measurements. The width is measured at the so-called "half power point", and is approximately equal to twice the modal damping (in Hz).

Finally, the mode shape information can be obtained using the "Quadrature method" of curve-fitting. From (displacement/force) or (acceleration/force) FRFs, the peak values of the imaginary part of the FRFs are taken as components of the mode shape. From (velocity/force) FRFs, the peak values of the real part are used as mode shape components.

3.3.3.2 Local MDOF methods

A brief description of two MDOF methods is given. The Complex Exponential (CE) and the Rational Fraction Polynomial (RFP) methods are two of the most popular local MDOF curve-fitting techniques.

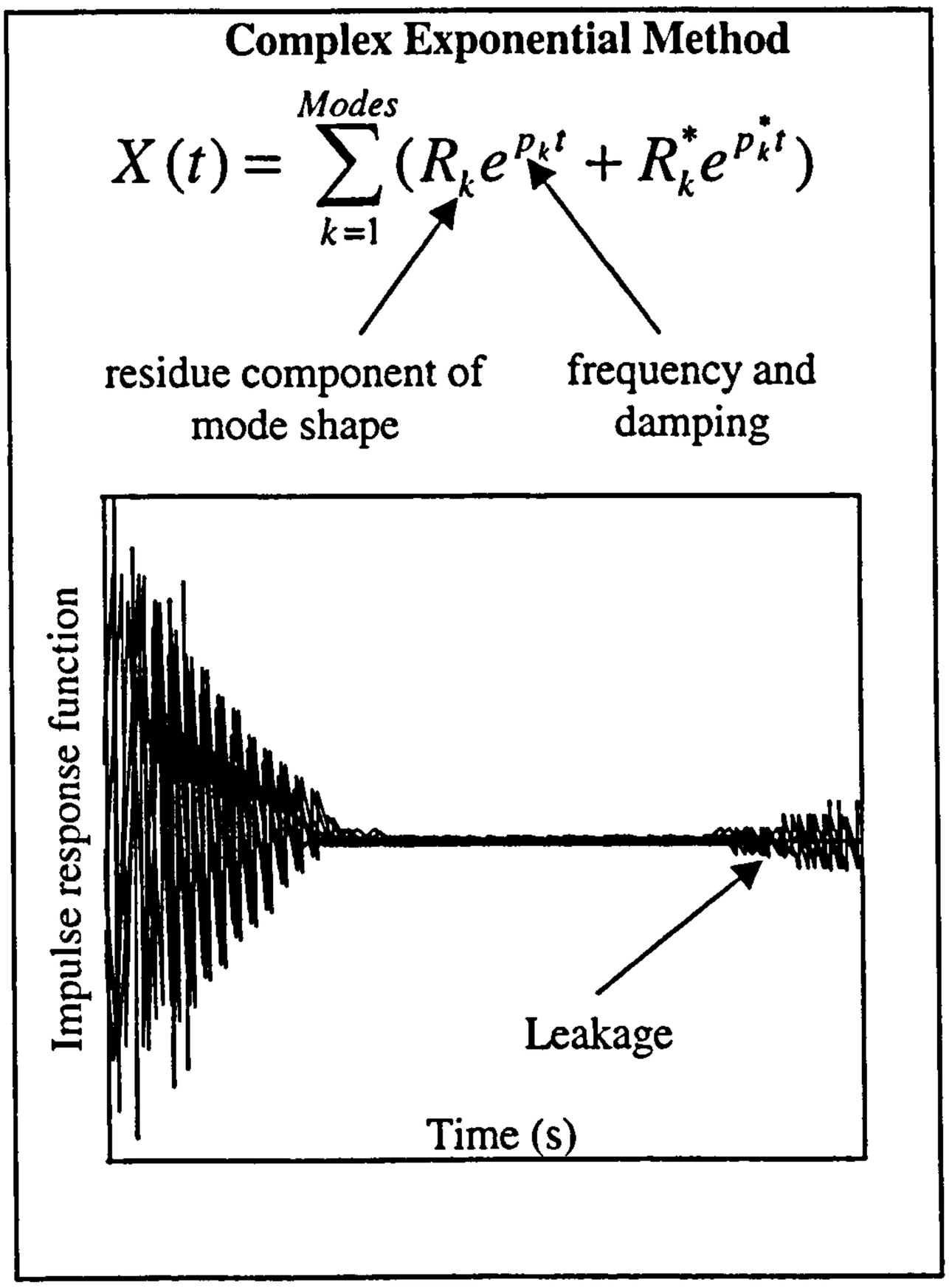

Figure 3.9.CE curve-fitting method [68]

CE algorithm curve-fits an analytical expression for a structural impulse response to experimental impulse response data. As the method uses the time-domain version of

system response data, in form of the Impulse Response Function, its application is limited to models incorporating viscous damping only. This is because hysteretic damping model presents difficulties for a time-domain analysis. A set of impulse response data is normally obtained by applying the Inverse FFT to a set of FRF measurements, as shown in (Figure 3.1).

Figure 3.9 shows the analytical expression used by CE curve-fitting. Also pointed out in Figure 3.9 is the leakage (wrap around error) caused by the inverse FFT, which distorts the impulse response data. This portion of the data cannot be used because of this error.

RFP method applies the rational fraction polynomial expression shown in Figure 3.10 directly to an FRF measurement. Its advantage is that it can be applied over any frequency range of data, and particularly in the vicinity of a resonance peak.

Rational Fraction Polynomial Method

Rational Fraction Form

$$H(\omega) = \left. \frac{\sum_{k=0}^{m} a_k s^k}{\sum_{k=0}^{m} b_k s^k} \right|_{s=j\omega}$$

Partial Fraction Form

$$H(\omega) = \left. \sum_{k=1}^{n/2} \left[\frac{r_k}{s - p_k} + \frac{r_k^*}{s - p_k^*} \right] \right|_{s=j\omega}$$

$p_k = k^{th}$ pole

r_k = residue for k^{th} pole

Figure 3.10. Alternate curve-fitting forms of the FRF [71]

Most other MDOF methods require that additional computational modes are used in order to compensate for the residual effects of out-of-band modes in the curve fitting frequency band. With some methods, these computational modes can often cause the

parameter estimates of the modes of interest to be in large error if the right number of computational modes is not used. Choosing the right number of computational modes can be a trial and error process. The RFP method, on the other hand, allows the use of additional numerator polynomial terms as a means of compensating for the effects of out-of-band modes. The use of these extra terms still permits the accurate estimation of the modal parameters of interest, and is, in general, a more fail-safe means of compensation than the use of computational modes [71].

3.3.3.3 Global and Multi-Reference methods

In local curve fitting methods natural frequencies and damping factors are performed on each of the individual FRF, however to obtain mode shape information a further stage of processing is required. Mode shapes are calculated through a combination of the individual eigenvector elements as modal constants. To anticipate this further stage of processing recent curve-fitting procedures capable of performing a multi-curve fit instead of working with individual curves, have been elaborated. In other words, they fit several FRF curves simultaneously, taking due account of the fact that the properties of all the individual curves are related by being from the same structure. A way in which a set of measurement FRF curves may be used collectively, rather than individually, is by the construction of a single composite FRF by adding several FRFs. Hence, from Eq. (3.9) it derives:

$$\sum_i \sum_k \alpha_{ik}(\omega) = \sum_{r=1}^{N} \frac{\psi_{ir}\psi_{kr}}{(\omega_r^2 - \omega^2 + j\eta_r\omega_r^2)} \tag{3.10}$$

These techniques are referred as Global and Multi-Reference methods. Both time domain (RFP) and frequency domain (CE) methods are amenable to the expansion to multi-curve analysis.

3.4 The design of a half-wavelength bar horn

Vibration theory, FEA and EMA are now applied to the design of the longitudinally resonant cylindrical bar horn shown in Figure 3.11. Ultrasonic systems often employ tuned bar horns which either operate as working tools or transmit vibrations to other tuned components.

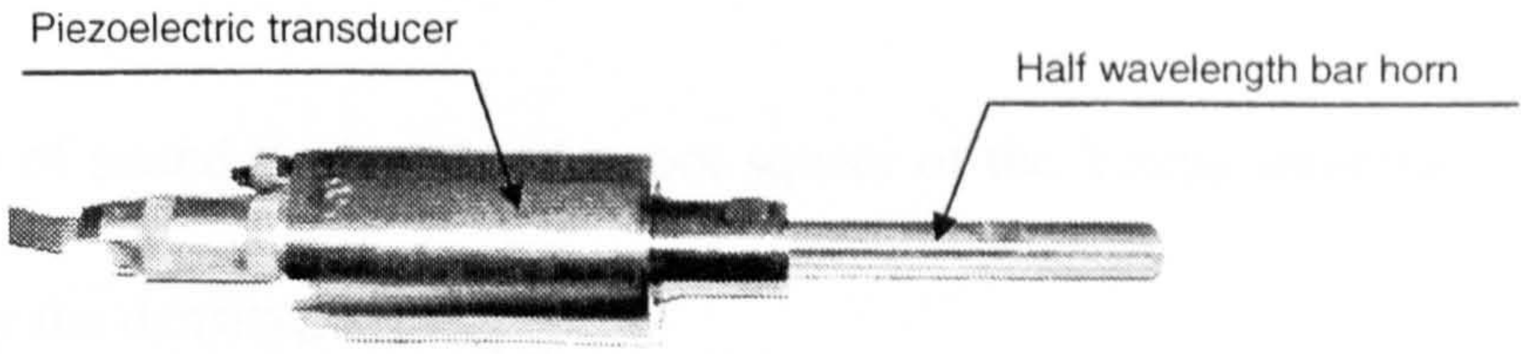

Figure 3.11. Half-wavelength bar horn screwed into transducer

In the design of ultrasonic systems it is usual procedure, firstly, to calculate the modal parameters of the vibrating components via FE modelling, and subsequently, to perform an EMA in order to confirm the predictions. However, the design of units with basic geometries can rely on mathematical formulas.

The requirements for the bar horn design are such that it responds in the first longitudinal mode of vibration at 35 kHz excitation frequency, and the used material is aluminium.

3.4.1 Calculation of the tuned length

The calculation of the tuned length and axial stress distribution of a cylindrical bar horn of unspecified tuned frequency and material is now derived [16]. Assuming free boundary conditions, isotropic material and no internal losses, the equation of motion for longitudinal waves propagating in the longitudinal direction is:

$$\frac{\partial^2 u}{\partial t^2} = (SV)^2 \frac{\partial^2 u}{\partial x^2} \tag{3.11}$$

where SV is the velocity of sound in the material and u is the displacement in the x (longitudinal) direction. The solution of Eq. (3.11) is of the type:

$$u = (A_1 e^{-jkx} + A_2 e^{+jkx}) e^{j\omega t} - u(x) e^{+j\omega t} \tag{3.12}$$

where A_1 and A_2 are constants, ω is the angular frequency of the vibrations and k is the wave number

$$k = \frac{\omega}{SV} \tag{3.13}$$

where the velocity of sound is given by the root square of the Young modulus of the material divided by the density, $SV = \sqrt{\frac{E}{\rho}}$.

Considering only the time-independent solution of Eq. (3.12), and given stress-free boundary conditions at the bar ends:

$$\frac{du(x)}{dx}\Big|_{x=0} = 0$$

$$\frac{du(x)}{dx}\Big|_{x=l} = 0 \tag{3.14}$$

the displacement function results:

$$u = u_o \cos(kx) \tag{3.15}$$

where u_o is the maximum displacement at the ends. Combining Eq. (3.13) and (3.15) the tuned length of the horn results:

$$kl = \pi \text{ or } l = \frac{\pi}{k} = \frac{\pi c}{\omega} = \frac{SV}{2f} \tag{3.16}$$

where $\omega = 2\pi f$.

Eq. (3.16) is valid for diameter (D) length ratios such that $D/l \leq 1$. Hence, substituting the tuned frequency value, $f = 35$ kHz, and the velocity of sound in aluminium, $SV \cong 5600$ m/s, in Eq. (3.16), it results $l = 80$ mm. Where l is the tuned length of the cylindrical bar horn resonating in the first longitudinal mode.

The stress associated with the longitudinal wave propagating in the horn can also be derived. The longitudinal stress distribution is related to the strain as shown in the well-known equation below:

$$\sigma(x) = -E\varepsilon(x) = E\frac{du(x)}{dx} \tag{3.17}$$

Using $SV = \sqrt{\frac{E}{\rho}}$ where ρ is the specific mass of the resonator material, the stress equation results as follows:

$$\sigma(x) = -\omega\rho c u_0 \sin(kx)\,. \tag{3.18}$$

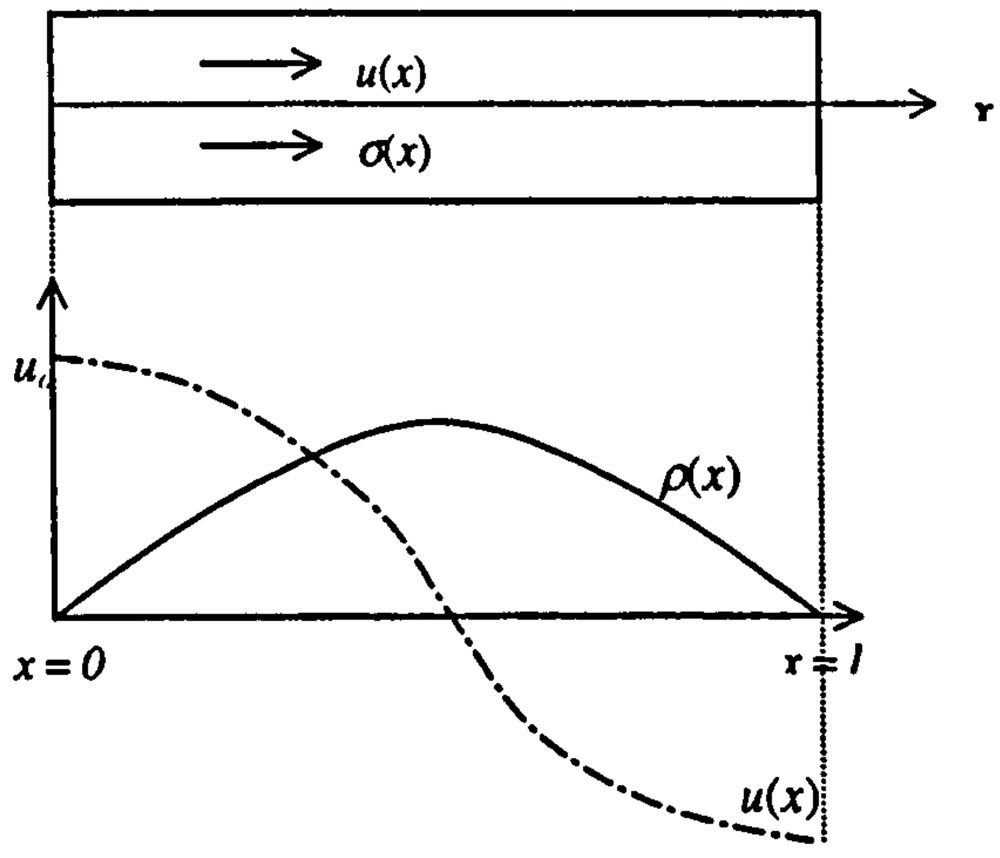

Figure 3.12. Displacement and stress distributions in the longitudinal mode

Figure 3.12 shows the stress and displacement distribution along the cylindrical horn axis derived from Eq. (3.16) and (3.18).

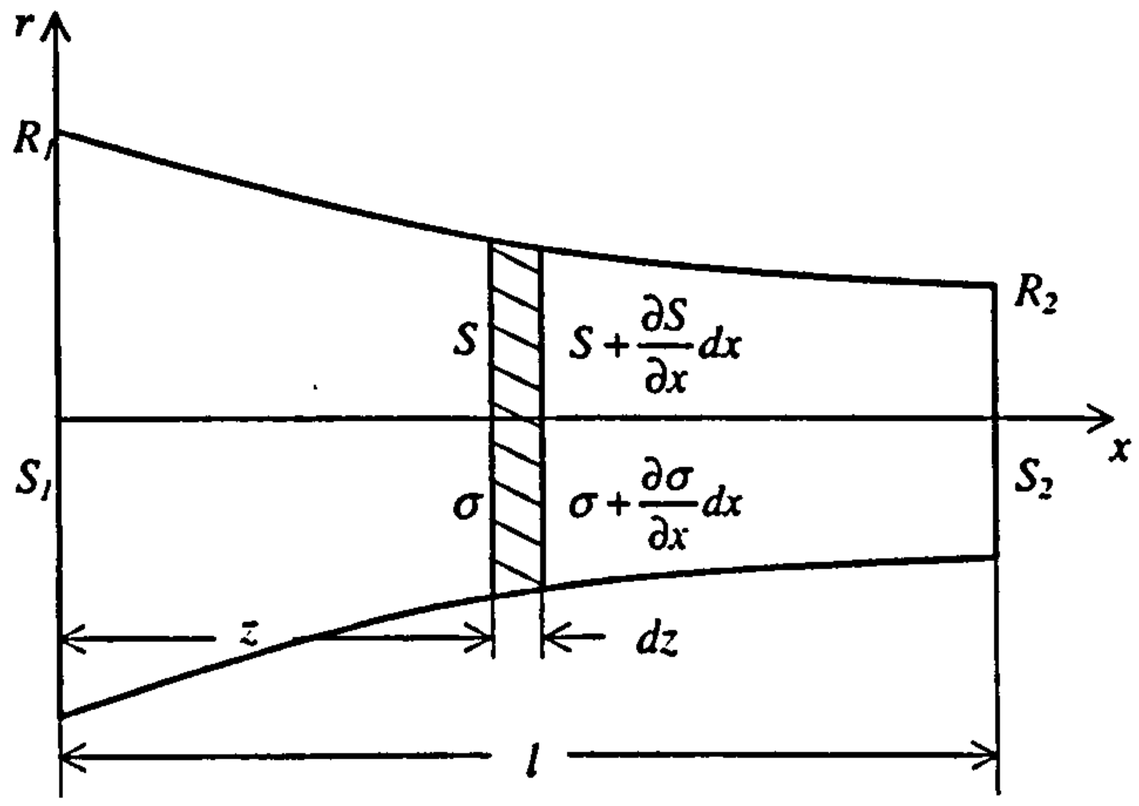

Figure 3.13. Tapered concentrator [12]

Analytical solutions for the design of bar-type resonators characterised by variable cross sections, producing amplitude gains towards the smaller face, can also be derived [12-15].

For the sake of completeness, the equations for calculating the tuned lengths of concentrators in longitudinal half-wave resonance in the form of conical, exponential, and catenoidal horns are now provided.

Calculations are conducted using the annotations in the literature [12]. The equation of motion of the highlighted layer of the generally tapered resonator shown in Figure 3.13 is:

$$\rho S dx \frac{\partial^2 u}{\partial t^2} = \frac{\partial \sigma}{\partial x} S dx + \frac{\partial S}{\partial x} \sigma dx \tag{3.19}$$

The boundary conditions for no external load are assumed:

$$\left.\frac{du(x)}{dx}\right|_{x=0} = 0 \qquad \left.\frac{du(x)}{dx}\right|_{x=l} = 0 \tag{3.20}$$

After substituting the expressions of the cross section variations along the axis of each considered horn profile, the tuned lengths of the three concentrators result:

for half-wavelength conical horn $$l = \frac{\lambda}{2}\frac{kl}{\pi} \tag{3.21}$$

for half-wavelength exponential horn $$l = \frac{\lambda}{2}\sqrt{\frac{(\pi)^2 + \ln^2(R_1/R_2)}{\pi^2}} \tag{3.22}$$

for half-wavelength catenoidal horn $$l = \frac{\lambda}{2}\sqrt{\frac{(\sqrt{k^2 - \gamma^2}\cdot l)^2 + (Arch(R_1/R_2))^2}{\pi^2}} \tag{3.23}$$

Where $\lambda = \frac{c}{f}\sqrt{\frac{E}{\rho}}$ is the length of the longitudinal wave travelling in a horn with

constant section. Figure 3.14 shows the stress and displacement distributions derived for the modelled concentrator profiles.

From the point of view of achieving large values of amplitude gains, for a given ratio between the input and output radius, the catenoidal concentrator offers a more beneficial solution compared with the other profiles. However, higher stresses arise in such concentrator configuration, which can be responsible for component fatigue failure. Amplitude gain and tolerable stress are the principal factors to account for at the design stage of ultrasonic components.

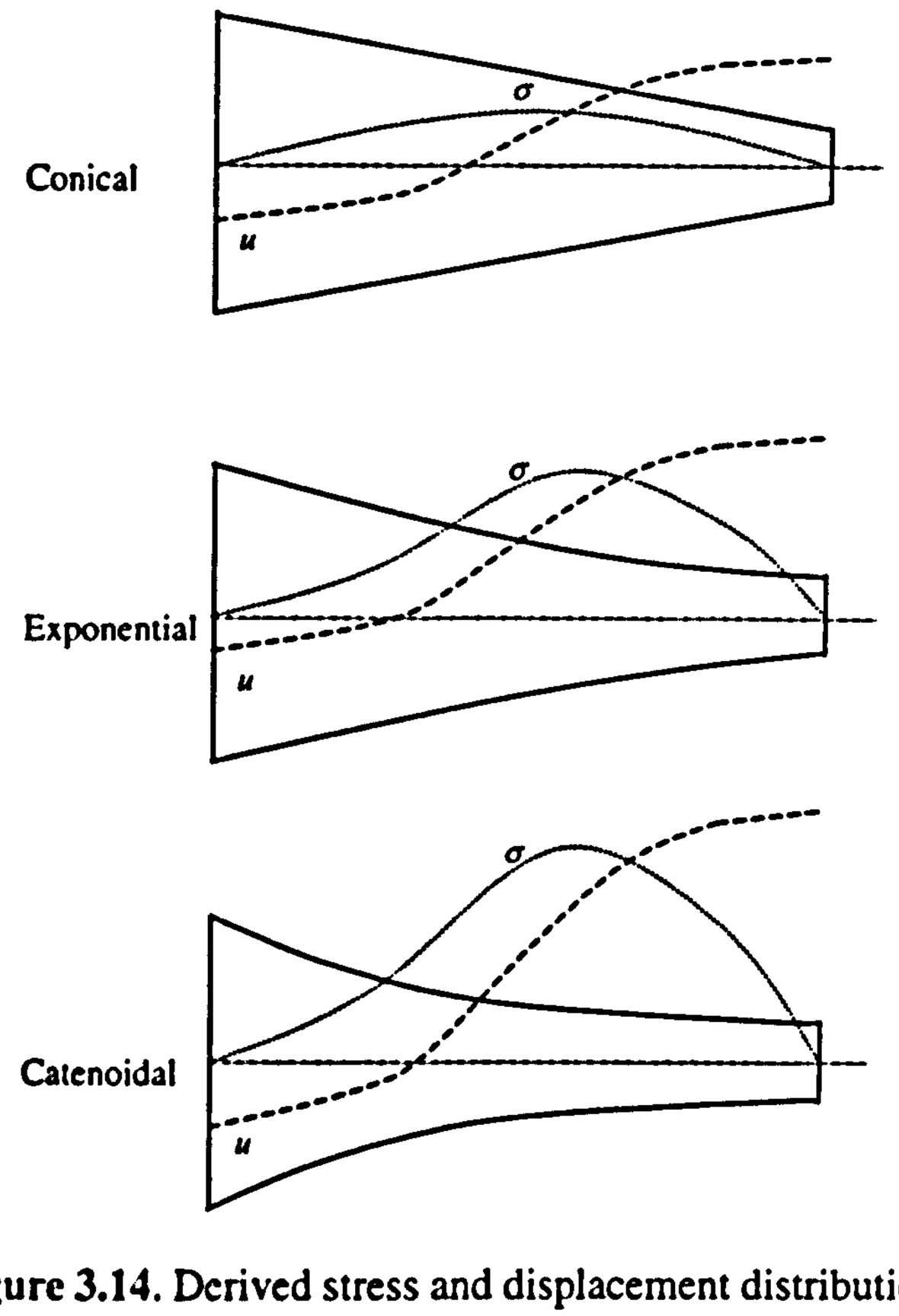

Figure 3.14. Derived stress and displacement distributions

3.4.2 The FE model

FEA is a computer-based methodology used to model static and dynamic behaviour of solids and fluids. Nowadays FEA is regularly performed to determine the vibration characteristics of ultrasonic systems and assembly prior to machining. The FE model is composed of many small elements, each of these mathematically described by a set

of equations. In vibration analysis, the solution to this set of equations allows prediction of the resonator's natural frequencies, mode shapes and associated stresses. The main steps for the FE modelling of the half-wavelength bar horn are now described. The FEA program used for this simulation is ABAQUS which interfaces with PATRAN, a CAD-like pre-processor that aid in constructing the model geometry and the mesh. Displacements or any other degree of freedom are directly calculated at the intersections of each element called nodes. At any other point in the element, the displacements are obtained by interpolating from the nodal displacements. The elements must be sufficiently small that the solutions for the natural frequencies converge. 20-noded brick (Hex20) and 15-noded wedge (Wed15) elements are used in the simulations carried out in this thesis.

First, the geometry of the cylindrical bar horn is defined using the tuned length determined by solving Eq. (3.16). Then, small elements describing the horn geometry are created. The required number of elements is determined through a study of convergence of modal frequencies. Figure 3.15 illustrates the frequencies of three bar horn modes predicted against the number of elements meshed along the axis of the bar horn. The first longitudinal, first bending and first torsional modes have been chosen as they are members of the three modal families excitable in the bar horn. The incorporation of a minimum of six elements along the horn axis is predicted to guarantee convergence of the considered natural frequencies. In particular, the predicted longitudinal mode frequency occurs at 34.9 kHz, proving that Eq. (3.16) provides a good estimate of the tuned length. Further, Figure 3.16 shows that the frequency of the modes characterised by bending and torsional motions are also dependent on the elements meshed around the horn circumference. Again at least six elements along the circumference are required to guarantee frequency convergence. The bar horn, being symmetric about the axis, could be modelled with a 2D mesh. However, while modelling only a 2D section of the resonator will save modelling and computing time, it also limits the FEA results, since asymmetric modes may not be extracted. Hence, a limited FEA model that precludes these modes can lead to unexpected problems when machined. Therefore, a 3D bar horn incorporating 224 elements (14 in the axial direction, 8 along the circumference and 2 radial) is modelled (Figure 3.17). A lower number of elements would assure convergence of the natural frequencies at the expense of mode shape definition.

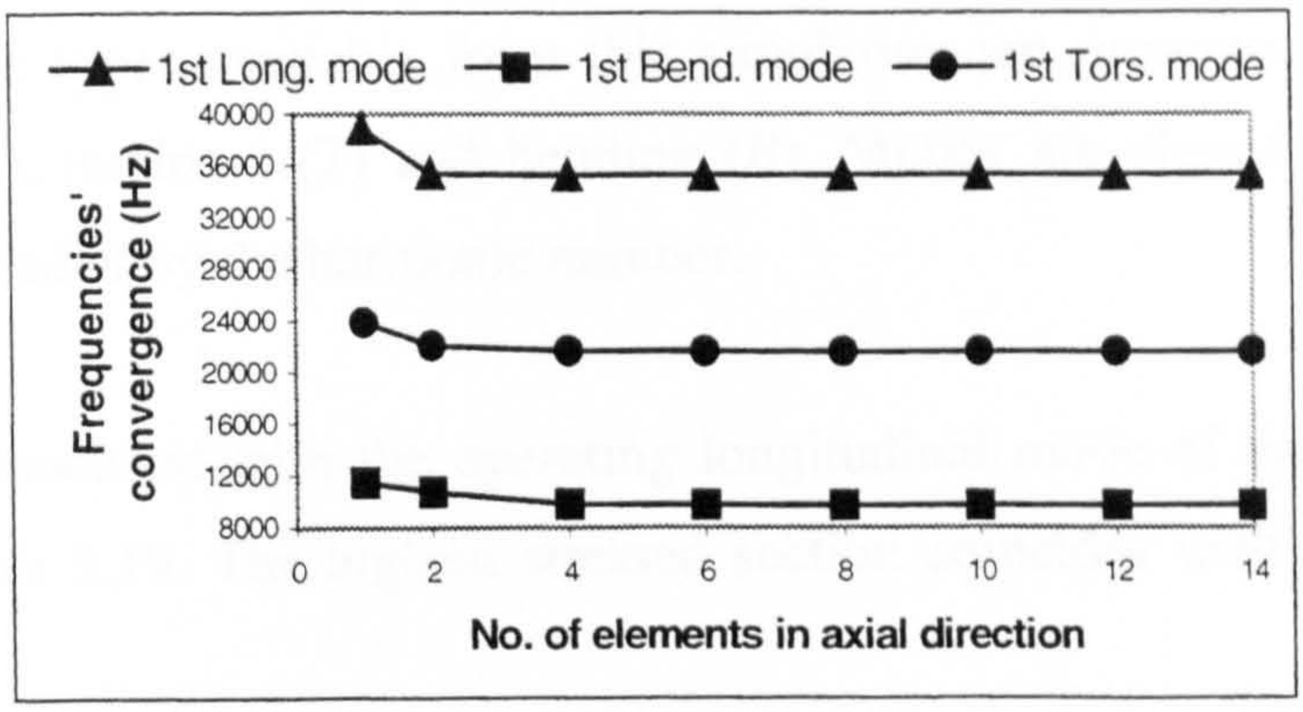

Figure 3.15. Mesh convergence in axial direction

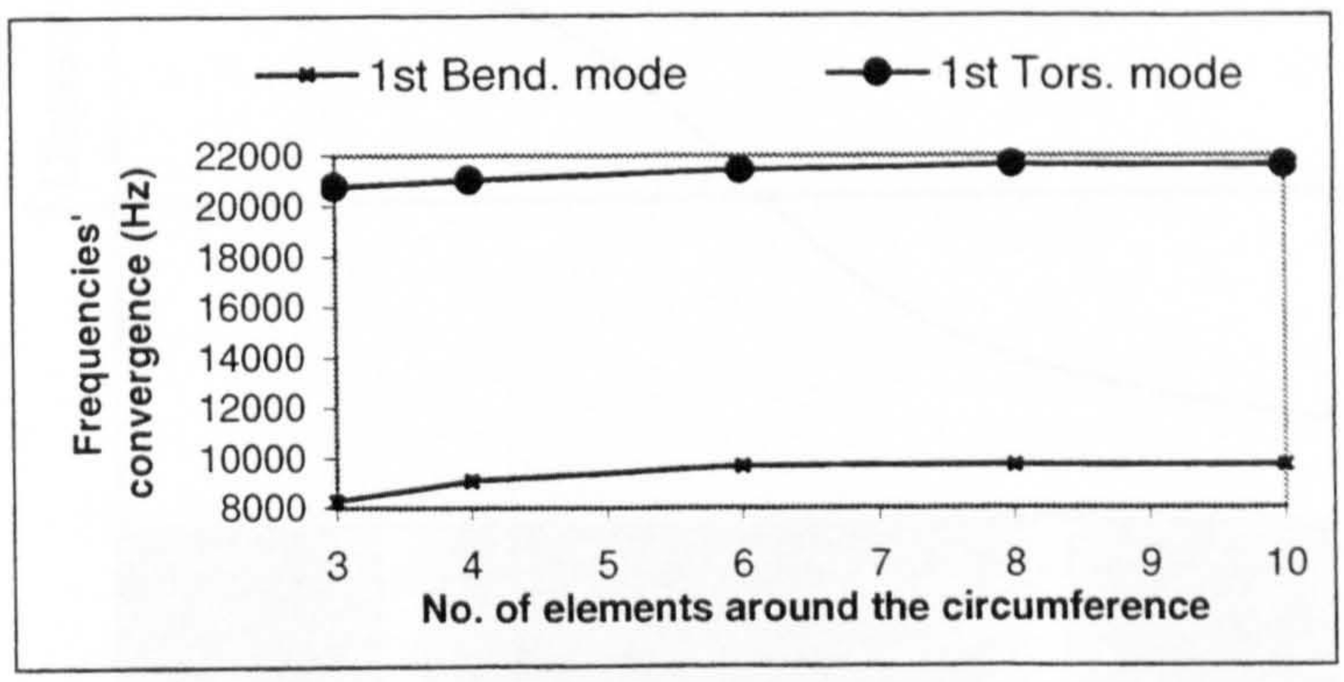

Figure 3.16. Mesh convergence around the circumference

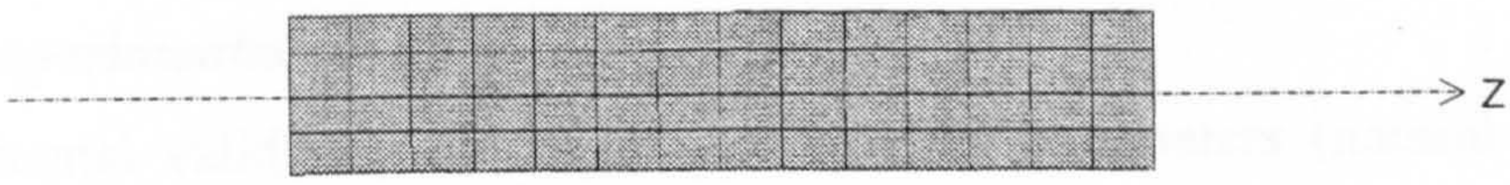

Figure 3.17. Bar horn FE model

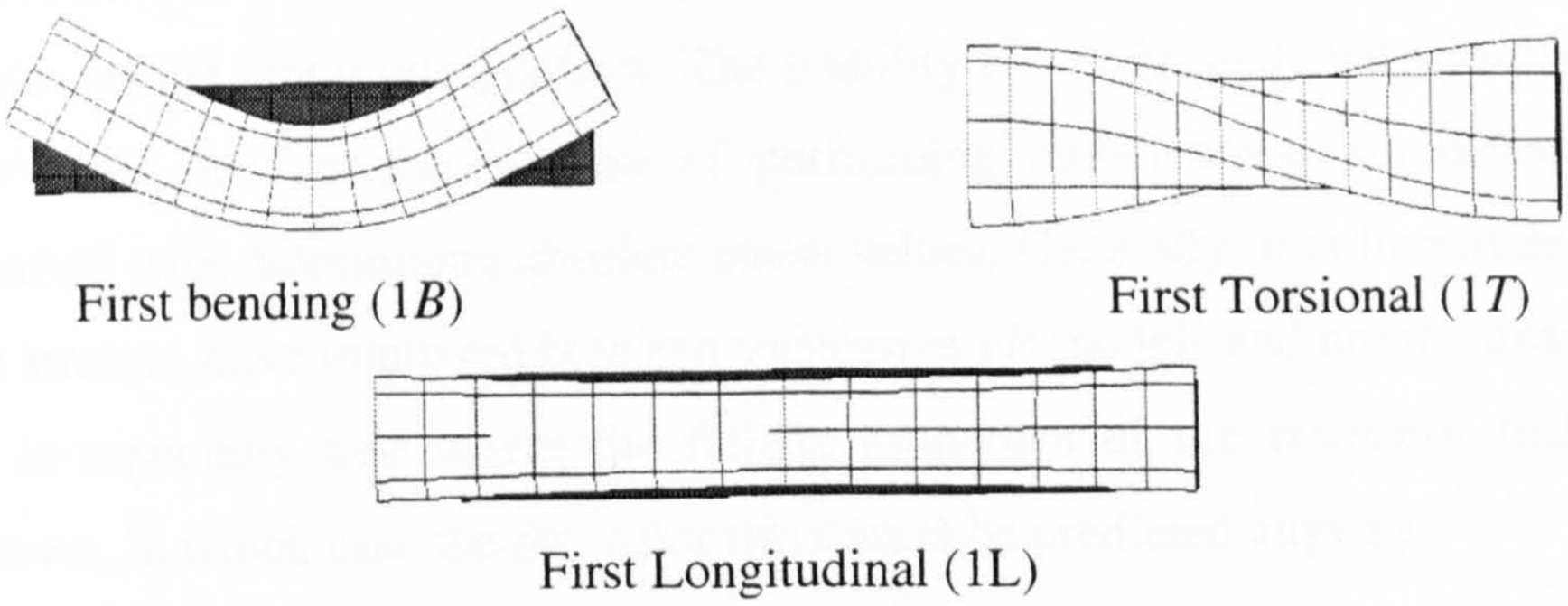

Figure 3.18. Mode classification by FE model of the bar horn

The three mode types available from this simulation are presented in Figure 3.18: longitudinal (L), torsional (T) and bending (B). Modes are classified by the above descriptors preceded by the harmonic number.

The stresses associated with the operating longitudinal mode of the horn model are shown in Figure 3.19. The highest stressed section coincides with the displacement node.

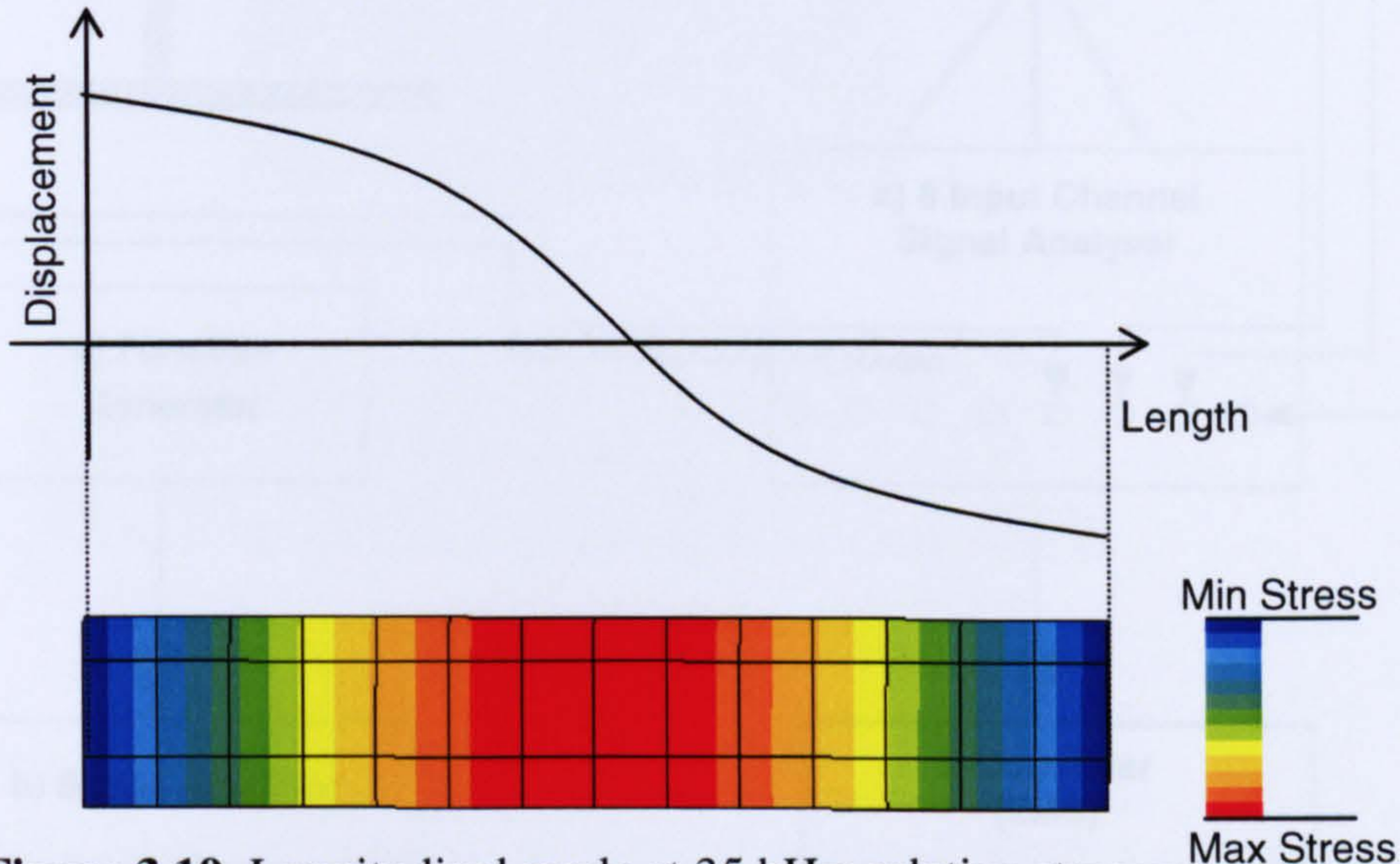

Figure 3.19. Longitudinal mode at 35 kHz: relative stresses

3.4.3 The experimental set-up

An experimental validation of the predicted modal parameters (natural frequencies and mode shapes) is now required to assess the accuracy of FE model. Since empirical stress data is usually not available, stress cannot be directly validated. However, the FE stresses will not be correct if the predicted mode shapes are not validated, as stress depends on the amplitude gradient. The inability to verify predicted stresses is not a major issue, in fact the purpose of performing model stress simulations is not concerned with determining absolute stress values. Generally, it is important to know if the stresses have improved between successive FE models and not the exact values. This is especially true where the fatigue properties of the resonator material are unknown, in which case the resonator life cannot be predicted anyway.

Figure 3.20 shows the experimental configuration used for the modal testing of the investigated aluminium bar horn manufactured in accordance with the FE model

dimensions. A function generator connected to a power amplifier drives the piezoelectric transducer connected to the bar horn.

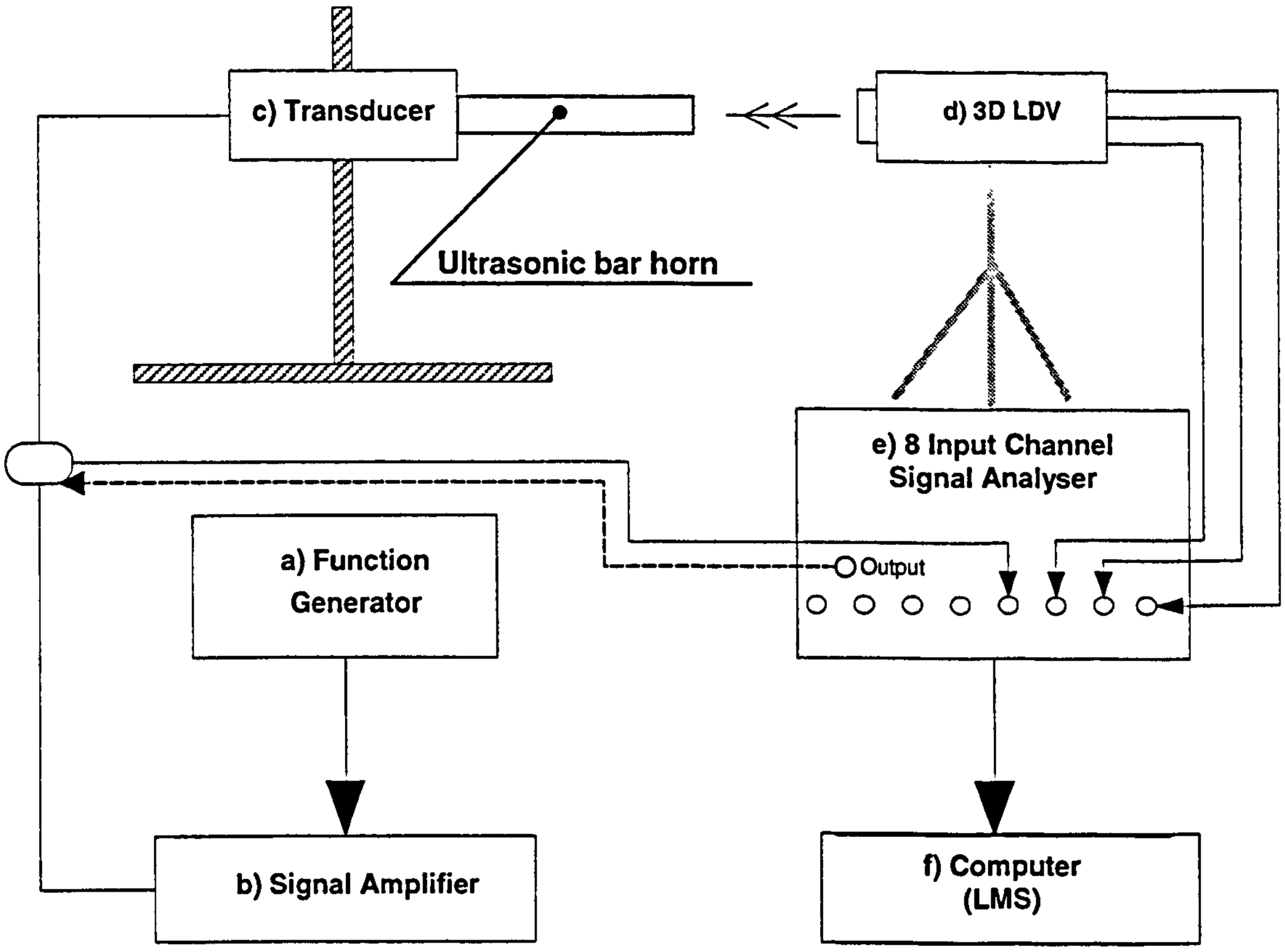

Figure 3.20. Experimental set-up for EMA

The responses of the ultrasonic systems are then measured in the Cartesian x, y and z coordinates by means of a 3D laser Doppler vibrometer (Polytec 3D LDV), allowing both in-plane and out-of-plane responses to be measured. Finally, a multi-channel data acquisition analyser connected to a portable computer, enables calculation of the FRFs from the identification of the excitation signal and responses, and via signal processing software.

3.4.3.1 Function generator and amplifier

The signal to excite the ultrasonic bar horn is in the form of a sine wave provided by the function generator (TTi TG550), shown in Figure 3.21(a). Fast sweeps of the excitation frequency over a 0–45 kHz range are performed. The TTi TG 550 is a precision 5 MHz function generator capable of generating waveforms of sine, triangle,

ramp, pulse and DC. The frequency range is 0.005 Hz to 5 MHz selected by a seven decade range multiplier and calibrated vernier. The generator output level is 20 V pk-pk. Internal sweep rates of the excitation frequency are adjustable from typically 20 ms to 20s. The excitation signal is amplified by the LDS PA 25E amplifier illustrated in Figure 3.21(b), which exhibits a harmonic distortion below 0.3%.

(a)

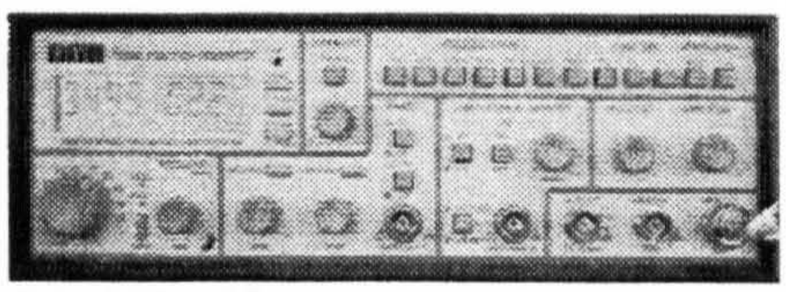

(b)

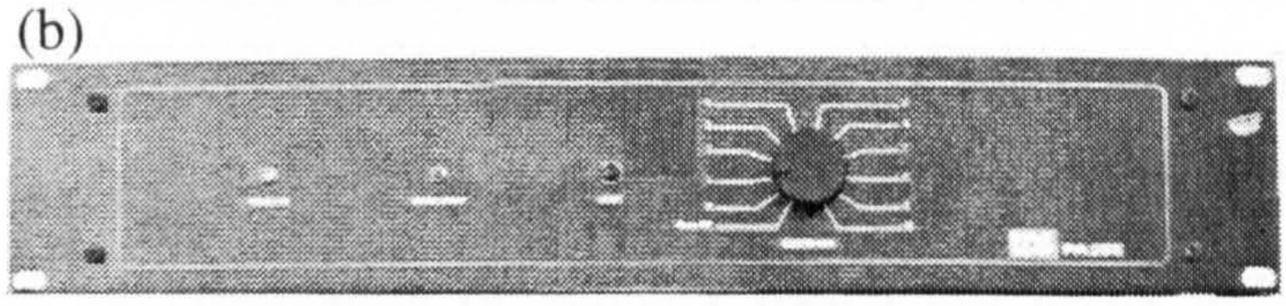

Figure 3.21. (a) Signal generator, (b) amplifier

3.4.3.2 Piezoelectric transducer

Ultrasonic transducers convert electrical power to mechanical vibrations by means of internal piezoelectric ceramics (PZT). PZTs are chemically inert materials, which have the characteristic of deforming when exposed to an electric field. In particular, if a piezoelectric ceramic element is exposed to an alternating electric field changes dimensions cyclically, at the frequency of the field.

Most high intensity ultrasound applications, such as ultrasonic cutting, require half-wave length longitudinal transducers with resonant frequencies between 20 kHz and 60 kHz. Figure 3.22 (a) shows a commercial 35 kHz longitudinal mode transducer (Martin Walter: MW 800) which is connected to the bar horn via a threaded stud. A schematic of the transducer and its internal elements is shown in Figure 3.22 (b). Piezoelectric ceramic disks (1) constitute the core of the transducer. Electrodes (2) are used on both sides of each ceramic disk to apply the alternating voltage which causes it to expand and compress along the axis of the transducer. Several disks are used to increase the movement generated. Using an even number of disks ensures that high voltage is applied only within the stack and both ends can be at zero volts. The ceramic disks are clamped together through the centre of the transducer by a clamping

bolt (3). To prevent them from cracking they should be kept under compressive stress even when the transducer is stretched to its maximum.

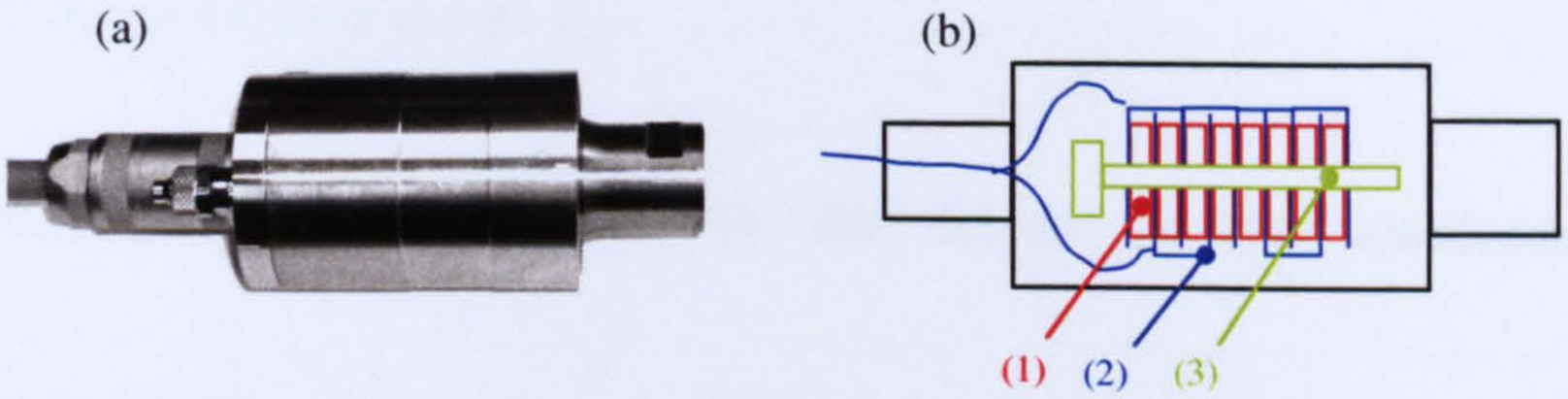

Figure 3.22. (a) Piezoelectric Transducer (MW 800), (b) composition of the transducer

3.4.3.3 3D laser Doppler vibrometer

Laser Doppler vibrometers (LDV) are based on the principle of the detection of the Doppler shift of coherent laser light scattered from a small area of the test object. The object scatters or reflects light from the laser beam and the Doppler frequency shift is used to measure the component of velocity which lies along the axis of the laser beam.

As the laser light has a very high frequency $\underline{W}$ (approx. 4.74 x10^{14} Hz), a direct demodulation of the light is not possible. An optical interferometer is therefore used to mix the scattered light coherently with a reference beam. The photo detector measures the intensity of the mixed light whose frequency is equal to the difference frequency between the reference and the measurement beam. Such an arrangement is shown in Figure 3.23.

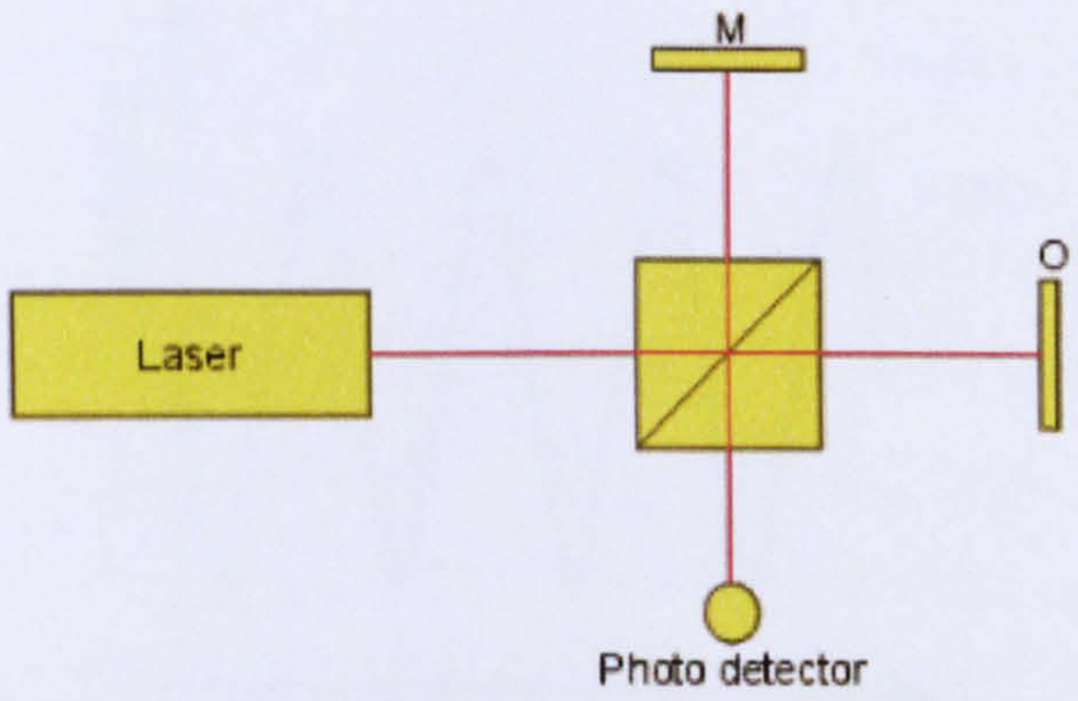

Figure 3.23. Schematic of a Michelson interferometer [Polytec]

A laser beam is divided at a beam splitter into a measurement beam and a reference beam which propagates in the arms of the interferometer. The distances the light travels between the beam splitter and each reflector are x_R and x_M for the reference mirror M and object O respectively.

The corresponding optical phase of the beams in the interferometer is:

Reference $\phi_R = 2kx_R$

Measurement $\phi_M = 2kx_M$

with $k = 2\pi/\lambda_l$. One usually defines $\phi(t) = \phi_R - \phi_M$

The photo detector measures the time dependant intensity $I(t)$ at the point where the measurement and reference beams interfere.

$$I(t) = I_R I_M R_{ef} + 2K\sqrt{I_R I_M R_{ef}}\cos(2\pi f_0 t + \phi)$$

Where I_R and I_M are the intensities of the reference and measurement beams, K is a mixing efficiency coefficient and R_{ef} is the effective reflectivity of the surface.

The phase $\phi = 4\pi\Delta L / l$ where ΔL is the vibrational displacement of the object and the wavelength of the laser light.

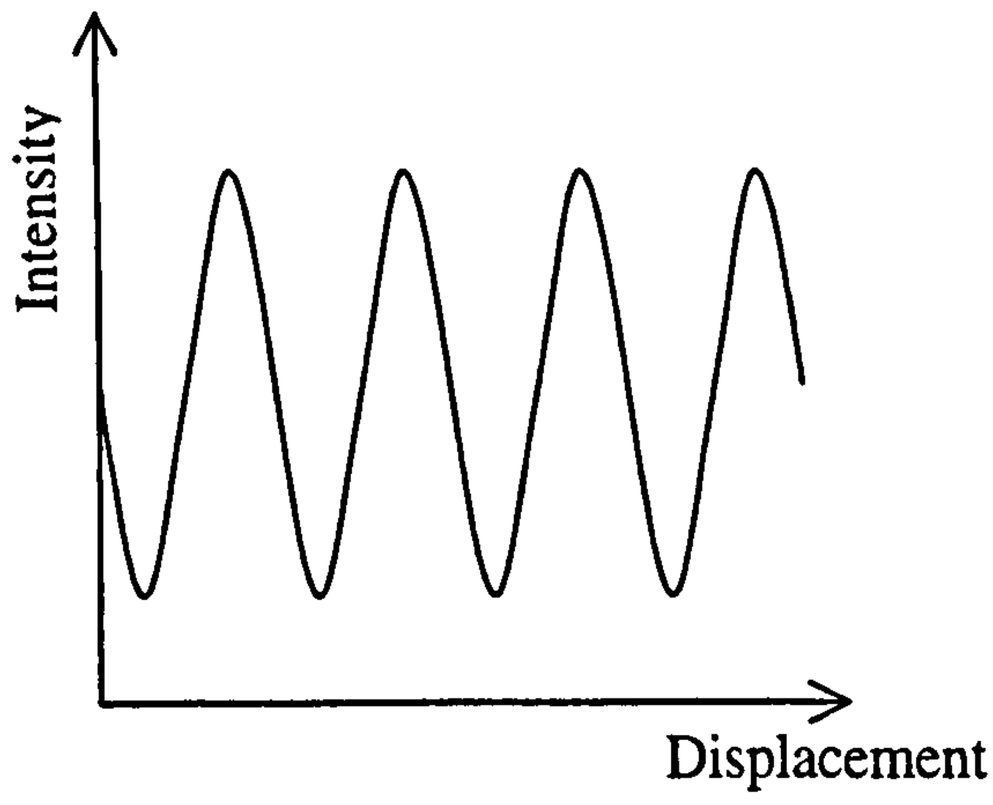

Figure 3.24. Light intensity

If ΔL changes continuously the light intensity $I(t)$ varies in a periodic manner as shown in Figure 3.24. A phase change ϕ of 2π corresponds to a displacement ΔL of l/2. The rate of change of phase ϕ is proportional to the rate of change of position which is the vibrational velocity V of the surface. This leads to the well known formula for the Doppler frequency, $f_D = 2\ V/\lambda_l$..

Due to the sinusoidal nature of the detector signal, the direction of the vibration is ambiguous. There are two ways to introduce a directional sensitivity:

- Introduction of an optical frequency shift into one arm of the interferometer to obtain a virtual velocity offset.
- Adding polarization components and an additional photo receiver in such a way, that at the interferometer output a second homodyne signal occurs being in quadrature to the primary photodetector output.

1D LDVs are commonly used to measure the out-of-plane component of the vibration velocity on the surface of ultrasonic units. The importance of mode shape characterisation is crucial in vibration analysis of ultrasonic systems. Hence, the detection of a single velocity component at each measurement point is not ideal, especially for investigating complex assemblies. A device able to measure in-plane as well as out-of-plane vibration velocities is therefore required.

In modal testing of the bar horn, a 3D LDV is used to perform non-contact measurements of the surface vibration velocity in three mutually orthogonal axes. The measurement apparatus shown in Figure 3.25 is a Polytec CLV-3D LDV. The system comprises a three-channel controller unit coupled to an optical sensor containing three independent optical systems, all focused to the same measurement point. The individual vibration components lying along the three respective laser beams are available as analogue outputs. Most importantly, a geometry-calculation module generates true V_x, V_y and V_z analogue outputs in real time, and can process vibration frequencies as high as 250 kHz. The optical sensor contains the optical components of three independent sensors. Each output laser beam is inclined at a 120° angle with respect to the surface, but from three slightly different directions. A 120° angle is small enough to allow the sensors to collect enough back-reflected light to make high-

quality measurement, but still large enough for good sensitivity to the in-plane vibration components.

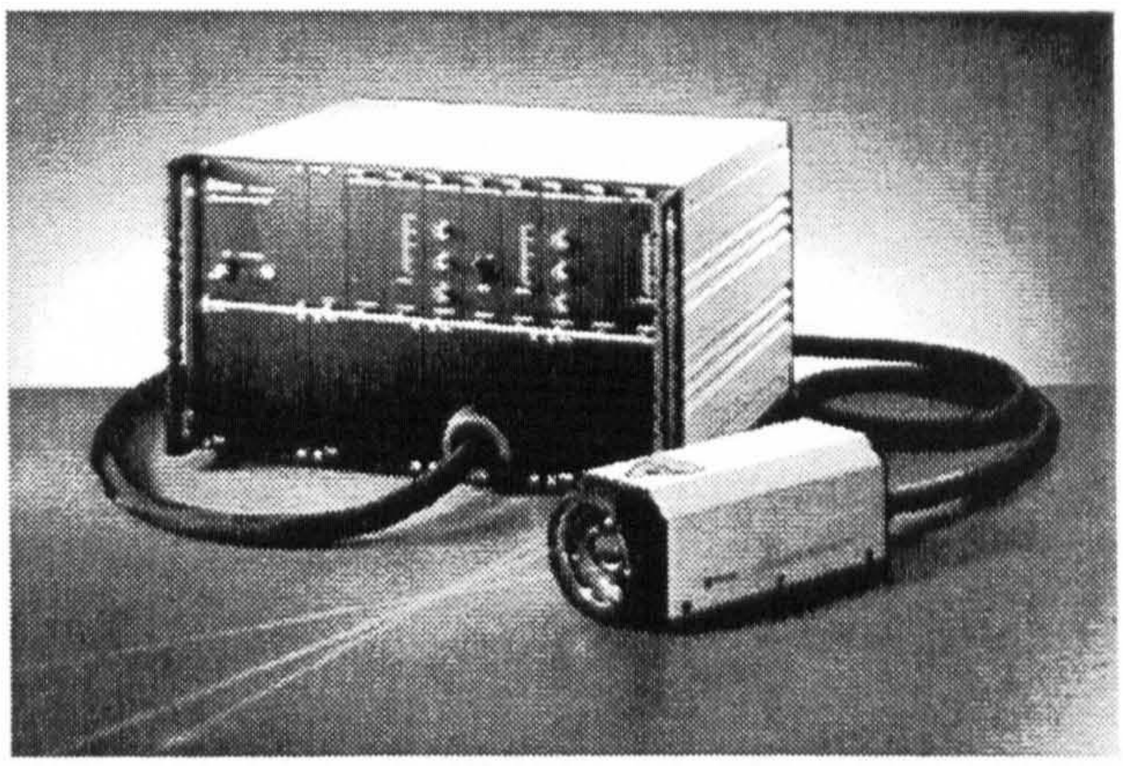

Figure 3.25. The Polytec CLV-3D laser vibrometer and a modular controller unit

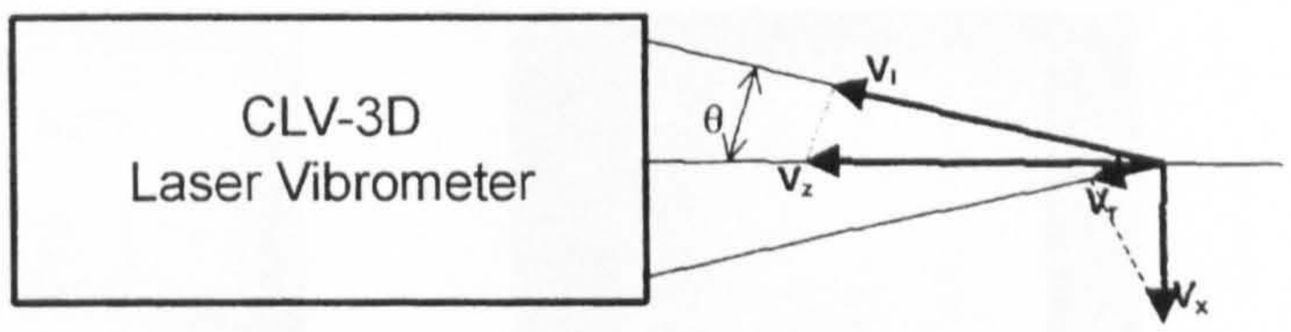

Figure 3.26. Top view of the probe beams and the coordinate system

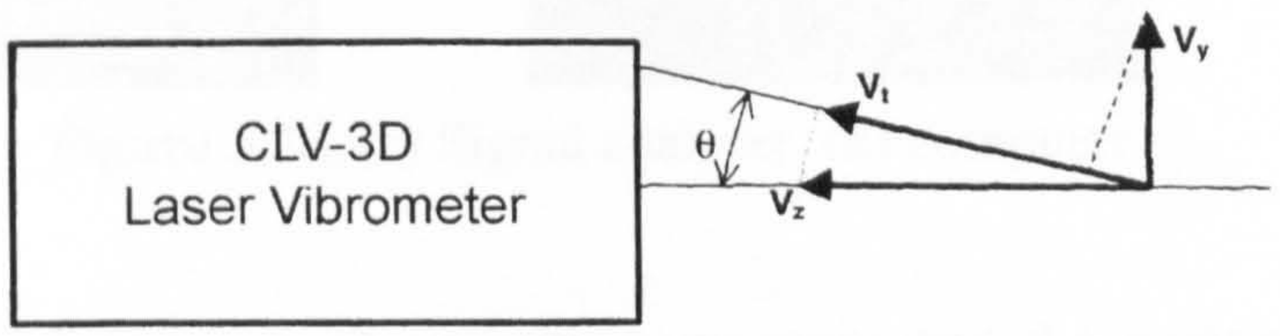

Figure 3.27. A side view of the sensor

Figure 3.26 and 3.27 show how the three beams converge into a measurement point. The CLV-3D sensor generates three laser beams: top, left and right, which measure components V_l, V_t and V_r respectively. When the sensor is pointed at a surface vibrating in three directions V_x, V_y and V_z, the true x- and z- components can be calculated using these relations with reference to Figure 3.26,

$$V_r = V_z \cos\theta + V_x \sin\theta \qquad \text{and} \qquad V_l = V_z \cos\theta + V_x \sin\theta$$

$$V_z = (V_r + V_l) / 2 \cos\theta \qquad \text{and} \qquad V_x = (V_r - V_l) / 2 \sin\theta$$

Similarly, viewing the sensor as in Figure 3.27, the true y-component is calculated using,

$$V_t = V_z \cos\theta + V_y \sin\theta$$

$$V_y = (V_t - V_z \cos\theta) / \sin\theta.$$

3.4.3.4 Multi-channel signal analyser

The measured signals (three-velocity responses and excitation force) are then collected and processed via FFT algorithm in the multi-channel signal analyser (SignalCalc 620) shown in Figure 3.28 (a).

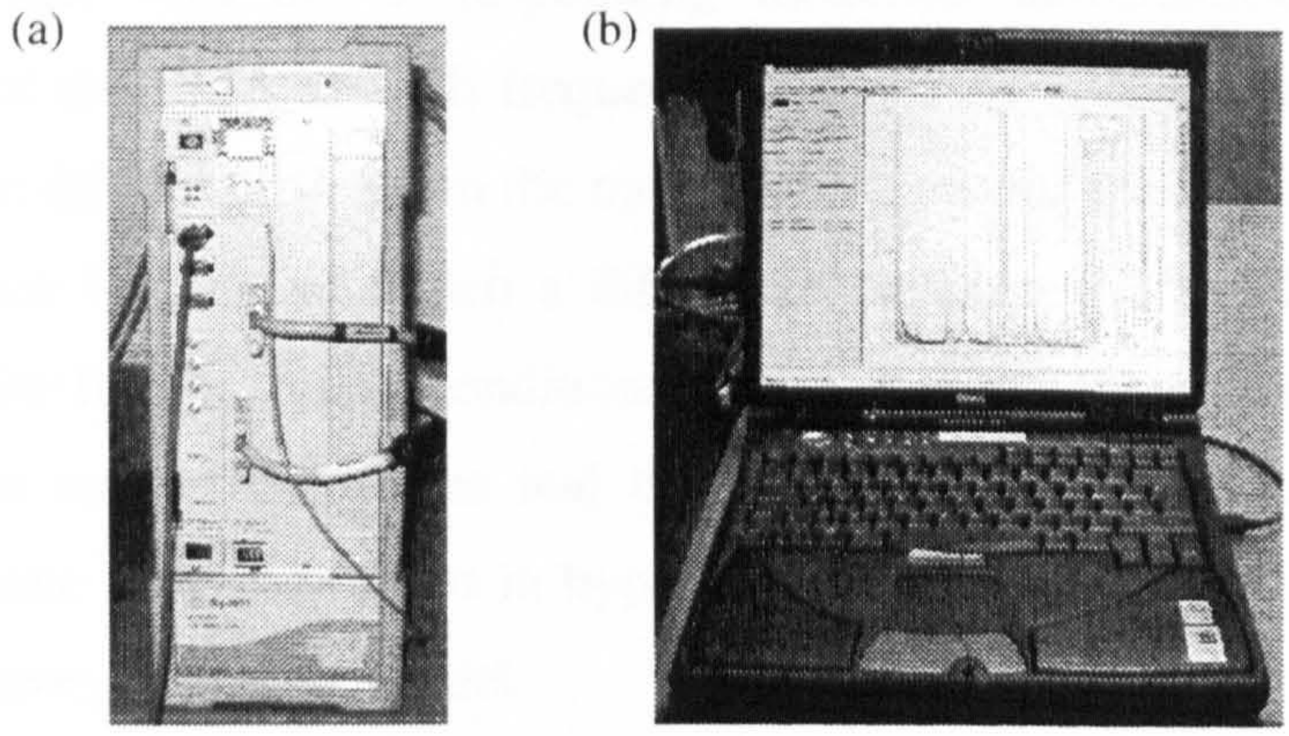

Figure 3.28. (a) Signal analyser, (b) computer

Transfer functions between each velocity component and the excitation force are available so that three FRFs (mobility) are provided for each measured point. The resolution adopted for the derivation of the FRFs from the raw signals measured on the horn surface is 12.5 Hz. 50 FRF averages are performed at each measurement point in order to eliminate disturbances. A Hanning window is also used to avoid the problem of leakage due to non-periodic signals.

3.4.3.5 Computer software

Measurements carried out on the bar horn, after being processed via SignalCalc 620, are curve-fitted in a modal analysis software (Star Modal) installed on a portable computer (Figure 3.28 (b)). Star Modal allows identification of modal parameters via

curve-fitting procedure including single DOF and multiple DOF time and frequency domain methods. The computer also constitutes the bench work from which all the operations are coordinated.

In the experimental investigations carried out in this thesis, another software for modal analysis, LMS, which interface with another brand multi-channel analyser, Scadas, has been used. LMS presents similar specifications to Star Modal with the main difference that it runs on a workstation. Also, in the tests performed with LMS the used signal is a random signal generated by the Scadas analyser, and not by the function generator.

3.4.4 Experimental validation by EMA

The measured mode shapes of the 1L mode and 1B mode shown in Figure 3.29 reveal good agreement with the corresponding modelled deformations (Fig. 3.18). A comparison of the EMA and FE frequency evaluations is presented in Table 3.1. A 4% maximum difference between the measured values and the FE values is estimated. A major factor because of which a difference between FE and EMA data occurs, stems from the free boundary conditions assumed in the FE simulation. Conversely, measurements are performed the real horn is fixed to the transducer. Also the FE predictions have been performed in hypothesis of elastic behaviour, however no real structure behaves as a linear model.

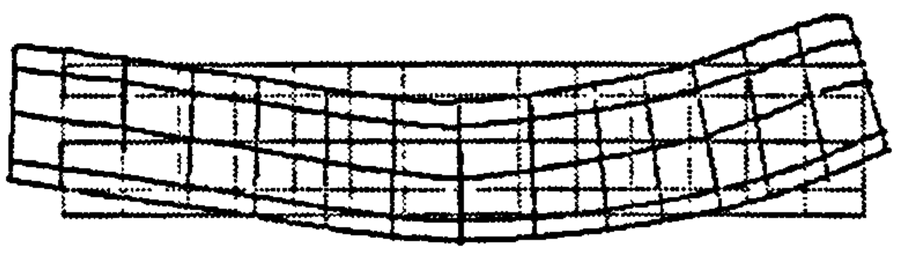

1B = 9923 Hz

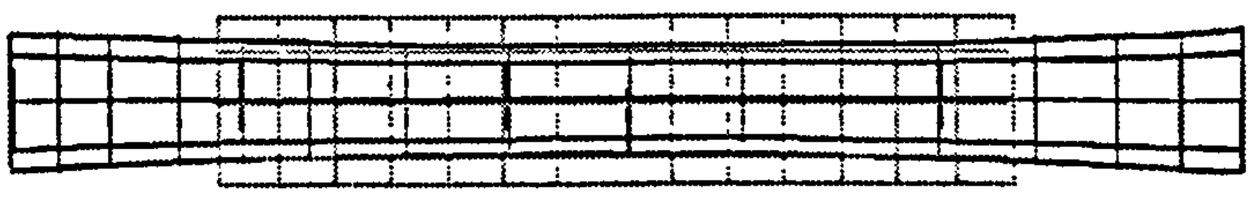

1L = 34932 Hz

Figure 3.29. Measured mode shapes

It can be seen that FEA predicts the existence of some modes of vibration which are not measured in the tested resonator. These are bending and torsional modal

frequencies. Although these modes exist, they are not easily excitable by a longitudinally resonant transducer and are, therefore difficult to detect by EMA.

	Blade Natural Frequencies (Hz)		
Mode	Finite Element Analysis (FEA)	Experimental Modal Analysis (EMA)	Error (%)
1B	9690	9923	-2.3
1T	21680	-	-
2B	24250	23971	1.1
1L	35290	34932	-1.0
3B	42610	-	-
2T	43360	45229	-4.1

Table 3.1. Bar horn mode frequencies in the range (0-45 kHz)

3.5 Conclusions

This chapter has presented the main concepts of EMA technique for vibration characterisation of structures. The main stages pertaining to modal testing: FRF measurement techniques and modal parameter estimation methods have been described.

To conclude, the vibration behaviour of a half-wavelength bar horn is characterised by EMA and FEA. A good correlation between the predictions and measurements of the modal parameters demonstrates that a combination of FE modelling and EMA constitutes a powerful tool in horn design.

CHAPTER 4

THE DESIGN OF ULTRASONIC CUTTING BLADES

4.1 Introduction

Cutting of food products with ultrasonically assisted tools has demonstrated significant benefits including reduced wastage and improved cut quality. Hence, tools for cutting of food products have largely been proposed in the last decade [2,5], where industries have sought to address the problems of blade stall and product waste associated with conventional cutting techniques. For successful operation and relative ease of tuning, many food slicers rely on integral tuned blades to achieve the required depth of cut.

Figure 4.1 shows a tool steel blade used in cutting food products tuned to the first longitudinal mode at 35 kHz. The cutting knife has to be thin and long enough to meet the depth cutting requirements of the product. A vibration amplitude of 60-70 μm at the blade tip has been found to be required to ensure an effective cutting operation. Since ultrasonic transducers are not capable of delivering such high amplitudes, amplitude gain is designed into ultrasonic blades by tapering of the their profiles. Depending on the depth of the material, half-wavelength or wavelength blades are employed.

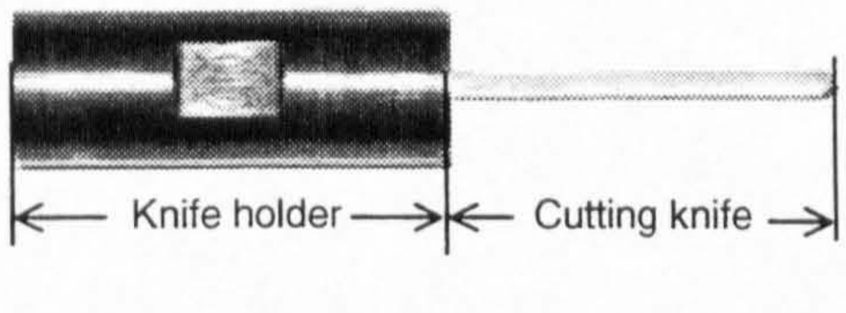

Figure 4.1. Half-wavelength ultrasonic blade

This chapter investigates the operation of a range of high power ultrasonic blades capable of cutting confectionary material in order to provide design strategies to

enhance system performance by reducing the effects of modal coupling and proposing component geometries which result in reduced stress levels. Blades with a gain between six and eight are examined. However, the outcomes of this study are useful in the design of cutting tools characterised by different amplitude gains.

4.2 Half-wavelength blades with built-in amplitude gain

Series of half-wavelength blades just like the one shown in Figure 4.1 are used to cut confectionary material on a production line, as illustrated in Figure 4.2. The tuned length of this blade type is 80 mm, and seven is the built-in amplitude gain factor. The tuned unit consists of a cutting knife, which length depends on the depth of the confectionary material, brazed on a cylindrical holder. Two symmetric arcs, whose chord length is equal to the cylinder diameter, define a 2 mm thick knife section (Figure 4.3). Hence, the material to be cut is compressed to such an extent as to enable it to pass through the blades. The blade dimensions are obtained via FE modelling. FEA allows fast calculations of blade tuned lengths which would otherwise result rather difficult to derive by solving analytically the partial differential equations of the profiles [12-15].

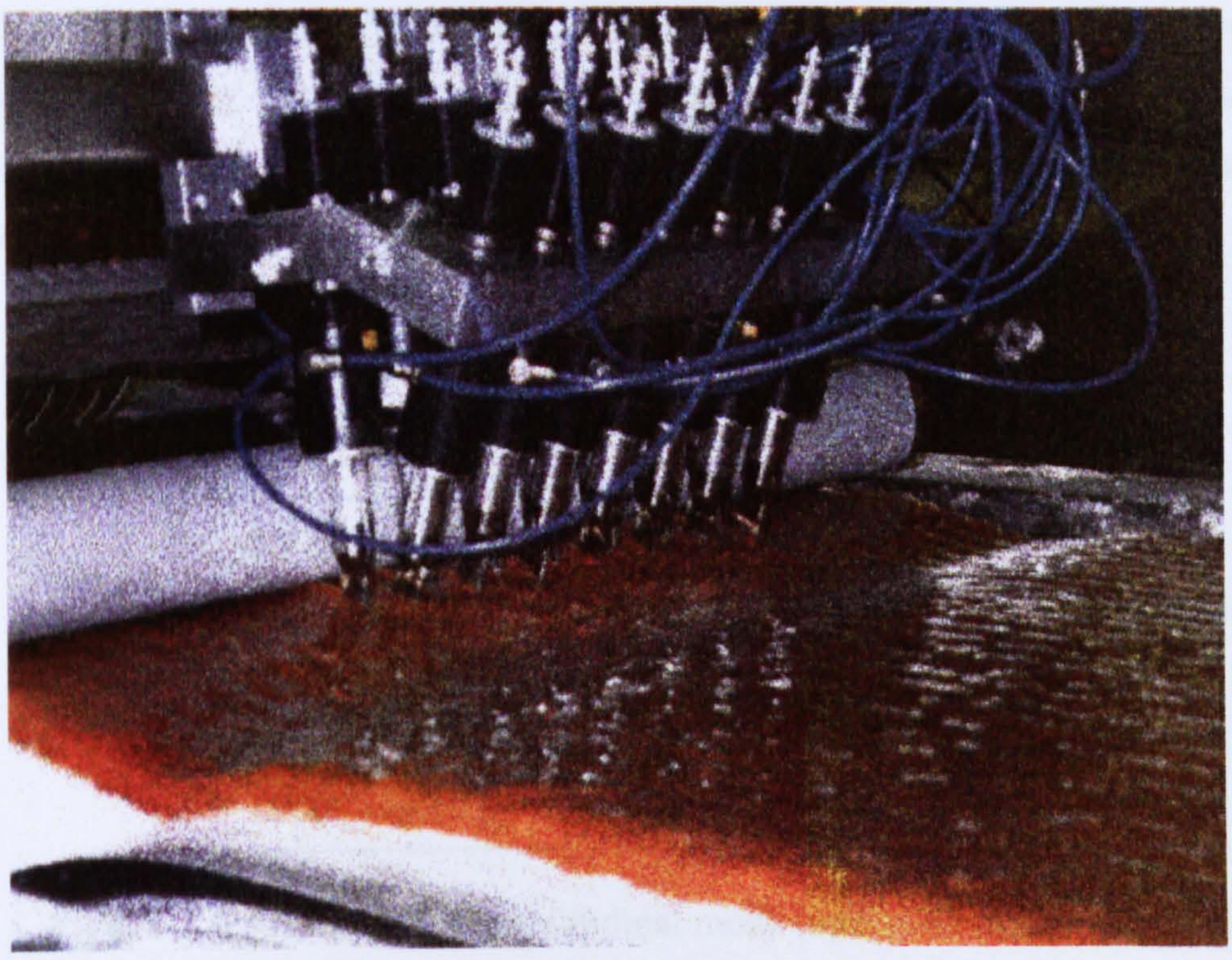

Figure 4.2. 15 blade cutting system [photo provided by Nestle' P.T.C., York, UK]

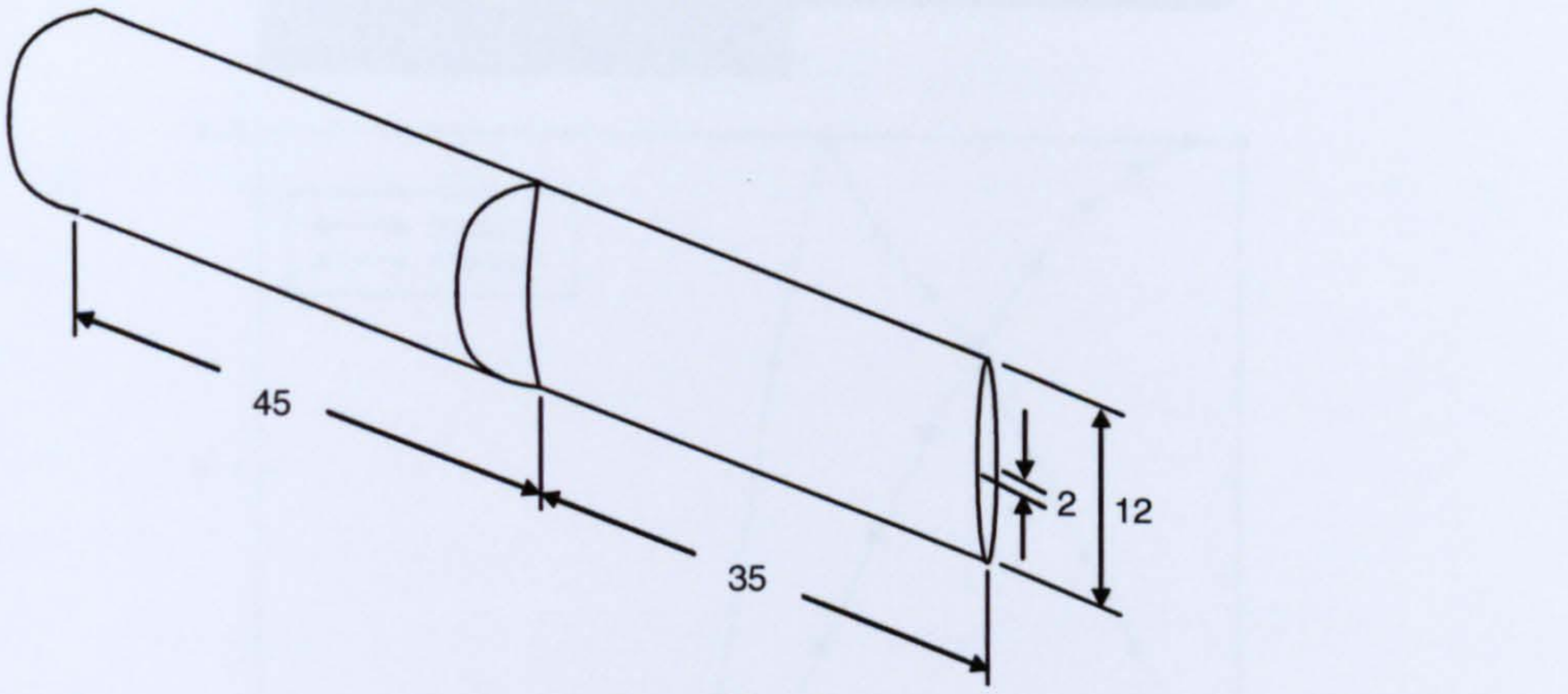

Figure 4.3. Blade dimensions

4.2.1 Stress distribution

Figure 4.4 shows the mode shape of the tuned longitudinal mode and the associated stress distribution, predicted by the blade FE model. As expected, maximum stress occurs at the section of transition from one diameter to the other, the step (or shoulder) which is the location of frequent failures. Great care must be taken when machining these parts, since any notch from damage or from poor design or machining in the nodal region will create stress raisers causing metal fatigue and almost guaranteed failure. Furthermore, the distributions of the normalised stress and displacement along the blade axis, illustrated in Figure 4.5, highlight that the longitudinal node is positioned at the blade step, thus maximising the stress at that location.

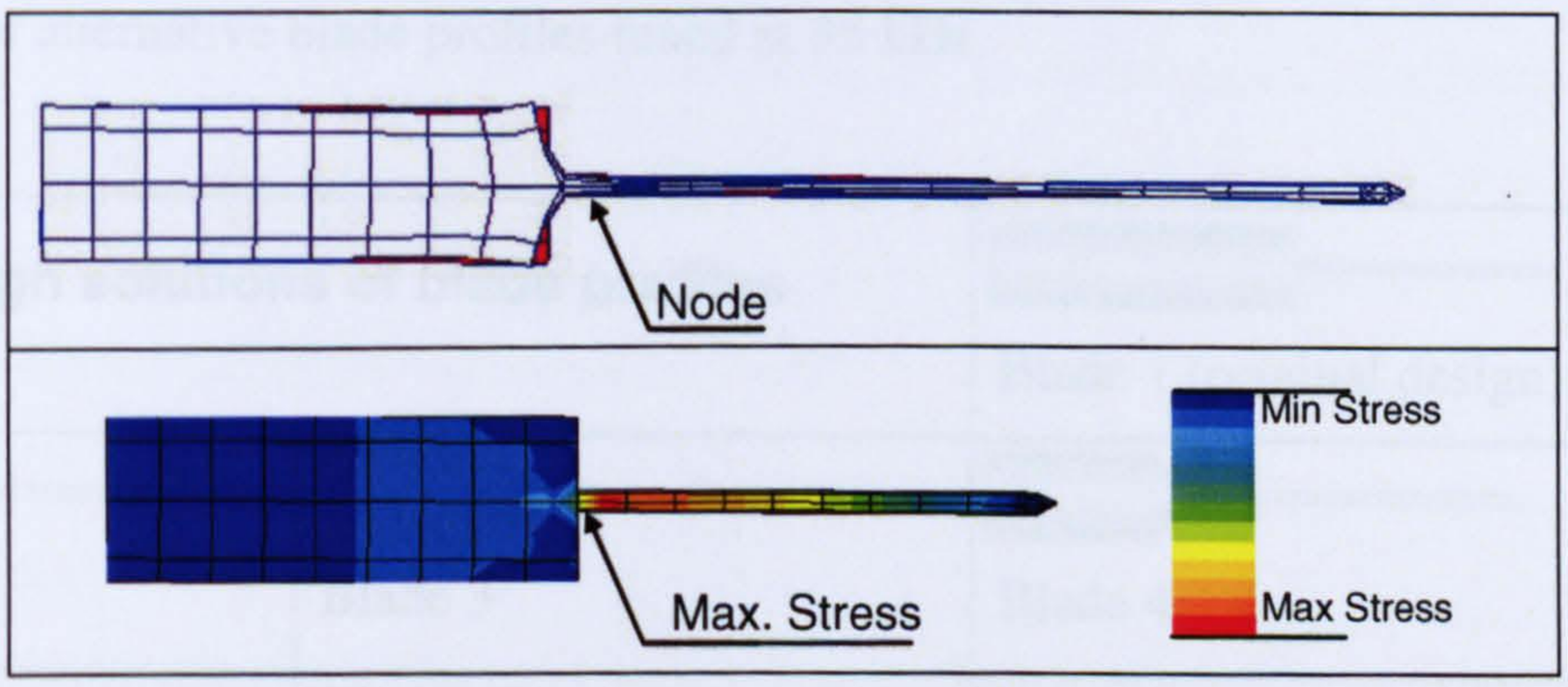

Figure 4.4. (a) Blade first longitudinal mode (operating mode) at 35.0 kHz, (b) stress contours

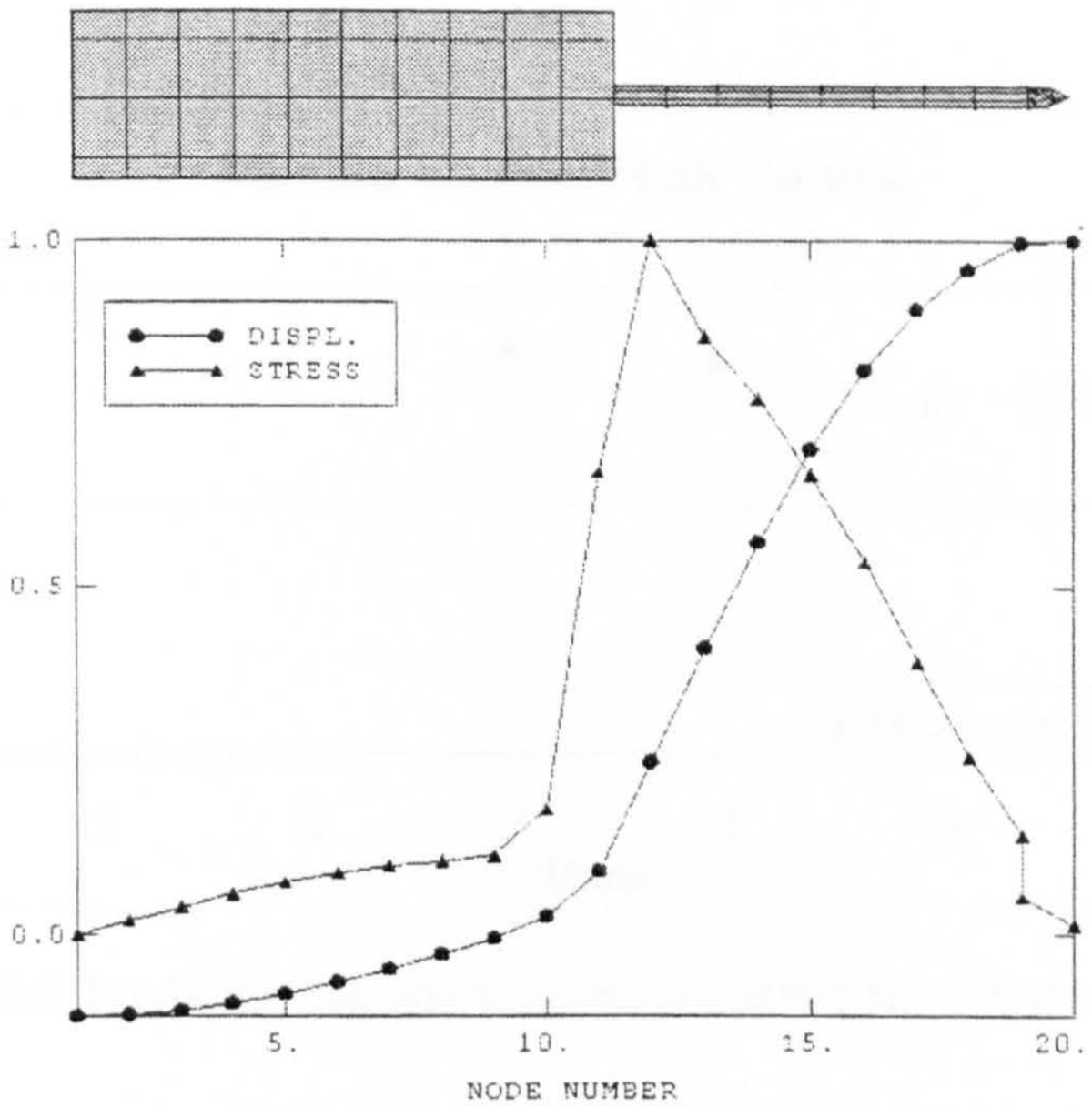

Figure 4.5. Predictions of normalised stress and displacement distribution along the axis of the half-wavelength stepped blade

4.2.2 Redesign of half-wavelength blades

Frequent fatigue blade failures have limited the exploitation of ultrasonic cutting using thin stepped blades. Therefore, there is a requirement for redesigned blades that deliver the necessary operating amplitude at the tuned frequency under lower stress conditions. A profile redesign strategy is undertaken here in order to reduce stress at the blade step. Design is carried out using FE modelling and EMA. The creation of alternative blade models is performed with the aim of reducing stress while preserving a minimum knife length necessary to cut through the material depth. Table 4.1 shows seven models of alternative blade profiles tuned at 35 kHz.

Redesign solutions of blade profiles		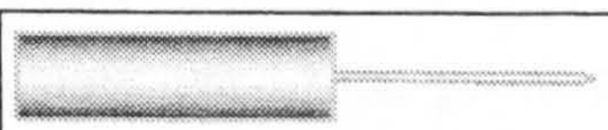 Blade 1 (original design)
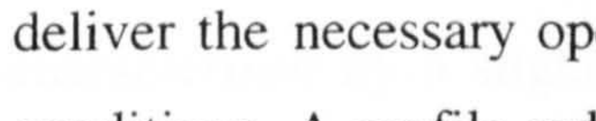 Blade 2	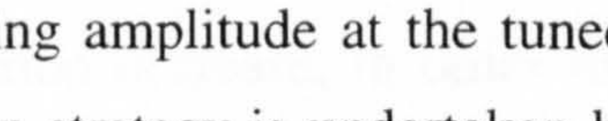 Blade 3	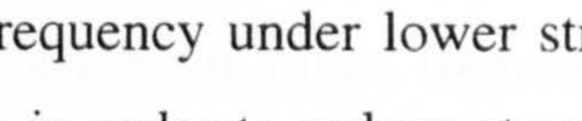 Blade 4
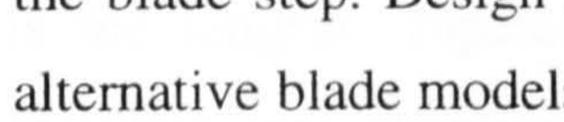 Blade 5	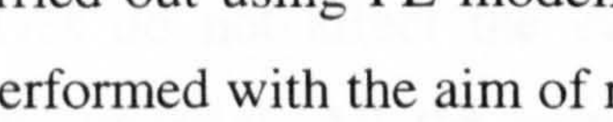 Blade 6	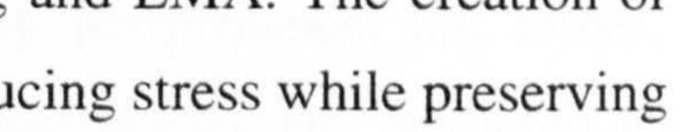 Blade 7

Table 4.1. FE models of alternative blade profiles

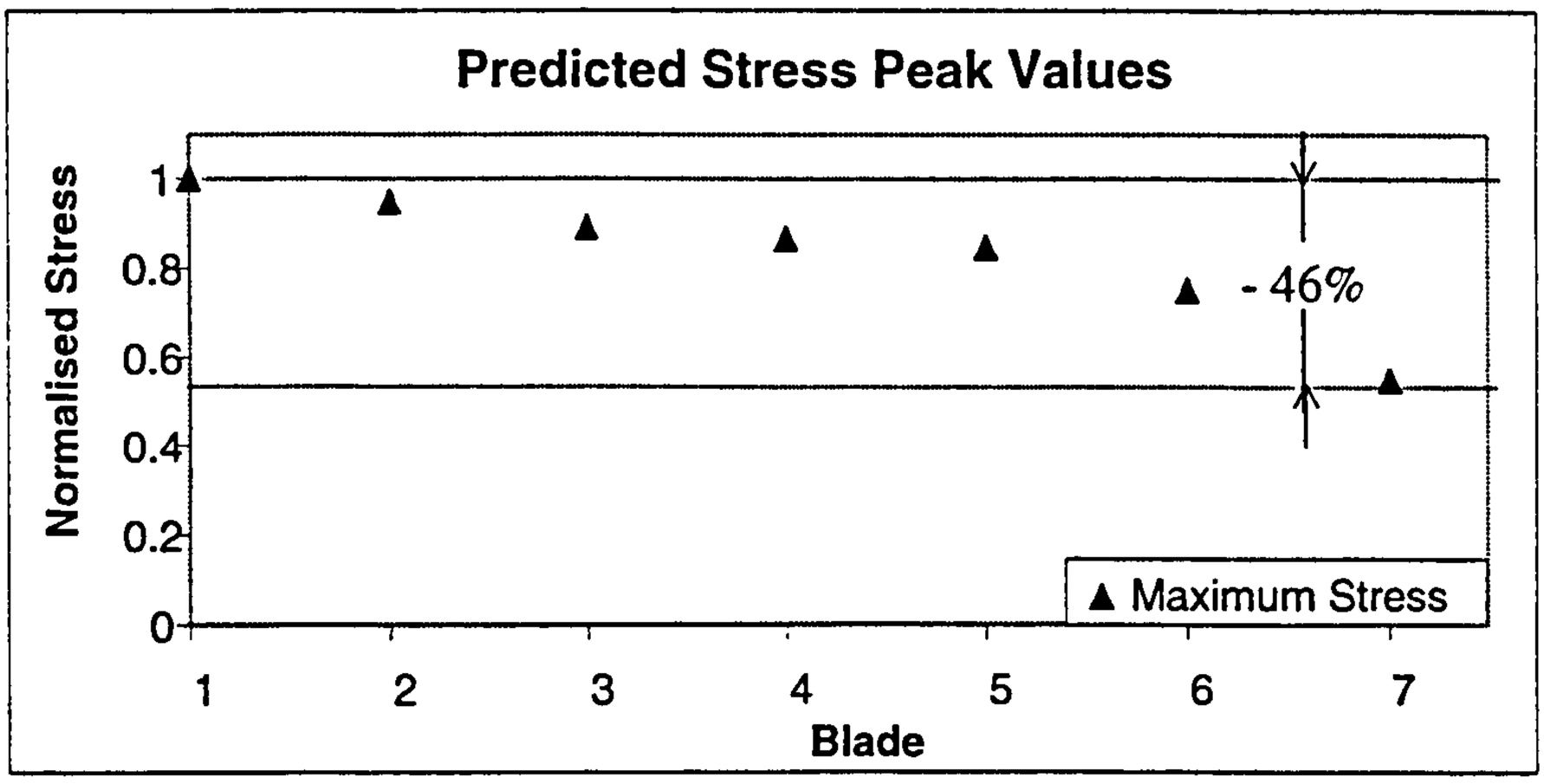

Figure 4.6. Predicted maximum stress for alternative blade profiles

All the blades are designed with smoother section reduction in order to reduce the stress level at the failure location. The redesigned blades 2-5 exhibit catenoidal, conical, exponential, and a combination of catenoidal and conical shoulder tapers, respectively. For these models the redesign approach does not alter the cutting knives, whereas cylinder lengths are adjusted in order to offset the tuned frequency shifts due to the step modifications. Conversely, the cutting knives of blades 6 and 7 are characterised by a slight section decrease, in order to preserve the tuned frequency, and are therefore longer. In particular, blade 7, which exhibits the steepest knife taper, is the longest. Tapered knives do not affect the cutting performance, but rather, facilitate tool insertion in the material. All the redesigned blades are predicted to exhibit lower stress at the step than the original design (Figure 4.6), thus, validating the assumption that a less steep section reduction results in lower stress. In particular, blade 6 and 7, with tapered cutting knives, are predicted to operate under significantly lower stress conditions. Slight variations of the blades' gains due to the geometric alterations, are also predicted for the modified models.

4.2.3 FEA and EMA comparison

A choice of blade model to manufacture is between blades 6 and 7. Blade 7 has the advantage of offering the lowest stress but at a cost of higher modal activity. In fact, many bending modes, associated with the longer knife, are predicted for blade 7 in the 30-40 kHz frequency range, with some of them very close to the tuned mode at 35

kHz. Hence, the excitation of a multi-modal response at the operating frequency, with consequent reduction of the blade performance, is expected to arise with blade 7. An additional mode or even modes being excited simultaneously, is called modal coupling. On the other hand, the FE model of the shorter blade (blade 6) predicts the modal frequencies to be well separated in the operation frequency range. As a result, Blade 6 is manufactured as a good compromise of low stress and modal activity.

An EMA of blade 6 mounted on the piezoelectric transducer is carried out in order to validate the modal predictions. 3D LDV is used to measure vibration velocities at several locations on the blade surface. Figure 4.7 shows the sum of the FRFs measured on the blade-transducer stack obtained by random excitation test in the frequency range 0 – 50 kHz. Agreement between the FEA and EMA data is within 6.3 % for all modes up to 50 kHz (Table 4.2). Figure 4.8 illustrates the blade modes predicted by finite element analysis alongside the corresponding modal analysis measurements. The blade exhibits responses in three mode families: torsional (Figure 4.8 (a,e) and Figure 4.8 (c,g)), bending (Figure 4.8 (b,f)) and longitudinal (Figure 4.8 (d,h)).

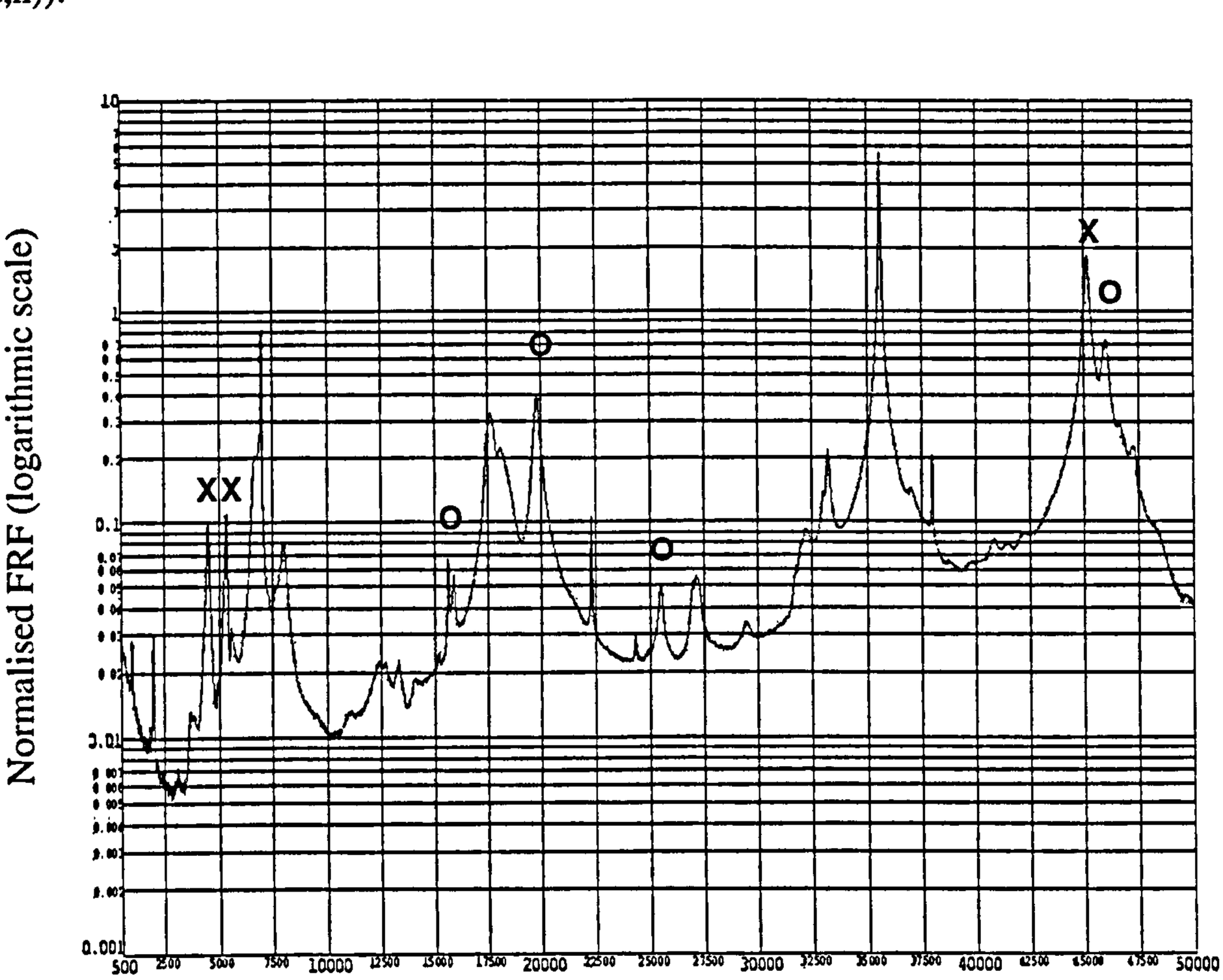

Figure 4.7. Sum of the FRFs measured in the transducer-blade stack

Blade Natural Frequencies (Hz)		
Finite Element Analysis (FEA)	Experimental Modal Analysis (EMA)	Error (%)
1418	-	-
6635	6626	0.1
7137	6990	2.1
8225	7971	3.1
16824	17463	-3.7
21435	22286	-3.8
25934	24325	6.2
28796	27202	5.5
34276	33256	3.0
36117(*)	35628	1.3
37358	37990	-1.7
38181	38278	-0.3
41634	41045	1.4
43245	42320	2.1
48756	47416	2.7

(*): Tuned longitudinal mode

Table 4.2. Blade mode frequencies in the range (0-50 kHz)

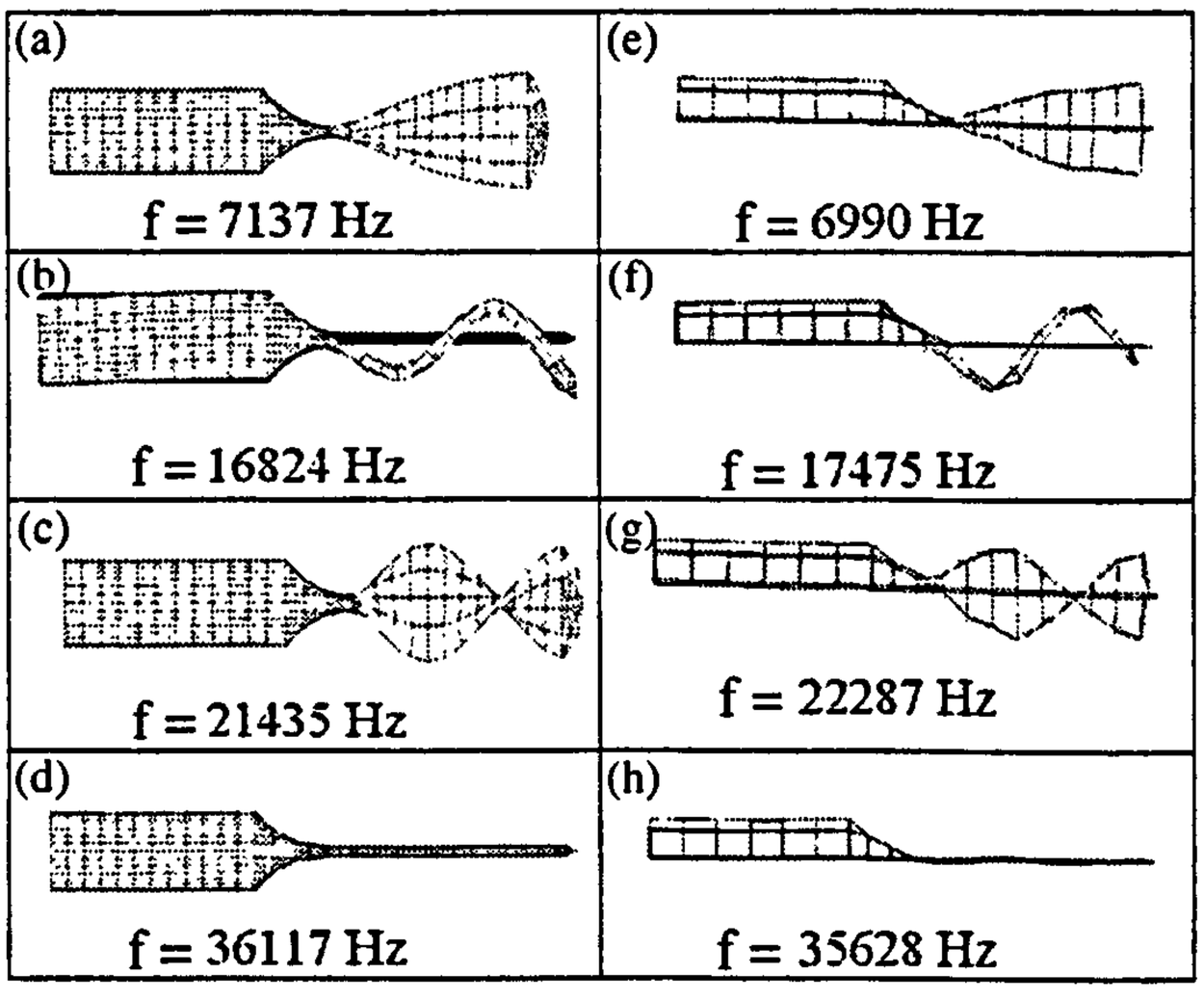

Figure 4.8. Blade modes of vibration: (a-d) FE modal data, (e-h) 3D LDV EMA data

4.2.4 Transducer influence on the blade modal behaviour

Alongside the blade modes predicted by FEA, highlighted with the squares (□), the spectrum of Figure 4.7 exhibits a number of resonances which require some further explanation. Analysis is therefore carried out of the mode shapes of such resonances, identified with circles (X) and crosses (O).

Figure 4.9 (a-b) shows two mode shapes which, at first glance, seem to resemble the 1st in-plane bending mode and the 2nd out-of-plane bending mode of the blade (where the reference plane is the knife plane). These blade modes, however, have been predicted and measured in good agreement at 8.0 kHz and 6.6 kHz, respectively, and are shown in Figure 4.9 (c,d).

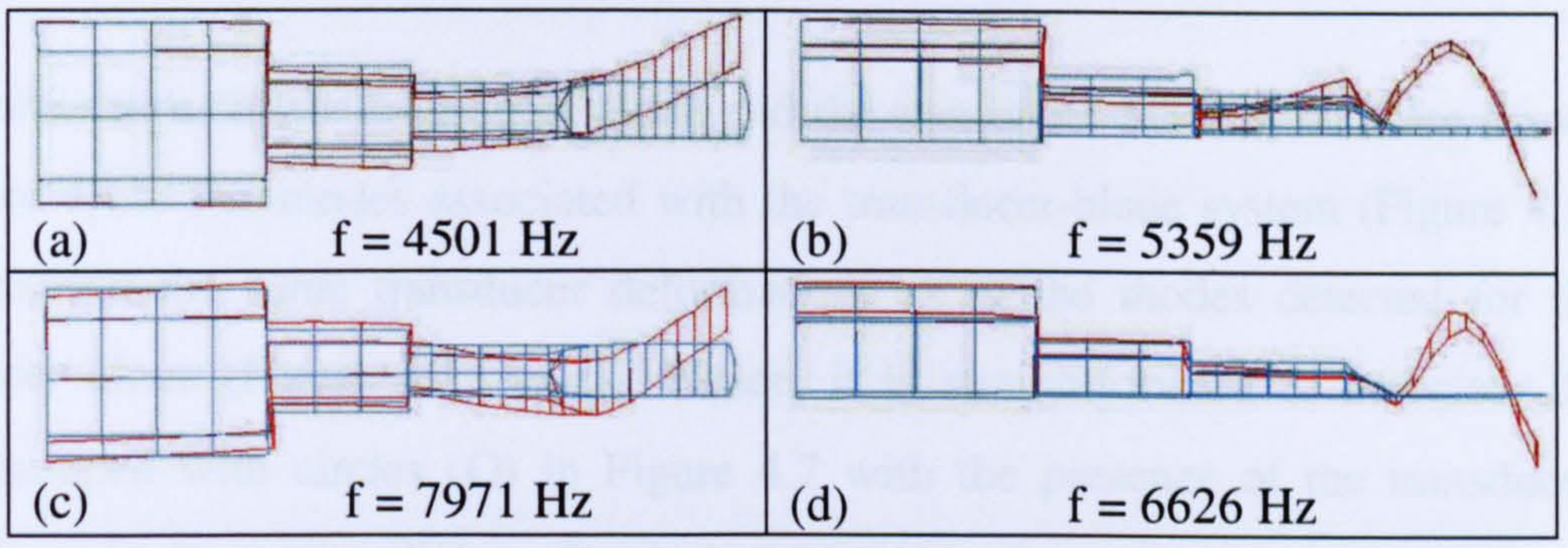

Figure 4.9. Measured modes of vibrations of the transducer-blade assembly

Careful inspection of the shapes of the modes occurring at 4.5 kHz and 5.4 kHz shows an involvement of the transducer in the bending motion of the blade. Hence, these natural frequencies (X) are associated with two modes of vibration of the entire blade-transducer stack and for this reason are not predicted by the FE model of the blade. These blade-transducer modes cannot be ignored, and must be included in the analysis.

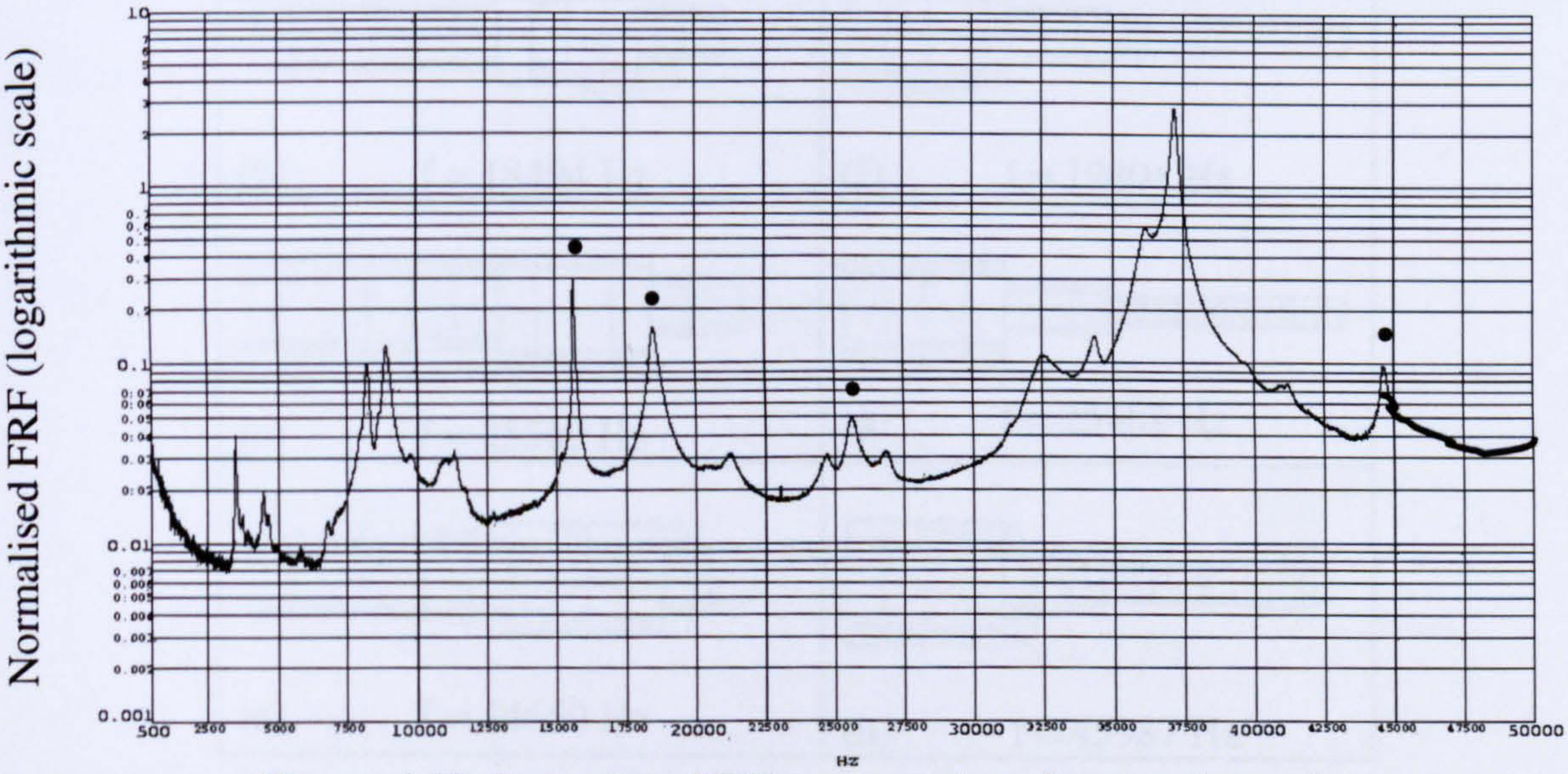

Figure 4.10. Sum of the FRFs measured on the transducer alone

To understand the nature of the modes corresponding to the remaining peaks (O) of the spectrum, a modal analysis of the transducer with no blade attached is performed. Figure 4.10 shows the sums of the FRFs measured on the transducer on its own. The transducer natural frequencies identified by dots (•) occur at frequencies very close to the peaks labelled with circles (O) measured for the transducer-blade assembly (Figure 4.7).

The mode shapes of the transducer alone and the transducer-blade system are shown in Figure 4.11. The modes associated with the transducer-blade system (Figure 4.11 (e-h)) exhibit the same transducer deformations as in the modes detected for the transducer alone (Figure 4.11 (a-d)). Hence, it is straightforward to associate the peaks grouped with circles (O) in Figure 4.7 with the presence of the transducer. From these findings, the choice of transducer is a key factor in the configuration of ultrasonic systems, as transducers tuned to the same frequency provided by different manufacturers have a different contribution to the vibration behaviour of the assembly.

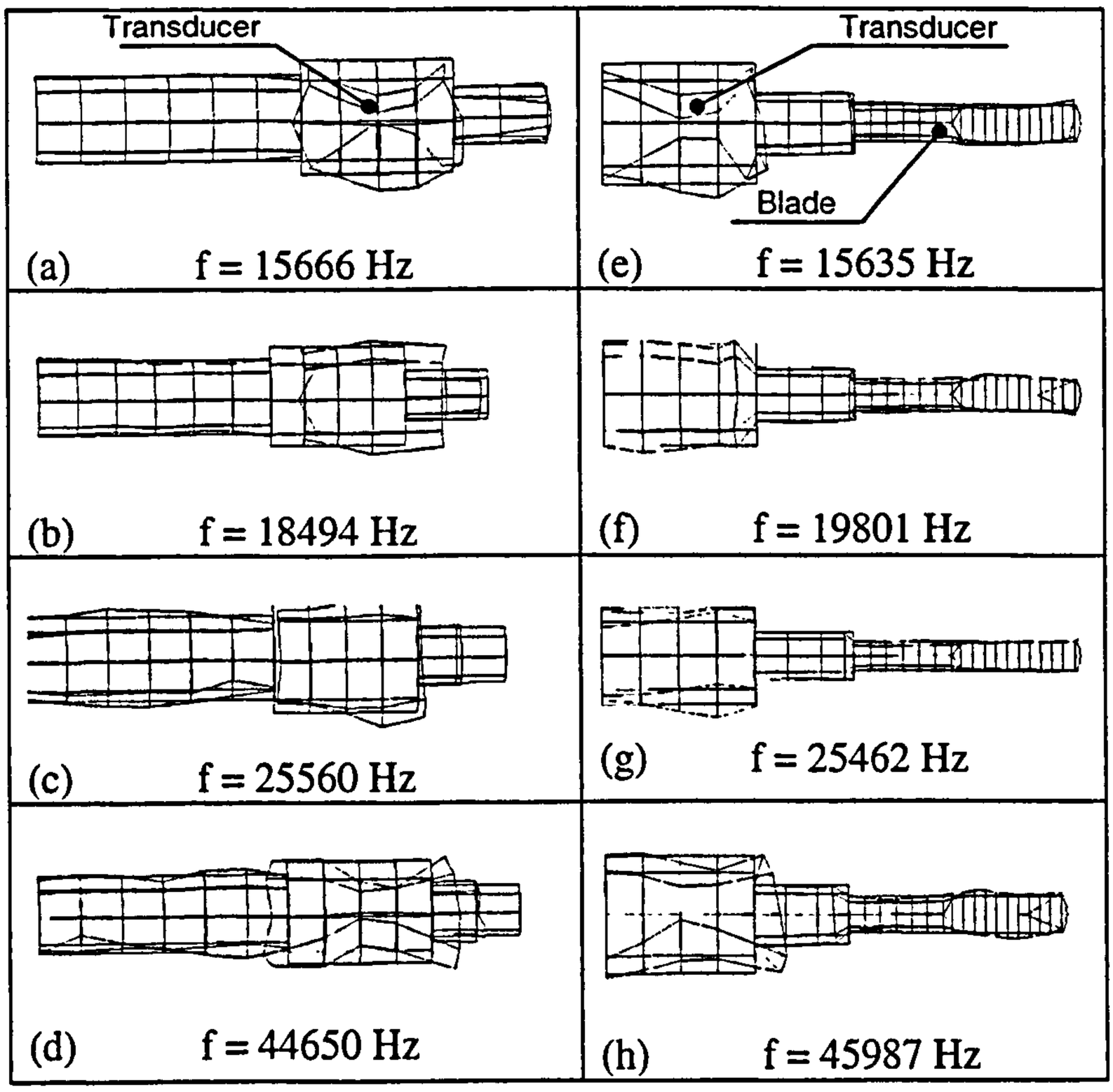

Figure 4.11. Transducer and corresponding transducer-blade measured modes of vibration

4.3 Wavelength blades with built-in amplitude gain

For cutting operations requiring greater depths of cut, wavelength blades are usually used. Figure 4.12 shows a wavelength blade designed to resonate in its second longitudinal mode of vibration at 35 kHz. The unit is 167 mm long, and is manufactured from tool steel. The knife holder is shaped as a half-wavelength stepped horn which transfers the vibration from the transducer to the cutting knife. In order to deliver the required amplitude at the knife tip, the holder is designed to provide a gain factor of two. The half-wavelength cutting knife is characterised by a tapered profile which supplies a gain factor of three to the vibration amplitude provided by the holder. The constant reduction of the section thickness of the knife from 2 mm at the holder interface to 0.6 mm at the tip also facilitates tool insertion in the material.

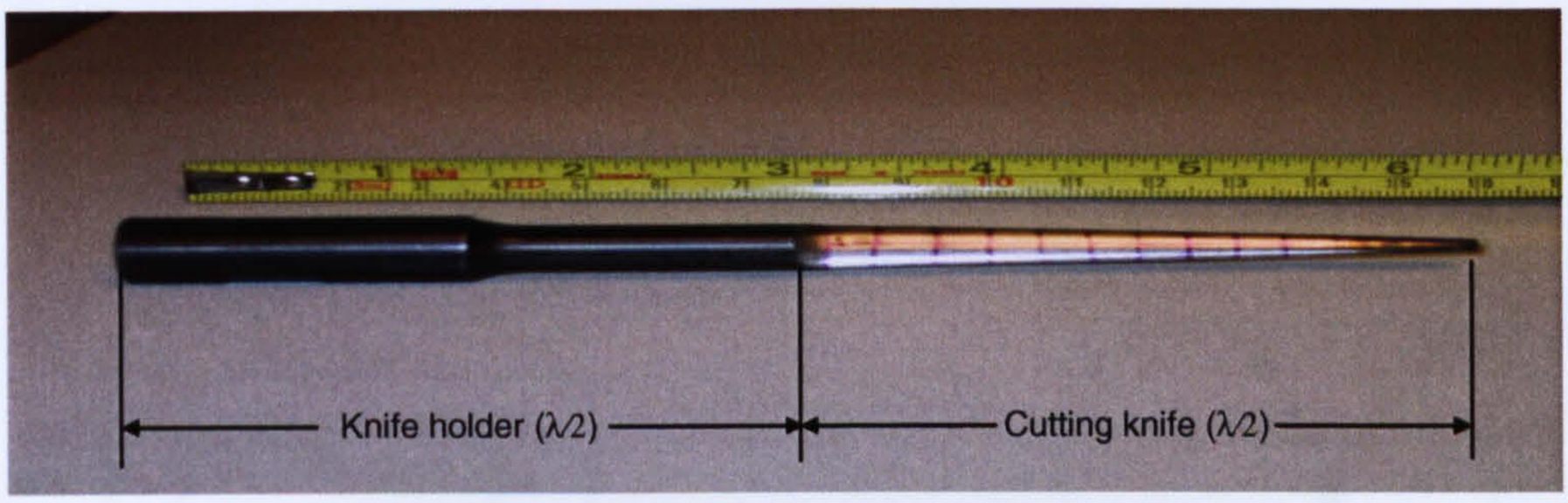

Figure 4.12. Wavelength ultrasonic blade

4.3.1 Stress distribution in a one-wavelength blade with built-in amplitude gain

Figure 4.13 (a) shows the predicted mode shape of the tuned second longitudinal mode of the blade. The two nodal points of zero displacement are indicated in the figure.

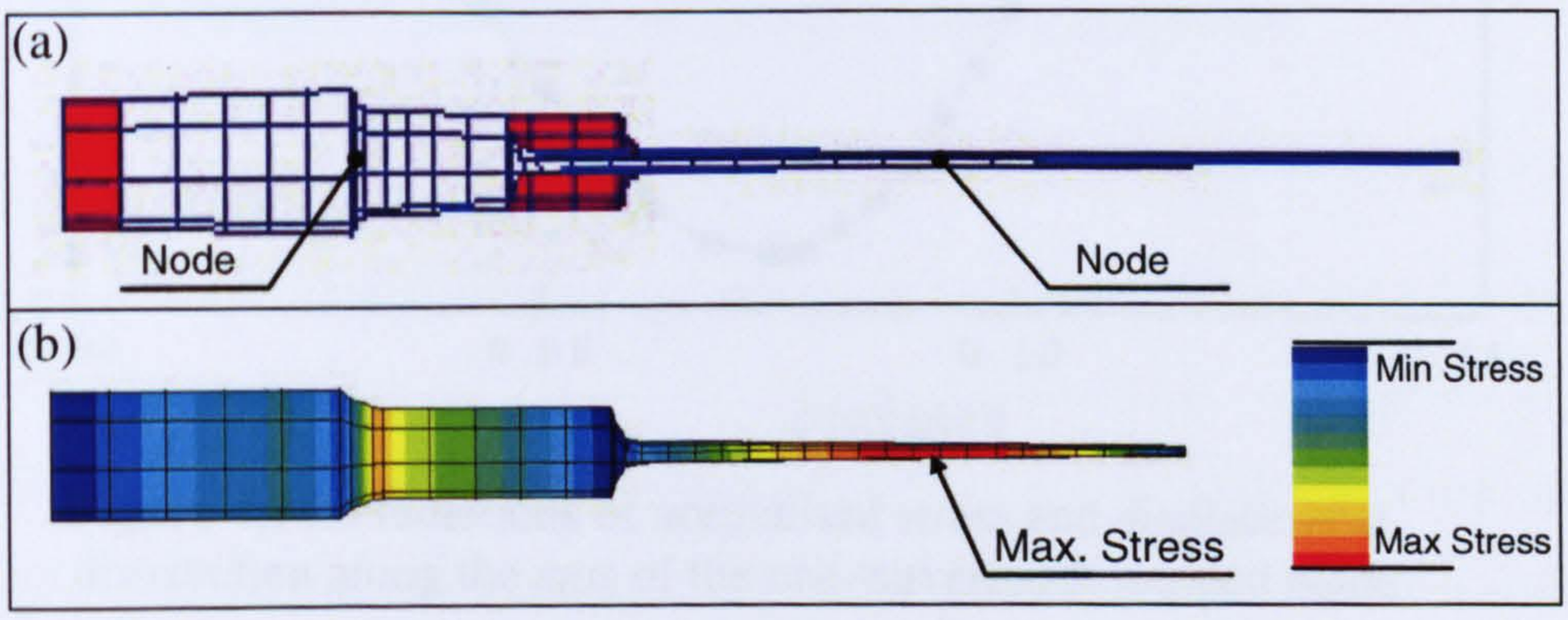

Figure 4.13. (a) Blade second longitudinal mode (operating mode), (b) Second longitudinal mode at 35.0 kHz: relative stresses

The stress associated with such motion (Figure 4.13 (b)) reveals that the highest stresses of the blade occurs just after the step of the knife holder and near the middle section of the cutting knife.

Moreover, the distributions of the normalised stress and displacement along the blade axis, shown in Figure 4.14, show that the maximum stresses occur in the vicinity of the nodes. The maximum stress predicted for the wavelength blade proves to be only 45 % of the maximum stress calculated for the original half-wavelength blade (blade 1) described in section 4.2. In fact, the tapered profile allows the knife to operate under reduced stress at the expense of a low gain. However, the stepped holder provides the additional gain needed to achieve the required amplitude at the knife tip.

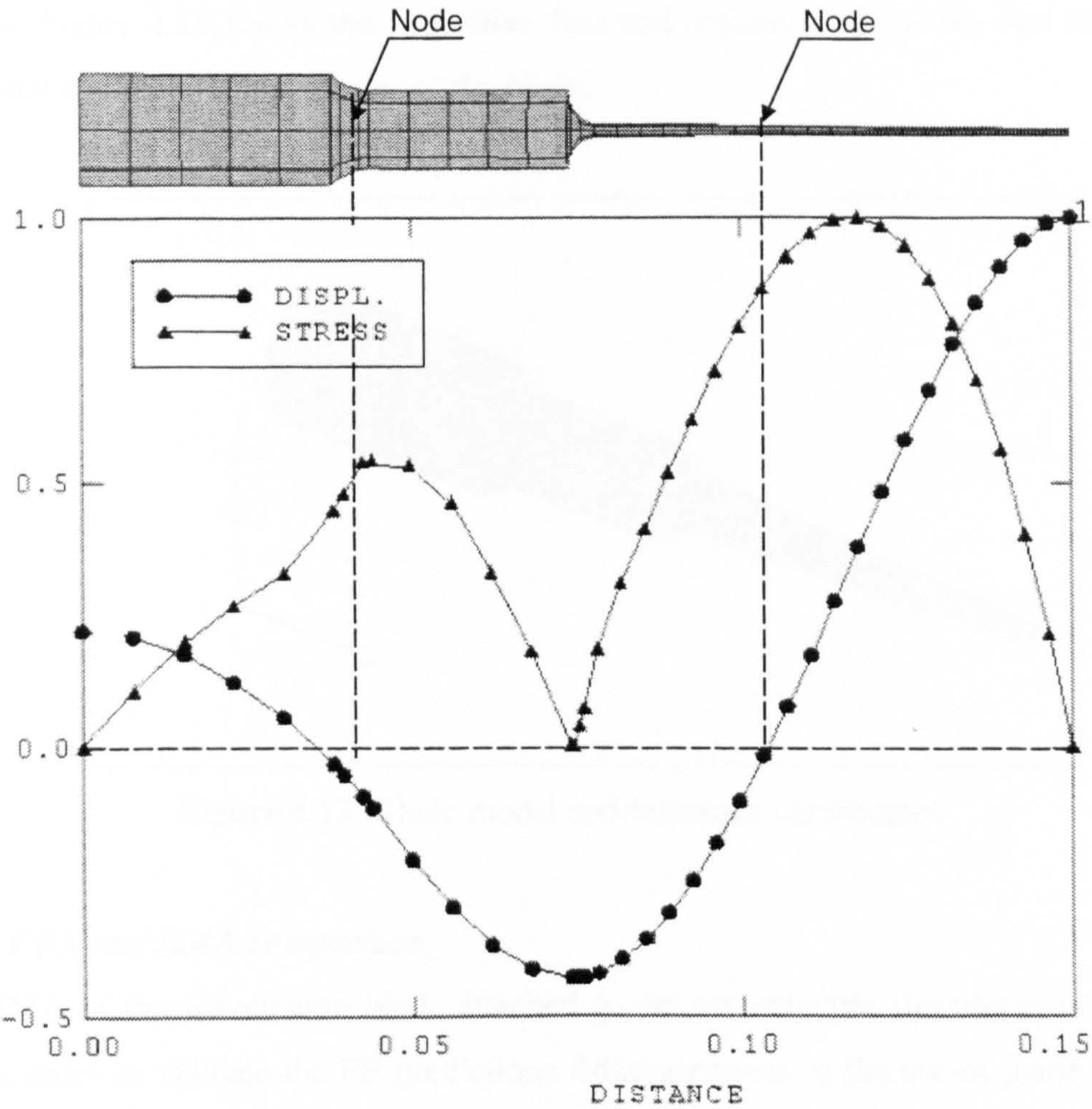

Figure 4.14. Predictions of normalised stress and displacement distribution along the axis of the one-wavelength stepped blade

Despite the advantages of offering greater depths of cut under low stress are characterised by a large number of modes, many predicted with frequencies in the

vicinity of the longitudinal mode. Hence, a sensitivity analysis is conducted of frequency sensitivity to blade profile parameters, in order to avoid modal coupling with the tuned mode.

4.3.2 Mode shapes classification

According to the nomenclature commonly used for the mode shapes of beam-like structures, the blade modes of vibration are classified by the harmonic number and the type of motion. The three translation degrees of freedom used as reference for the blade model are illustrated in Figure 4.15. The bending modes can occur in the x-direction, x-y plane, therefore named B_x modes, and also in the y-direction, y-z plane, therefore named B_y modes. Torsional modes occur around the z-axis, therefore called T_z-modes. The longitudinal modes occur in the z-direction, are hence named the L_z modes. Figure 4.16 shows the respective first and second mode of the two bending, torsional and longitudinal modes of the blade.

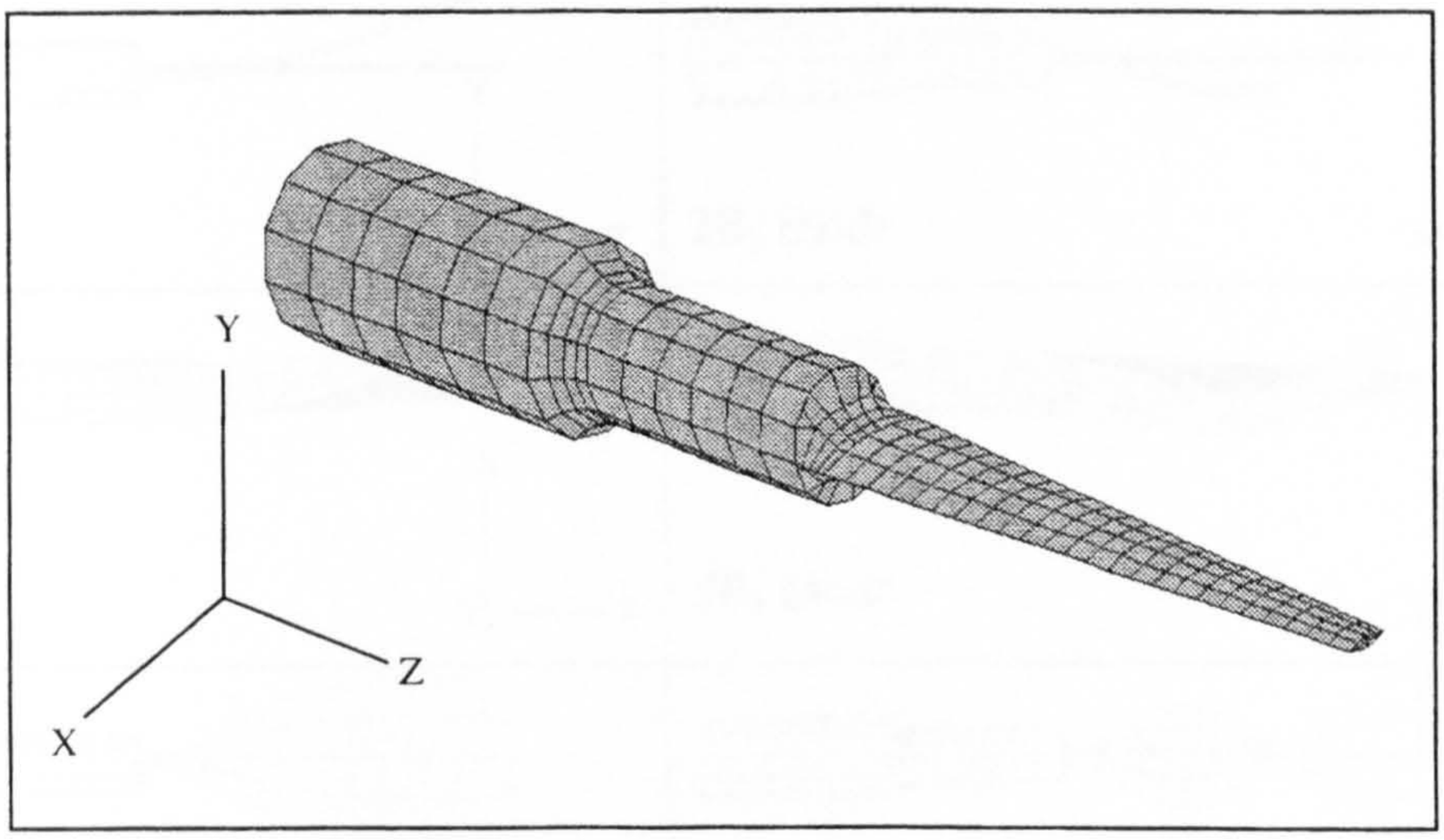

Figure 4.15. Blade model and reference coordinates

4.3.3 FEA and EMA comparison

An EMA of the wavelength blade attached to the piezoelectric transducer is carried out in order to validate the FE predictions. Measurements of the out-of-plane and in-plane components of the blade surface vibration velocities are performed using the 3D LDV. Figure 4.17 shows the sum of the FRFs measured on the blade-transducer assembly, where the modes, determined by a random excitation test in the 0 – 60 kHz frequency range, are identified. A comparison of the calculated and the

experimentally obtained modal frequencies shows good correlation (Table 4.3). Hence, the FE model is considered for geometry alteration to improve the accuracy of the design. In particular, the measured frequency of the 2Lz tuned mode results in very good agreement with its FE prediction, as an error of only 0.01% is estimated.

Identification of the measured mode shapes is sometimes difficult as modal coupling between some modes in the spectrum results in indistinct motions. Such an effect is not encountered in the FE predictions where the mode shapes are calculated without taking account of coupling effects.

Modal coupling becomes detrimental for the system performance when involves the tuned mode couples with one or more modes. In this case, from the FE predictions and measurements the frequency of the $11B_y$ mode results very close to the tuned $2L_z$ longitudinal mode frequency.

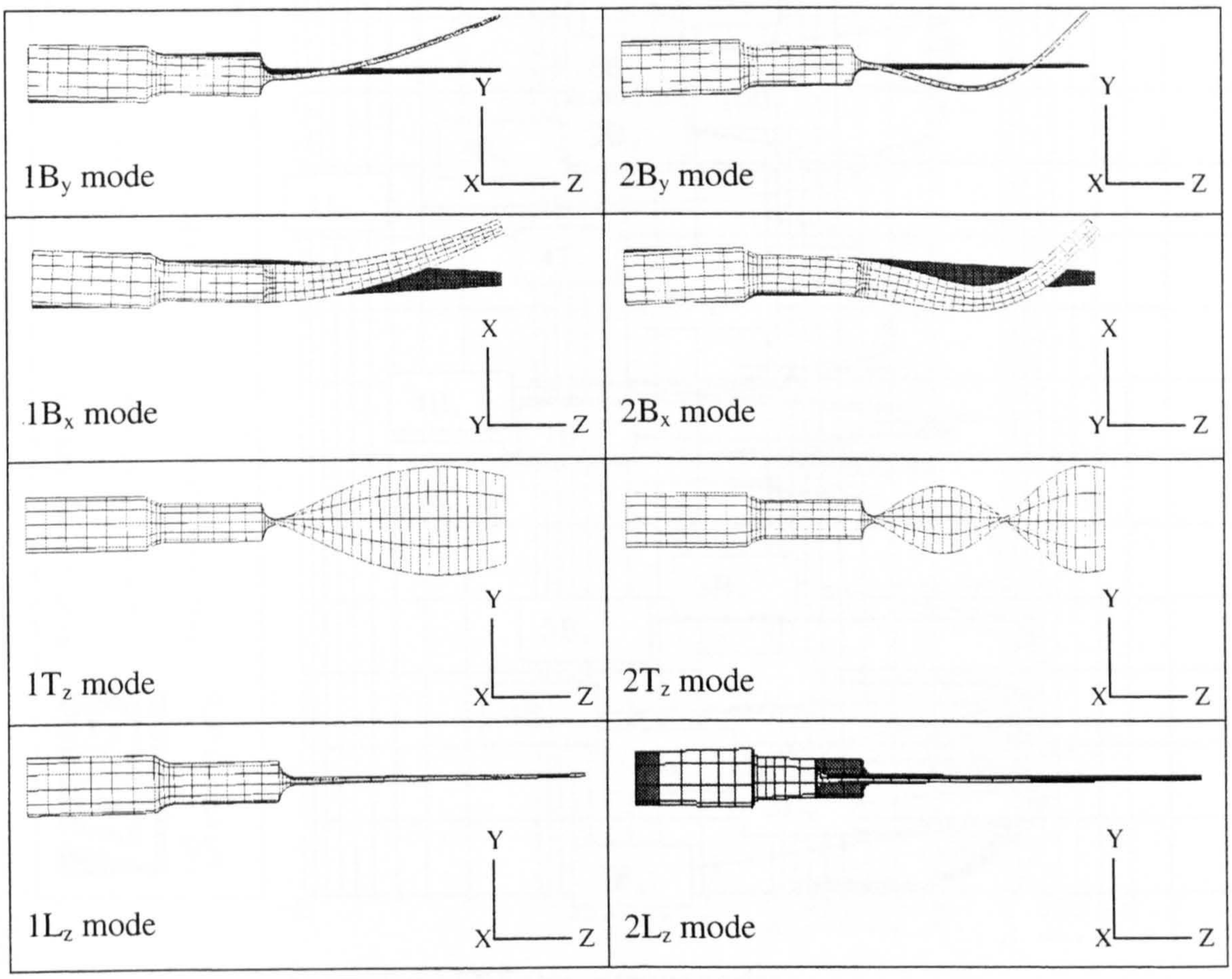

Figure 4.16. Mode classification

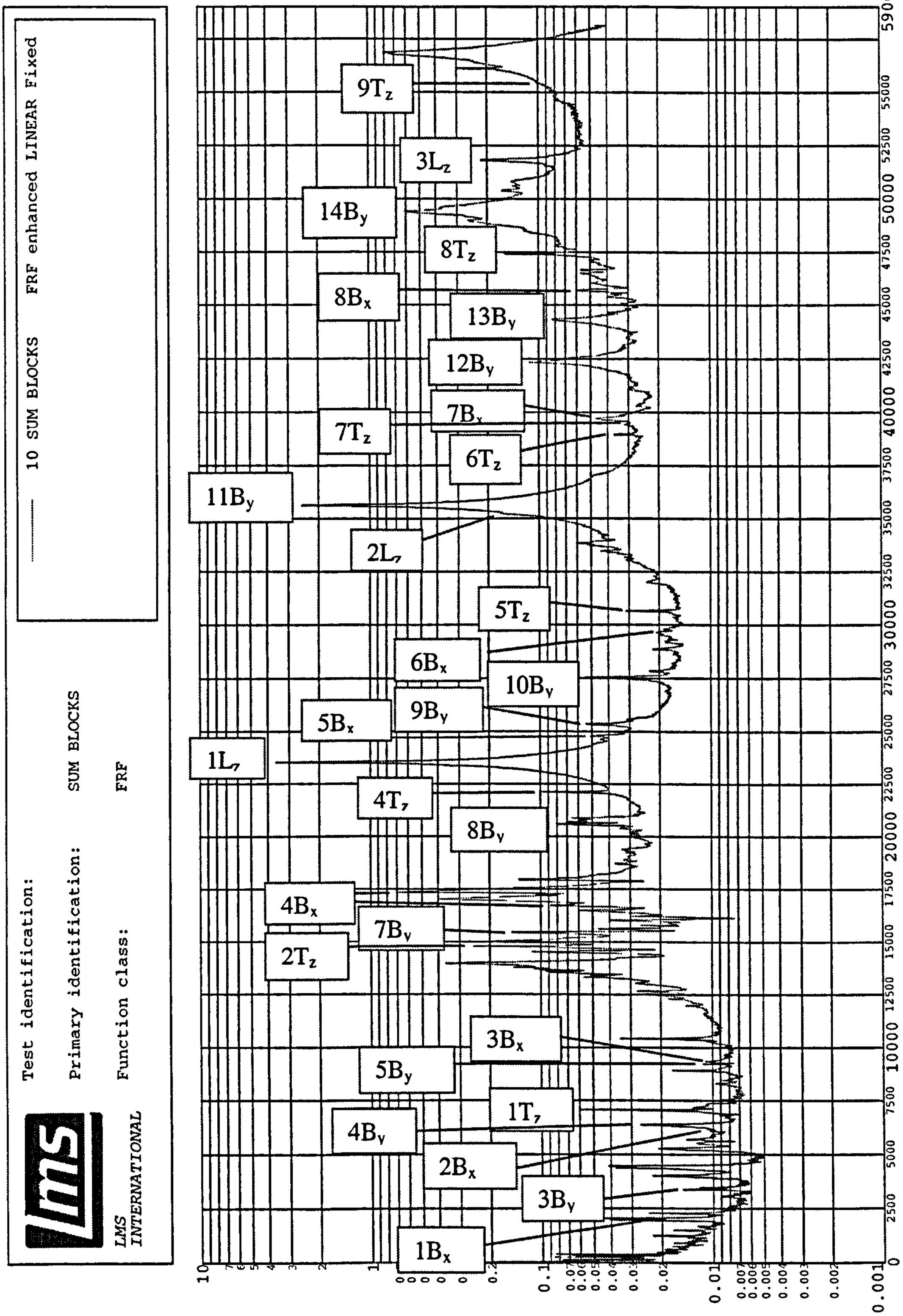

Figure 4.17. Sum of FRFs of original wavelength blade

	Blade Natural Frequencies (Hz)		
Mode	Finite Element Analysis (FEA)	Experimental Modal Analysis (EMA)	Error (%)
1By	410	-	-
2By	1479	-	-
1Bx	2016	2051	-1.7
3By	3497	3432	1.9
2Bx	6212	6219	-0.1
4By	6418	6383	0.5
1Tz	7079	7067	0.2
5By	9316	9216	1.1
3Bx	10184	9345	8.9
6By	11025	-	-
2Tz	14132	14796	-4.5
7By	15554	15451	0.7
4Bx	16247	16754	-3.0
8By	21165	20860	1.5
1Lz	22080	23522	-6.1
4Tz	22516	22115	-1.8
5Bx	25078	24749	1.3
9By	25873	25404	1.8
10By	28600	27529	3.9
6Bx	30184	29630	1.9
5Tz	30192	30645	-1.5
2Lz(*)	35268	35263	0.01
11By	35516	35630	-0.3
6Tz	38415	38956	-1.4
7Tz	39676	39821	0.1
7Bx	40836	39756	2.7
12By	41998	42363	0.8
13By	44925	44310	1.4
8Bx	46621	46429	0.4
8Tz	47146	47419	-0.6
14By	53002	49758	6.5
3Lz	53966	51822	4.1
9Tz	55866	56130	0.5
9Bx	59818	-	-

(*): Tuned longitudinal mode

Table 4.3. Blade modal frequencies in the range (0-55 kHz)

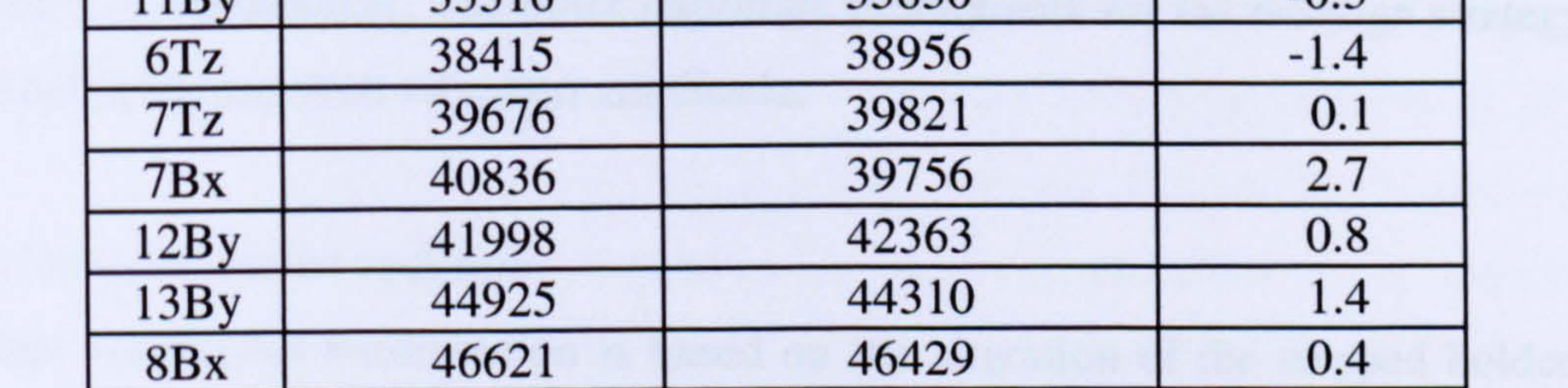

Figure 4.18. Modal coupling between 2Lz mode and 11By mode

Examination of the frequency response (Figure 4.17) in the region of the operating frequency shows that the $11B_y$ mode corresponds to the response peak at 35.6 kHz, whereas the $2L_z$ mode at 35.3 kHz. Hence, the mode shape of the tuned mode illustrated in Figure 4.18 shows the $11B_y$ mode participation in the longitudinal mode as a result of modal coupling. The $11B_y$ motion superimposed on the longitudinal motion results in higher stress and therefore shorter life expectancy of the blade. As the FE modal data correlates well with the measurements, a redesign strategy to achieve isolation of the tuned frequency based on geometry alterations of the blade model is investigated next.

4.3.4 Design modifications

To adjust the modal behaviour of the blade for isolation of the longitudinal mode, a sensitivity analysis of the tuned frequency is conducted based on altering blade profile parameters. A frequency separation of the tuned mode from close modes by at least ± 1000 Hz is estimated to be sufficient to remove problems of modal interference and mode switching [4], with the latter due to the generator frequency tracking onto the wrong resonance. The aim is to identify one or more blade dimensions on which the coupled mode ($11B_y$) frequency is highly dependent and the longitudinal mode frequency is independent. The other important prerequisite for the redesign strategy is maintaining the required vibration amplitude.

4.3.4.1 Stepped holder redesign

The first considered modification is based on the alteration of the stepped holder of the blade. Figure 4.19 shows the geometric dimensions of the original stepped holder. The length of cylinder 1 is increased from 38 mm to 63 mm, whereas cylinder 2 is shortened by the same amount to maintain the holder length constant.

Since a slight increase in the $2L_z$ frequency occurs for this modification, the length of cylinder 1 is increased to compensate for the variation of tuned frequency. Frequency retuning could also be obtained by lengthening cylinder 2 and/or the cutting knife, however, in order to maintain a consistent rule, adjustments are only applied to cylinder 1. Hence, a length increase of 3 mm in cylinder 1 is predicted to retain the tuned frequency of the modified blade to the $2L_z$ frequency of the original blade.

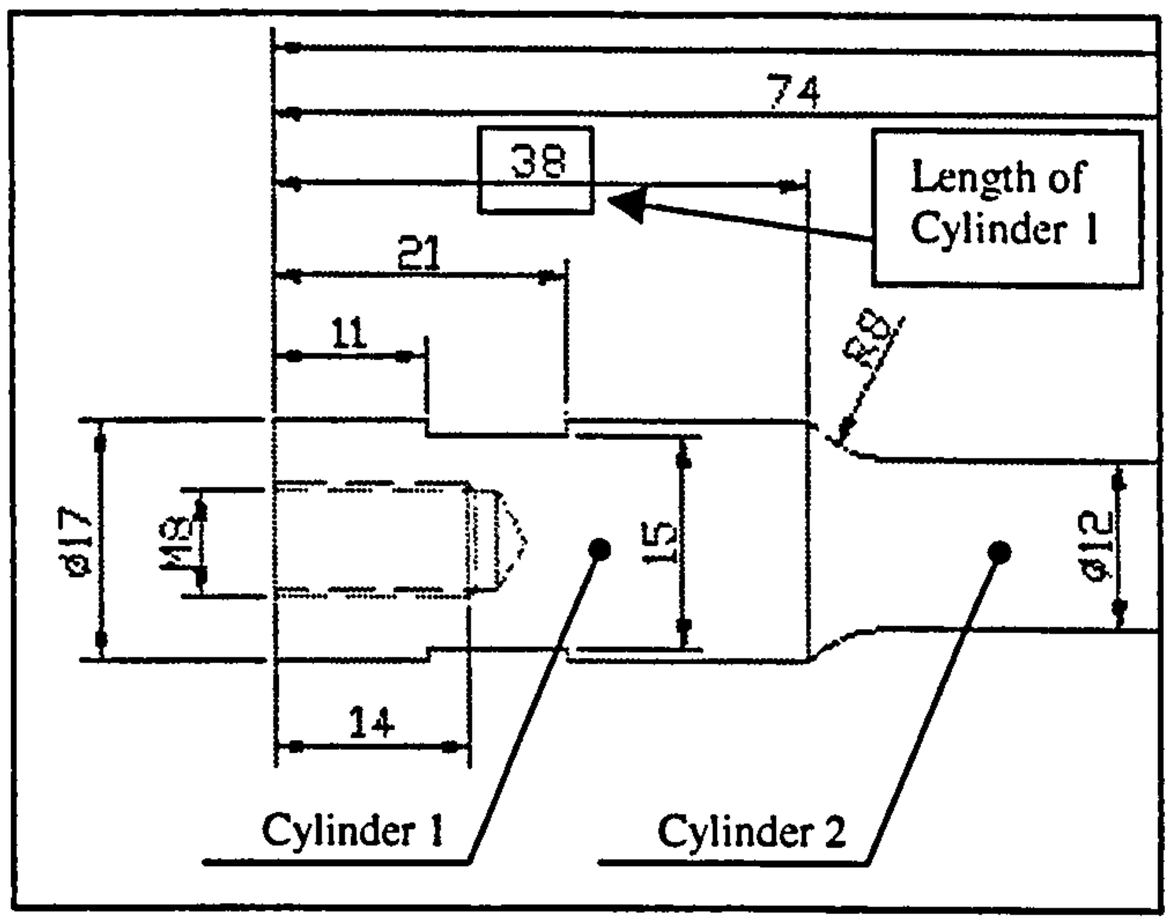

Figure 4.19. Stepped holder dimensions

Conversely, a $2L_z$ frequency decrease is expected when the lengths of cylinders 1 and 2 are decreased and increased, respectively. In this case, a length reduction of cylinder 1 from 38 mm to 23 mm is followed by a further reduction of 9.2mm in order to maintain frequency tuning.

Figure 4.20 shows the predicted mode sensitivities from 3 data points for the described length alterations of the original model. It can be seen that the alteration of the stepped holder does not have a significant effect on the modal frequencies in the frequency range considered (25-47 kHz), except for the $7T_z$ mode (Figure 4.21) frequency which proves to be appreciably affected by the modification. In particular, the $11B_y$ mode, regarded as the dangerous mode due to its vicinity to the $2L_z$ mode, appears totally unaffected by the modifications.

Figure 4.22 illustrates the effects on the predicted tuned mode amplitude using this redesign strategy. The longitudinal displacements of the original blade and the redesigned models are calculated along the knife axis. The nodal point appears at a constant location for the three depicted curves, as no considered alteration affects the knife geometry and the tuned frequency is maintained constant for each redesign. The longitudinal amplitude is highest for the case the length of cylinder 1 is decreased to 23 mm and lowest for the case in which the length is increased to 63 mm. In particular, an amplitude increase of 20.3% and decrease of 12% in comparison to the

original blade are predicted. These amplitude variations stem from altering the stepped holder amplitude gain due to the step repositioning.

In particular, with the length of cylinder 2 increased, and its cross section being smaller than the length and cross-section of cylinder 1 the holder gain increases.
An increase of the holder gain enables a higher longitudinal amplitude at the knife interface to be attained with the result that, for an unmodified knife, the amplitude reached at the knife tip is higher.

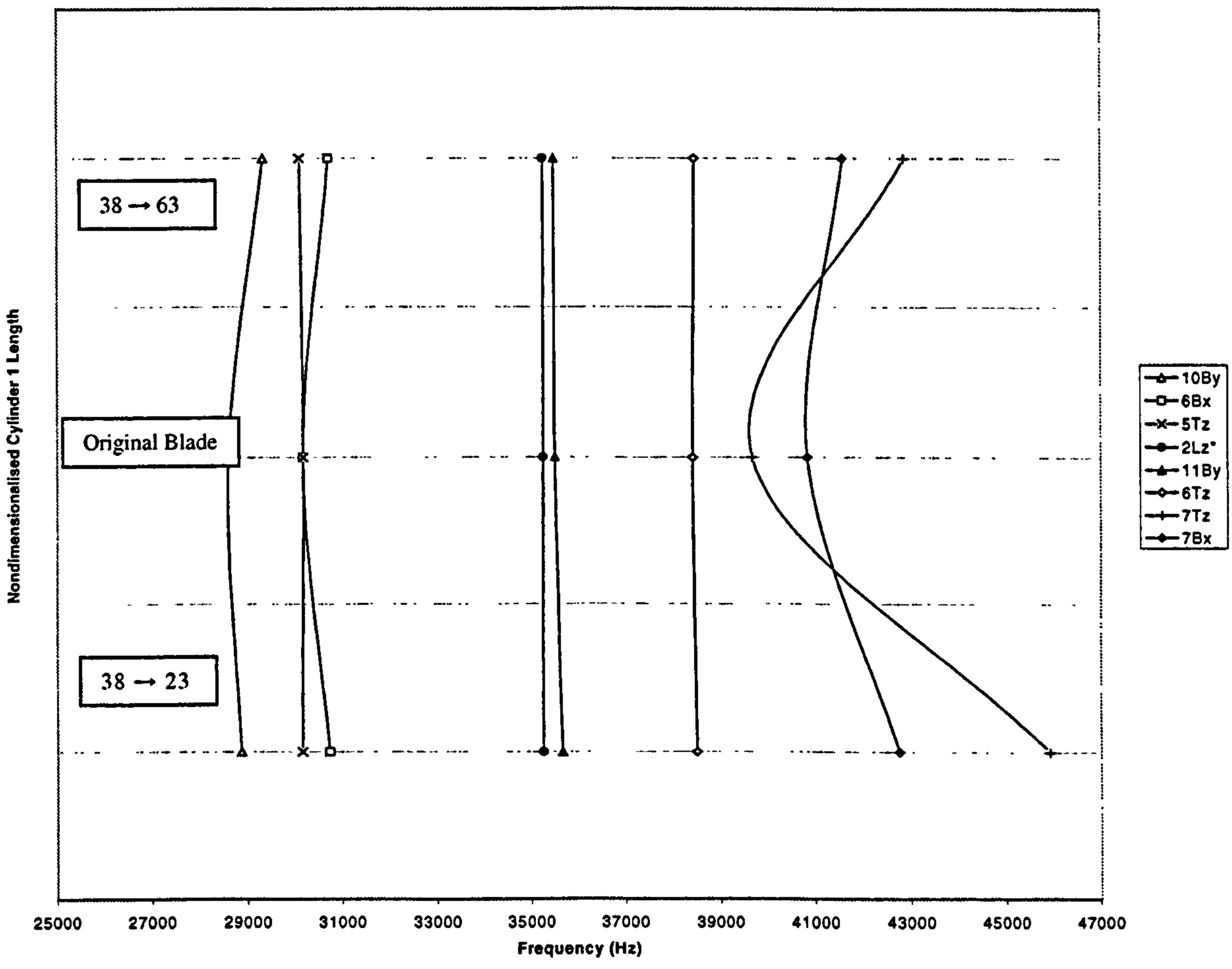

Figure 4.20. Effect of length variation of cylinders 1 and 2

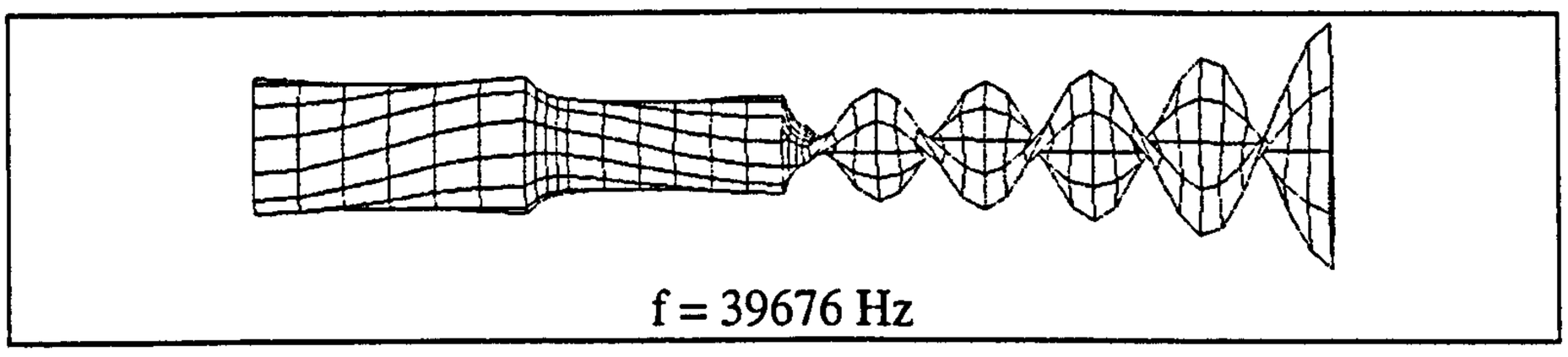

Figure 4.21. Predicted mode shape of the $7T_z$ mode

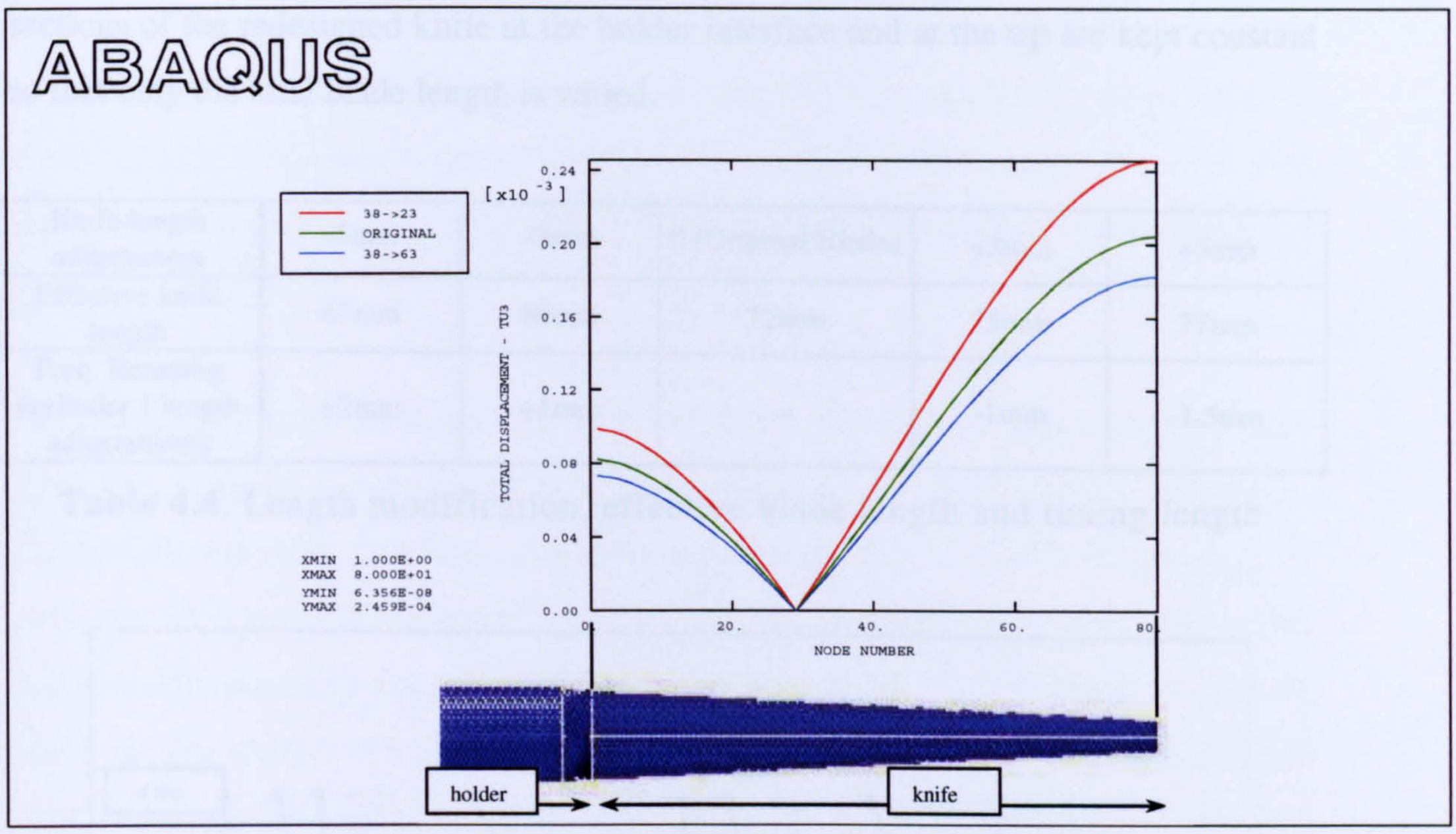

Figure 4.22. Amplitude variation of the cutting knife

4.3.4.2 Cutting knife redesign

Since the alterations of the holder lengths have failed to uncouple the $2L_z$ and $11B_y$ modes another redesign approach is investigated. Modifications of the cutting knife are now studied in order to isolate the tuned mode. Figure 4.23 shows the cutting knife dimension to be varied.

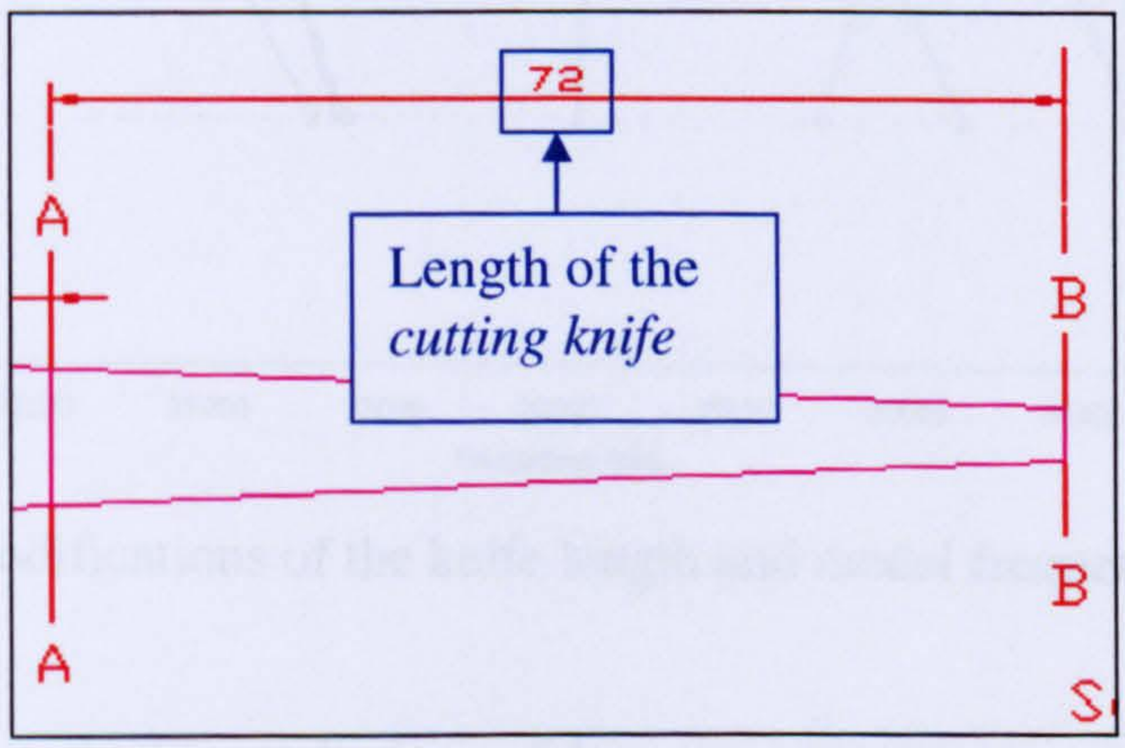

Figure 4.23. Modification of knife length

Initially, the effects of four variations of the knife length from the original blade model are considered. Table 4.4 summarizes these length alterations along with the

adjustments of cylinder 1 length estimated to maintain the tuned frequency. The cross-sections of the redesigned knife at the holder interface and at the tip are kept constant so that only the total blade length is varied.

Knife length adjustament	-5mm	-3mm	0 (Original Blade)	+3mm	+5mm
Effective knife length	67mm	69mm	72mm	75mm	77mm
Freq. Retuning (cylinder 1 length adjustament)	+2mm	+1mm	–	-1mm	-1.5mm

Table 4.4. Length modification, effective blade length and tuning length

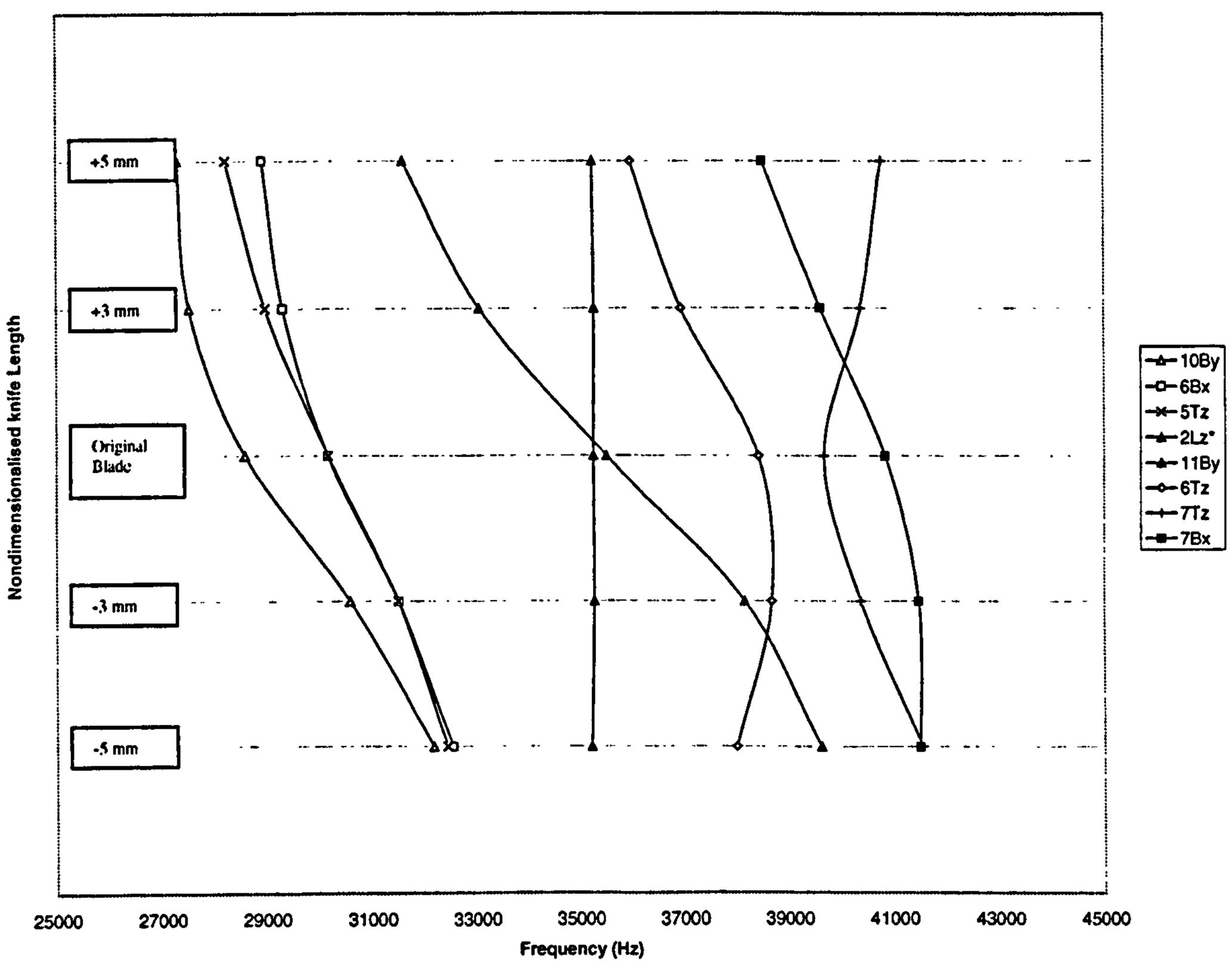

Figure 4.24. Modifications of the knife length and modal frequency separation

Figure 4.24 illustrates the FE predictions of frequency sensitivity to length alterations of the cutting knife. It appears that a decrease of the knife length is responsible for frequency increases of the bending modes in the 25-45 kHz range. The 11By mode frequency is influenced by the length modification. Alternatively, the trend of the 6Tz and 7Tz-modes cannot be readily explained, as their frequencies increase and

decrease unpredictably with the knife length. A frequency separation of more than 3000 Hz is predicted on either side of the tuned mode frequency for reductions of the knife length between 3 mm and 5 mm. Figure 4.25 shows a more detailed representation of the sensitivity of the modal frequencies in this region. It can be seen that the best frequency separation (3200 Hz) is predicted for a length reduction of 3.4 mm.

The predicted amplitude sensitivity to these knife alterations is presented in Figure 4.25. The diagram shows small amplitude increases for knife length reductions, whereas considerable amplitude decreases are predicted for the knife lengthening. In particular for a length increase of 5 mm, the loss of amplitude is over 30%. This effect is due to the repositioning of the nodal point as a result of the length alterations, which moves towards the knife tip (gain decrease) when the knife is lengthened and away from the tip (gain increase) when the knife is shortened. Hence, the best frequency separation of the tuned frequency, achieved when the knife length is reduced by 3.4mm, also corresponds to a 4% amplitude increase.

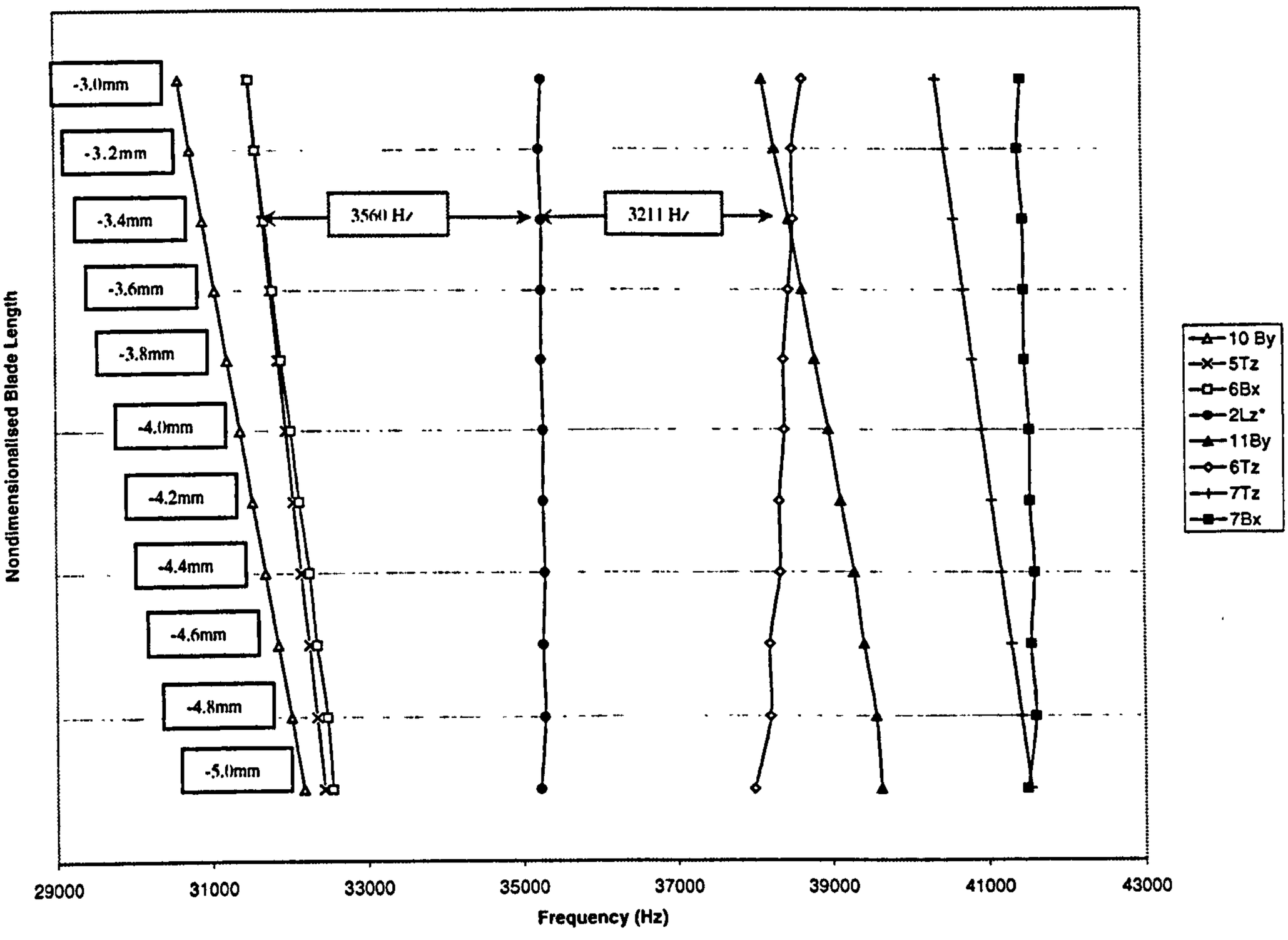

Figure 4.25. Detailed altering of knife length and frequency separation

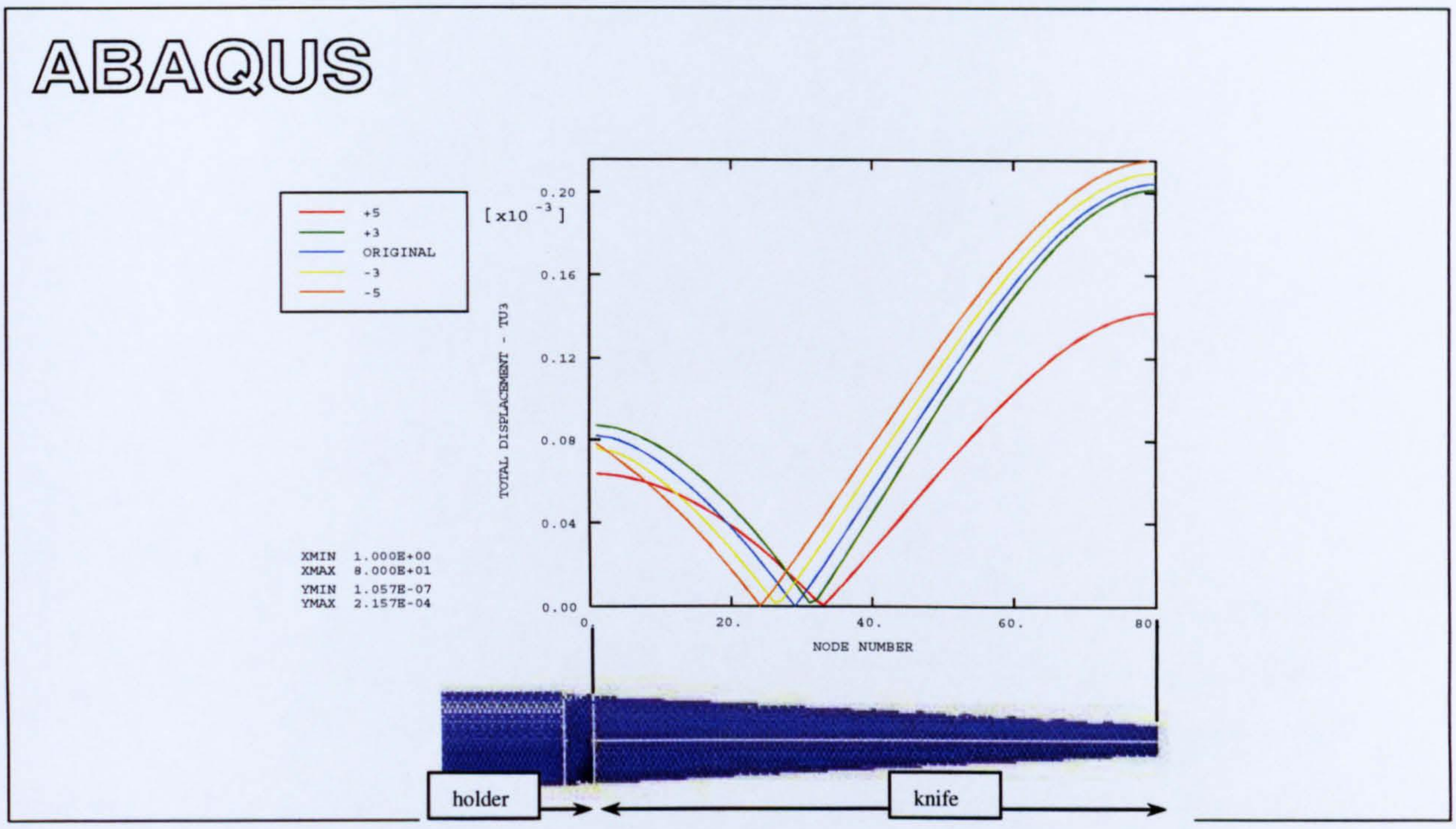

Figure 4.26. Amplitude variation of the cutting knife

4.4 Conclusions

This chapter reports on the main research challenges in the design of half-wavelength and wavelength ultrasonic blades used for cutting of food products. Ultrasonic cutting can be a reliable technology but the often conflicting design requirements for the isolation of the operating frequency and low stress distributions during cutting can only be addressed by vibration analysis. The vibration behaviour of these systems is characterised using a combination of FEA and EMA using a 3D LDV. The effects of geometry modifications on vibration responses and associated stresses have been discussed and improvements for enhanced performance proposed. Finally, it has shown how FE models can be used effectively to predict the sensitivity of modal parameters to geometry modifications to improve the design of cutting blades.

CHAPTER 5

THE DESIGN OF ULTRASONIC BLOCK HORNS

5.1 Introduction

Ultrasonic block horns are used in numerous industrial applications, such as welding and cutting, where they either operate as a tool directly vibrating on the work surface, or as an intermediate component acting as a transmission element between the transducer and the tool. Usually block horns are tuned to the first longitudinal mode at a frequency in the of 0 – 40 kHz range. Reliable operation of block horns is associated with the amplitude of vibration, uniformity of vibration amplitude at the working surface and the avoidance of modal participation by non-tuned modes at the operating frequency [4,6]. Although in the last ten years various researchers have provided practical design strategies to enhance the performance of simple block horns [3,4,7], block horns with elaborated geometries still exhibit reliability problems.

In this chapter the vibration behaviour of half-wavelength block horns is investigated in order to provide extra design insights to improve their performance. Initially the conventional principles of block horn design are illustrated with reference to the literature. Subsequently the vibration behaviour of a multi-slotted block horn of a multi-component cutting device is modelled and validated by EMA. The importance of mode shape characterisation is discussed and modes are classified using experimental data from 1D and 3D laser Doppler vibrometer measurements and finite element analysis.

5.2 Classification of resonators with wide output cross-sections

Usually ultrasonic components with wide output cross-sections are utilised in place of slender rod-type resonators (bar horns) for those applications requiring a large output area. The size of the horn output surface depends on the dimensions of the workpiece in contact with the ultrasonic tool. A classification of longitudinal mode components

with wide output surface on the basis of their geometrical shapes is given by Derks [16]. The three main groups are:

- cylindrical type, diameter > $\lambda/3$ (Figure 5.1(a))
- blade type, only one dimension > $\lambda/3$ (Figure 5.1(b))
- block type, both dimensions > $\lambda/3$ (Figure 5.1(c)),

where $\lambda/3$ corresponds to one third of the wavelength of the longitudinal wave. For the sake of simplicity, all components with at least one lateral dimension exceeding $\lambda/3$ will be called block horns.

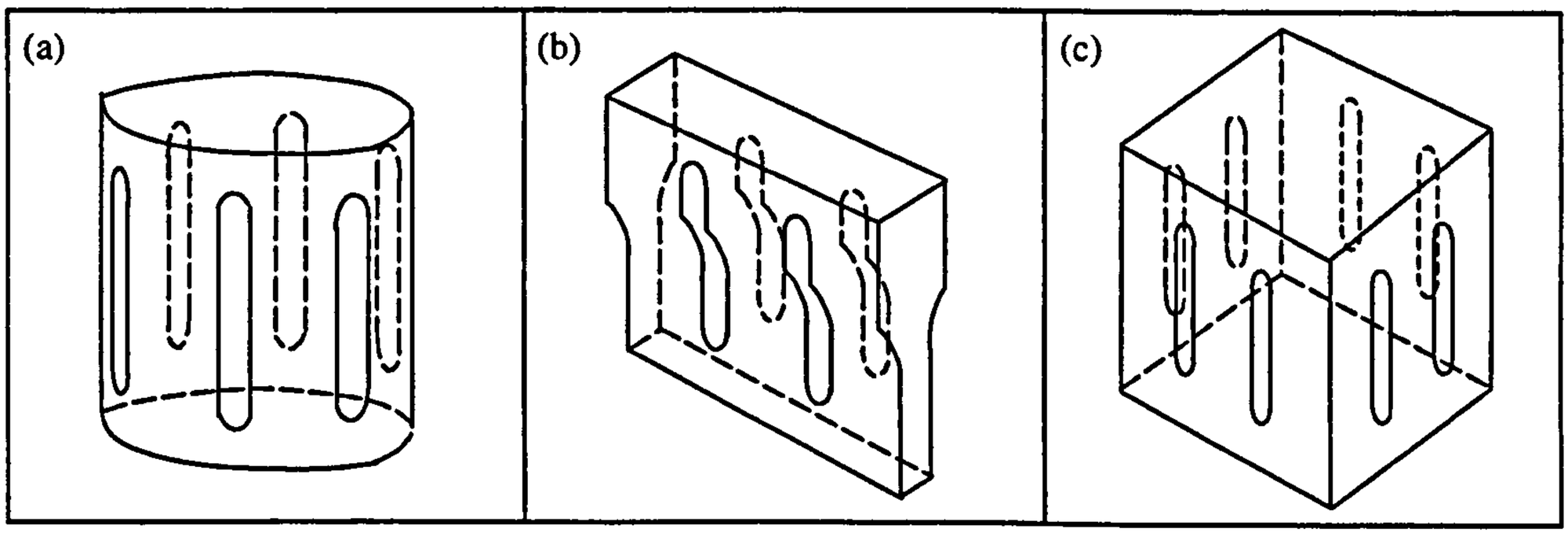

Figure 5.1. Horn classification: (a) cylindrical type, (b) blade type, (c) block type

Whereas the design of simple half-wavelength rod-type horns is possible by solving the equation of motion derived in section 3.4.1, theoretical calculation of the tuned length of block horns proves to be more complicated. Although Derks has provided validated theoretical models to calculate the dimensions of some basic block horn shapes, FE modelling currently constitutes the standard method used in horn design.

Despite the numerous manufacturing applications and the design experience gained through the use of FEA, the performance of block horns is often still unsatisfactory. Block horn problematic behaviour is mainly due to the modal density in the region of the excitation frequency. This is investigated in this section.

5.3 Design principles

Generally, the design of ultrasonic block horns is focused on satisfying three main performance criteria: isolation of the operating frequency from close non-tuned modal

frequencies, uniformity of amplitude at the working surface and sufficient amplitude in the operating mode. Research has shown that improved amplitude uniformity and frequency separation can be achieved by the inclusion of slots in the horn configuration [4,6], whereas higher vibration amplitudes are obtainable in block horns with tapered profiles [6,55].

A detailed strategy to control the vibration behaviour of block horns based on FE models was presented by O' Shea [4]. Formerly block horn design mainly relied on experience and a trial and error approach. O' Shea provided a design methodology for large ultrasonic horns through investigation of the effects of slot length, slot width, and the number of slots on mode shapes and natural frequencies. According to this method, uniformity of amplitude at the output surface and isolation of the longitudinal mode frequency could be predicted prior to machining.

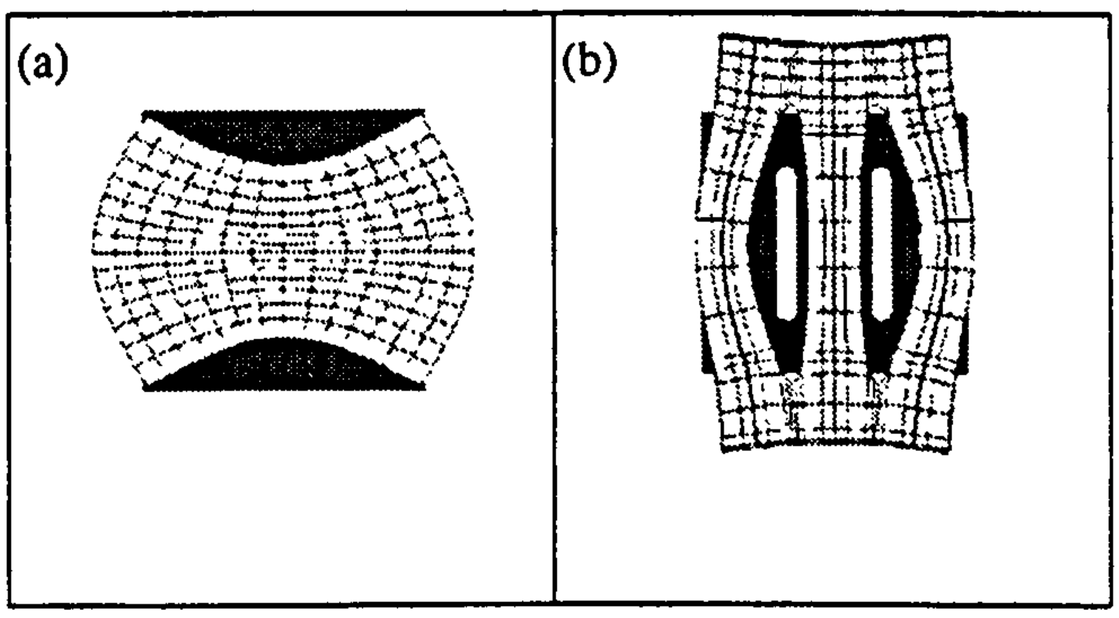

Figure 5.2. Longitudinal mode of block horns: (a) block horn with no slots, (b) double-slotted block horn

Figure 5.2(a) shows an FE model of the longitudinal mode at 35 kHz of a solid block horn with a lateral dimension exceeding $\lambda/3$. Poor uniformity of vibration amplitude on the block faces, due to Poisson's effect in the longitudinal mode, is predicted for this configuration. The uniformity requirement for a welding block horn, measured as the ratio of minimum to maximum response amplitude on the output surface, U_{min}/U_{max}, is estimated to be at least 80% [4]. A double-slotted block horn having the same global dimensions, modelled following the design rules for slotting introduced by O'Shea, is shown in Figure 5.2(b). Incorporation of two slots, having length, width and slot spacing of 1/3, 1/24 and 1/4 wavelength respectively, results in good amplitude uniformity (90%) and adequate isolation of the longitudinal mode (2300

Hz). According to O'Shea, a frequency isolation of at least 1 kHz of the tuned mode is necessary to avoid problems of modal coupling during operation.

Design techniques to isolate the tuned mode from close modes of differently profiled block horns, have also been proposed by Lucas [55] and Graham [7]. With a combination of laser based measurement techniques, ESPI and 1D LDV modal analysis and FEA, block horn dimensions were identified which could be modified in order to shift coupled modal frequencies away from the operating frequency. In particular, it was shown that the frequencies of the out-of-plane bending and torsional modes are highly dependent on horn thickness and the in-plane bending and longitudinal modes are largely independent. Hence, modal coupling between the longitudinal mode (in-plane mode) and out-of-plane modes was avoided via opportune horn thickness dimensioning.

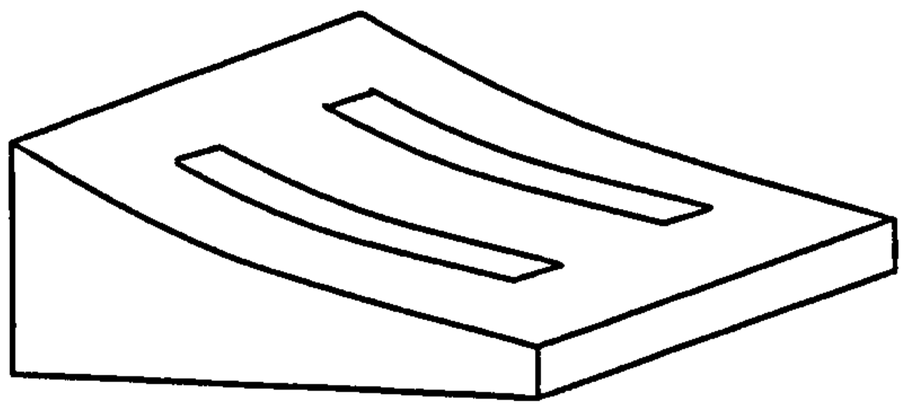

Figure 5.3. Model of an exponential block horn for welding applications

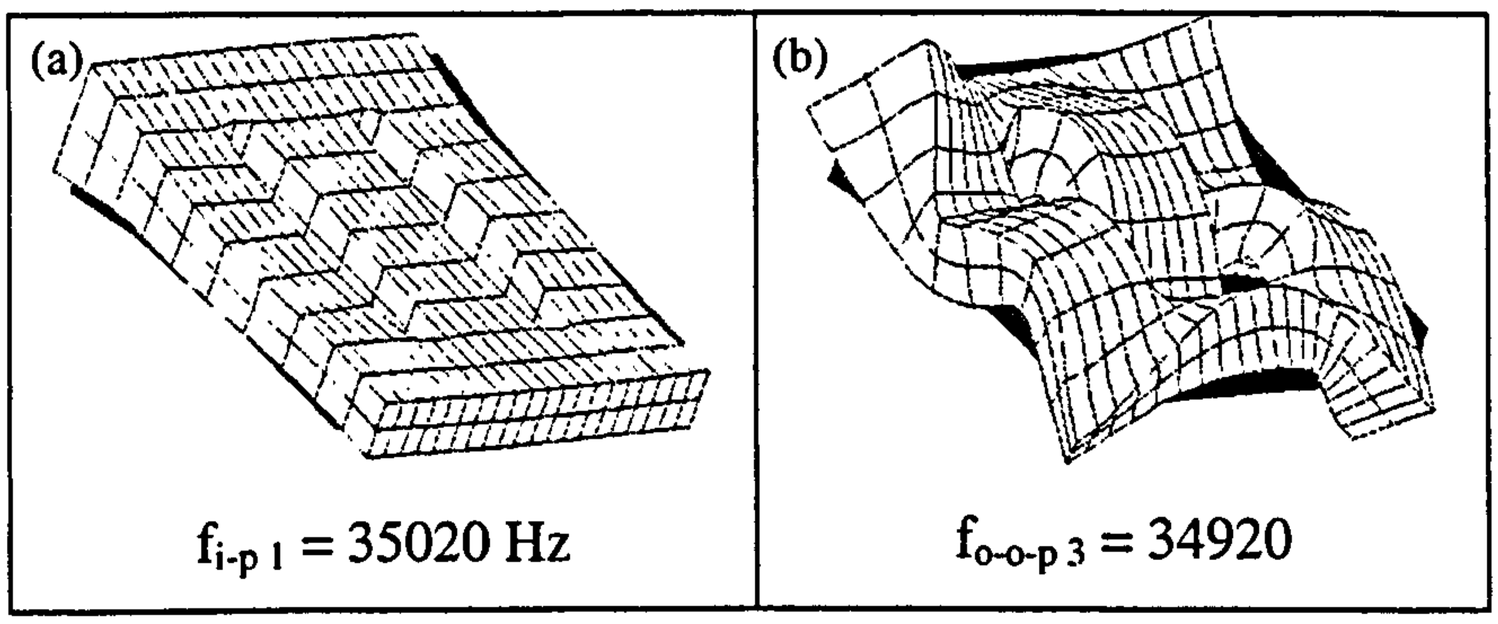

Figure 5.4. FE modal data: (a) Longitudinal mode,
(b) coupled out-of-plane bending mode

An application of this redesign approach is shown here for a double-slotted tapered welding block horn depicted in Figure 5.3. Results of the FE model of the horn predict the existence of modal coupling between the longitudinal mode (Figure 5.4 (a)) and an out-of-plane bending mode (Figure 5.4 (b)). The plot in Figure 5.5

illustrates the FE predictions of mode sensitivity to thickness alterations of the horn in the 20 - 45 kHz frequency range. Out-of-plane modes are indicated with the descriptor "o-o-p", whereas in-plane modes are indicated with the descriptor "i-p". A number, increasing with the modal frequency, is associated with the above descriptors to distinguish between modes of the same category. A thickness reduction of 10% is estimated to provide a 1 kHz frequency isolation of the tuned modal frequency (i-p 1) from the close out-of-plane modal frequency (o-o-p 3), thus, removing problems of modal coupling.

Despite the effectiveness of this design approach, it is not effective for block horns characterised by non-regular profiles, as simultaneous realization of all the performance criteria cannot be readily achieved. In particular, the required frequency isolation of the longitudinal mode is difficult to achieve for those components with highly tapered profiles and/or many slots, as they exhibit numerous bending modes near the operating frequency. Hence, careful identification of all the mode shapes and a measure of their responsiveness are required. Where there are a large number of modes at frequencies close to the tuned frequencies, identifying each mode and its responsiveness allows it to be categorised in terms of its participation in the response of the tuned mode via modal coupling. Strongly coupled modes can therefore be prioritised for shifting their modal frequencies in the redesign of the block horn. A multi-slotted block horn is studied to demonstrate this approach.

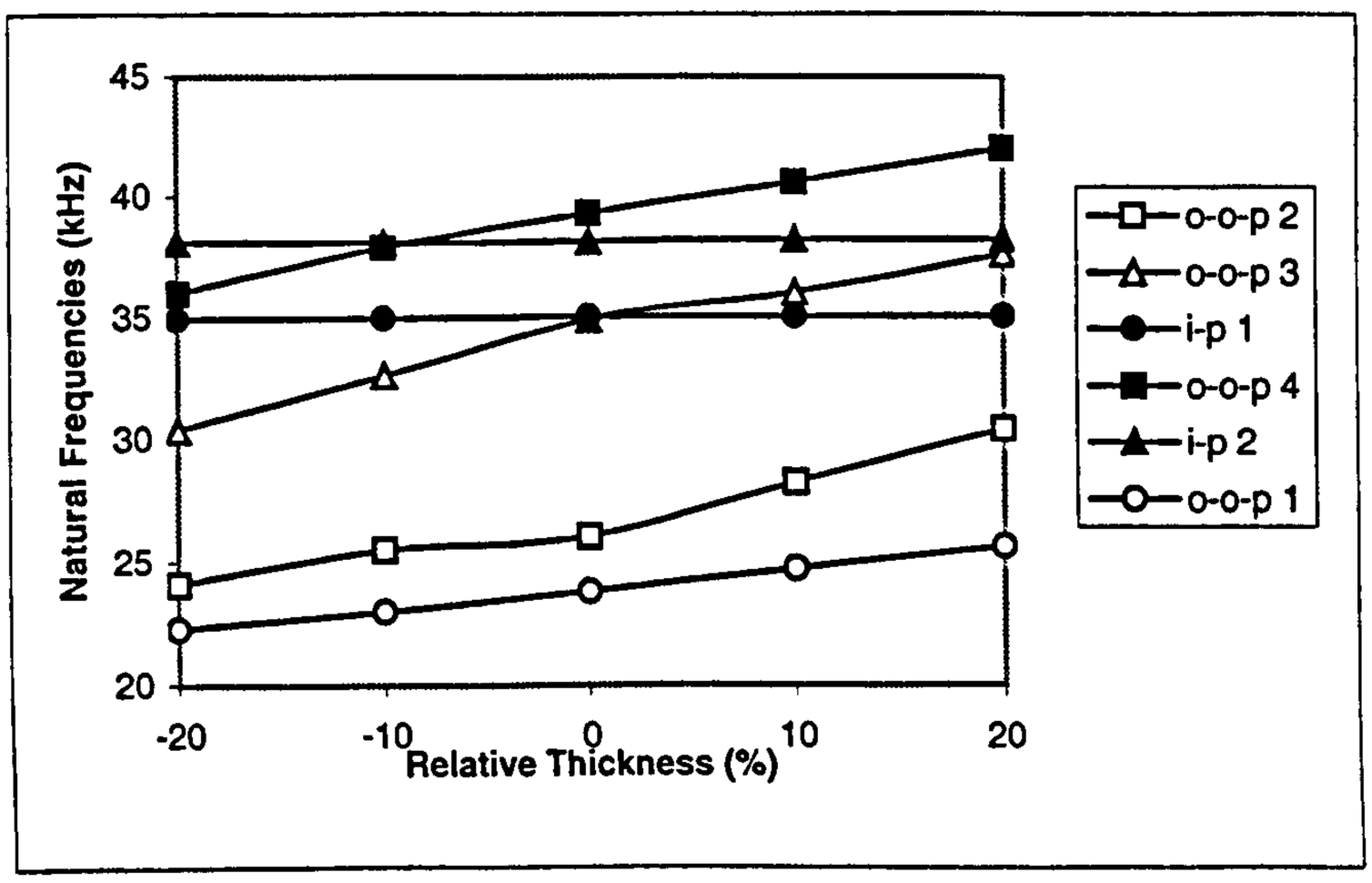

Figure 5.5. Effect of horn thickness on natural frequencies

5.4 Design of a half-wavelength block horn with fine slots

The vibration behaviour of an aluminium half-wavelength double-slotted block horn is investigated (Figure 5.6). The block horn is used as the intermediate component between the piezoelectric transducer and three cutting blades in an ultrasonic cutting device. The block horn also includes six fine slots, as shown in the figure, incorporated to improve amplitude uniformity on the output face of the block. The additional masses on the input surface are also used to improve amplitude uniformity.

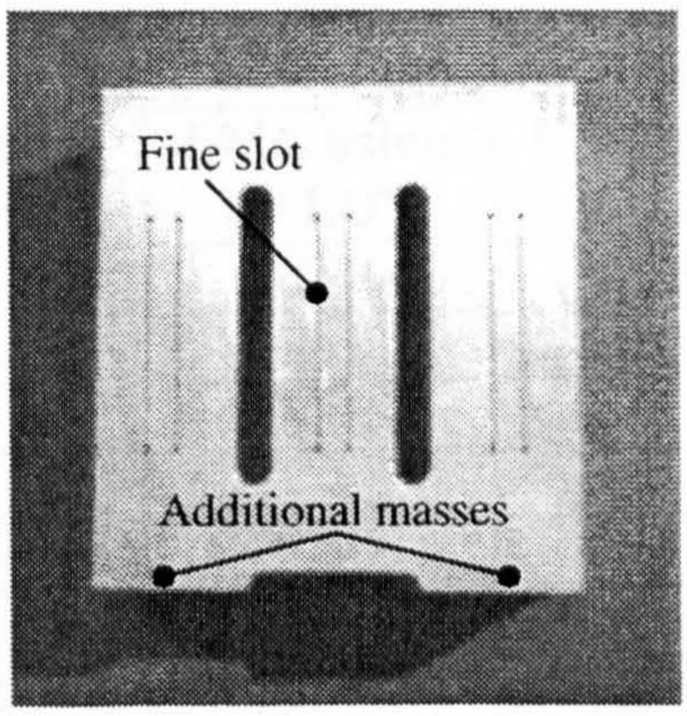

Figure 5.6. Double-slotted block horn with six fine slots

FEA and EMA of the block horn are performed to investigate its vibration behaviour. In order to demonstrate the importance of measuring vibration velocities in the space, first, measurements using a 1D LDV, which detects only normal to surface responses, are performed. The modal frequencies are determined by random excitation test in the 0-40 kHz frequency range. The 2^{nd} and 3^{rd} columns of Table 5.1 show a comparison of the predicted and measured natural frequencies, respectively. Experimental values, although in good agreement with the calculations, allow identification of only some of the predicted modes of vibration. This is partly because the ultrasonic transducer is unable to excite all the natural frequencies of the attached component. Also, as the 1D LDV measures only the normal to surface component of velocity, a number of modes involving in-plane motions of the horn columns turn out to be either undetected or incomplete. Figure 5.7 depicts the FE and EMA modal data of two in-plane modes of the horn involving bending motions of the columns. For instance, correlation between the predicted mode shapes (Figure 5.7 (a,b)) and the corresponding measurements performed with 1D LDV (Figure 5.7 (c,d)) proves inadequate for allowing validation of the FE model.

Subsequently, EMA is performed using a 3D LDV, which allows one out-of-plane and two in-plane components of the vibration velocity response of the surface of the block to be detected. The corresponding measured data, reported in the 4th column of Table 5.1, clearly shows how the 3D LDV improves the experimental modal analysis allowing the identification of almost all the predicted modes in the considered frequency range. The ability to measure the three components of velocity provides very accurate mode shapes (Figure 5.7 (e-f)), improving validation of FE results.

Block Horn Modal Frequencies (Hz)				
Mode No.	Finite Element Analysis (FEA)	EMA using 1D LDV	EMA using 3D LDV	Error (%) (FEA- 3D LDV)
22	28155	28349	28396	- 0.8
23	28642	-	27922	2.6
24	28824	28146	28135	2.4
25	30071	-	-	-
26	30474	-	30192	0.9
27	31151	-	30415	2.4
28	32522	32910	32893	- 0.1
29 (*)	34921	34951	35024	- 0.1
30	35404	35454	35468	0.0
31	36040	35847	35944	0.1
32	36096	35177	35172	2.5
33	36118	35218	35214	2.5
34	37000	-	38039	- 2.7
35	37002	35324	35320	4.7
36	38672	-	-	-
37	39786	-	37470	6
38	39824	38691	38716	2.8

(*): Tuned longitudinal mode

Table 5.1. Block horn mode frequencies in the range (28kHz – 40kHz)

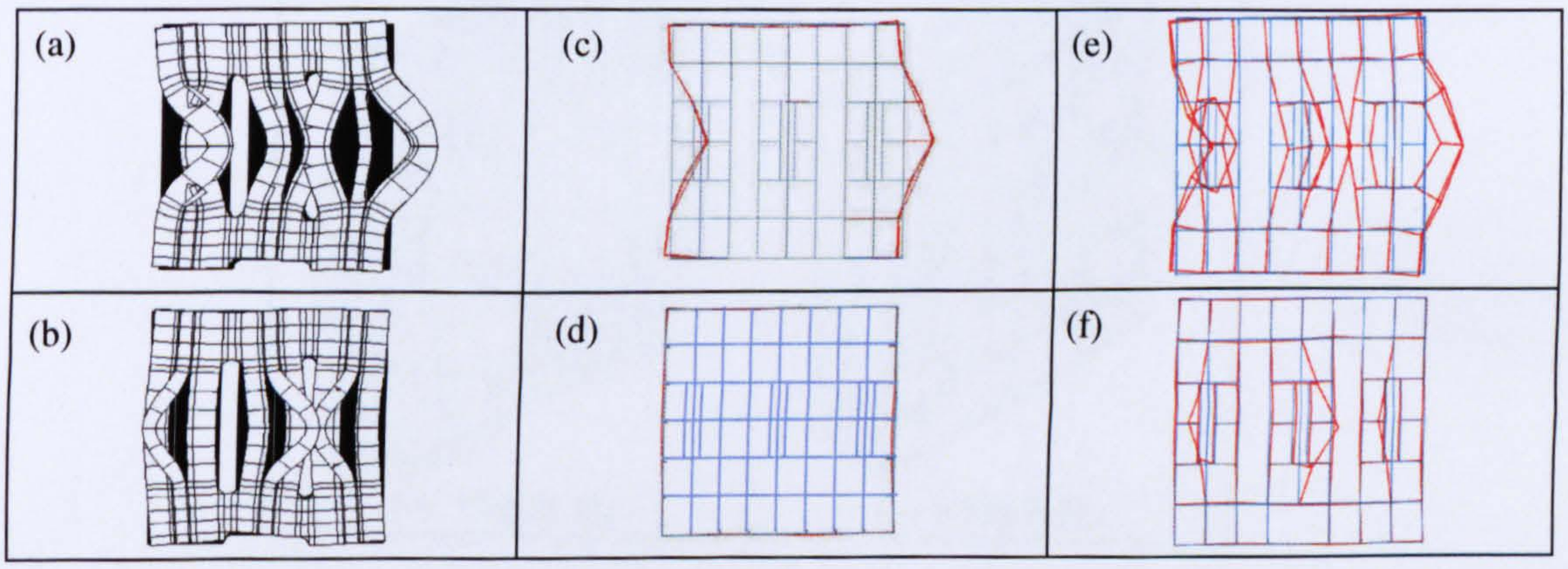

Figure 5.7. Comparison of mode shapes determined by FE (a-b), 1D LDV (c-d), 3D LDV (e-f)

5.4.1 Modal coupling

Predictions and measurements of the block horn vibration behaviour highlight the presence of three modes of vibration occurring at frequencies 35172 Hz, 35214 Hz and 35468 Hz, very close to the longitudinal frequency at 35024 Hz. Since a frequency separation of 1 kHz of the tuned mode is required, according to O'Shea's method, a horn modification should be made to isolate the operating frequency from these three modal frequencies.

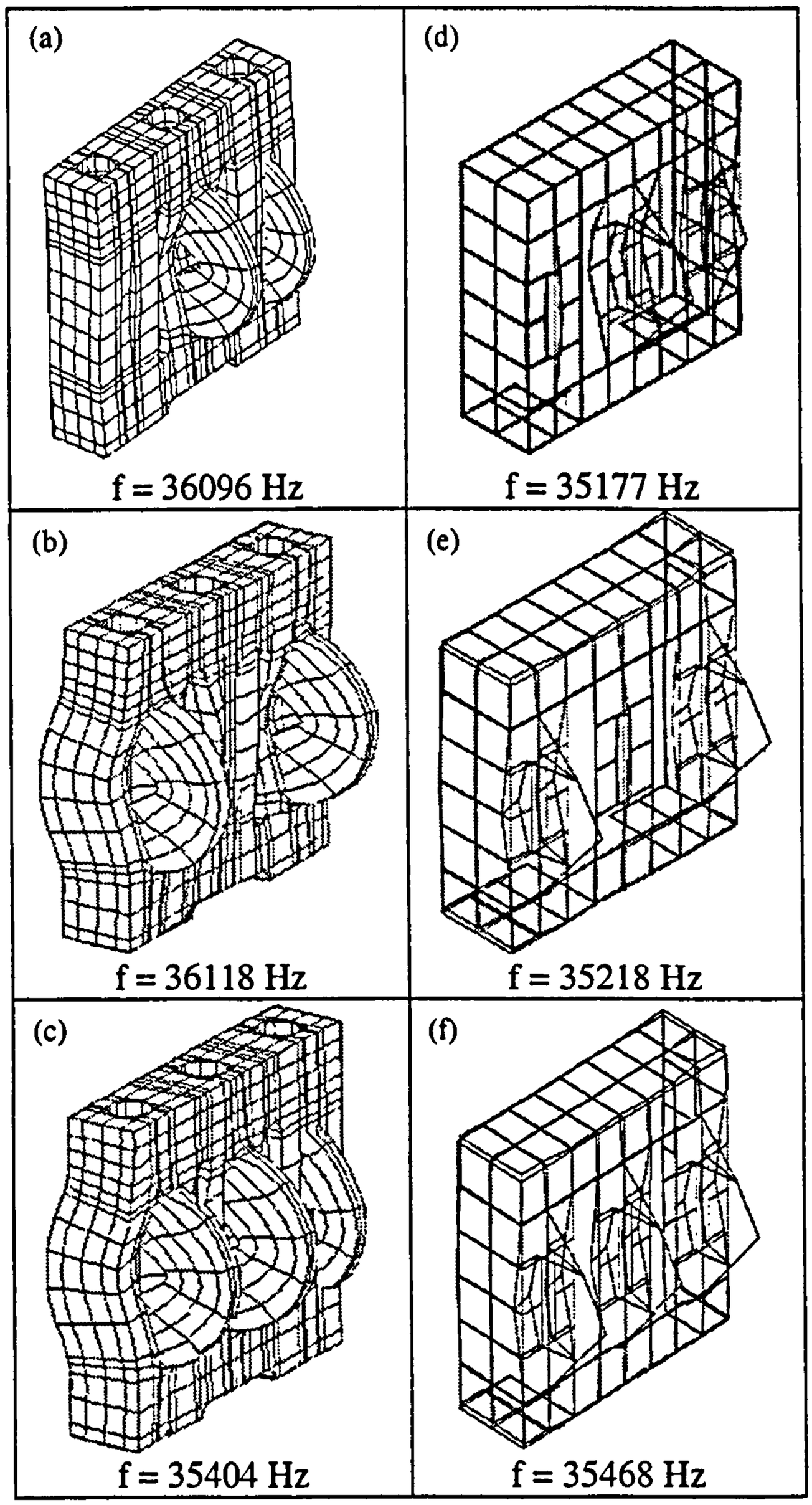

Figure 5.8. Comparison of mode shape due to the flexural motion of the inner columns determined by (a-b-c) FEA, (d-e-f) EMA using 3D LDV

First, two observations regarding the three modes can be made. As shown in Figure 5.8, with a correlation between FEA and EMA data lower than 3%, the modes are characterised by different phase variations of the out-of-plane vibration of the horn columns, none of which involve deformation of the output surface. Also, the sum of the FRF measurements illustrated in Figure 5.9 shows that the modes are largely unexcited by the transducer. Consequently, modal coupling between the longitudinal mode and these neighbouring modes does not prevent the system from running in the operating mode with high amplitude uniformity, as shown in Figure 5.10. For these three modes, although they all couple with the longitudinal tuned mode, it is not necessary to shift their modal frequencies because their response participation in the tuned mode is negligible under longitudinal excitation.

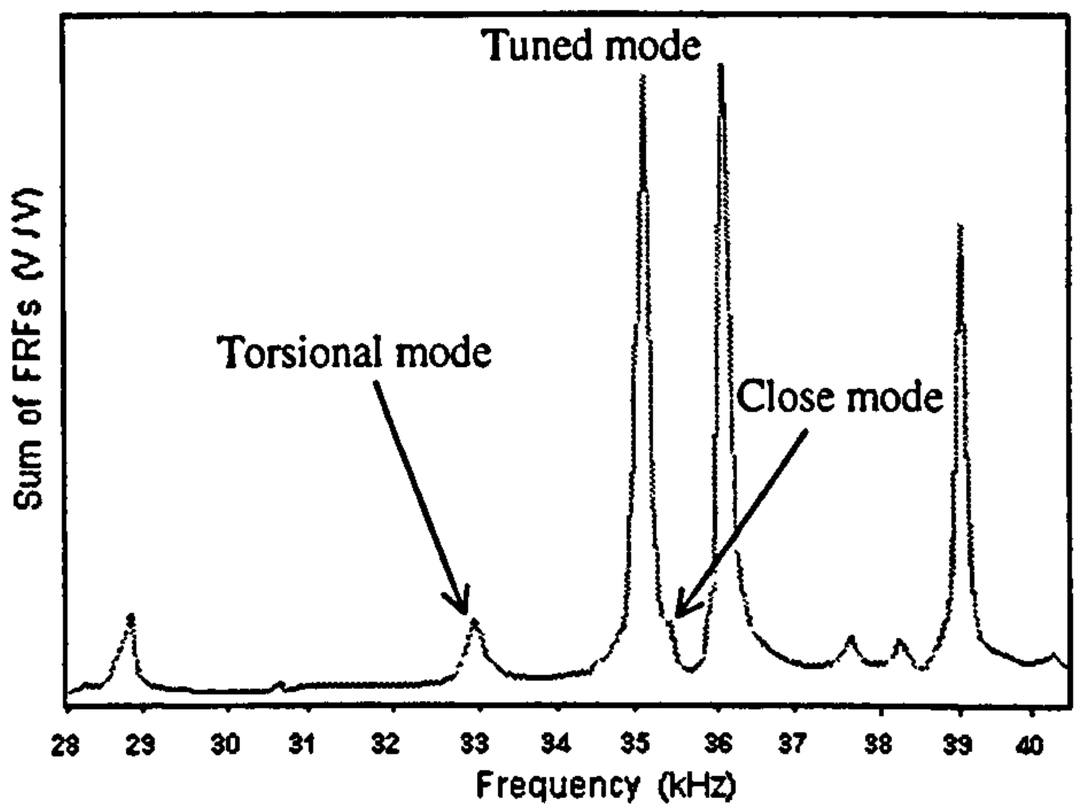

Figure 5.9. Sum of the FRFs measured on the block horn with fine slots

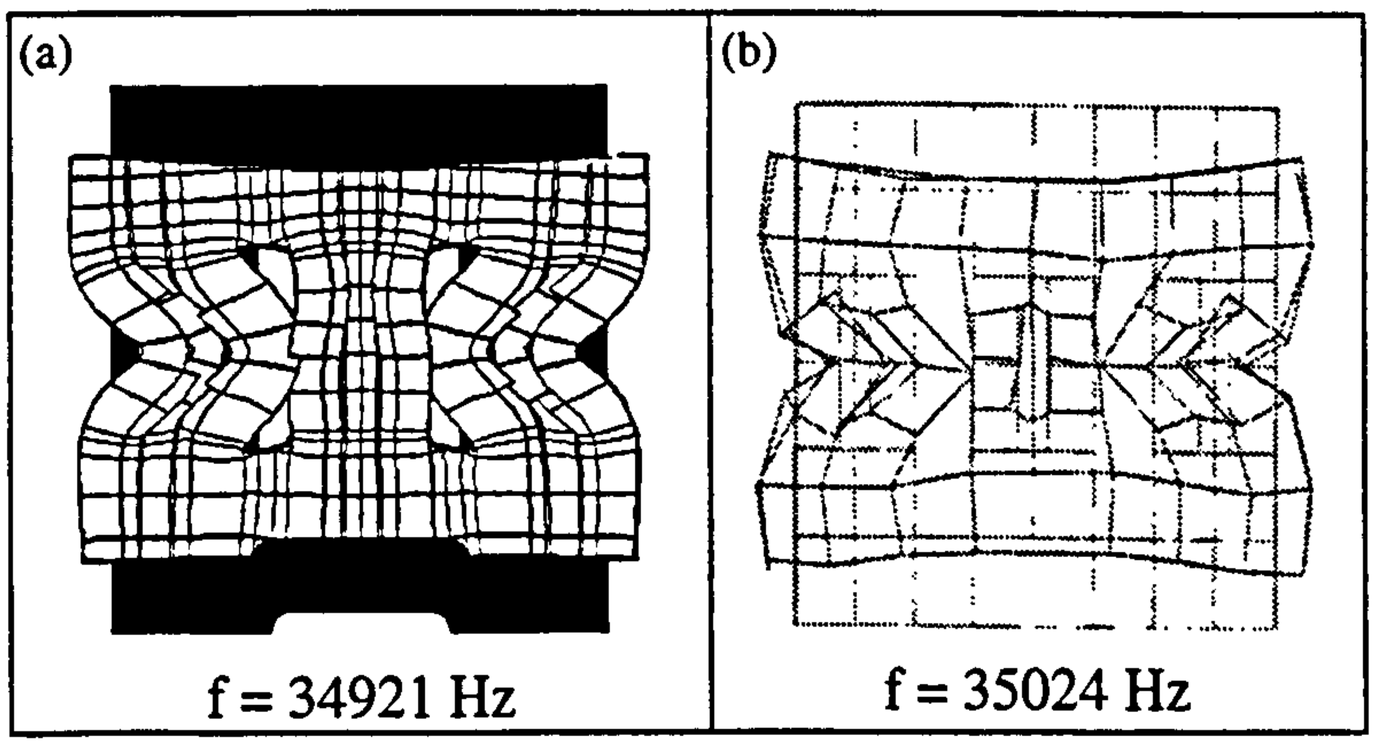

Figure 5.10. Comparison of longitudinal mode shape determined by (a) FEA, (b) EMA using 3D LDV

The modal frequency sensitivities to altering the thickness of the block horn are shown in Figure 5.11 for a number of modes with modal frequencies close to the tuned frequency. Sufficient frequency isolation of the tuned mode is predicted for a 20% increase in the horn thickness. However, it is also necessary to consider the effects on other natural frequencies which critically lie outside the frequency range of concern. For example, the frequency of the torsional mode, Figures 5.9 and 5.12, is predicted in Figure 5.11 to increase for thickness increases, reaching 34.01 kHz for the estimated thickness adjustment, barely satisfying O'Shea's requirement for frequency separation.

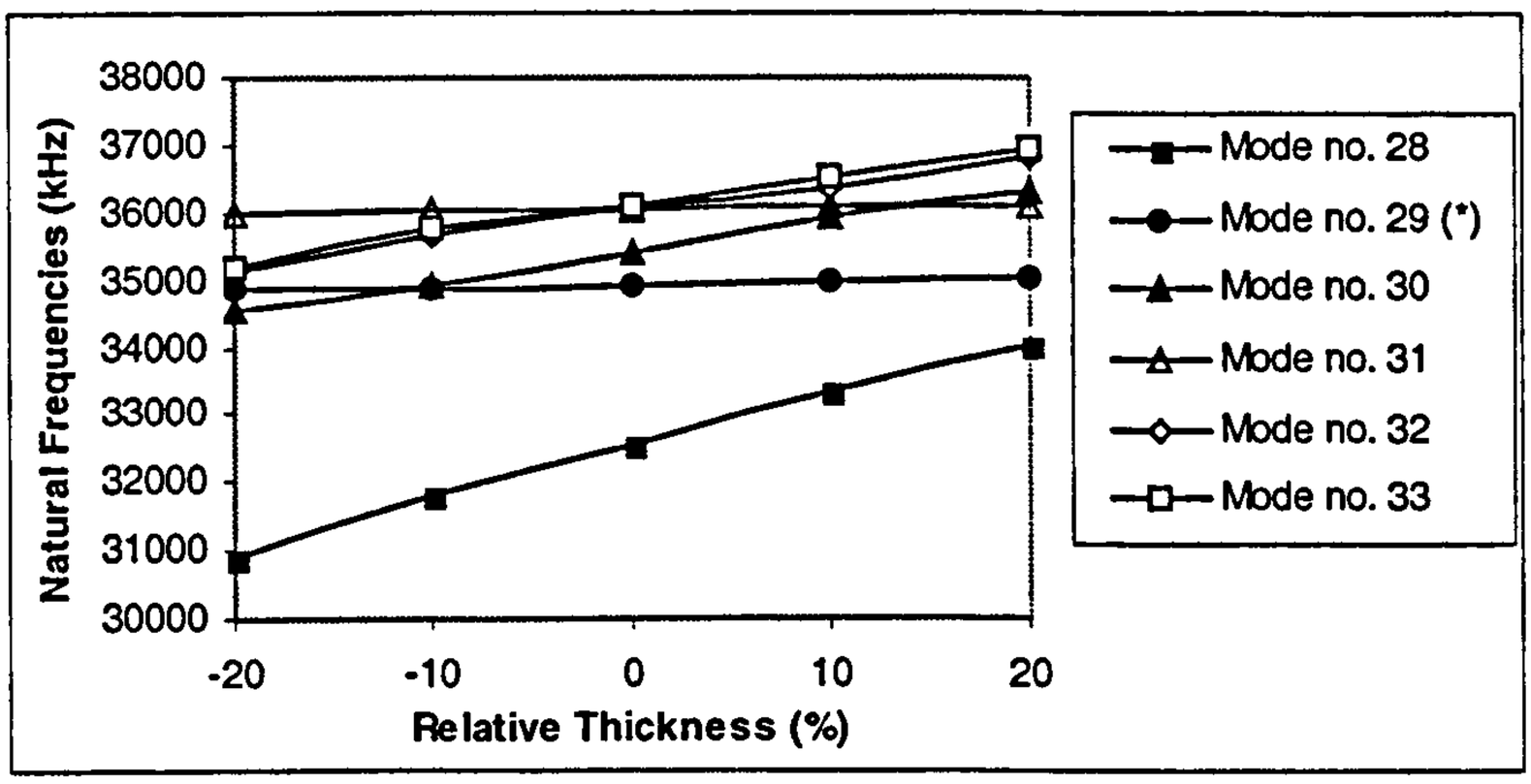

Figure 5.11. Effect of horn thickness on natural frequencies

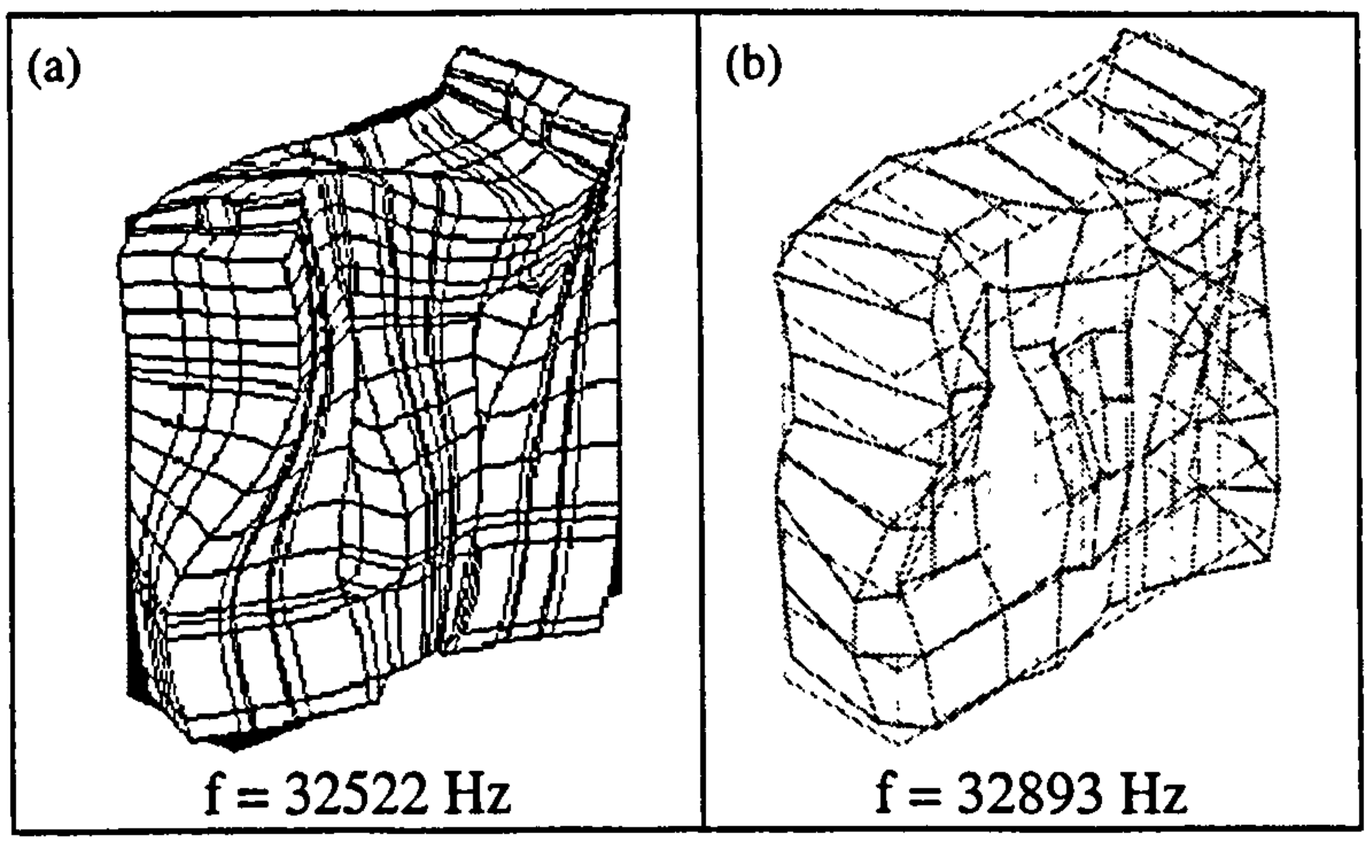

Figure 5.12. Comparison of torsional mode shape determined by FE (a), (b) 3D LDV

Since a small error (< 4%) between the measured and predicted torsional and longitudinal frequencies of the redesigned block horn is typical, modal coupling

between these modes is possible. A torsional contribution to the longitudinal vibration of the output surface would lead to poor performance of the block horn.

Hence, having established that modal coupling in the original horn profile is not affecting the performance, whereas alterations of the horn thickness may result in unwanted torsional motions, no alteration of the block horn is performed.

5.4.2 Modal families

From the FEA and EMA results it emerges that incorporation of slots considerably enriches the number of modes of a block horn and incorporating fine slots results in numerous modes appearing in the frequency spectrum. The response is characterised by the appearance of mode families. These are families of multiple modal frequencies, characterised by a common mode shape of the columns with each mode being differentiated by spatial phase variations between adjacent columns. A mode family usually appears as a cluster of modes in a narrow frequency band and the excitation of these families significantly enriches the frequency response spectrum. Figure 5.13 shows two such mode families whose common feature is the in-plane motion of the horn columns. Their experimental detection and identification with predicted modes is only possible through 3D LDV measurements.

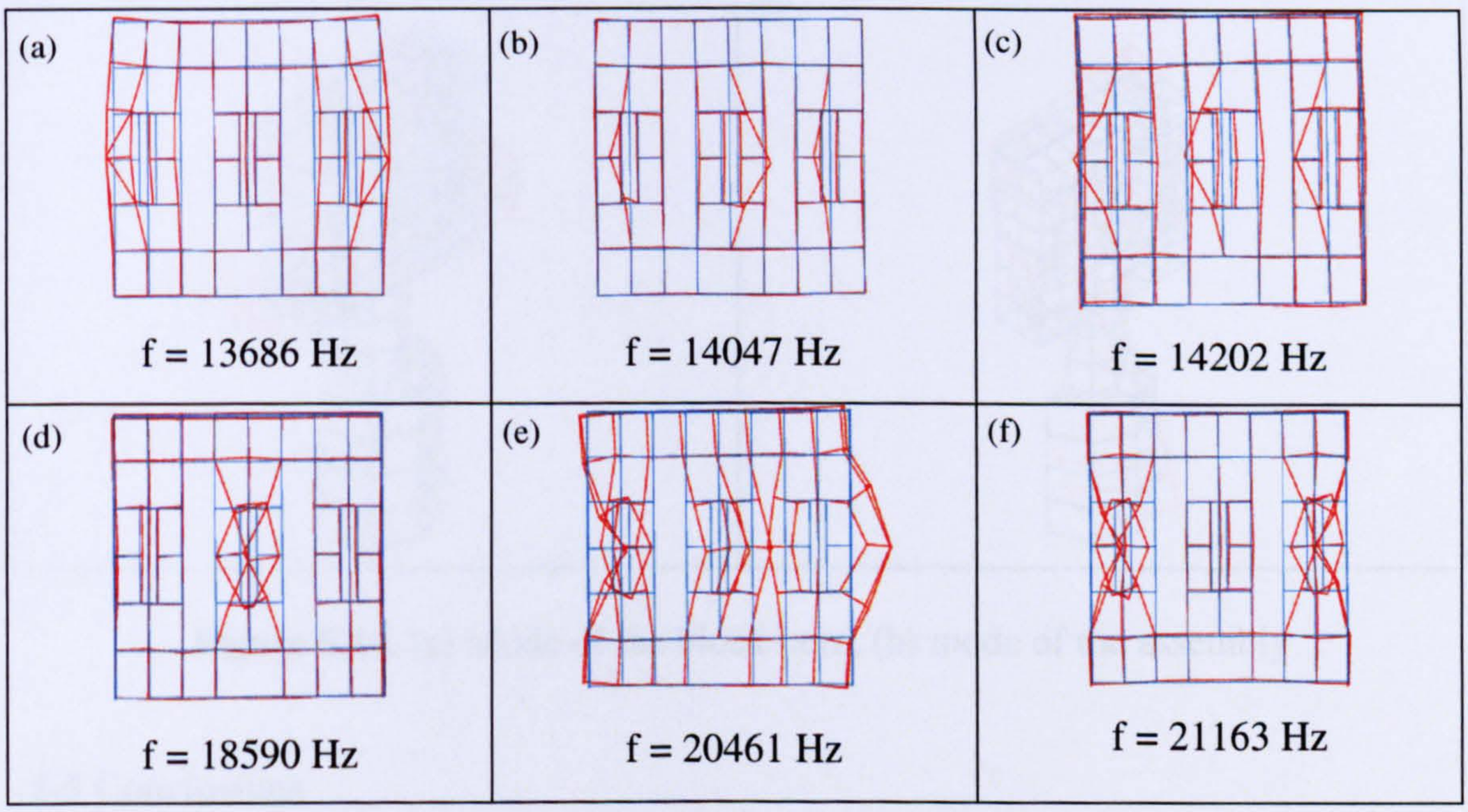

Figure 5.13. Two measured mode families characterised by spatial phase variations between adjacent columns: (a-c) first family, (d-f) second family

5.4.3 The effect of transducer coupling

Previous research on transducer-horn assemblies has shown that excitation of all the vibrational modes predicted for the horns is not possible [6]. Similarly, for the investigated transducer-block horn stack, despite the great accuracy of the 3D LDV measurements, several modes predicted for the horn model are undetected in the 0-40 kHz range due to the difficulty in exciting a measurable response using the longitudinal transducer. However, modal measurements do highlight the presence of a number of modes which are not predicted by the block horn FE model. EMA of the whole assembly, including measurement of the transducer surface, allows identification of these modes. Such modes, characterised by simultaneous responses of the transducer and block horn, cannot be anticipated by FE modelling of the block horn alone. Figure 5.14 (a) depicts a measured mode shape characterised by in-plane motion of the block, which has been predicted by the horn FE model. On the other hand, Figure 5.14 (b) illustrates the detected mode shape of a system mode composed of out-of-plane motions of the horn and transducer, which is not predicted by FE model. Measurement of whole system modes proves to be as important as detection of the horn modes, and this highlights the importance of including the transducer in the FE model.

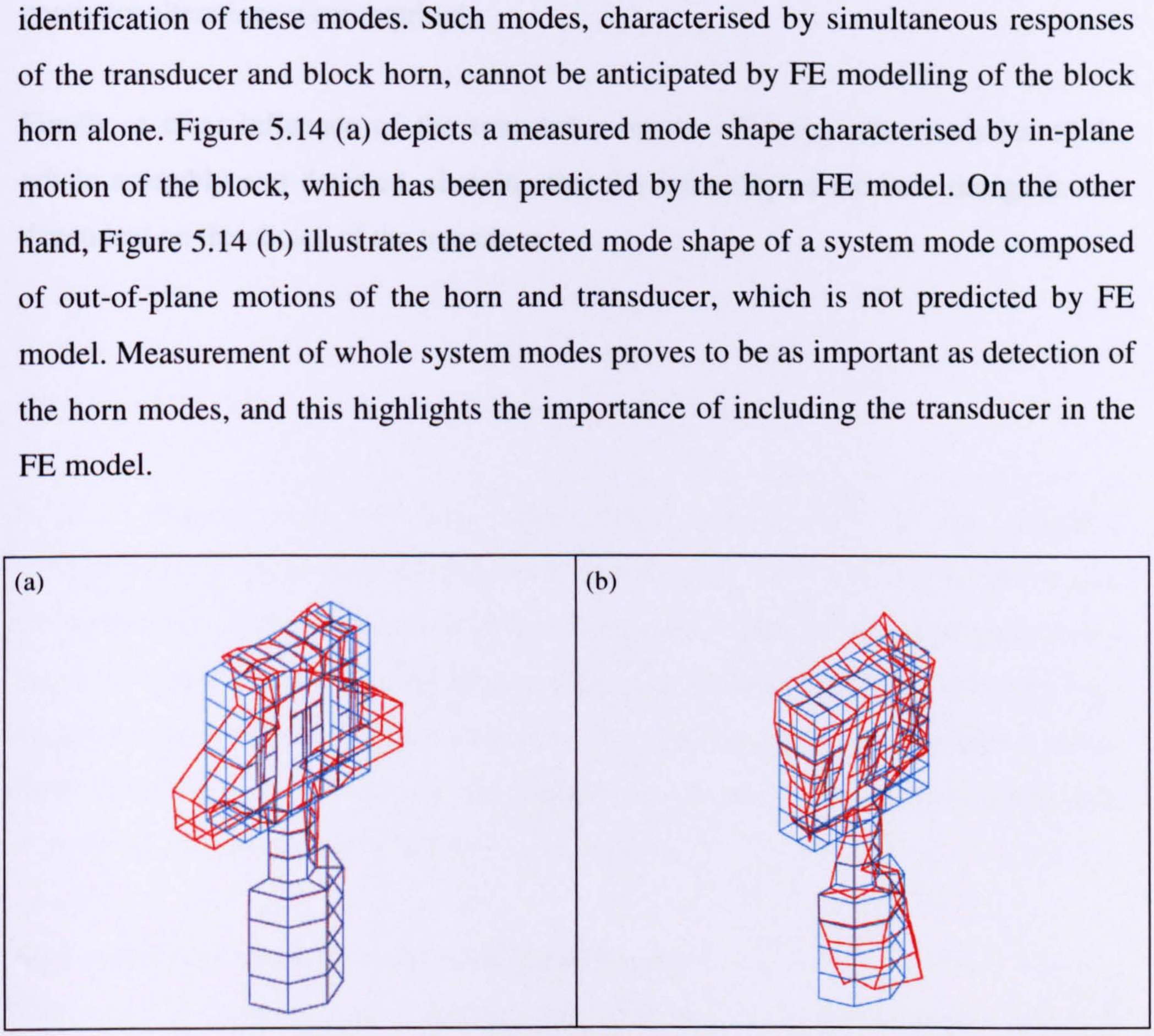

Figure 5.14. (a) Mode of the block horn, (b) mode of the assembly

5.5 Conclusions

This chapter has concentrated on the identification and classification of modal behaviour of block horns. To achieve accurate mode identification a combination of

FEA and EMA have been performed. It has been demonstrated that the ability to measure the three components of vibration velocity using the 3D LDV provides very accurate mode shapes allowing improved validation of FEA models.

The use of 3D LDV was also crucial in the response characterisation of a block horn incorporating fine slots. Due to the multi-slotted profile the horn spectrum was characterised by the appearance of numerous modes, with three of them coupling with the tuned mode. Measurements of the response amplitude of the coupling modes revealed that their participation in the tuned mode was negligible; therefore no geometry alterations were required.

Finally, a clear influence of the transducer on the vibration characteristics of the whole assembly was detected, showing that the reliability of the horn design is also dependent on the choice of the transducer.

CHAPTER 6

THE DESIGN OF ULTRASONIC CUTTING HEADS

6.1 Introduction

High power ultrasonics can be applied in manufacturing operations requiring a large number of tools, such as multiple-blade cutting operations or simultaneous multiple-welding tool operations. However, in order to make these applications cost-effective, where possible it is advantageous to minimise the number of generator and transducer systems. For example, several cutting blades can be attached to a wide output face block horn driven by a single transducer. For multiple welding tool operations, the number of tools can be kept small if the output face of the welding block horn is as large as possible. However, the vibration behaviour of such complex systems leads to frequent component failures and poor operating performance.

In this chapter, numerical and experimental investigations of the vibration characteristics of multi-blade cutting heads, tuned to resonate in a longitudinal mode, are performed. A characterisation of the effects of the individual components on the assembly's performance is carried out in order to provide the basis for improved design strategies of complex ultrasonic systems. In particular, the importance of mode shape identification is discussed and modes are classified using experimental data from 3D LDV measurements and FEA.

6.2 Three-blade cutting heads – Design principles

The design of complex cutting systems consisting of three high-gain blades attached to an intermediate block horn, such as the one depicted in Figure 6.1, is the subject of this section. Usually, each component of a cutting assembly is designed in the form of a half-wavelength unit resonating in the first longitudinal mode of vibration at the frequency provided by the transducer. The most practical solution is to attach the cutting blades to the block horn via threaded studs, as manufacturing the entire stack in one piece is problematic.

For simplicity, the block horn depicted in the figure has a constant cross section. However, amplitude gain can be designed into the block may be needed at the blade tips, which can be achieved through tapering of the horn profile. Distribution of the amplitude gain between the system components by using tapered block horns can also be a useful way to reduce blade stress.

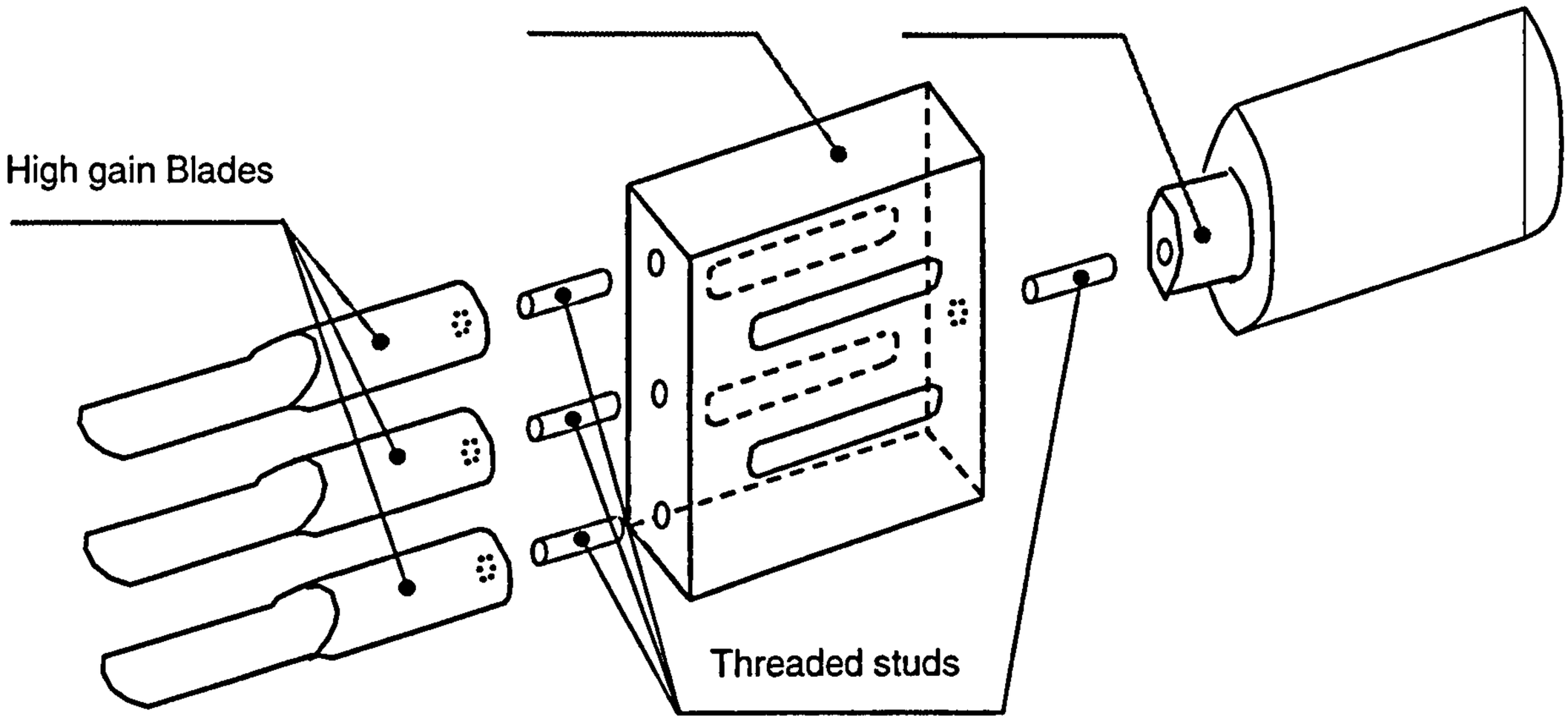

Figure 6.1. A three-blade cutting head assembly

In the previous chapter, it was shown that reliable performance of block horns is normally associated with uniformity of the amplitude of vibration at the working surface and the avoidance of modal participation by coupled non-tuned modes at the operating frequency. The design of block horns acting as transmission elements between the transducer and attached blades requires, perhaps, even more care than the design of block horns used as working tools. Certainly, the longitudinal mode at the tuned frequency should be such that, at the output surface where the blades are attached, the vibration amplitude is as uniform as possible. In this case, the blades will have equal and in-phase vibration displacement input. If the surface amplitude is not uniform, for instance due to Poisson's effect in the longitudinal mode, the required operating amplitude at the blade tips would not be achieved. However, even for systems where the block horn output surface exhibits very high uniformity of vibration amplitude, the attached blades can exhibit non-identical vibration responses, including bending and torsional responses. Furthermore, isolation of the tuned mode

frequency from other modal frequencies is particularly difficult to achieve for complex systems because they are characterised by a high number of modes of vibration.

The design of a three-blade cutting head is investigated by analysing the effects of block horn and blade geometries on the vibration response and stress condition. Design improvements are suggested and the general applicability of these issues in ultrasonic system design is discussed.

6.2.1 Vibration analysis of a three-blade cutting head

Figure 6.2 shows an ultrasonic cutting head used for cutting food products, where a double-slotted block horn drives three equally spaced tuned cutting blades. All components of this system are half-wavelength units tuned longitudinally to 35 kHz. The system is used to slice slabs of food product. This cutting device is designed to provide 65 μm pk/pk of amplitude at the tip of each blade when driven in resonance by the transducer. The block horn and blades of the assembly have been discussed previously in Sections 5.4 and 4.4.2, respectively.

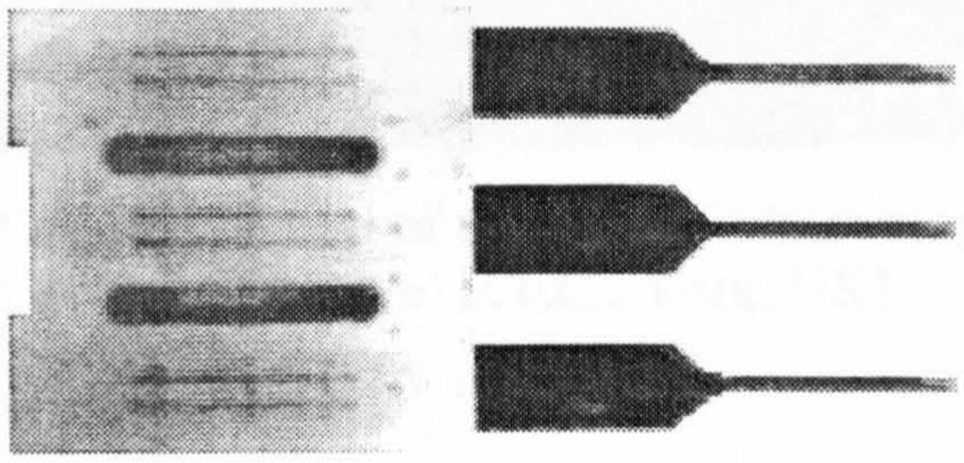

Figure 6.2. Three-blade cutting head

Figure 6.3 shows the experimental rig set-up to determine the fatigue life of the cutting head. Tests have been carried out on a single head under the power loading and amplitude that the system would undergo in normal use on a production line. On a production line, ten cutting heads would stand side by side separated by a few millimetres. Trial outcomes showed that the assembly cuts effectively when immersed in the material, but blade failures occur when the head is withdrawn from the material. Also, the system becomes noisy in air and the response suddenly changes into a multi-

frequency response exhibiting what appears to be a nonlinear behaviour. Hence, a number of factors seem to be responsible for blade failure.

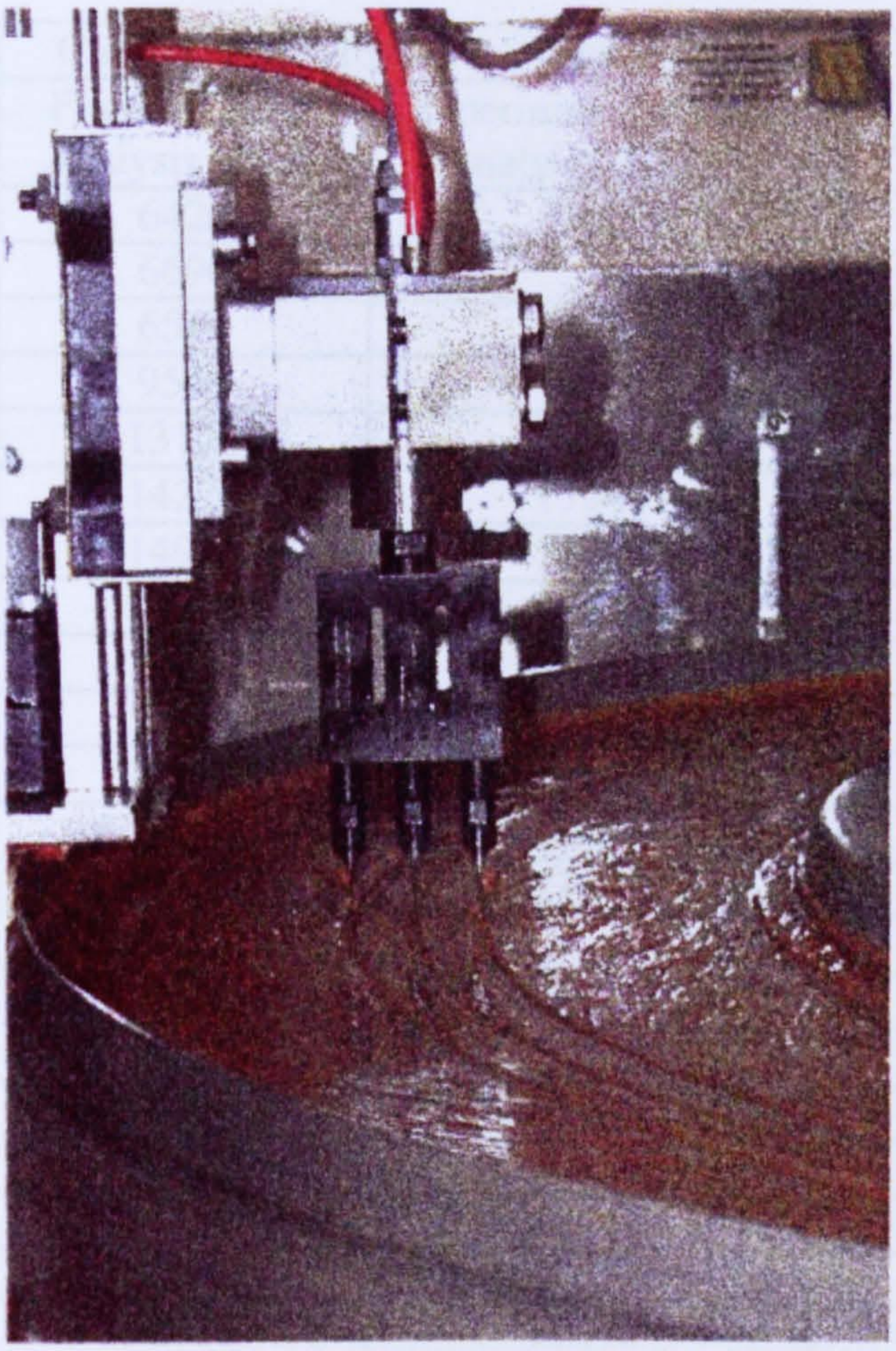

Figure 6.3. Fatigue trial of the three-blade cutting head
[photo provided by Nestle' P.T.C., York, UK]

In order to understand the vibration behaviour of the head, a FE model of the whole assembly is created and subsequently validated by EMA performed using a 3D LDV. Finite element results correlate well with the measured modal behaviour at low excitation, allowing identification of almost all the predicted modes in a 0-40 kHz frequency range as shown in Table 6.1. The large number of modes is the result of the complexity of the cutting assembly.

Four mode categories are identified: (a) modes where blade responses dominate, (b) modes where block horn responses dominate, (c) modes of the block and blades assembly, and (d) modes of the transducer, block and blades assembly. The last group

is neglected in the following discussion, since all the detected modes are predicted by the head model without including the transducer.

	Cutting Head Modal Frequencies (Hz)		
Mode no.	Finite Element Analysis (FEA)	Experimental Modal Analysis (EMA)	Error (%)
1	6420	6645	-3.3
2	6690	-	-
3	6550	6699	-2.3
4	9540	9842	-3.1
5	13120	13374	-1.9
6	14220	13946	2.0
7	14970	14614	2.3
8	17020	16559	3.0
9	17040	16773	2.6
10	17120	17037	1.0
11	17130	17165	-0.1
12	18800	18669	0.1
13	20710	21019	1.5
14	21135	-	-
15	21380	-	-
16	22230	21995	2.0
17	22270	22151	0.5
18	22280	22378	-0.4
19	28890	30215	-4.4
20	31510	32426	-2.8
21	32010	33110	-3.3
22	32600	33596	-3.0
23*	34580	34999	-1.2
24	35890	35298	1.7
25	34840	35330	-1.4
26	36370	36382	0.0
27	36500	-	-
28	36920	36954	0.0
29	37330	37330	0.0
30	37900	37582	-
31	38380	37976	1.0
32	38170	37991	0.5
33	39770	38630	2.9
34	40130	39881	0.1

Table 6.1. Cutting head modal frequencies in the range (0-40 kHz)

6.2.1.1 Head modes dominated by blade responses

Experimental modal data has shown that many modes of vibration of the three-blade cutting head are essentially characterised by blade motions. The frequencies of such

modes are very close to the natural frequencies measured in the single blade system investigated in Section 4.2.3, where an identical single blade is driven by the transducer.

Modes of the transducer-blade system	**Mode families of the three-blade cutting head**		
	1st mode	2nd mode	3rd mode
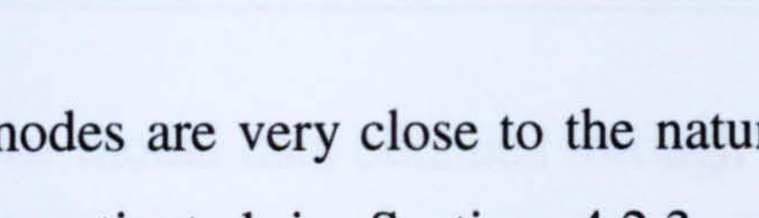 EMA: f= 6631 Hz	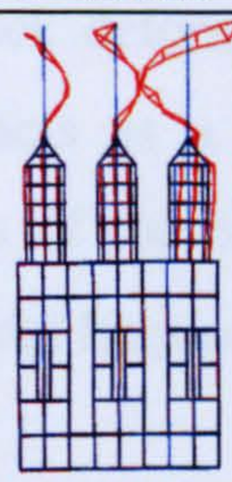 EMA: 6645 Hz	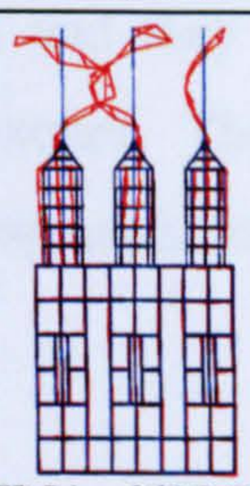 EMA: 6699 Hz	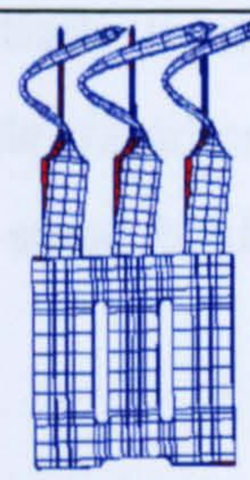 FE: 6690 Hz
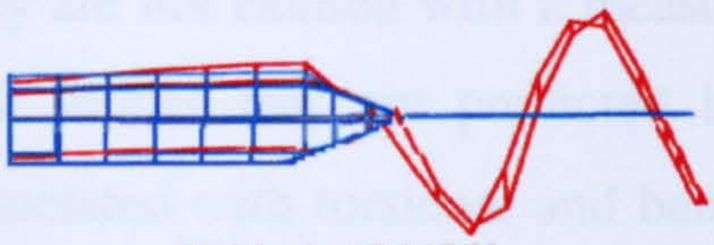 EMA: f=17465 Hz	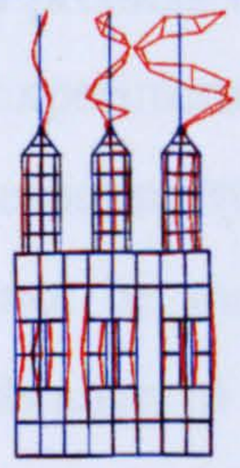 EMA: 16559 Hz	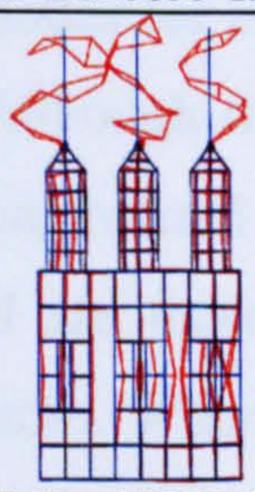 EMA: 16773 Hz	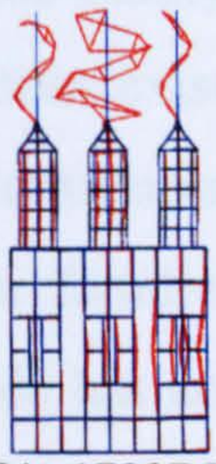 EMA: 17037 Hz
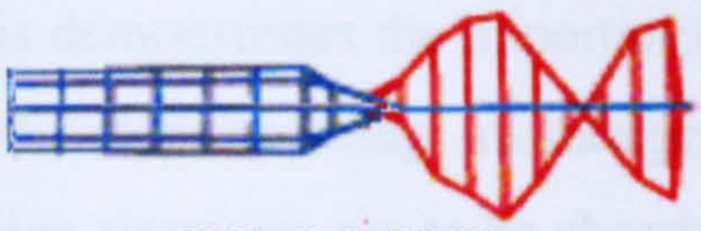 EMA: f=22287 Hz	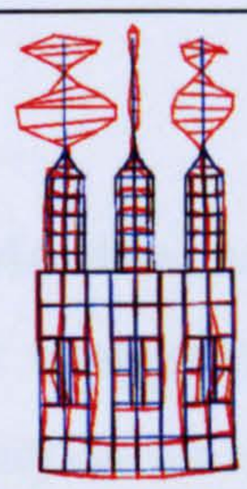 EMA: f=22378 Hz	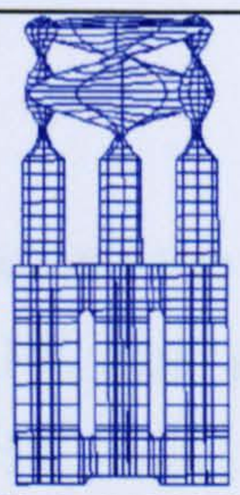 FE: f=21380 Hz	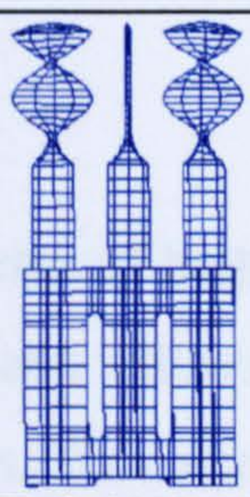 FE: f=21135 Hz
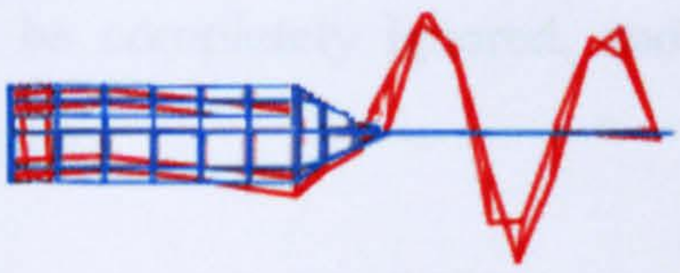 EMA: f=33250 Hz	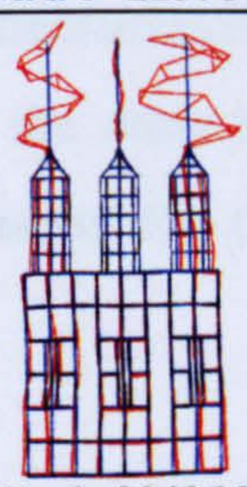 EMA: f=32426 Hz	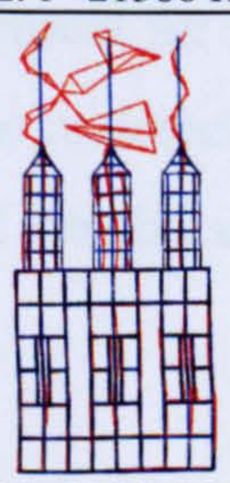 EMA: f=33110 Hz	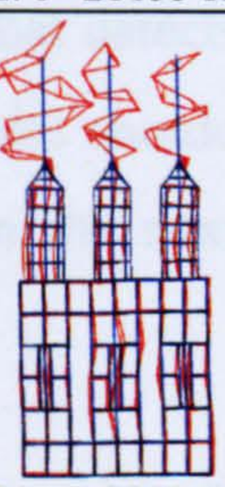 EMA: f=33596Hz
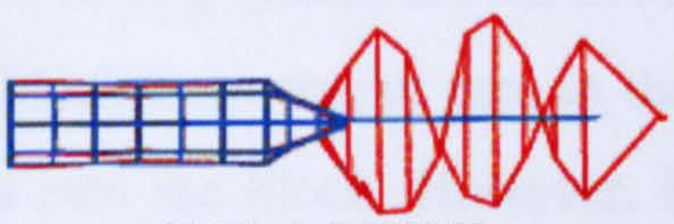 EMA: f=37989 Hz	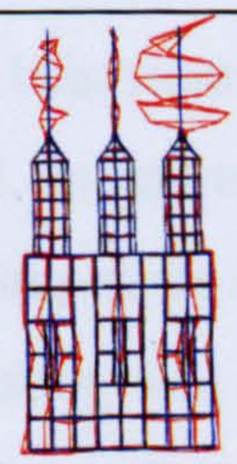 EMA: f = 37582 Hz	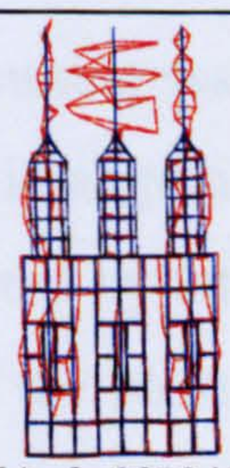 EMA: f=38194 Hz	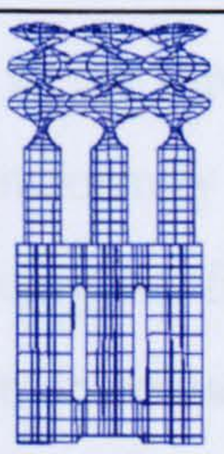 FE: f =36500 Hz

Figure 6.4. Comparison between the modes of the single blade system and the three-blade head determined by EMA and FEA

The modal data obtained through EMA of the single blade system and the three-blade assembly are shown in Figure 6.4. Visual comparisons between the mode shapes of the single-blade system and the corresponding blade responses detected in the three-blade head, illustrate how a mode of the single blade system develops into a mode family in the three-blade assembly. The mode shapes of the three-blade configuration at these frequencies do not exhibit block deformations, and they essentially typify blade modes, where the block horn acts as a stiff exciter. The mode families, associated with spatial phase variations of the blade responses for the same blade mode, occur in clusters of very close modal frequencies.

The FE model of the three-blade system predicts three modes for each mode family, however, not all of them are detected experimentally. Although these modes exist, they are not excited with a measurable response by the longitudinal mode transducer. The modes that are predicted but cannot be measured are mostly from families associated with torsional and bending vibration of the blades. Where a mode has not been measured, the FE predicted mode of the mode family has been included in Figure 6.4.

This demonstrates the importance of EMA data, which prevents the problems of high modal density being misinterpreted or exaggerated by FE data alone and allows design strategies not to be abandoned only on the basis of FE model results. This also demonstrates the importance of using a measurement instrument for EMA that detects in-plane and out-of-plane responses. On the other hand, the undetected modes should not be completely ignored, and the reasons for this will be discussed in the next chapter.

6.2.1.2 Head modes dominated by the block horn

The block horn also affects the vibration behaviour of the cutting system. In the three-blade cutting system shown in Figure 6.2, an improvement in amplitude uniformity on the block horn output face in the operating mode is achieved by introducing six fine slots into the block. However, incorporating fine slots in the block horn introduces families of modes mainly associated with bending responses in the increased number of columns. These modes are numerous as they excite several frequencies for each mode family. Figure 6.5 illustrates the measured mode shapes and frequencies of the

block horn, as investigated in Section 5.4 (Table 5.1), alongside the detected modes of the three-blade cutting head.

	Mode families of the transducer-block horn system			**Mode families of the three-blade cutting system**		
	1st mode	2nd mode	3rd mode	1st mode	2nd mode	3rd mode
1st modal family	 f = 13686 Hz	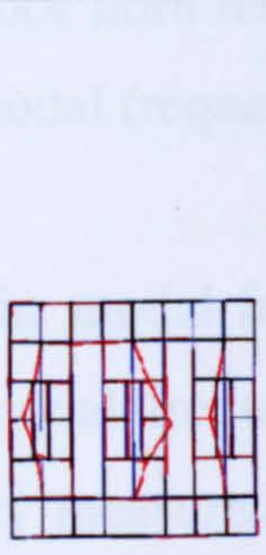 f = 14047 Hz	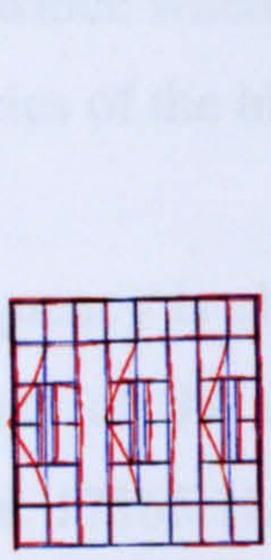 f = 14202 Hz	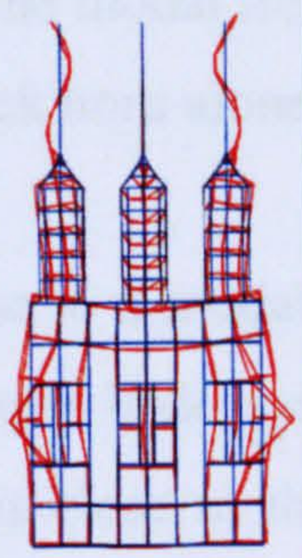 f = 13374 Hz	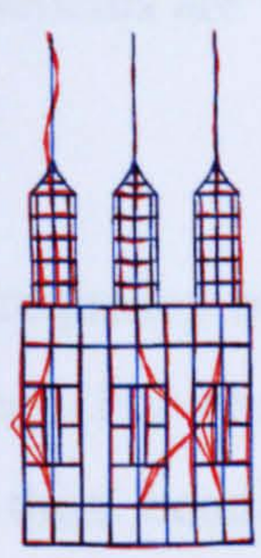 f = 13946 Hz	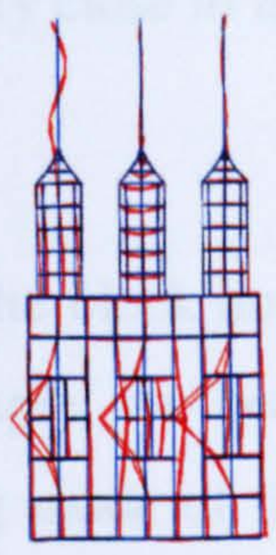 f =14614 Hz
2nd modal family	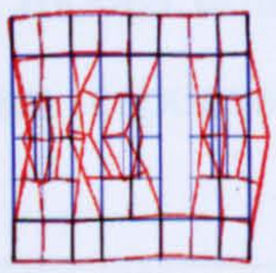 f = 16775 Hz			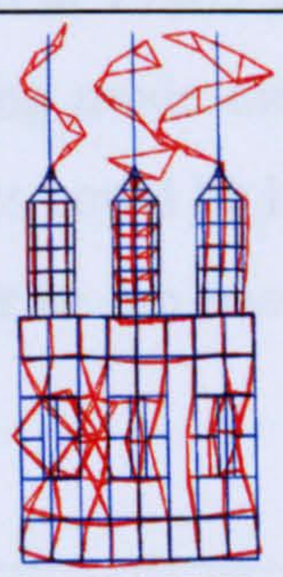 f = 17165 Hz		
3rd modal family	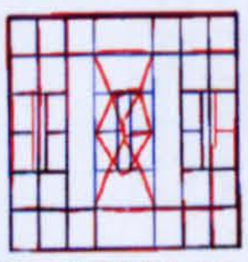 f = 18590 Hz	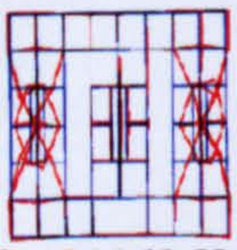 f = 21163 Hz		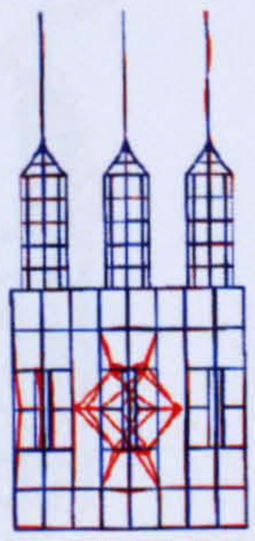 f = 18669 Hz	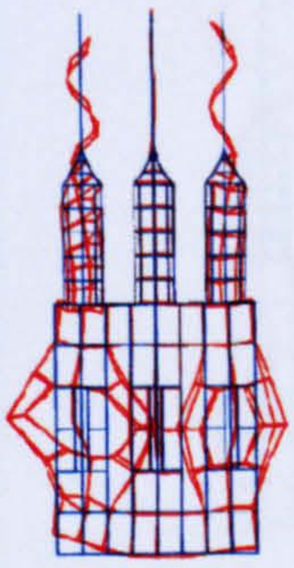 f = 21019 Hz	
4th modal family	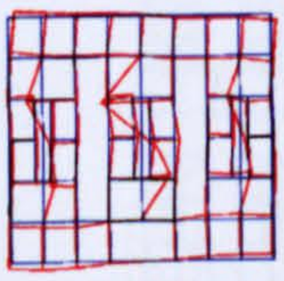 f = 37470 Hz	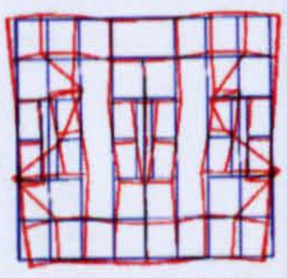 f = 38716 Hz	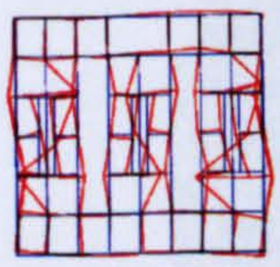 f = 40175 Hz	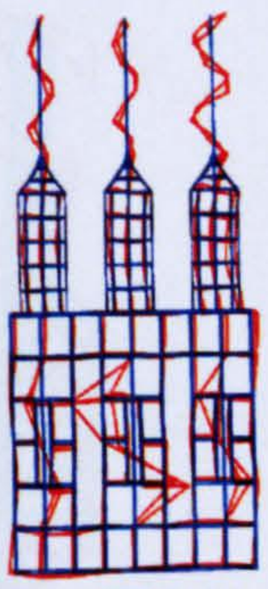 f = 37330 Hz	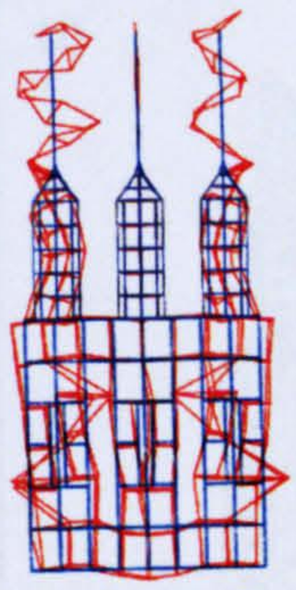 f = 38630 Hz	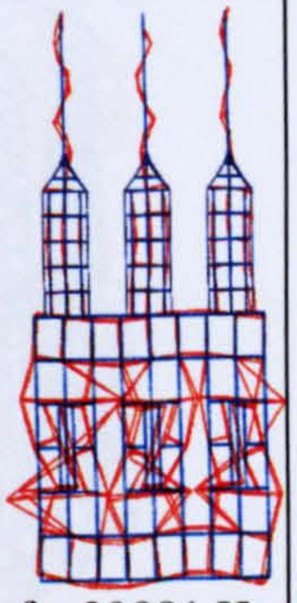 f = 39881 Hz

Figure 6.5. Comparison between the modes of the block horn and the three-blade head determined by EMA

Mode families, characterised by spacial phase variations of the bending responses of the block horn columns for the same column mode, are shown for the block horn alone and for the cutting head. The modes of each family occur at very close frequencies for both system configurations. The cutting head modes in Figure 6.5 often exhibit blade and block responses, but it can be argued that the modes are dominated by block horn resonance where the modal frequencies are very close to the corresponding modal frequencies of the block horn alone.

In other cases, the modal frequency is close to a modal frequency of the block horn alone and the modal frequency of the single bade system. For example, the head natural frequency measured at 17165 Hz is close to the third bending mode of the single blade system which has been detected at 17465 Hz, whereas the head mode at 38630 Hz is close to the blade sixth bending mode measured at 38278 Hz (Section 4.2.3, Table 4.2). Consequently, these modes could be included either in the category of modes dominated by blade responses, or in the head modes dominated by block horn responses.

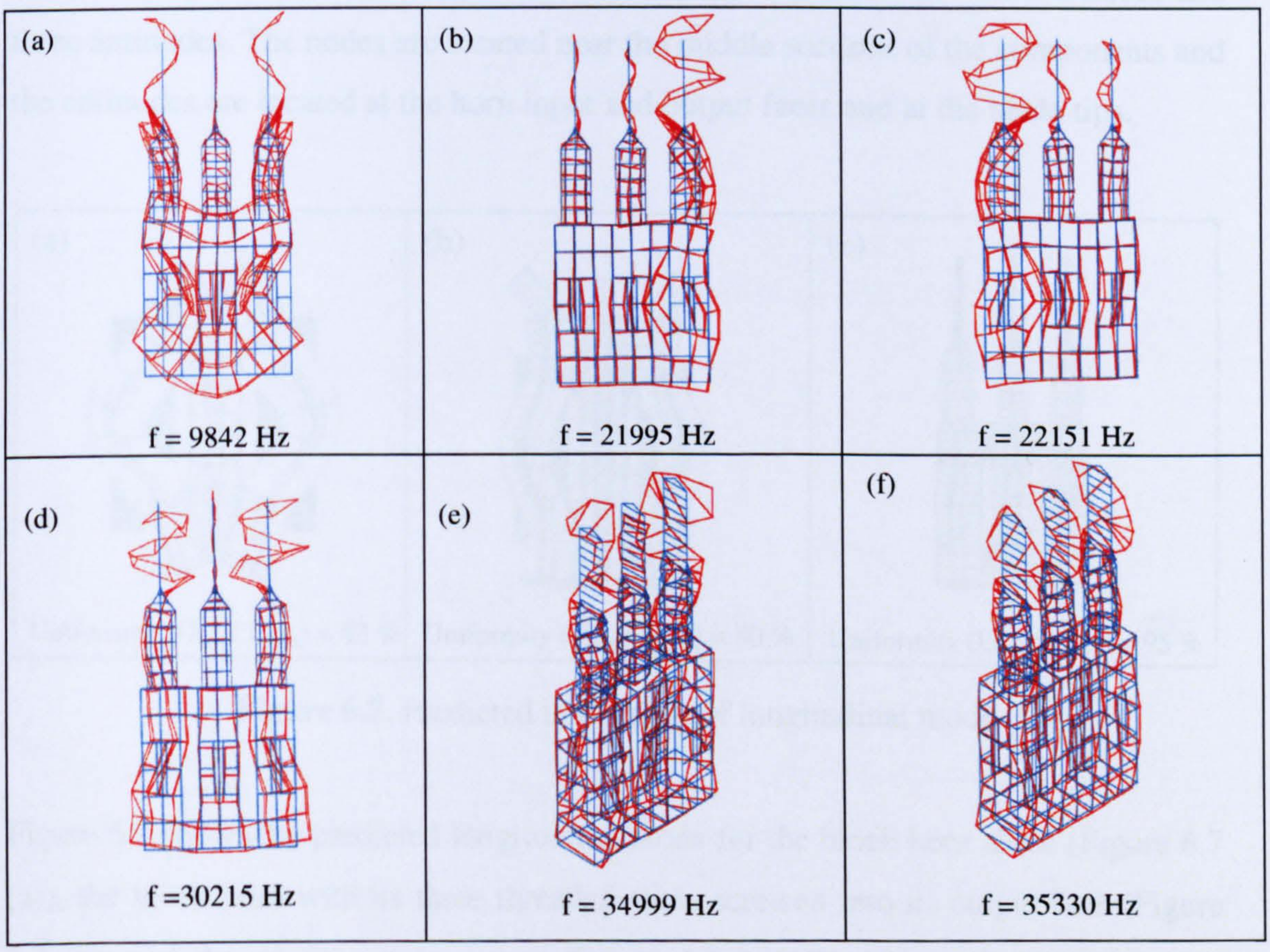

Figure 6.6. Measured compound modes of the three blade head determined by EMA

6.2.1.3 Modes of the block-blades assembly

Another group of modes of vibration of the three-blade head exists, whose frequencies do not correspond to the natural frequencies of the block horn or blades components separately. The modes in this category are whole assembly modes, characterised by continuous deformations of all the components of the assembly. Figure 6.6 shows the mode shapes of six of the numerous modes of the assembly measured for the three-blade cutting head. From the mode shapes it is evident that the columns of the block horn exhibit bending and torsional responses which result directly in bending and torsional responses in the blades. The modes shown in Figure 6.6 (e) and (f) occur at frequencies very close to the tuned frequency, measured at 35298 Hz.

6.2.2 The tuned longitudinal mode

The tuned mode of the three-blade head is a mode of vibration characterised by the simultaneous longitudinal motion of the block horn and the cutting blades. The horn and the blades are tuned individually to resonate in their first longitudinal mode at 35 kHz, which is the excitation frequency of the transducer. Hence, the operating mode of the block and blades assembly is the second longitudinal mode with two nodes and three antinodes. The nodes are located near the middle sections of the components and the antinodes are located at the horn input and output faces and at the blade tips.

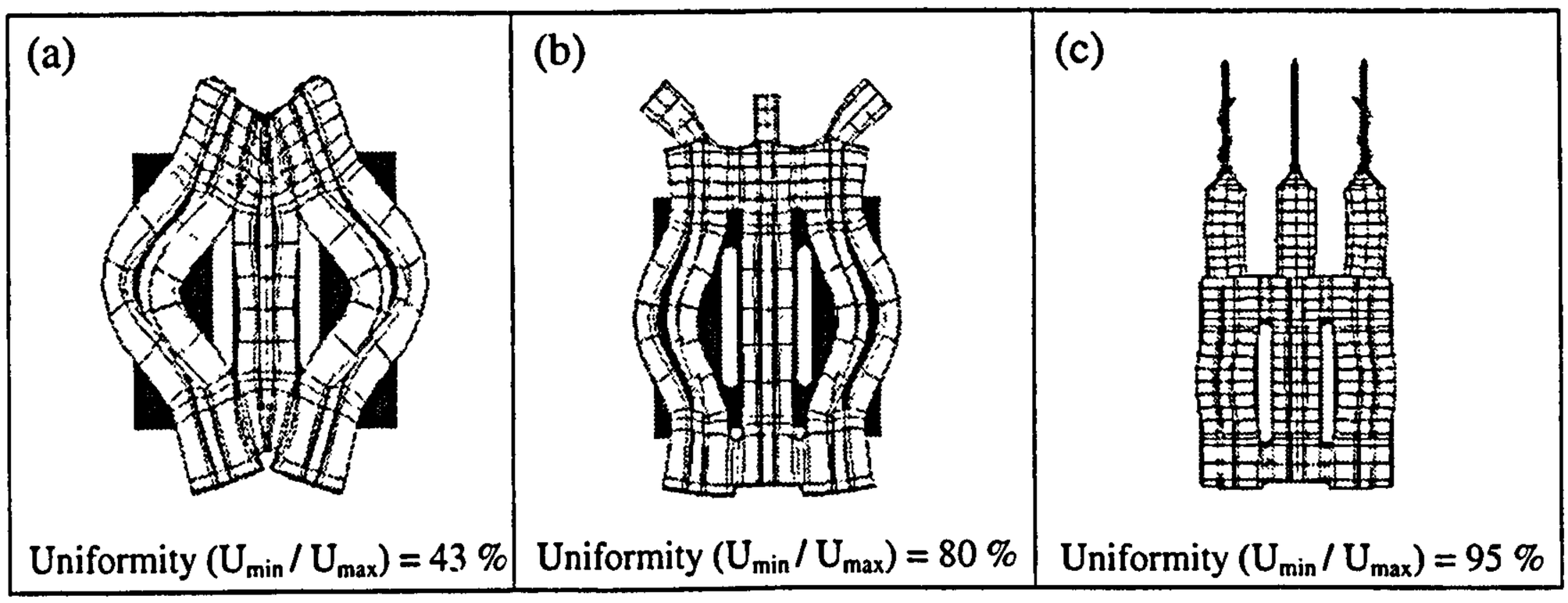

Figure 6.7. Predicted uniformity of longitudinal mode

Figure 6.7 shows the predicted longitudinal mode for the block horn alone (Figure 6.7 (a)), the block horn with its three threaded studs screwed into its output face (Figure 6.7 (b)) and the whole cutting system (Figure 6.7 (c)). The figure demonstrates that although high amplitude uniformity (95%) is achieved on the face of the block horn

for the complete cutting system, the block horn modelled alone predicts an amplitude uniformity of only 43%. It is clear that the block horn cannot be designed in isolation for such multiple component systems.

Figure 6.8 presents the responses of the tuned mode of the cutting head predicted by FEA and measured by EMA at 35.9 kHz and 35.3 kHz respectively. The measurements of the longitudinal motions correlate well with the predicted mode shape. In the second longitudinal mode of the system, the elongation half-cycle of the block horn coincides with the compression half-cycle of the cutting blades, and vice versa. The mode shape reveals that while the middle blade vibrates in a purely longitudinal mode, the outer blades are characterised by longitudinal and bending responses. Bending responses in the outer columns of the block horn are responsible for the bending responses in the outer blades. This behaviour gives rise to dynamic stresses in the two outer blades, which can cause failure. Hence, a design strategy needs to constrain bending responses in the blades.

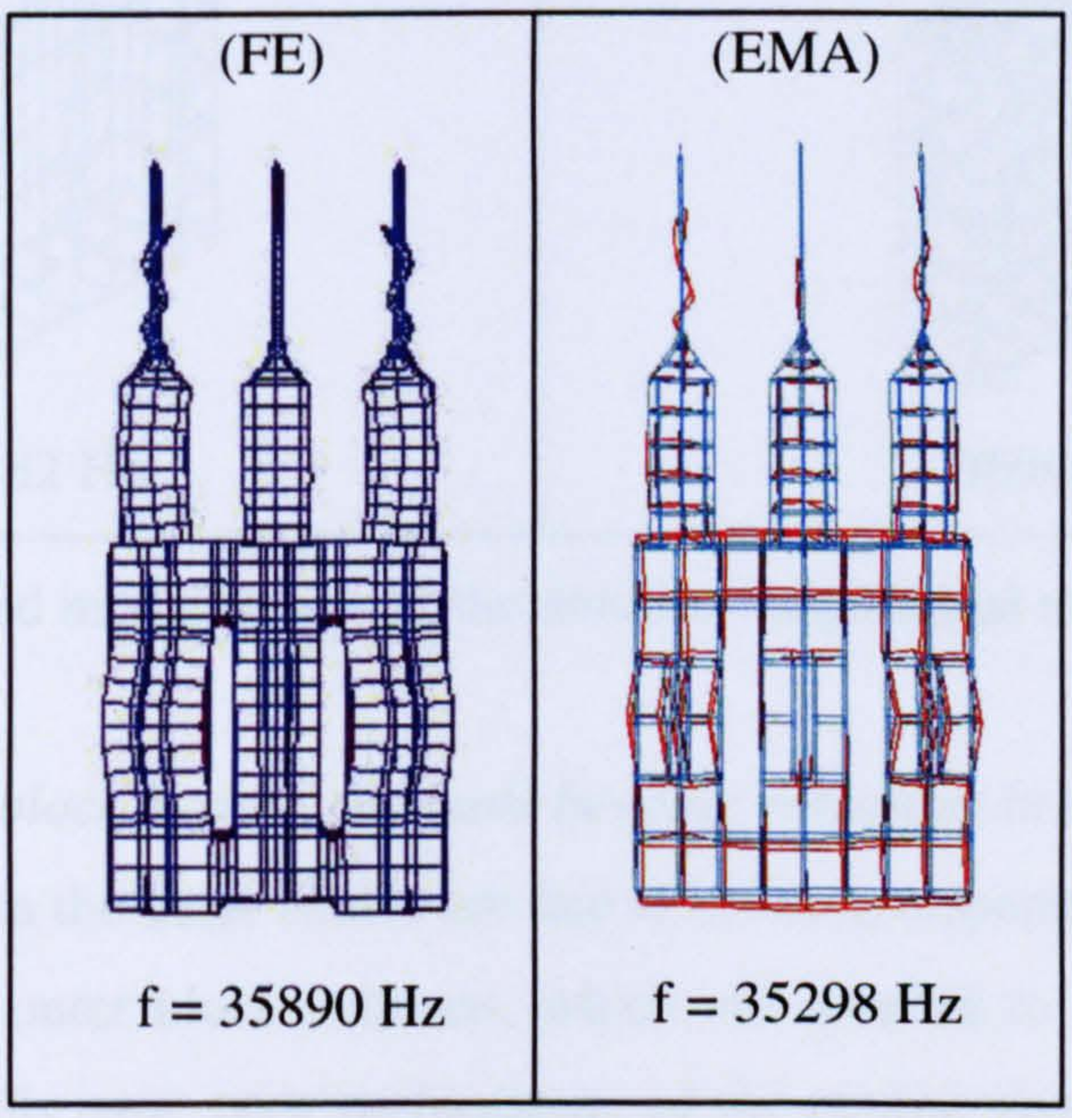

Figure 6.8. Predicted and measured mode shape of the tuned mode

The mode shapes of two other modes, which are excited close to the tuned frequency and exhibit longitudinal and bending responses in the blades, are shown in Figure 6.9. These two modes and the tuned mode are of the same mode family and differ only in the phase relationships between the bending responses and the longitudinal responses

in the different blades. Tuning the transducer excitation frequency to either of these modal frequencies would not produce the required vibration at the blade tips.

FE and EMA data also highlight the presence of two modes of the whole assembly occurring at frequencies close to the longitudinal mode frequency. The mode shapes and frequencies were presented in Figure 6.6 (e) and (f). Modal coupling between the tuned longitudinal mode and these modes exhibiting bending responses in the blades, can prevent the system from running in its operating mode and increase stress, particularly in the blades. The issues of modal coupling, therefore, also need to be addressed.

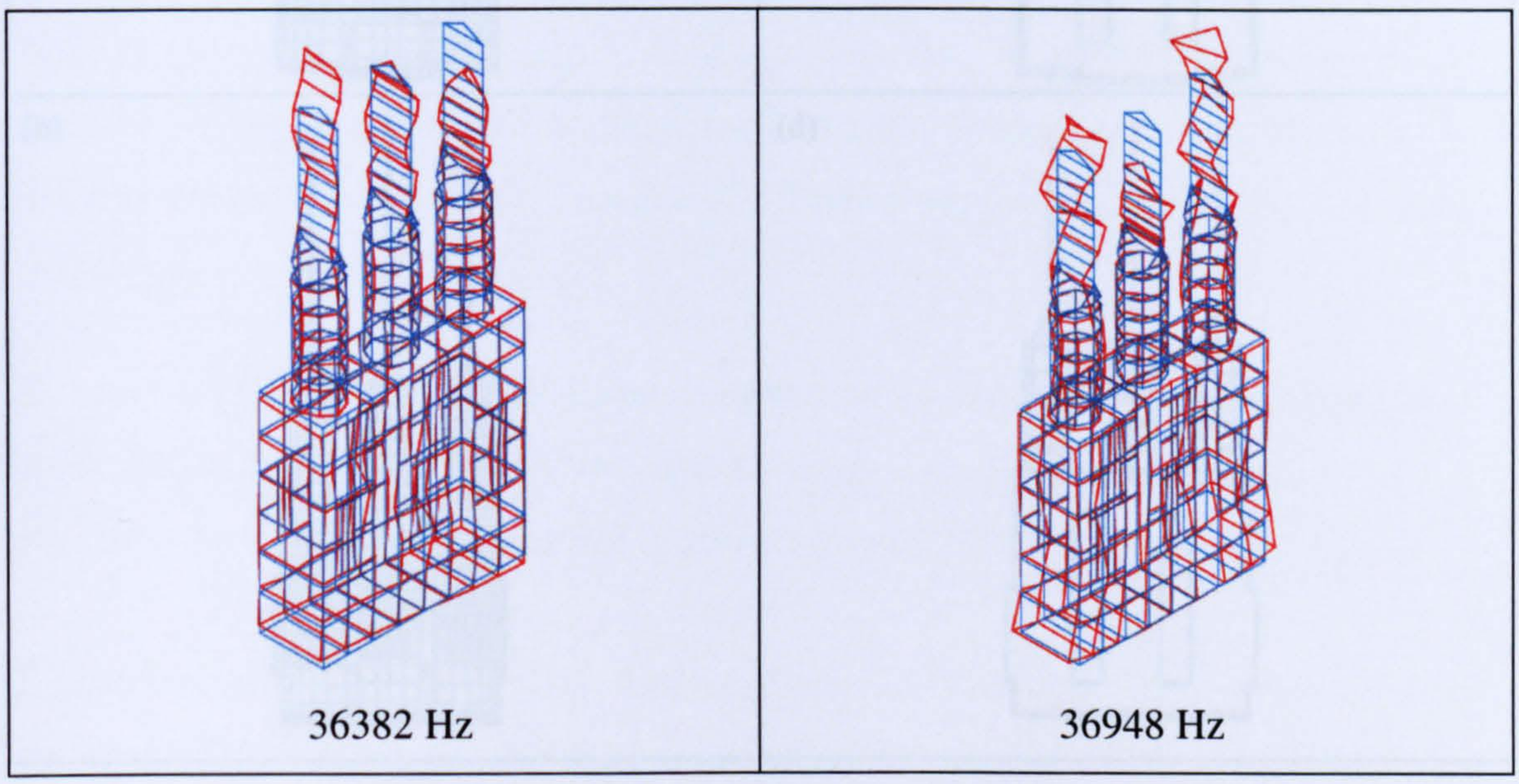

Figure 6.9. Measured modal shapes of the untuned longitudinal modes of the blades

6.2.2.1 Redesign of block horn to eliminate bending responses in the outer blades

Bending responses in the outer blades are due to bending responses in the block horn, in particular in the outer block columns, which are coupled to the outer blades via threaded studs. In this case, poor performance of the cutting system is not connected to poor amplitude uniformity at the output surface of the block, which is 95% and unlikely to be significantly improved. In fact, the method used to improve block amplitude uniformity is the cause of blade bending responses. Additional masses of the horn input face and the incorporation of fine slots produces high amplitude uniformity together with increased bending responses in the outer columns and consequently in the outer blades. Although equal and in-phase vibration of the three

blades can only be achieved through uniformity of the horn output surface, participation of bending responses in the longitudinal mode is a major source of increased stress in the outer blades and poor cutting reliability.

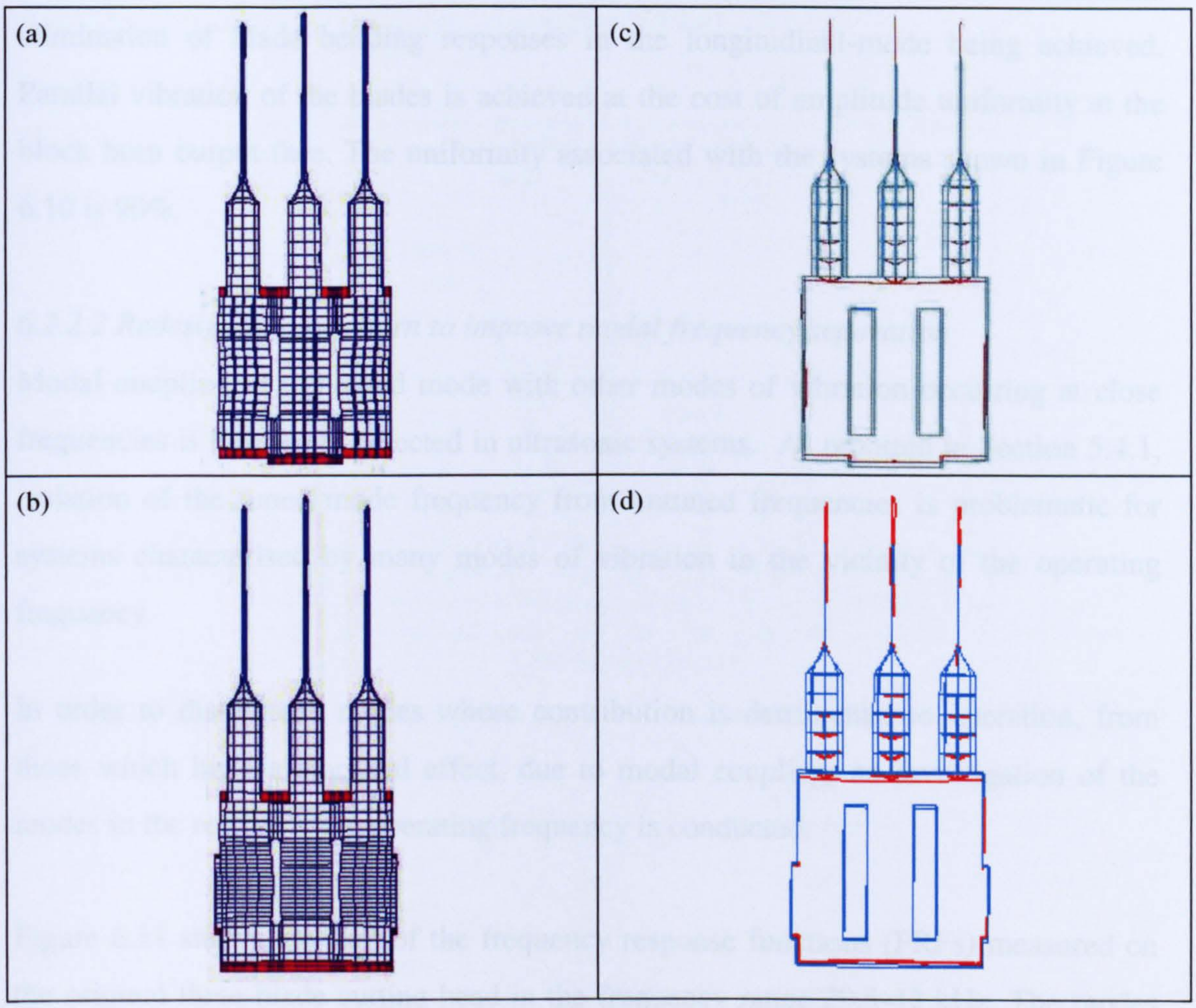

Figure 6.10. Comparison of predicted and measured responses using longer horn central column (a) FEA, (c) EMA, and castellation of horn outer columns (b) FEA and (d) EMA

A block horn redesign strategy based on modifications of the horn columns in the FE model of the assembly is performed. As shown in Figure 6.10(a), a castellated block horn with a longer central column is predicted to remove blade bending responses from the longitudinal mode. An alternative block horn with a form of castellation of the sides of the outer columns is shown in Figure 6.10(b). This restricts bending motion of the outer columns in the longitudinal mode, resulting in equal and in-phase longitudinal motion of all three blades, as evident in the figure.

Subsequently, the redesigned block horns were manufactured. An experimental modal analysis using a 3D LDV is performed on the new cutting heads incorporating the alternative horns. Measurements shown in Figure 6.10(c) and 6.10(d) reveal high correlation with the predicted mode shapes of the tuned mode, with successful elimination of blade bending responses in the longitudinal-mode being achieved. Parallel vibration of the blades is achieved at the cost of amplitude uniformity at the block horn output face. The uniformity associated with the systems shown in Figure 6.10 is 90%.

6.2.2.2 Redesign of block horn to improve modal frequency separation

Modal coupling of the tuned mode with other modes of vibration occurring at close frequencies is frequently detected in ultrasonic systems. As reported in Section 5.4.1, isolation of the tuned mode frequency from untuned frequencies is problematic for systems characterised by many modes of vibration in the vicinity of the operating frequency.

In order to distinguish modes whose contribution is detrimental to operation, from those which have a marginal effect, due to modal coupling, an investigation of the modes in the region of the operating frequency is conducted.

Figure 6.11 shows the sum of the frequency response functions (FRFs) measured on the original three-blade cutting head in the frequency range 29.5-42 kHz. The modes of the assembly of Figure 6.6 (e) and 6.6 (f) also occur in the FRF but are present in the figure within the bandwidth of the response of the longitudinal mode.

The tuned longitudinal mode response, illustrated in Figure 6.12, reveals a bending response contribution in the longitudinal response of the block horn and the blades. This is clear evidence of modal coupling between the operating mode and the bending mode measured just 30 Hz above the tuned frequency and presented in Figure 6.6 (f).

On the other hand, the mode shape of the longitudinal mode does not present evidence of additional responses associated with the torsional mode of the assembly measured 300 Hz below the tuned frequency and shown in Figure 6.6 (e). This mode, whose response is identifiable as the small spike at 35 kHz, is barely excited by the

transducer, and therefore does not contribute significantly to the longitudinal mode response. The existence of modal coupling is not always a detrimental feature of ultrasonic operations. There are applications where the simultaneous excitation of two modes of vibration, i.e. longitudinal/torsional modes or longitudinal/bending modes, has a positive effect on the system operation [63,64].

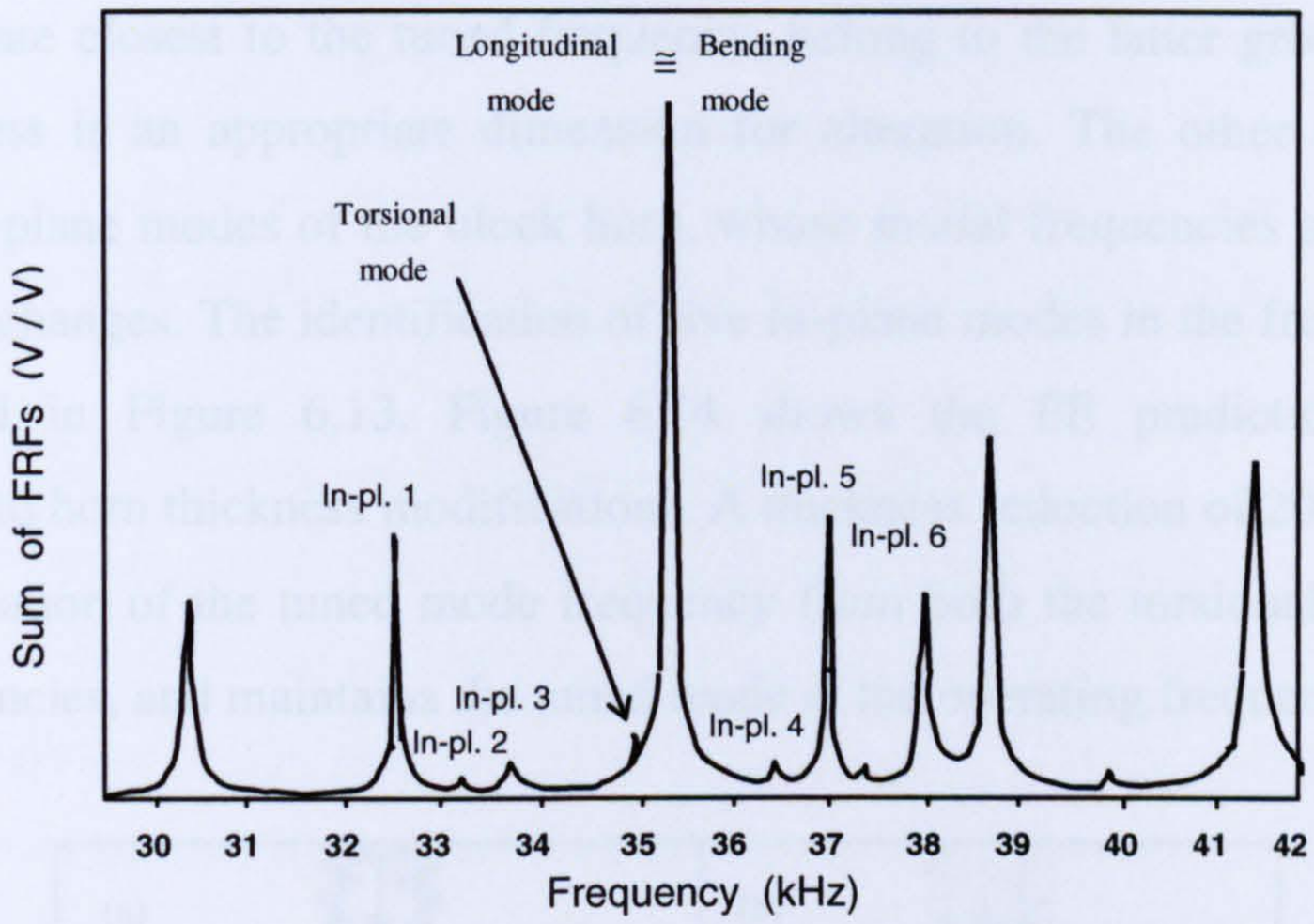

Figure 6.11. 3D LDV frequency response function measurement of cutting head

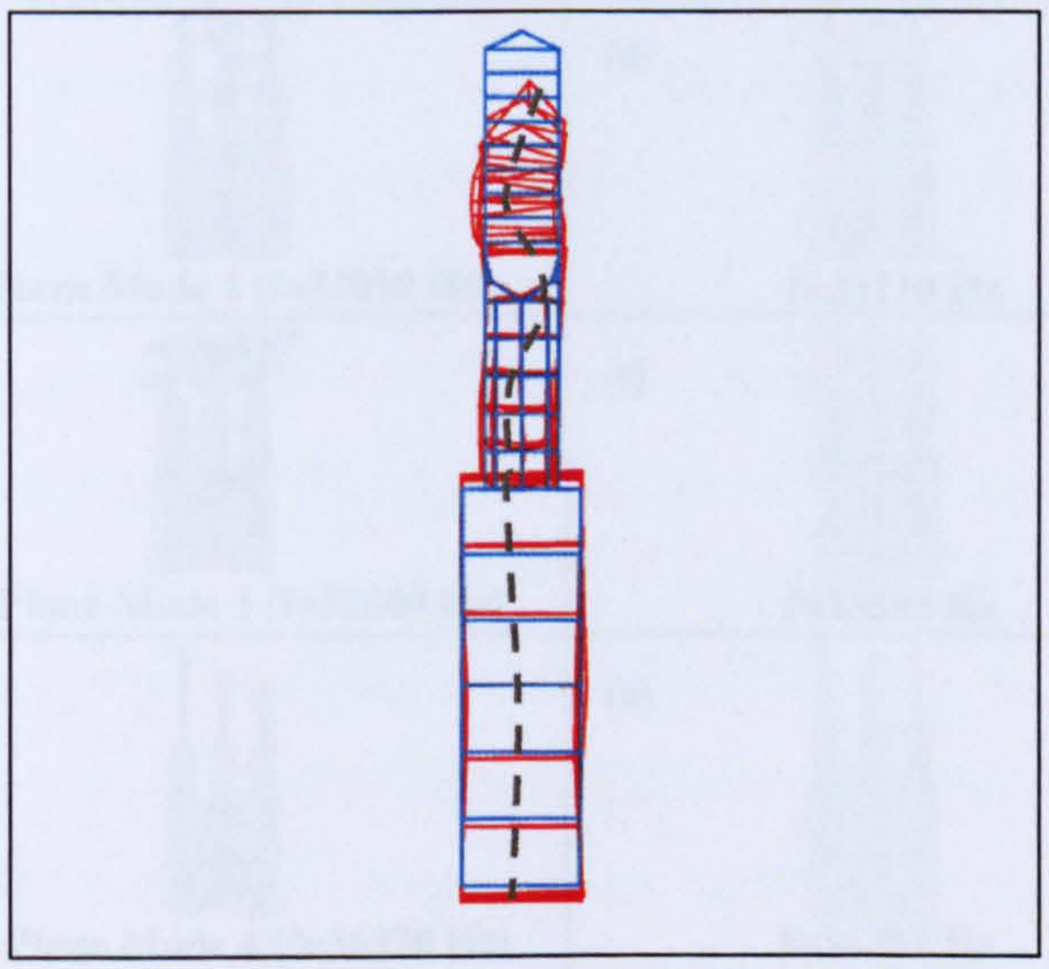

Figure 6.12. Side view of the longitudinal mode

A redesign strategy to isolate the longitudinal mode frequency of the three-blade head from close modal frequencies is proposed to provide practical insight in the design of systems where modal coupling cannot be tolerated. Since the blade dimensions are dictated by the operation requirements (amplitude gain and cutting depth), the block

horn geometry is modified to improve isolation of the longitudinal mode frequency. Block horn modes in an 8 kHz frequency range around 35 kHz are classified into two main categories: a) in-plane modes whose frequencies are highly dependent on block width and/or length, but independent of block thickness, and b) out-of-plane modes (including bending and torsional modes), which are highly sensitive to block thickness. Both of the modes discussed previously (torsional and bending), whose frequencies are closest to the tuned frequency, belong to the latter group. Therefore horn thickness is an appropriate dimension for alteration. The other modes in the range are in-plane modes of the block horn, whose modal frequencies are insensitive to thickness changes. The identification of five in-plane modes in the frequency range is illustrated in Figure 6.13. Figure 6.14 shows the FE predictions of mode sensitivities to horn thickness modifications. A thickness reduction of 20% results in a 2.5 kHz isolation of the tuned mode frequency from both the torsional and bending mode frequencies, and maintains the tuned mode at the operating frequency.

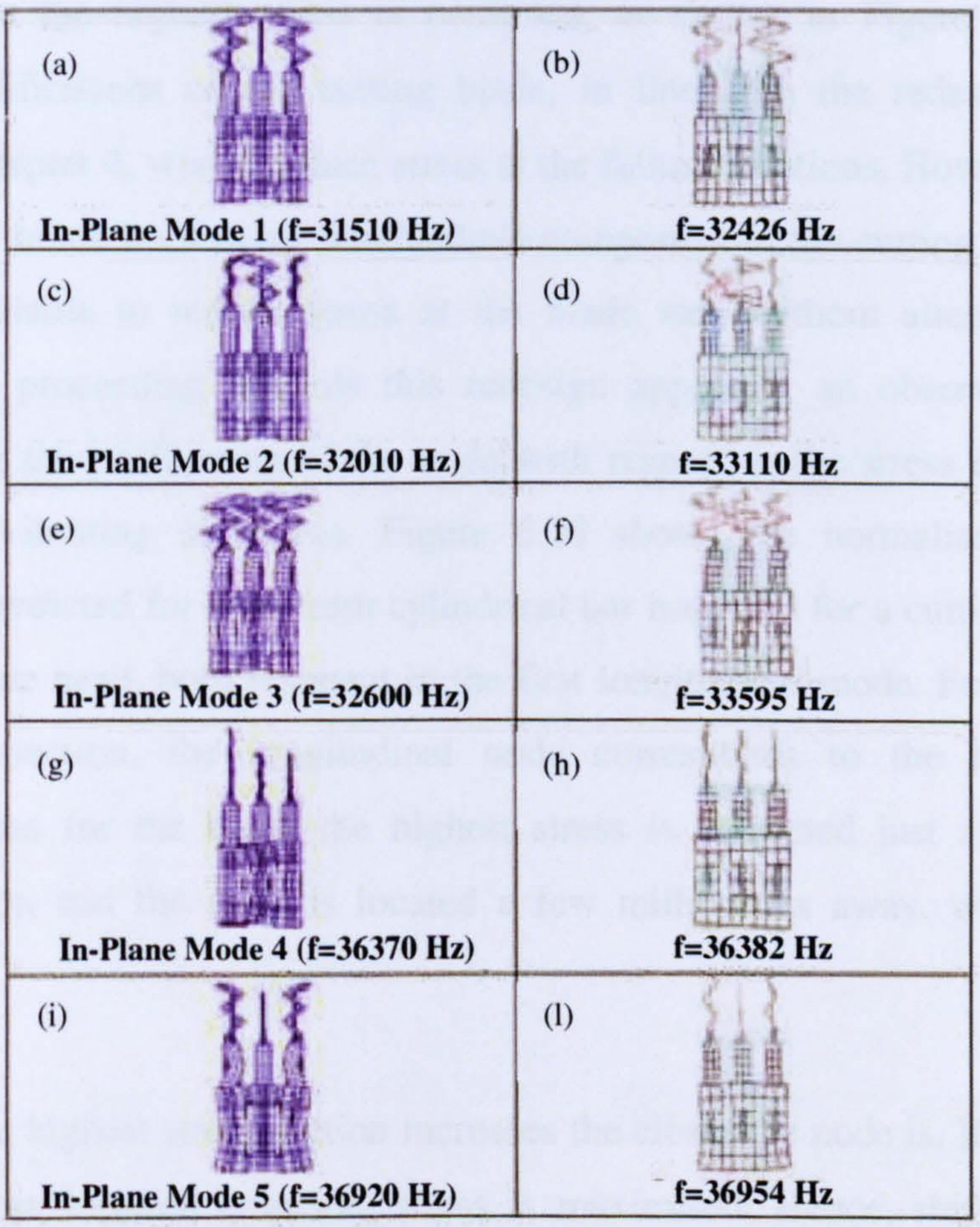

Figure 6.13. Mode classification by FE (a, c, e, g, i), experimental data (b, d, f, h, l)

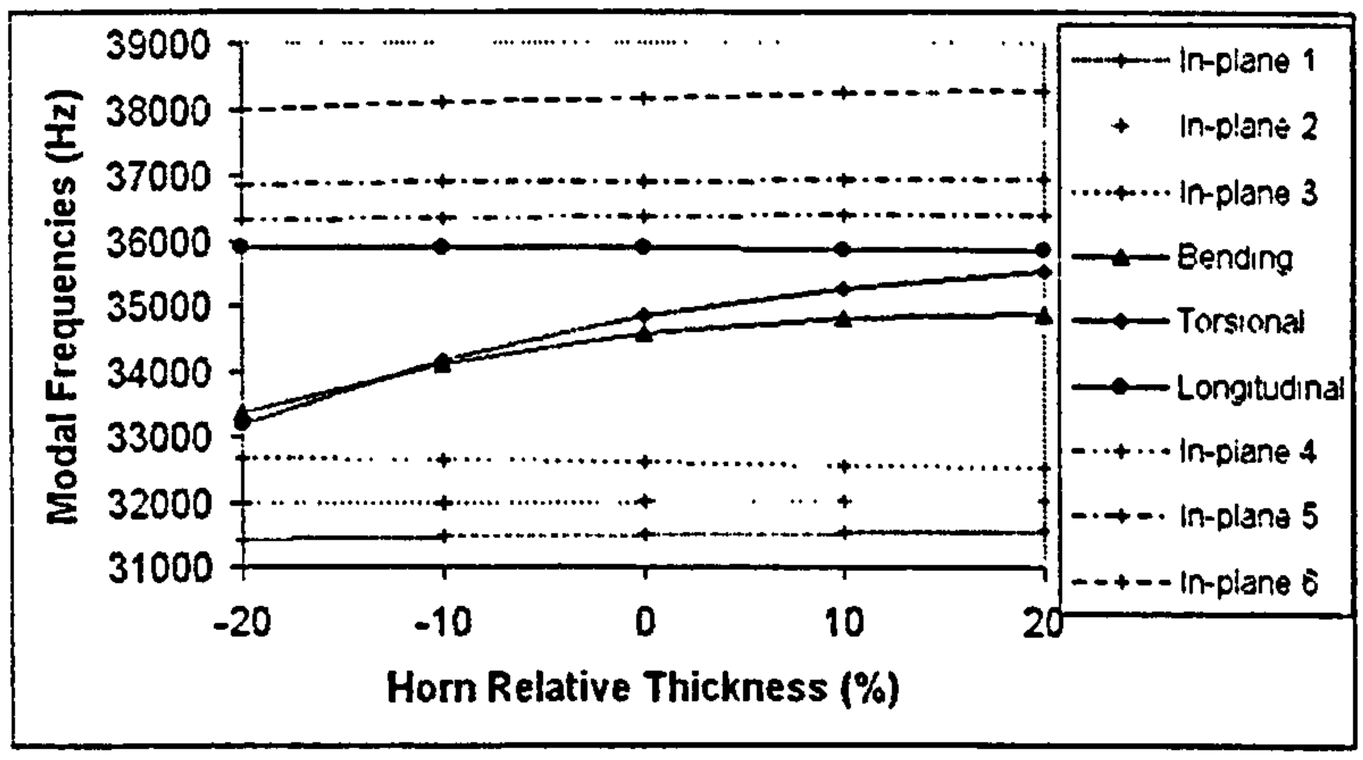

Figure 6.14. Predicted effect of horn thickness on modal frequencies

6.2.3 Cutting head component detuning to reduce stress

Fatigue trials carried out on three-blade cutting heads have resulted in failures due to high dynamic stresses in the cutting blades under operating conditions. Equally, in the single blade system investigated in Section 4.2.1, fractures occur at the blade step which is where the highest stress is predicted, as shown in Figure 6.15. Hence, geometric modifications of the cutting blade, in line with the redesign strategies discussed in Chapter 4, would reduce stress at the failure locations. However, with the presence of the block horn as an intermediate component in the cutting head, another strategy is available to reduce stress at the blade step without altering the blade profile. Before proceeding towards this redesign approach, an observation can be made regarding the positioning of the node with respect to the stress distribution in longitudinally vibrating structures. Figure 6.16 shows the normalised stress and displacement predicted for a uniform cylindrical bar horn and for a cutting blade used in the three-blade head, both resonant in the first longitudinal mode. For the bar with constant cross-section, the longitudinal node corresponds to the highest stress location, whereas for the blade the highest stress is predicted just after the steep section reduction and the node is located a few millimetres away, within the step profile.

The stress at the highest stress section increases the closer the node is. If the node and the highest stress location coincide, stress is maximised. Hence, shifting the node further away into the thicker blade section, reduces stress at the highest stress section. The technique to achieve this is to detune the block and blades, thus shifting the node

into the cylindrical end of the blades, in particular by tuning the block horn longitudinal mode to a lower frequency, whilst maintaining the original tuned frequency of the assembly.

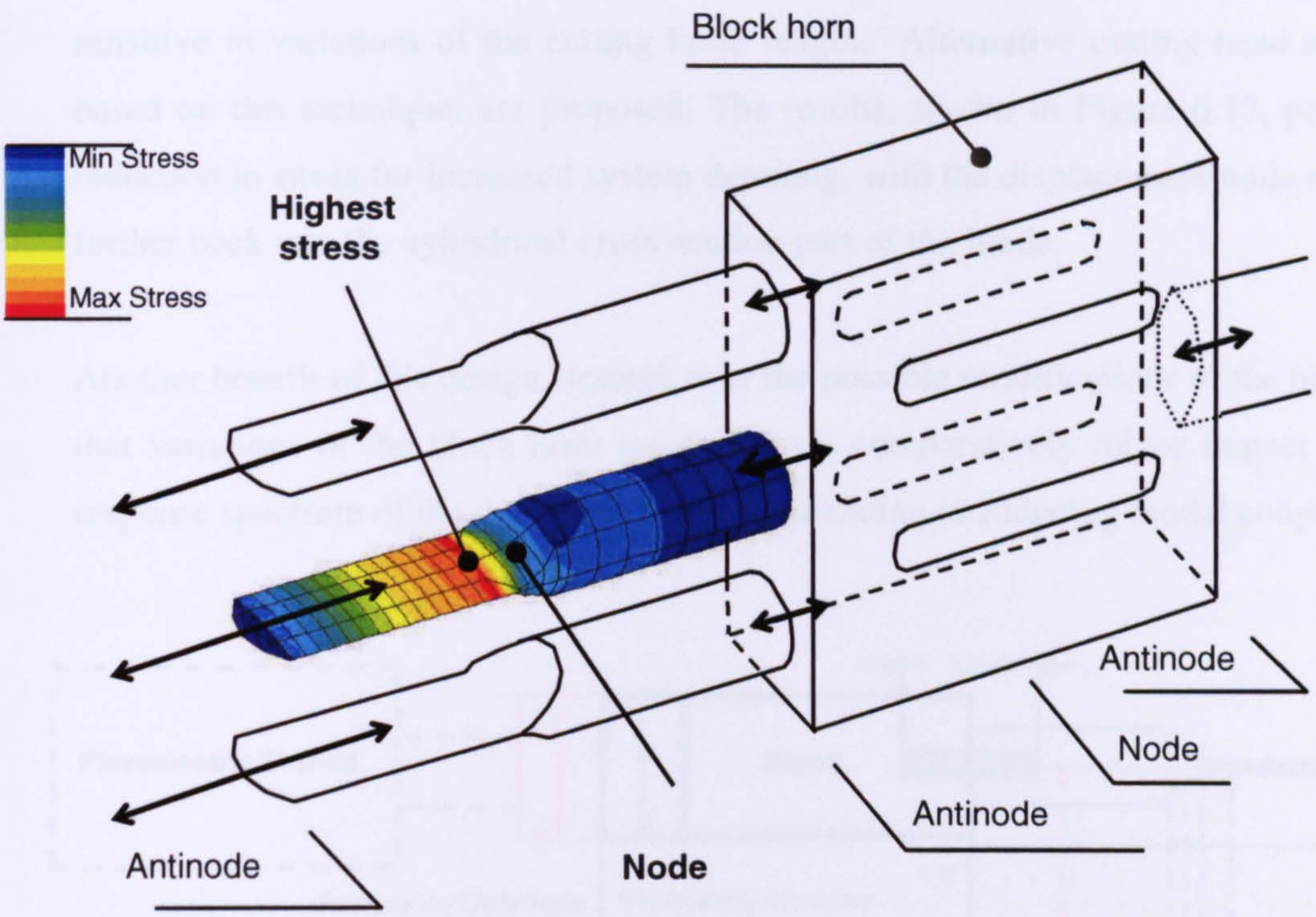

Figure 6.15. Predicted stress distribution in the central blade of three-blade head

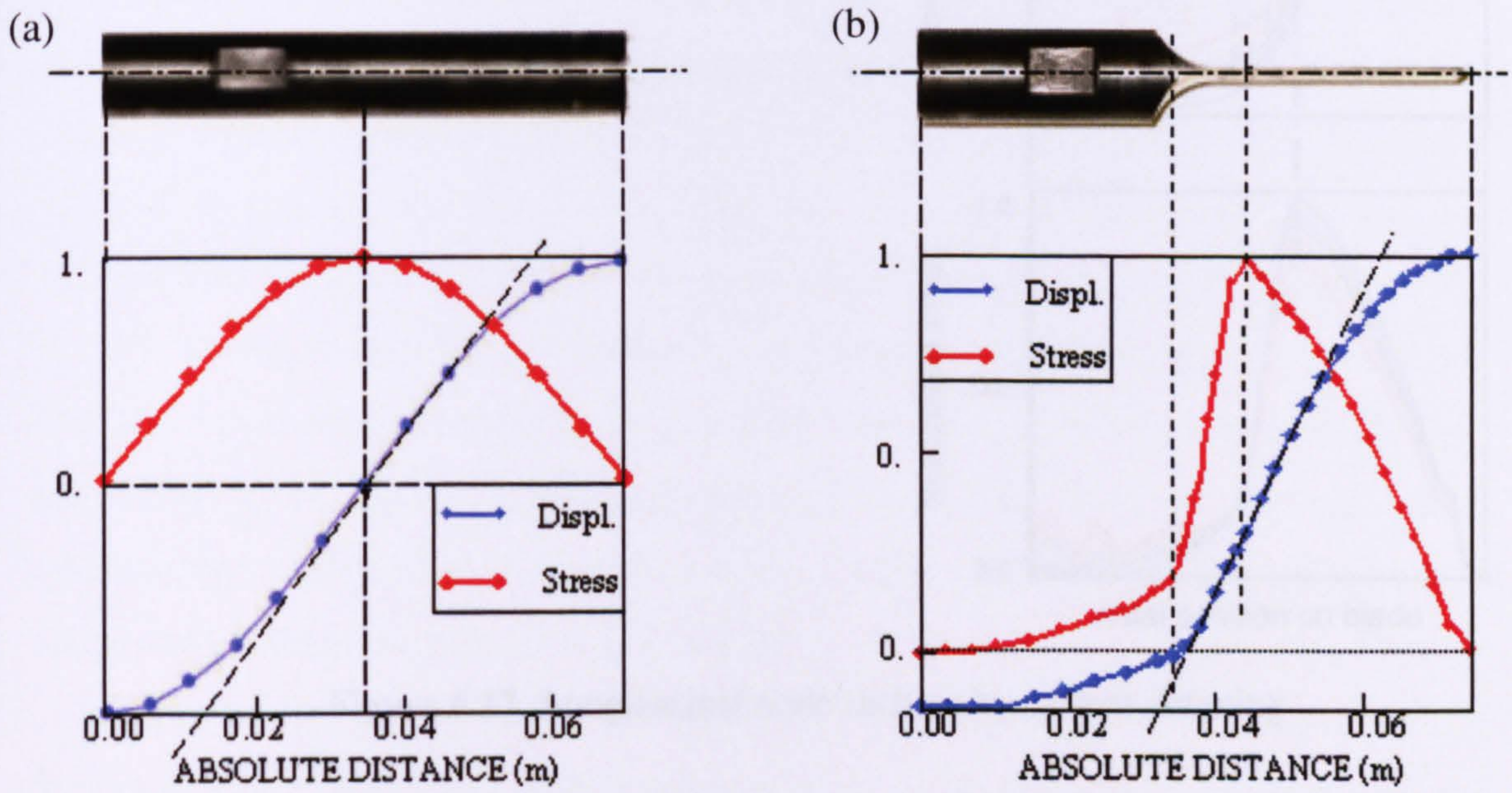

Figure 6.16. Normalised Stress and Displacement in: (a) bar horn, (b) cutting blade

Small modifications of the block horn length do not significantly influence the longitudinal frequency of the whole assembly, which in contrast is particularly sensitive to variations of the cutting knife length. Alternative cutting head models, based on this technique, are proposed. The results, shown in Figure 6.17, predict a reduction in stress for increased system detuning, with the displacement node moving further back into the cylindrical cross-section part of the blade.

Another benefit of this design strategy over the possible modifications of the blades is that variations of the block horn length have a comparatively minor impact on the response spectrum of the assembly, therefore avoiding introducing modal coupling.

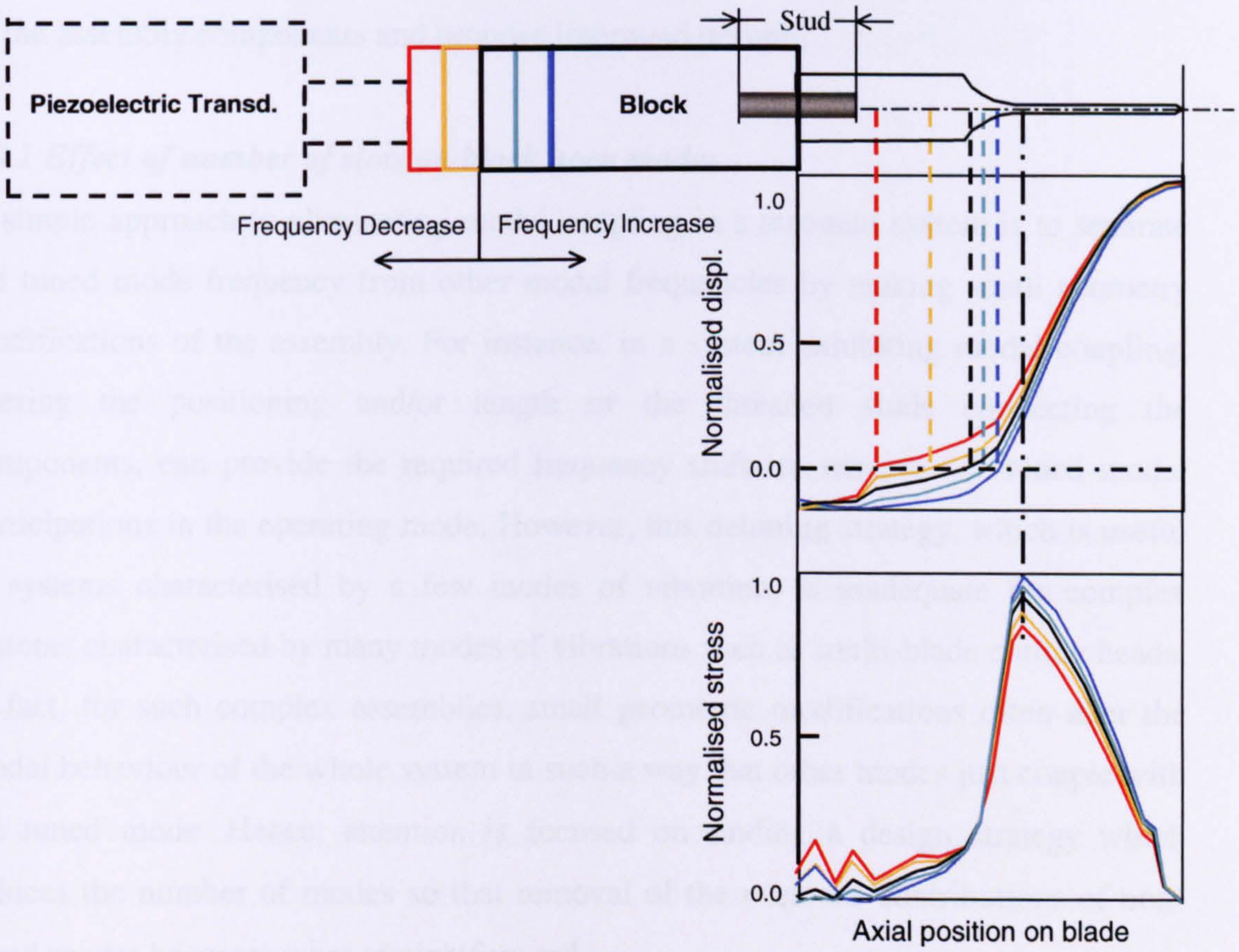

Figure 6.17. Longitudinal node shifting by system detuning

6.3 Design strategies for improved vibration behaviour of cutting systems

The characterisation of the vibration behaviour of single ultrasonic components and complex assemblies has revealed that the number of modes of an ultrasonic system depend on the quantity and the geometry of its constituent units. In Section 6.2.1, it

was shown how mode families are excited in cutting systems comprising a block horn driving three cutting blades. The blades, due to their tapered profiles, are characterised by numerous bending modes which become easily excited when a slotted block horn is used as an intermediate resonator. In addition, the slotted configuration of the horn considerably increases the number of modes of the whole assembly, increasing the risk of coupling the tuned frequency with close natural frequencies (linear modal coupling). The characterisation of energy leakage from the operating frequency to well-separated modes (nonlinear modal coupling) will be the subject of the next chapter.

In this section, design strategies to eliminate the effects of linear modal coupling in three-blade cutting systems, by focusing on reducing the number of vibration modes, are proposed. Finite element models are used to characterise the vibration behaviour of the assembly components and propose improved designs.

6.3.1 Effect of number of slots on block horn modes

A simple approach to eliminating modal coupling in a resonant system is to separate the tuned mode frequency from other modal frequencies by making small geometry modifications of the assembly. For instance, in a system exhibiting modal coupling, altering the positioning and/or length of the threaded studs connecting the components, can provide the required frequency shifts to remove non-tuned modal participations in the operating mode. However, this detuning strategy, which is useful in systems characterised by a few modes of vibration, is inadequate for complex systems characterised by many modes of vibrations such as multi-blade cutting heads. In fact, for such complex assemblies, small geometric modifications often alter the modal behaviour of the whole system in such a way that other modes just couple with the tuned mode. Hence, attention is focused on finding a design strategy which reduces the number of modes so that removal of the response contributions of non-tuned modes becomes more straightforward.

We have seen that in multi-blade cutting systems, block horns are responsible for the presence of a large number of modes and the incorporation of slots results in a highly enriched response spectrum. Reducing the number of slots in block horns for wavelength systems therefore provides a strategy for decreasing the number of modes.

In Section 6.2.2 it was shown that for a double-slotted block horn, the output face vibration amplitude in the longitudinal mode was very uniform, but that the outer columns of the block horn exhibit bending responses which result in bending and longitudinal vibration of the outer blades. It was also shown that purely longitudinal vibration of the three blades could be achieved through the incorporation of castellations in the block horn profile (Section 6.2.2.1). For a block horn with no slots, the longitudinal mode visibly exhibits curvature on the faces of the block due to Poisson's effect.

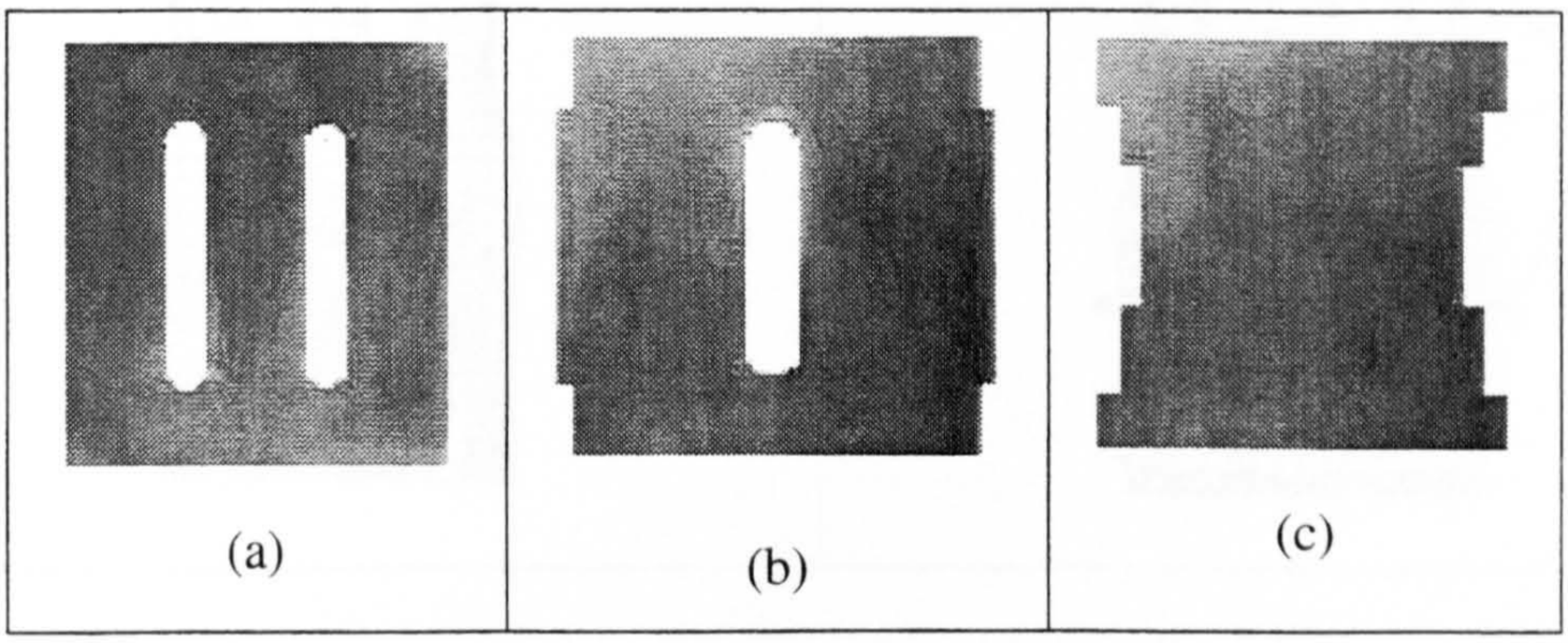

Figure 6.18. (a) Double-slotted block horn, (b) single-slotted block horn, (c) solid block horn, for wavelength cutting head

For a three-blade cutting head this effect would also lead to the outer blades exhibiting longitudinal and bending responses. Therefore, the solution for design aimed at reducing the number of modes of the cutting head, is to decrease the number of slots and use castellations to eliminate the effects of curvature in the response at the output face of the block horn. Three block horns are shown in Figure 6.18. The double-slotted block horn is designed based on standard slotting configurations, whereas the other two blocks are a single-slotted and solid block geometry incorporating castellated faces to improve uniformity of the output face vibration amplitude and constrain the bending responses in the outer blades. The single slotted block horn in Figure 6.18 exhibits 20% fewer modes than the double-slotted block horn and the solid block exhibits 40% fewer modes in a 0 – 50 kHz frequency range. The predicted shape of the tuned mode resulting from incorporating a single-slotted block horn with no castellations, is shown in Figure 6.19 (a). Poor uniformity of the horn output face and bending motions of the outer columns and blades, are evident. However, as shown in Figure 6.19 (b), a form of castellation of the outer columns of

the block horn is predicted to provide uniformity at the output face and to remove bending motion from the longitudinal motion of the blades.

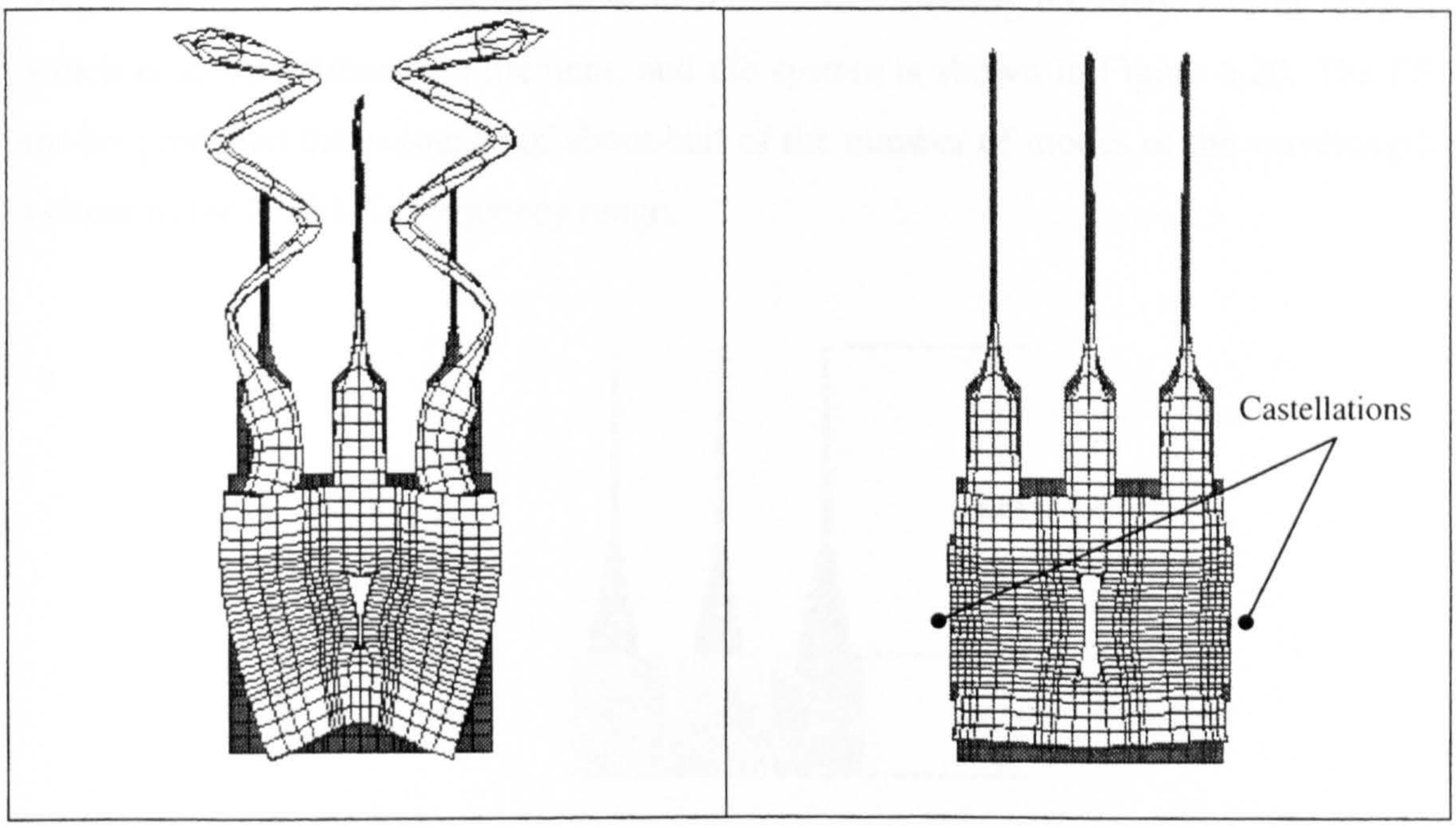

Figure 6.19. Mode shapes of the tuned mode predicted for the same magnification factor; (a) no castellation,(b) castellations of the horn outer columns

6.3.2 Short-block design for a half-wavelength system

The characterisation of the vibration behaviour of the three-blade cutting head investigated in Section 6.2.1 revealed that the mode families associated with the three identical blades, each consist of a cluster of modal frequencies. Increasing the number of identical blades mounted on the block horn does not significantly increase the possibilities for exciting modal coupling. In fact, the number of modes of each mode family increases but their modal frequencies tend to be very close, with the response dominated by one or two of the modes, under longitudinal excitation of the assembly. More significantly, it is the length of the whole assembly which directly affects the number of modes. It is usual to assemble ultrasonic systems from a series of tuned half-wavelength components. Where, in cutting systems, a block horn acts as the intermediate component between the transducer and blades, the system is one-wavelength. An opportunity therefore exists to reduce the number of modes by designing a block and blade assembly within a half-wavelength.

Wavelength block horn and blade assemblies are tuned to operate in the second longitudinal mode. In order to reduce the number of modes, a half-wavelength three-blade cutting system is designed by finite element modelling, tuned to the first longitudinal mode. The redesign is achieved without altering the blade cutting length, which is an operational requirement, and the system is shown in Figure 6.20. The FE model predicted the existence of about half of the number of modes of the wavelength system in the 0-50 kHz frequency range.

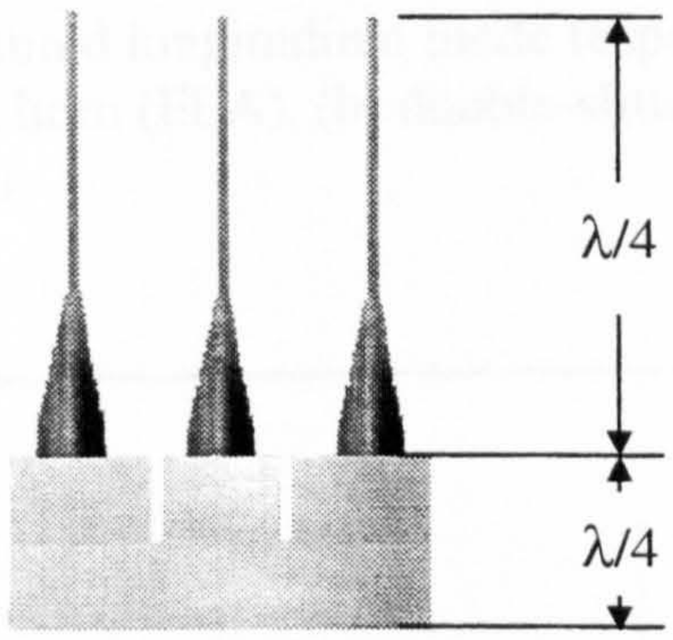

Figure 6.20. Half-wavelength three-blade cutting head

6.3.2.1 Incorporating slits to eliminate bending responses

For the half-wavelength cutting system, it is possible to accommodate slits into the design, which constrains bending responses in the outer blades and results in a pure longitudinal mode response of the system with parallel, in-phase responses in the blades. The predicted longitudinal mode response for a half-wavelength cutting head, without and with slits, is shown in Figure 6.21 (a) and (b), respectively. Subsequently an EMA is conducted on the redesigned cutting head. The sum of the FRFs measured on the half-wavelength cutting head in the frequency range 0-50 kHz is shown in Figure 6.22. Figure 6.21 (c) presents the measured longitudinal mode shape of the head. The measurements confirm that bending responses in the outer blades are eliminated by the introduction of the slits in the block horn.

The half-wavelength cutting head, due to its reduced number of modes, provides straightforward opportunities to remove the adverse effects of modal coupling, where they exist, by making small geometry modifications to the design using a sensitivity analysis as described previously in Section 6.2.2.2.

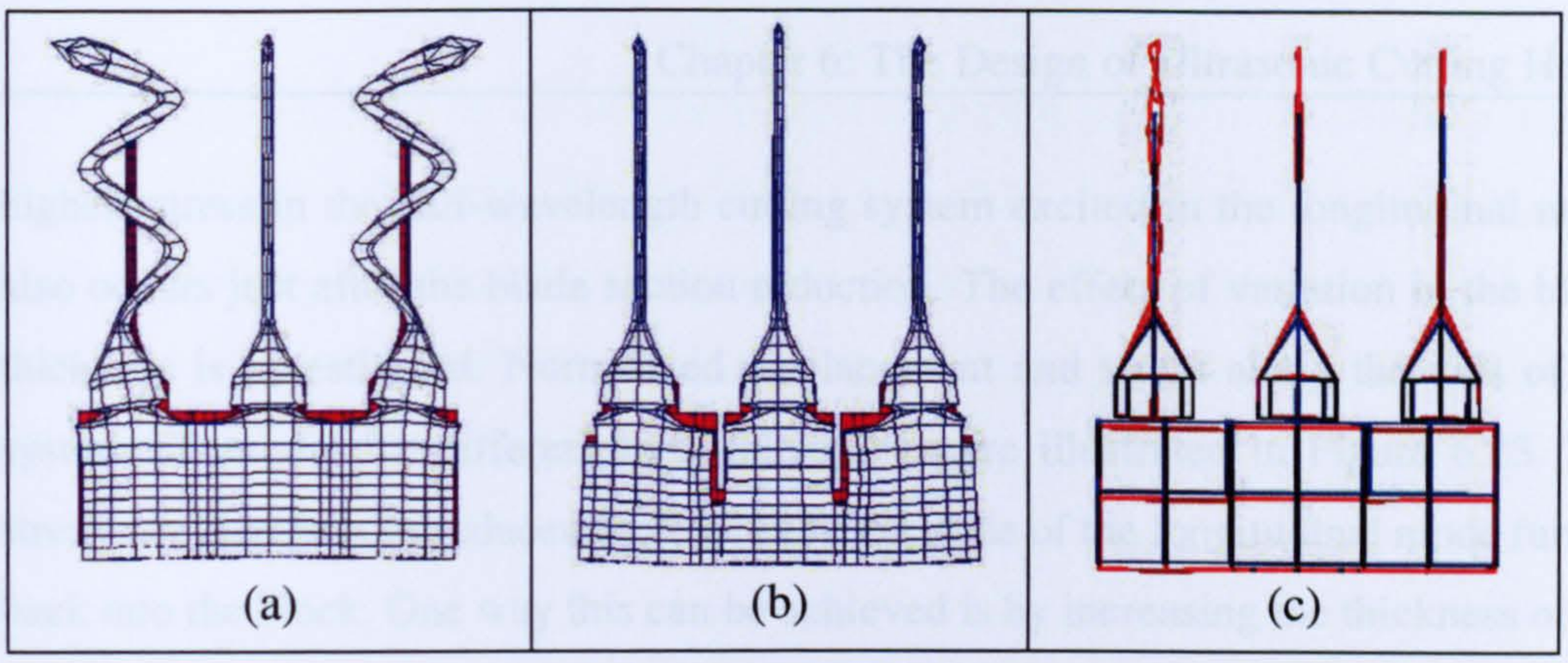

Figure 6.21. Predicted and measured longitudinal mode response of half-wavelength cutting head with (a) solid block horn (FEA), (b) double-slitted block horn (FEA), (c) double-slitted block horn (EMA)

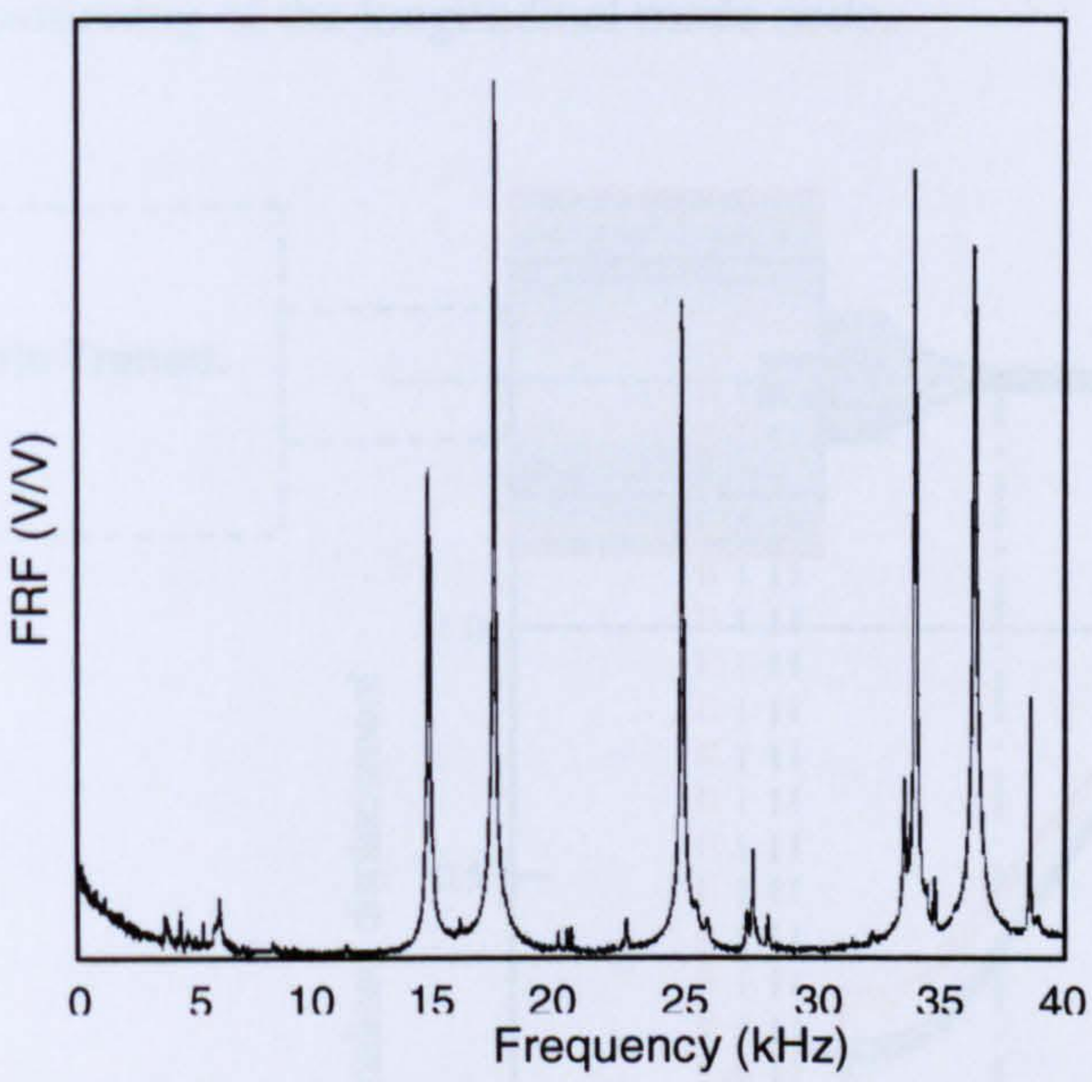

Figure 6.22. Sum of the FRFs measured in the half-wavelength three-blade head

6.3.2.2 Design strategies for reducing stress

An important consideration in the design of ultrasonic components is the stress condition. It has been shown that amplitude gain is achieved by using steep section reductions in the blade profiles and by altering the thickness and profile of the blocks. The result is that weak points exist that become failure locations in operation, and the most common failure location in cutting systems occurs just after the steepest section reduction in the blades. As discussed previously, the removal of bending responses in the cutting blades significantly reduces the number of blade failures, but other geometry modifications can also improve the reliability of the cutting assemblies. The

highest stress in the half-wavelength cutting system excited in the longitudinal mode also occurs just after the blade section reduction. The effect of variation in the block thickness is investigated. Normalised displacement and stress along the axis of the system FE model for different horn thicknesses are illustrated in Figure 6.23. The stress can therefore be reduced by relocating the node of the longitudinal mode further back into the block. One way this can be achieved is by increasing the thickness of the block. Figure 6.23 shows the reduction in stress at the highest stress location due to variation of block thickness in 2 mm increments, where increasing the thickness moves the node backwards, thus reducing the slope of the modal displacement curve. Altering other geometry parameters can also be used to improve the stress condition by judicious repositioning of the longitudinal mode node.

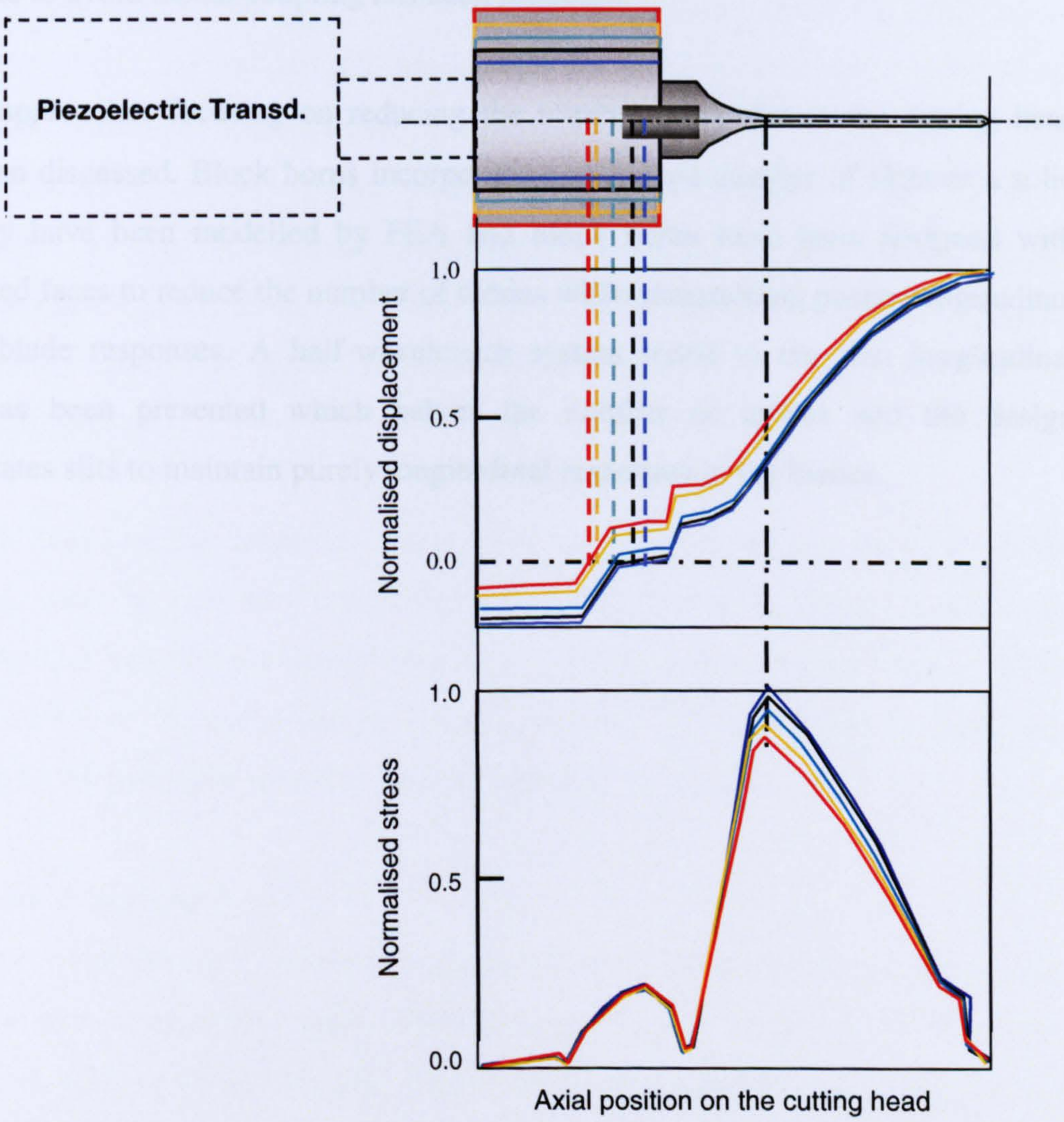

Figure 6.23. Predicted normalised axial displacement and stress for half-wavelength cutting head

6.4 Conclusions

This chapter has presented a numerical and experimental characterisation of the vibration behaviour of a three-blade ultrasonic cutting head used for cutting food products. Significant improvements in experimental validation of the FE models are achieved by the use of a 3D LDV, which allows modal analysis from both in-plane and out-of-plane response measurements, which are necessary for the classification of the modes of the system.

Strategies for reducing the maximum stress in the components of the assembly have been proposed. Stress reduction at the failure locations of the cutting blades is achieved by detuning the different system components while maintaining the system tuned frequency, and using geometry modification such as castellations to eliminate participation of bending motion in longitudinal-mode systems. Also, a design technique to avoid modal coupling has been proposed.

Design approaches focusing on reducing the number of modes in the cutting head have been discussed. Block horns incorporating a reduced number of slots or a solid geometry have been modelled by FEA and block horns have been designed with castellated faces to reduce the number of modes while maintaining purely longitudinal cutting blade responses. A half-wavelength system tuned to the first longitudinal mode has been presented which halves the number of modes and the design incorporates slits to maintain purely longitudinal responses in the blades.

CHAPTER 7

MODAL INTERACTIONS IN ULTRASONIC SYSTEMS

7.1 Introduction

Ultrasonic devices driven at high power in a longitudinal mode are often characterised by surprising phenomena such as frequency shifts, and particularly multiple responses, which tend to affect their performance. Evidence suggests that modal interactions are characteristic of ultrasonic systems where special relationships exist between two or more linear mode frequencies and the excitation frequency. Especially in devices characterised by many modes of vibration, external excitation of the tuned mode may excite one or multiple modes through what appears to be a nonlinear mechanism. Typically, systems tend to leak energy into lower modes [8], with the consequence for ultrasonic systems being that energy is leaked into audible modal frequencies and that the response of a tuned longitudinal mode includes bending and/or torsional contributions. The immediate consequence is that less energy excites the operating mode and stress is raised due to the additional responses, causing component failures.

Although multi-modal responses have been discussed and reported for simple structures, such as bars and beams [72-76], the reliability problems in ultrasonic tooling devices have not previously been linked to these phenomena. The focus of this study is therefore to investigate multi-modal responses in ultrasonic devices, with reference to the published models of simple dynamic systems.

7.2 Review of literature

In the last three decades, considerable research work has been carried out on the theoretical and experimental study of modal interactions of simple dynamic systems such as rods and cantilevered beams. This research effort has attempted to understand the vibration behaviour of flexible space structures characterised by many modes of

vibration. In these systems it was found that if the natural frequencies ω_i are matched with an external harmonic excitation, under a certain condition of the excitation (parametric excitation), energy exchanges between modes can occur. In particular, internal resonances or autoparametric resonances can exist when the external excitation frequency is close to a modal frequency which, in turn, corresponds to the sum or difference of two or more modal frequencies, depending on the degree of nonlinearity and the number of modes involved. These autoparametric resonances have been successfully treated by a number of authors using the widely used perturbation method of multiple scales. This method has been associated with several researchers but can mainly be attributed to Nayfeh [72]. The principle behind this technique is that the dependent variables of the equations of motion of a system are expanded in terms of two or more independent variables, or scales, instead of a single variable, thus taking better account of slow and fast oscillations within the system, this being a commonly occurring feature within nonlinear and parametric systems.

In 1980, Crespo da Silva [73] presented a theoretical study of autoparametric resonances in a base-excited cantilever beam using the perturbation method. Calculations showed that the beam's whirling (nonplanar) motions were the result of a modal coupling between bending and torsional modes. A previous work from Dugundji and Mukhopadhyay [74] dealt with the simultaneous excitation of two (bending and torsional) modes of a thin beam under parametric excitation. However, in this case the excitation frequency did not correspond to a natural frequency of the beam, but to the sum of the frequencies of the excited modes (parametric vibrations). A large body of experimental results, which show good agreement with the perturbation results, has also been published [75,76]. Important observations for a fundamental understanding of parametric stability, together with a detailed description of developments in practical applications, are encompassed in a review paper published by Barr [77]. In this work the effects of including small parametric terms in the equations of the modelled structures are characterised for those conditions under which they become of considerable significance.

In 1987 Cartmell [78] demonstrated that it is possible for two or more combination resonances to be excited simultaneously in vibrating structures under single frequency

external parametric excitation, and that an effect generated by a weaker type of coupling can in fact modify that of a stronger coupling to a significant extent. As in the work of Dugundji and Mukhopadhyay [74], a flexible cantilever beam undergoing axial excitation was investigated. A theoretical model of the system to first and second order approximation accurately predicted the observed laboratory behaviour within a range of excitation accelerations. A re-examination of this study has been published recently [79].

Research has shown that other nonlinear phenomena, such as chaotic motions, can be observed in parametrically excited system. Haddow and Hasan conducted an experimental investigation of a parametrically excited cantilever beam excited close to twice the natural frequency of its fourth bending mode [80]. They observed that during a slow frequency sweep of the excitation frequency, a planar periodic response that essentially consisted of the fourth mode of the beam internally excited via principal parametric resonance, lost stability and a nonplanar chaotic motion took place. Hence, the energy seemed to leak through the modes. A similar experiment was carried out in 1988 by Burton and Kolowith [81] who identified the modes involved in the chaotic motions.

Nonlinear systems under parametric excitations can also be characterised by a particular type of interaction between high and low-frequency modes, distinct from typical autoparametric resonances. Anderson et al. [82] conducted experiments on a parametrically excited cantilever beam and found that interactions could occur between two high-frequency modes and the fundamental mode, with the excitation of the fundamental mode not due to parametric internal resonance. Rather, it appeared that slow modulations of the high-frequency modes were responsible for energy transfer to the fundamental mode. In a later publication, Nayfeh and Nayfeh [83] experimentally investigated a cantilever beam with circular cross-section subject to axial excitation. One-to-one autoparametric resonances were found at each natural frequency of the beam due to its axial symmetry, with the result that the mode in the plane of the excitation interacted with the out-of-plane mode resulting in a nonplanar whirling motion. More importantly, it was observed that when the beam was excited near the natural frequency of its third or any higher mode, a large first-mode response appeared in the spectrum. As in the work of Anderson et al. [82], the appearance of

the first mode was accompanied by modulations of the amplitudes and phases of the high frequency modes.

Modal interactions via modulations have also been reported in ultrasonic systems externally excited at a frequency in the vicinity of the longitudinal mode of vibration. Graham and Lucas published an experimental study of the vibration behaviour of a multi-component ultrasonic tool, where the system resonance and component tuning are typically at variance with the transducer tuned frequency, due to inherent manufacturing tolerances [8]. Energy transfer into a system natural frequency, due to the input excitation, causes the system to vibrate with an amplitude modulation related to the driving frequency and equal to the separation between the tuned frequency and the driving frequency.

7.3 Introduction to parametric vibrations

In 1990, Cartmell published a book in which the subject of parametric vibrations is presented through the analysis of practical examples [84]. The theoretical analyses of relevance to the characterisation of ultrasonic systems is discussed here.

7.3.1 Parametric systems

The prediction of the response of harmonically excited dynamic systems can be complicated due to the participation of one or several modes in the response. The issue of modal interactions often depends on the type of applied excitation and the system nonlinearity. For instance, the effects of parametric excitation of a simple structure are such that very large responses may be generated in a plane perpendicular to that of the excitation, provided that certain relationships exist between the frequency of excitation and the frequency of the excited mode or modes. The term parametric is descriptive of cases where the external excitation appears as a time varying modification of a system parameter. In contrast, in forced vibrations the response of the system to the excitation depends entirely on whether a resonance condition is present, and there is no resulting time variation in the system parameters.

A case of forced vibration and two typical parametric configurations, for which there is a parameter varying with harmonic excitation, are given in Figure 7.1, where a simple beam is in turn excited in the three spatial directions by a harmonic force.

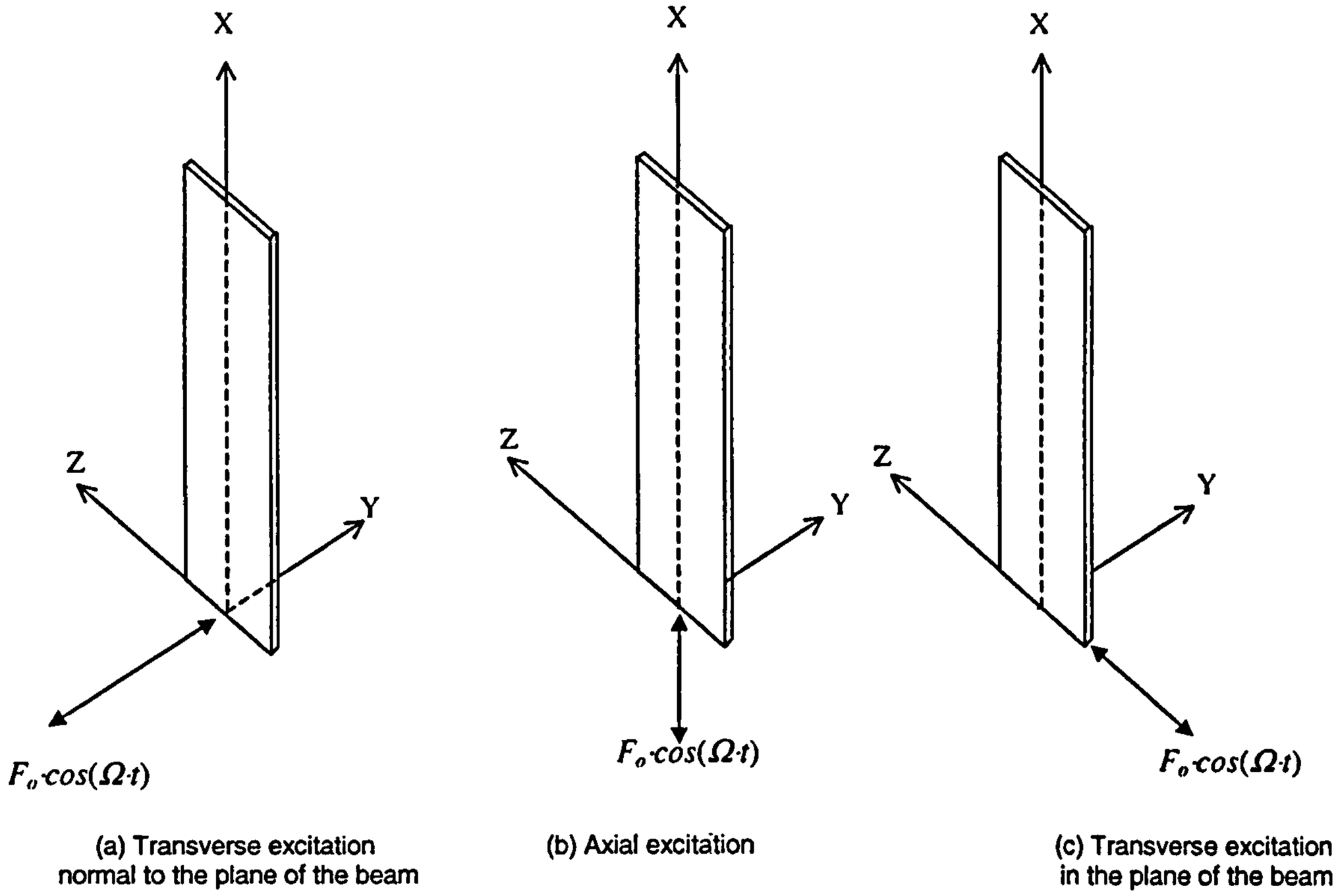

(a) Transverse excitation normal to the plane of the beam

(b) Axial excitation

(c) Transverse excitation in the plane of the beam

Figure 7.1. Examples of (a) a forced and (b,c) two parametric configurations of a harmonically excited beam

In general mathematical terms, the inhomogeneous differential equations of motion for a forced system are replaced by homogeneous forms, in which there exist a varying periodic coefficient in the parametric case. This is typified by the fundamental Mathieu-Hill equation

$$\ddot{q} + (a + b\cos\Omega t)q = 0\,. \tag{7.1}$$

A more generalised version for which the excitation function $f(t)$ is periodic, but not necessarily harmonic, is the Hill equation,

$$\ddot{q} + (a + f(t))q = 0\,. \tag{7.2}$$

Parametric systems respond when the frequency of excitation is related to the natural frequency (or frequencies) by a resonance condition, and this does not imply synchronicity between these frequencies.

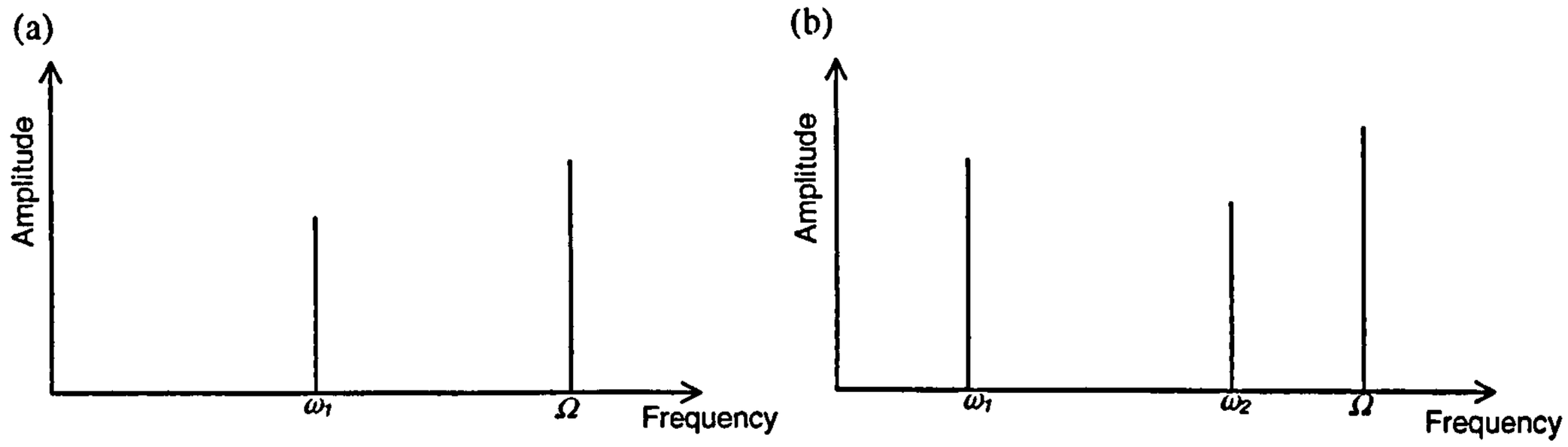

Figure 7.2. Frequency spectra for typical parametric combination resonances; (a) two modes modal interaction (principal parametric resonance), (b) three modes interaction

So, large responses may be generated in cases where the excitation frequency is remote (but related through an integer or fractional multiple of some sort) from the natural frequency or frequencies. Figure 7.2 illustrates the spectral plots of two combination resonances typical of parametrically excited systems, where internal modes are related to the external excitation frequency through the following resonance conditions (or internal couplings):

$$\Omega \cong 2\omega_1 \text{ and } \Omega \cong \omega_1 + \omega_2 \tag{7.3}$$

7.3.2 Autoparametric systems

An autoparametric system consists of a primary system, which is an externally excited forced oscillator, coupled to a secondary system which is parametrically excited by the response of the primary system. Assuming that the primary system is excited close to resonance, such that $\Omega \cong \omega_1$, then if the excitation frequency is such that, for instance, $\omega_1 \cong 2\omega_2$, where ω_2 is a natural frequency of the secondary system, the secondary system's response will be a principal parametric resonance. For this case, there can be an energy flow that results in responses in both modes, at ω_1 and ω_2. In general, an autoparametric system is one where internal coupling exists between two or more modes and a response relationship exists between these modes and the excitation frequency.

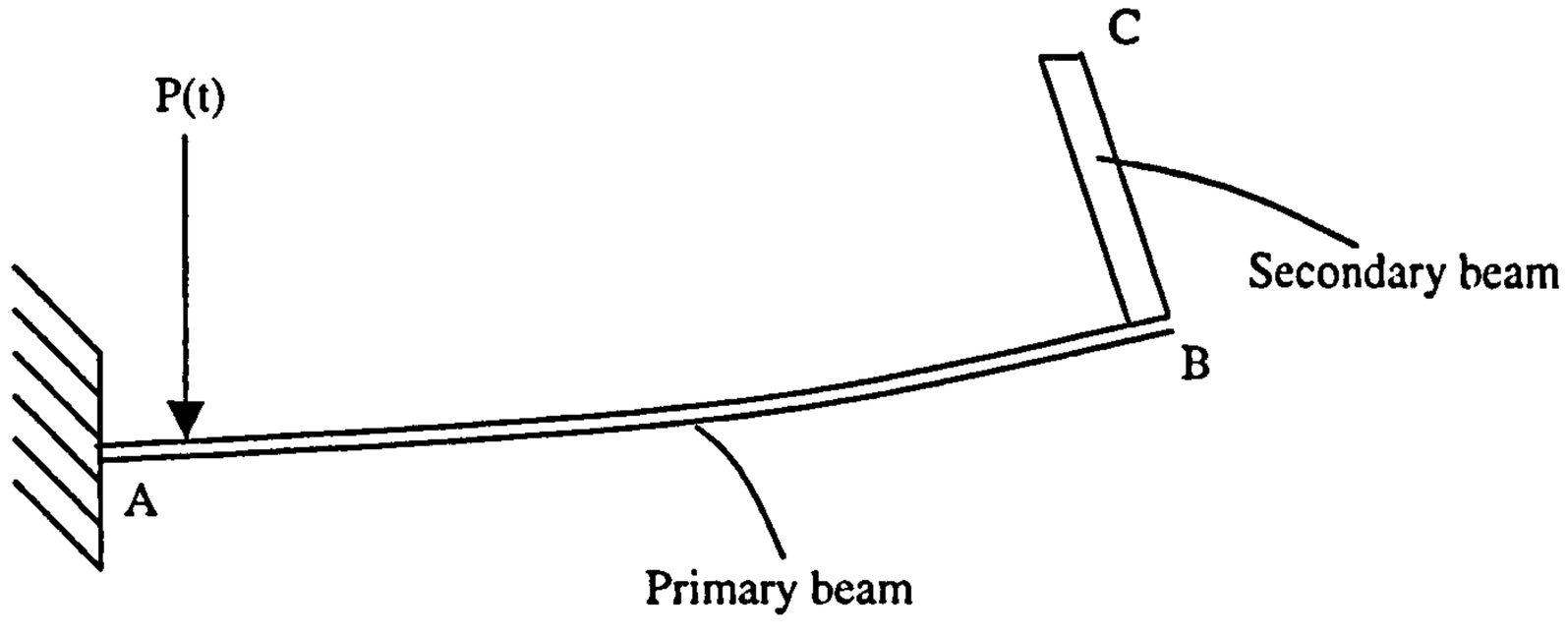

Figure 7.3 Coupled beam interaction problem showing primary response resulting from an imposed external excitation P(t) [84]

Cartmell [84] has shown that for an example of a two DoF system of two coupled beams, illustrated in Figure 7.3, the responses of the primary and secondary systems of the two-mode autoparametric system can be solved using the following equations of motion:

$$\ddot{x}+2\xi_1\omega_1\dot{x}+\omega_1{}^2x-\varepsilon\mu(\dot{y}+y\ddot{y})=P_0\cos\Omega t, \tag{7.4}$$

$$\ddot{y}+2\xi_2\omega_2\dot{y}+\omega_2{}^2y-\varepsilon\ddot{x}y=0, \tag{7.5}$$

where ξ_1, ξ_2 are damping ratio terms and ε and μ are constants.

The nonlinear coupling between the two equations is apparent in the terms $\varepsilon\mu(\dot{y}+y\ddot{y})$ and $\varepsilon\ddot{x}y$. Eq. (7.4) can be reduced to a linear forced oscillator (with one degree-of-freedom) if the nonlinear term disappears. The other equation of motion, Eq. (7.5), is clearly a parametric type equation where $\ddot{x}$ acts as a coefficient of the coordinate y.

The calculated primary and secondary system responses are represented in Figure 7.4, where P_0 indicates a chosen excitation level. The region of modal interaction is bounded by ABCD in Figure 7.4 (a) and (b). Outside this region Eq. (7.4) drops the nonlinear term and becomes the equation of motion for a forced linear oscillator, as stated above.

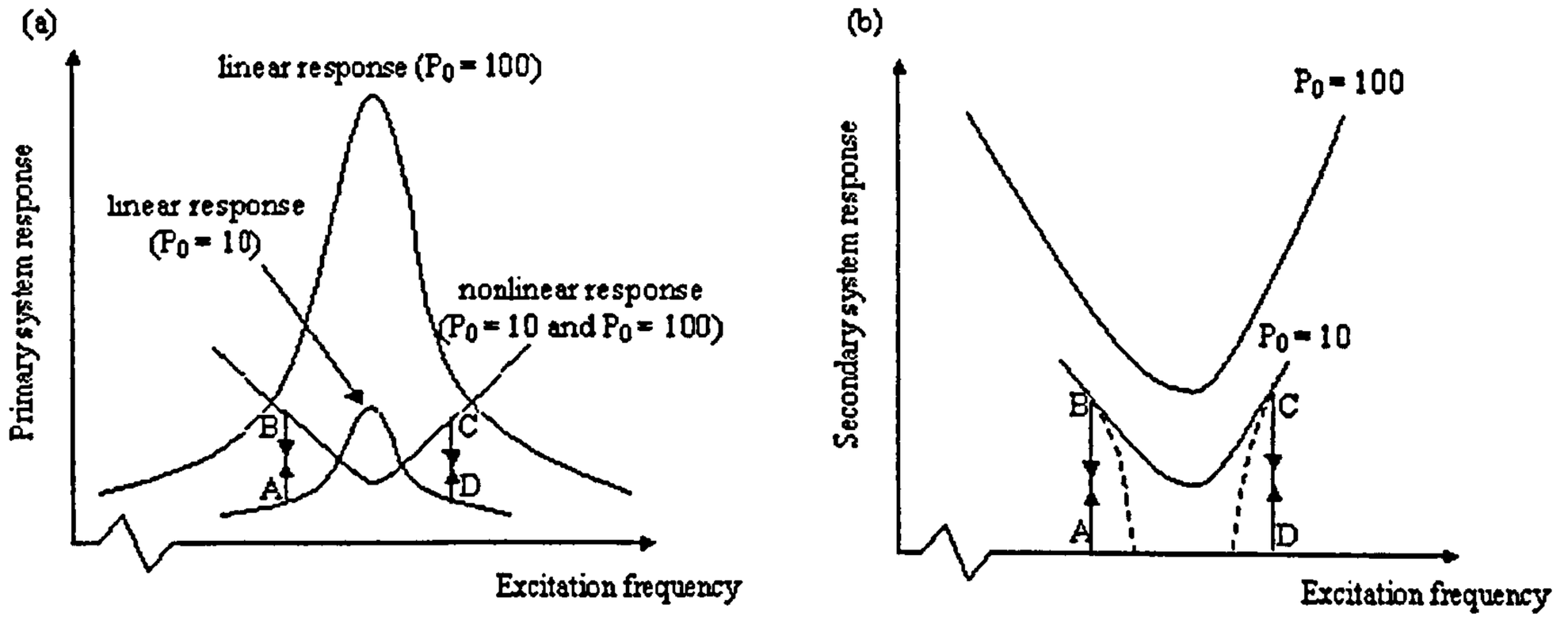

Figure 7.4. Responses for two-mode autoparametric coupling: (a) theoretical primary response, (b) theoretical secondary response [84]

In Figure 7.4 (a) there is an exact relationship, $\omega_1 = 2\omega_2$. The linear response, for the chosen excitation level $P_0 = 10$, is replaced by a v-shaped curve where nonlinear autoparametric interaction occurs. The secondary system response, shown in Figure 7.4 (b), follows the linear curve in a sweep-up of the excitation frequency until reaching point A, where the response jumps from A to B, and continues along the nonlinear curve to point C, where the response jumps from C to D and then returns to a linear response. Jumps AB and CD are symmetrical about the linear resonance. A larger excitation level ($P_0 = 100$) would extend the frequency region over which the nonlinear characteristics occur and would increase the magnitudes of responses. The nonlinear primary response in Figure 7.4 (a) is independent of P_0, in fact an increase in P_0 to $P_0 = 100$ would simply promote jumps AB and CD at points further away from ω_1 than the lower excitation level of $P_0 = 10$.

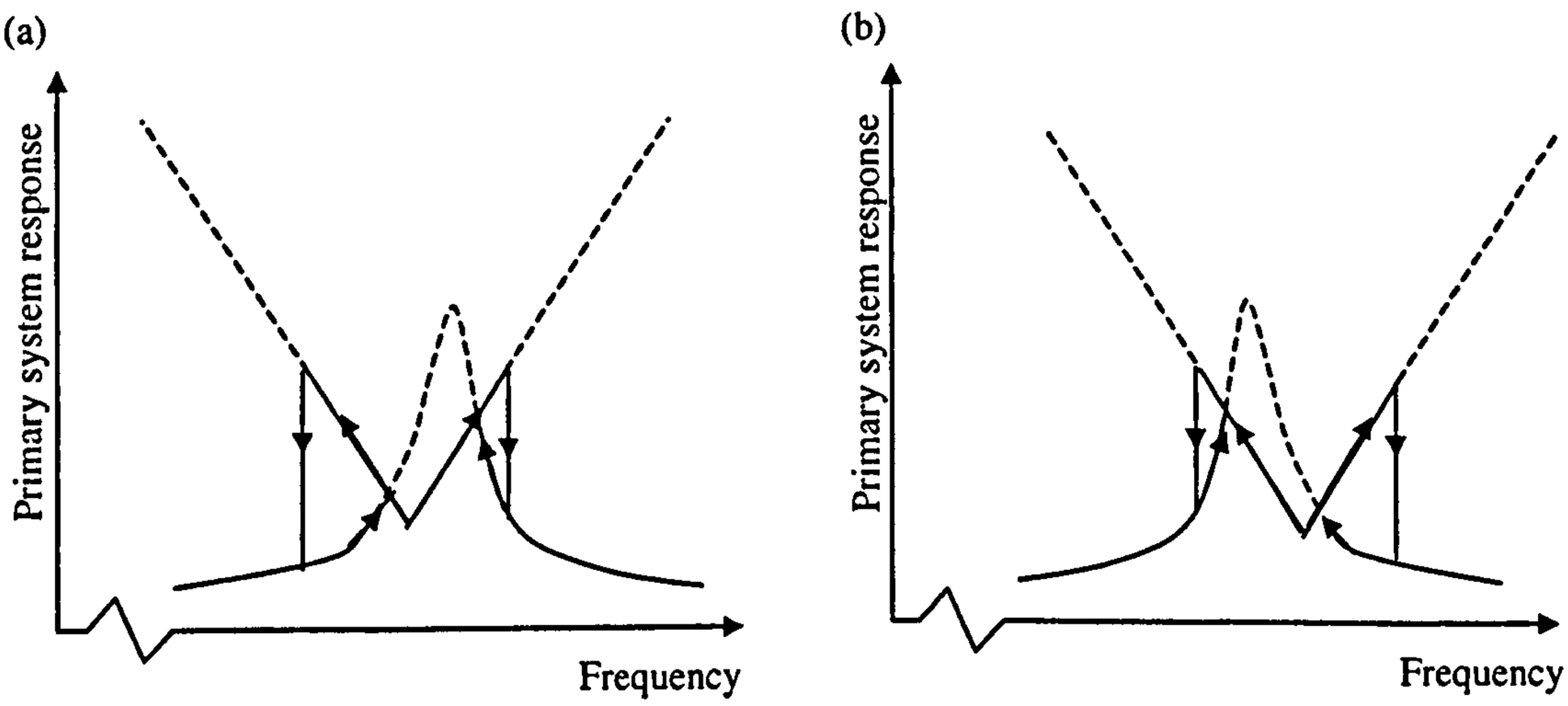

Figure 7.5. Theoretical primary responses: (a) $(\omega_2/\omega_1) = 0.48$, (b) $(\omega_2/\omega_1) = 0.52$

Where an exact relationship does not exist, and $\omega_1 \cong 2\omega_2$, the primary system response loses this symmetry about the linear resonance, as illustrated for two cases where $\omega_2/\omega_1 = 0.48$ and $\omega_2/\omega_1 = 0.52$ in Figure 7.5.

7.4 Combination resonances in ultrasonic systems

In ultrasonic cutting systems, energy can leak into bending and torsional modes at frequencies lower than the excitation frequency, as a direct result of tuning and exciting the system in a longitudinal mode of vibration. In particular, the principal parametric resonance $\omega_1 \cong 2\omega_2$ and relationships involving combination resonances, $\omega_1 \cong \omega_2+\omega_3$, where ω_2 and ω_3 are two internal modes, are typically identified in ultrasonic systems. The vibration behaviour of these complex ultrasonic devices can therefore appear to be similar to published models of autoparametric systems.

In this section the vibration behaviour of single-component and multiple-component ultrasonic systems are experimentally characterised to illustrate the excitation of combination resonances.

7.4.1 Combination resonance in an ultrasonic block horn

The first resonator under investigation is a double-slotted block horn used as the intermediate component in a three-bladed cutting head, shown in Figure 7.6.

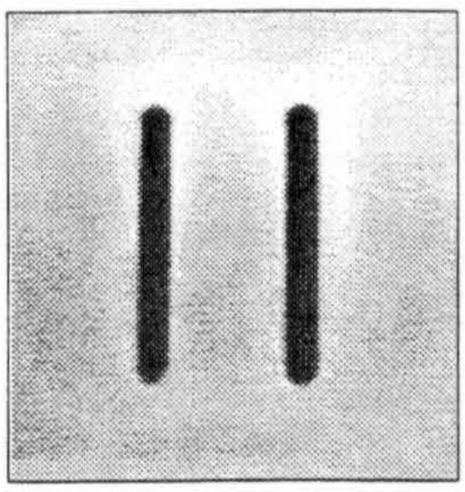

Figure 7.6. Double-slotted block horn

As discussed in Session 5.3, conventional block horn design relies on the use of standard slotted geometries and profiles. Block profiles are largely based on the required amplitude gain for the output face, while slots are used to control the vibration amplitude uniformity on the output face, and also control the separation of

non-tuned modal frequencies from the tuned frequency. As a result, slotted block configurations result in the presence modes of vibration associated with the width of the horn columns.

An FE model of the block horn is performed in order to predict its modes of vibration in a 0 – 40 kHz frequency range. Furthermore, a steady-state dynamics step, calculating the amplitude of the horn response caused by harmonic excitation over the same frequency range, is created in order to simulate the transducer excitation.

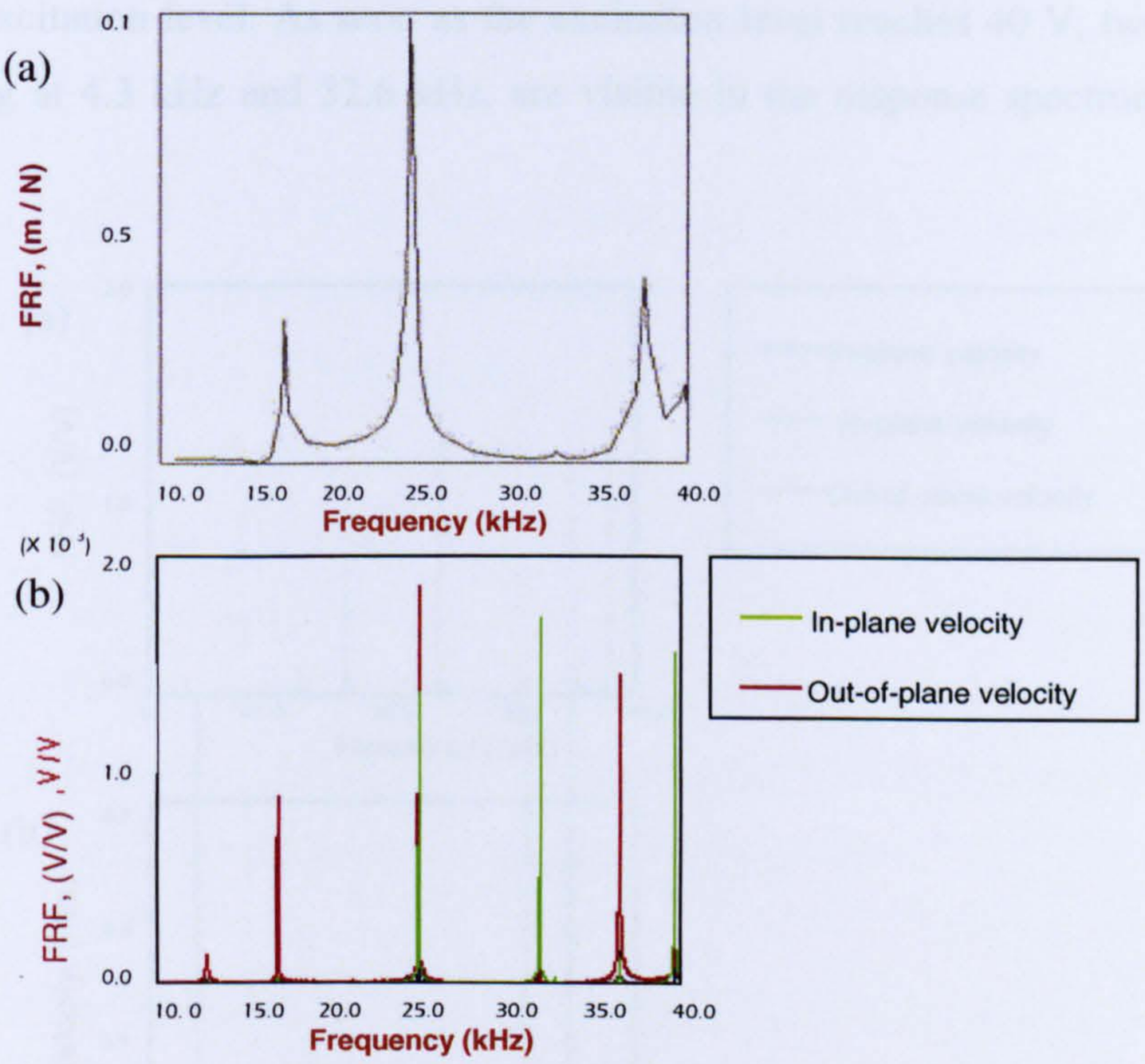

Figure 7.7. FRFs from block horn:
(a) predicted, (b) measured

The FRF of the block horn is also measured using the experimental rig used for swept-sine excitation as described in Section 3.4.3. The response of the block horn-transducer system is measured by the 3D LDV over the same frequency range as the numerical simulation. The predicted and measured FRFs at a corner of the block horn are shown in Figure 7.7. Good correlation between the predicted and measured modal frequencies is achieved. However, the predicted FRF (Figure 7.7 (a)) exhibits a lower

number of modes than the measured one (Figure 7.7 (b)), and there are differences between the predicted and measured responsiveness of the modes. Such discrepancies are due to the simplistic model of the transducer-block horn, which neglects the modes introduced by the transducer.

Subsequently, to inspect whether modal interactions occur during the operation of the transducer-horn stack, an experimental sweep of the excitation frequency is performed in a small frequency band around the horn's longitudinal frequency (37 kHz). The frequency is gradually swept over a range of 300 Hz with the sweep repeated for 5 V increments of the excitation level. As soon as the excitation level reaches 40 V, two responses, occurring at 4.3 kHz and 32.6 kHz, are visible in the response spectrum (Figure 7.8 (b)).

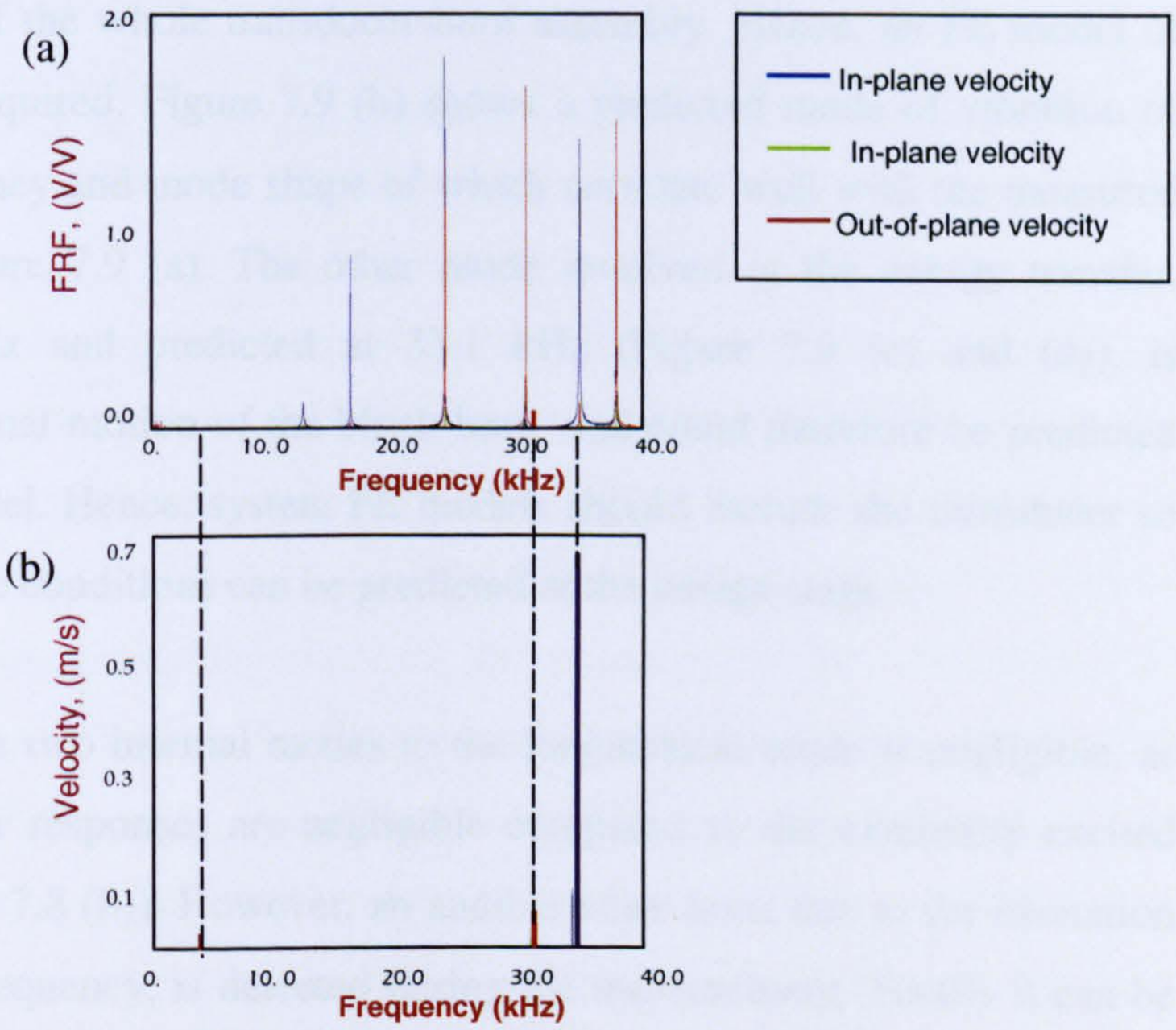

Figure 7.8. (a) FRF of the block horn measured in 0-50 kHz frequency range, (b) three-mode combination resonance

The ratios of the velocity response of the directly driven longitudinal mode and the other two responses in the spectrum, are of the order of 20:1. The sum of the frequencies of the indirectly excited responses is equal to the frequency of the externally driven mode. The response detected at 32.6 kHz corresponds to a mode of vibration, as evident in the measured FRF (Figure 7.8 (a)). Conversely, the FRF does

not exhibit any resonant mode at the frequency of the other response component, detected at 4.3 kHz (Figure 7.8 (b)). An EMA of the system carried out by FRF measurements of the entire surface of the block, and partially of the transducer, allows the classification of 4.3 kHz also as a mode of vibration. This demonstrates the importance of EMA which prevents the problem of missing modal responses performing single FRF measurements. The block horn-transducer system behaves as an autoparametric system where the driven mode and the indirectly excited modes form a combination resonance involving three system modes. The experimentally detected mode shapes of the two internal modes excited through the combination resonance, are illustrated in Figure 7.9. The low frequency mode, shown in Figure 7.9 (a), is a bending mode of the transducer and block horn assembly in the plane of the block.

The FE model of the block horn alone does not predict the 4.3 kHz mode, because it involves the motion of the whole transducer-horn assembly. Hence, an FE model of the entire system is required. Figure 7.9 (b) shows a predicted mode of vibration of the system, the frequency and mode shape of which correlate well with the measured bending mode of Figure 7.9 (a). The other mode involved in the energy transfer, measured at 32.6 kHz and predicted at 33.1 kHz (Figure 7.9 (c) and (d)), is characterised by torsional motion of the block horn, and could therefore be predicted by the block horn model. Hence, system FE models should include the transducer so that potential resonance conditions can be predicted at the design stage.

The contribution of the two internal modes to the longitudinal mode is negligible, as the amplitudes of their responses are negligible compared to the externally excited mode response (Figure 7.8 (b)). However, an audible noise level due to the excitation of the lowest modal frequency, is detected during the measurement. Finally it can be observed that, whereas at the low excitation levels required for EMA, untuned bending and torsional modes are not excited by the longitudinal mode transducer, at higher excitations the system can lose stability, self-exciting bending and torsional responses.

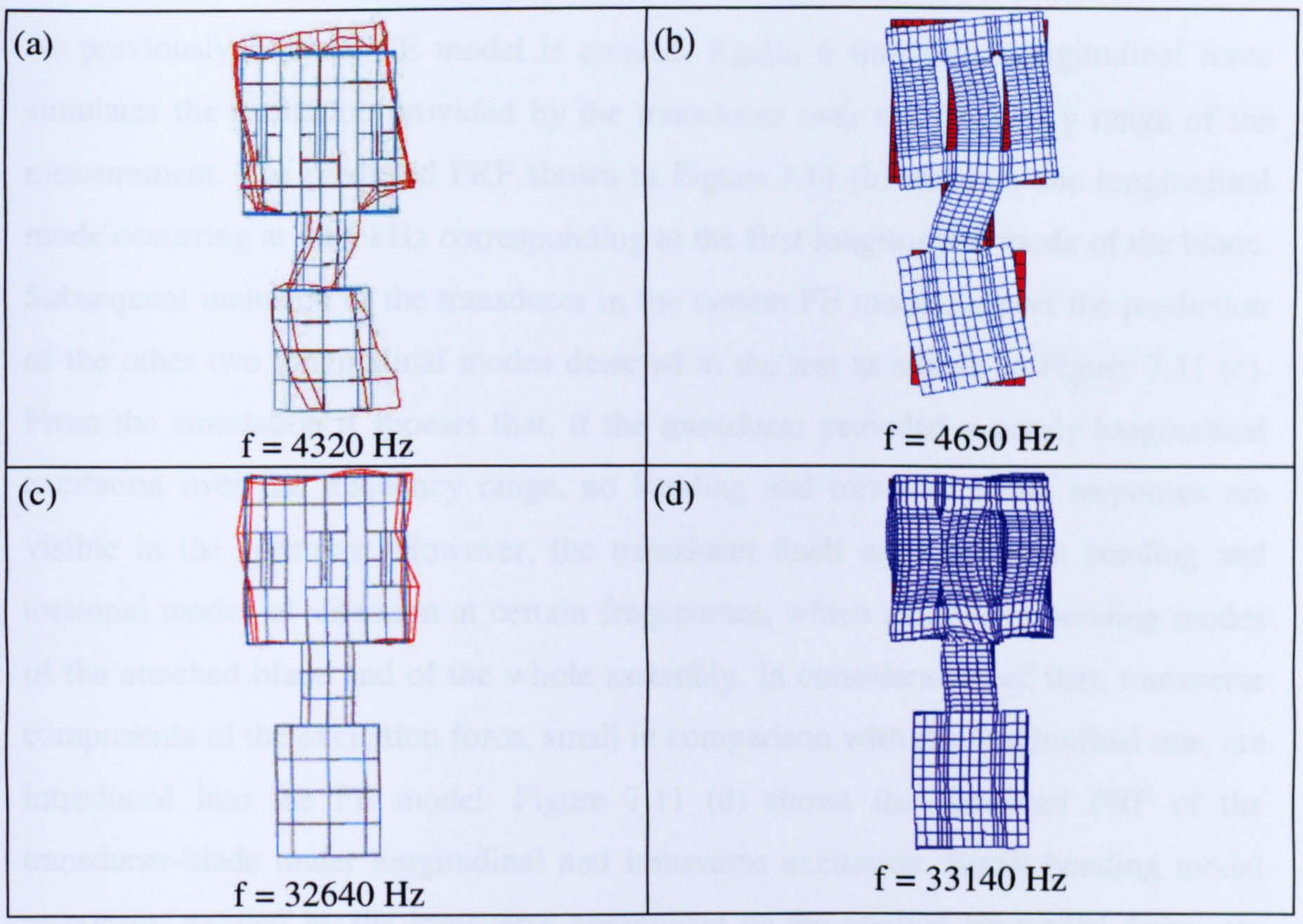

Figure 7.9. Measured and predicted mode shapes of the combination modes of the assembly: transducer-block horn bending mode (a) measured, (b) predicted; block horn torsional mode (c) measured, (d) predicted

7.4.2 Combination resonances in a single-blade cutting system

A test is also conducted to study the vibration characteristics of the single-blade ultrasonic cutting system shown in Figure 7.10, whose modes of vibration were predicted and validated in Section 4.2.3 through FEA and EMA. A complete EMA of the cutting device enabled classification of all the modes by random excitation test in the 0 – 50 kHz frequency range. The FRFs measured from a point at the tip of the blade are shown in Figure 7.11 (a). The figure highlights the presence of three responsive modes corresponding to three longitudinal modes of the transducer-blade assembly, alongside several small resonance peaks matching the frequencies of bending and torsional modes.

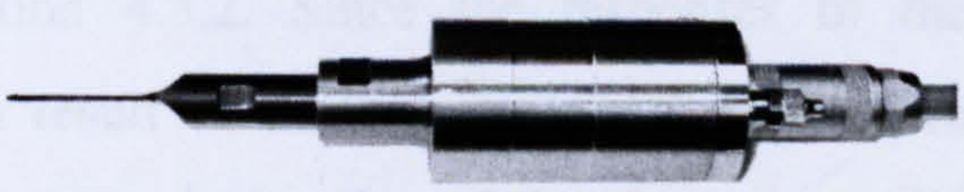

Figure 7.10. Transducer-blade ultrasonic cutting system

As previously, a blade FE model is created. Again, a sinusoidal longitudinal force simulates the excitation provided by the transducer over the frequency range of the measurement. The predicted FRF shown in Figure 7.11 (b) exhibits one longitudinal mode occurring at 35.5 kHz corresponding to the first longitudinal mode of the blade. Subsequent inclusion of the transducer in the system FE model, allows the prediction of the other two longitudinal modes detected in the test as shown in Figure 7.11 (c). From the simulation it appears that, if the transducer provided a purely longitudinal excitation over the frequency range, no bending and torsional mode responses are visible in the spectrum. However, the transducer itself exhibits some bending and torsional modes of vibration at certain frequencies, which can excite bending modes of the attached blade and of the whole assembly. In consideration of that, transverse components of the excitation force, small in comparison with the longitudinal one, are introduced into the FE model. Figure 7.11 (d) shows the predicted FRF of the transducer-blade under longitudinal and transverse excitation. Small bending modal responses, excited by the transverse component of the applied sinusoidal force, are predicted in a frequency region around 5 kHz, improving agreement with the measurement of Figure 7.11 (a).

Modal interactions are experimentally identified from a slow frequency sweep over a narrow frequency band around the tuned longitudinal mode frequency at 35.3 kHz, at constant increments of the excitation voltage. The excitation frequency is swept forward and backward over a range of 300 Hz at increments of 5 V. At 30 V excitation, two peaks appear in the spectrum which correspond to frequencies identifiable in the FRF (Figure 7.12 (a) and (b)) at 16.8 kHz and 18.3 kHz, corresponding to the third bending mode, $f_{3B_y}^{BT}$, and to the second torsional mode, $f_{2T_z}^{BT}$, of the transducer-blade assembly, respectively (Figure 7.13). The superscripts BT indicates that both blade (B) and transducer (T) are involved in the motion, whereas the subscripts, $3B_y$ and $2T_z$, indicate the mode types according to the classification of Section 4.3.2. Since the responses of the bending modes are particularly low, as a result of the mainly longitudinal excitation provided by the transducer, a logarithmic scale is adopted for the measured FRF and the response spectra.

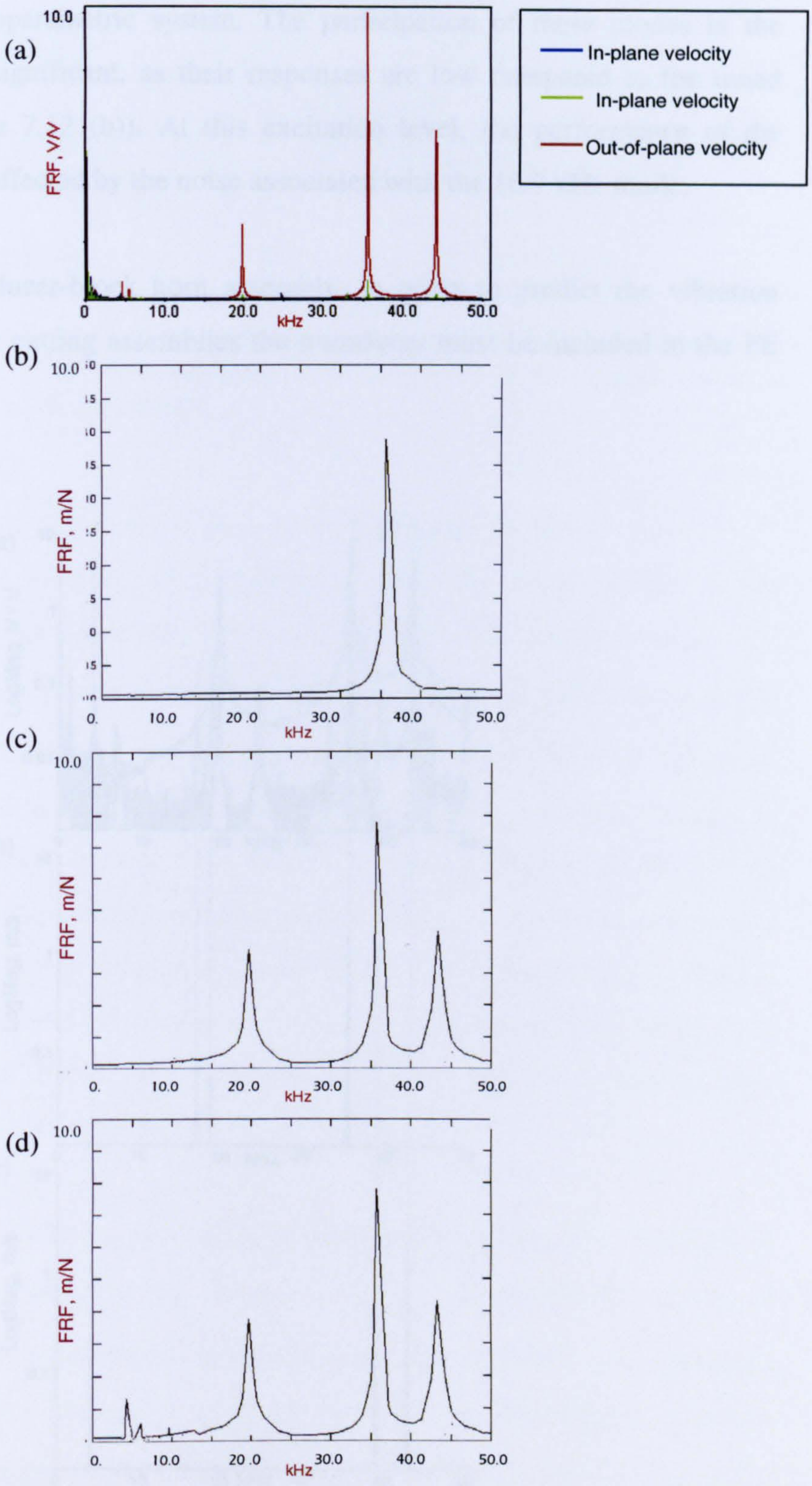

Figure 7.11. FRFs: (a) measured, (b) predicted for the blade (axial excitation) (c) predicted for the blade-transducer assembly (axial excitation), (d) predicted for the blade-transducer assembly (axial and transverse excitation)

The sum of the internally excited modal frequencies is equal to the frequency of the driven mode, $f_{2L_y}^{BT}$, which is evidence of a combination resonance, $f_{2L_y}^{BT} \approx f_{3B_y}^{BT} + f_{2T_y}^{BT}$, and typical of an autoparametric system. The participation of these modes in the overall response is insignificant, as their responses are low compared to the tuned mode response (Figure 7.12 (b)). At this excitation level, the performance of the cutting system is only affected by the noise associated with the 16.9 kHz mode.

As seen for the transducer-block horn assembly, in order to predict the vibration behaviour of ultrasonic cutting assemblies the transducer must be included in the FE model.

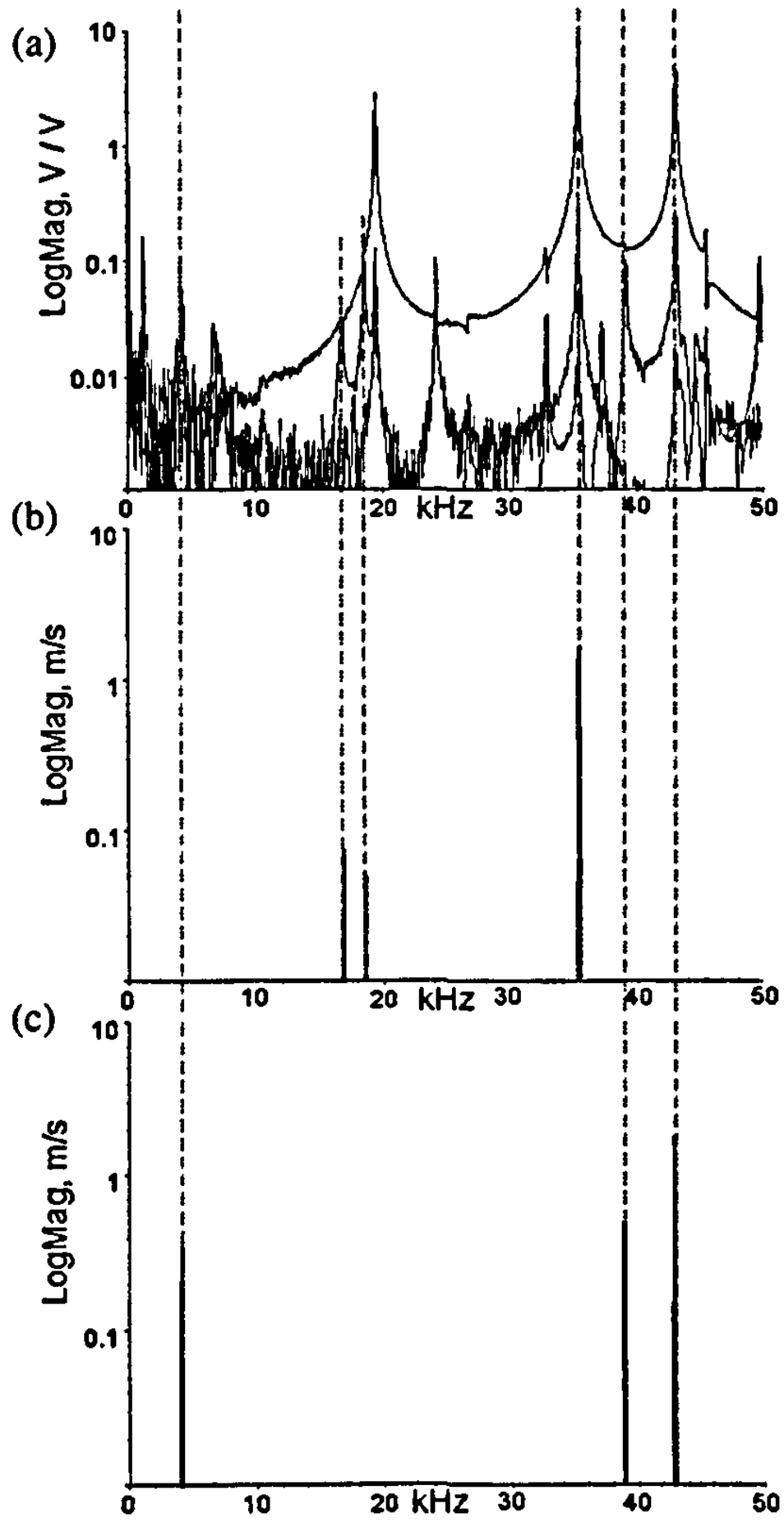

Figure 7.12. (a) FRF from transducer-blade system, (b) combination resonance I, (c) combination resonance II

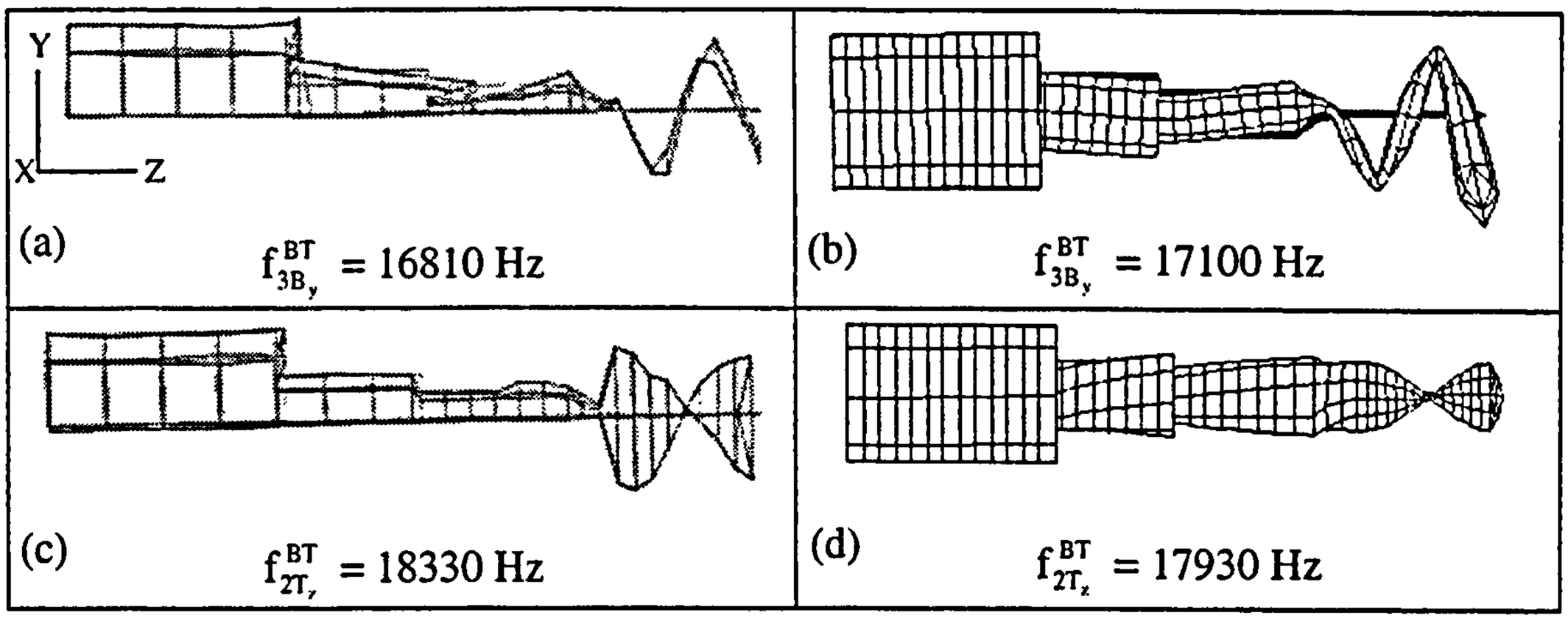

Figure 7.13. (a,c) Measured and (b,d) predicted mode shapes of an internal resonance; (a,b) third bending mode of the transducer-blade assembly, (c,d) second torsional mode of the transducer-blade assembly

7.4.2.1 Single-blade cutting system driven in lower and higher frequency modes

In order to investigate whether other resonance conditions are detectable in the system, the transducer-blade assembly is driven in the first longitudinal mode at 19.7 kHz ($f^{BT}_{1L_z}$), which is not the tuned mode of the system. The excitation frequency is again swept over a 300 Hz range at 5 V increments of the excitation level. However, in this case no combination resonances are measured at any excitation voltage. In principle, energy exchanges between the excited mode and untuned modes can be both upward and downward, but experiments indicate a preference for modes to pass energy downwards to lower frequency modes [77]. When the cutting system is externally driven in a lower frequency at its first longitudinal mode (19.7 kHz), there is a smaller number of modes at frequencies below the driving frequency, thus combination resonances are less likely occur.

The system is finally driven at 42.9 kHz, corresponding to the third longitudinal modal frequency of the assembly, $f^{BT}_{3L_z}$ (Figure 7.12 (c)). As previously, a sweep of the excitation frequency is performed. In this case, at 20 V excitation two responses, corresponding to the first in-plane bending mode of the transducer-blade assembly and the third torsional mode of the blade, occur at 4.8 kHz ($f^{BT}_{1B_x}$) and 38 kHz ($f^{B}_{3T_z}$) respectively, and satisfy the internal resonance, $f^{BT}_{3L_z} \approx f^{BT}_{1B_x} + f^{B}_{3T_z}$. Figure 7.14 illustrates the measured and predicted mode shapes of the excited modes of the

combination. The FE model of the blade alone predicts the higher frequency mode of the pair as illustrated in Figure 7.14 (d), this mode exhibiting only blade responses (Figure 7.14 (c)). The transducer contributes to the bending motion of the lower frequency mode as visible in Figure 7.14 (a). Hence, this mode can only be predicted by including the transducer in the FE model of the system (Figure 7.14 (b)).

In this case, the response of the internally excited modes are of the same order as the externally driven mode (Figure 7.12 (c)). In addition, the 4.3 kHz mode is clearly audible.

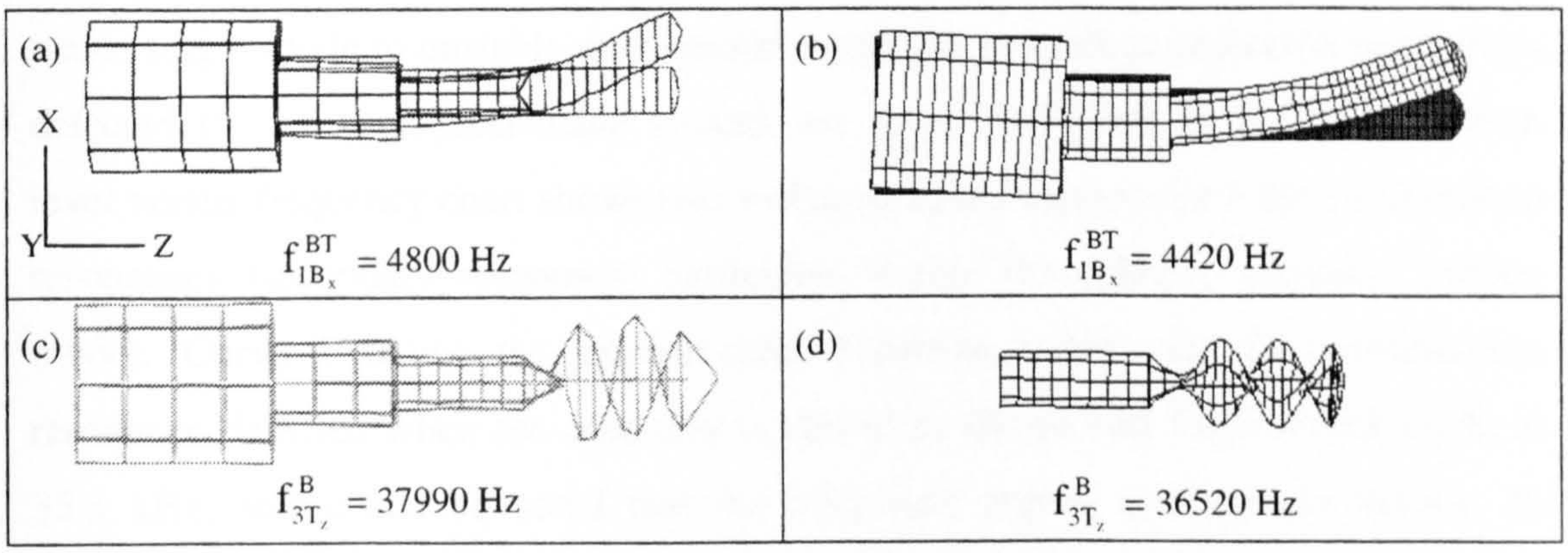

Figure 7.14. Mode shapes of an internal resonance of the assembly; (a) measured and (b) predicted 1st in-plane bending mode, (c) measured and (d) predicted 3rd torsional mode

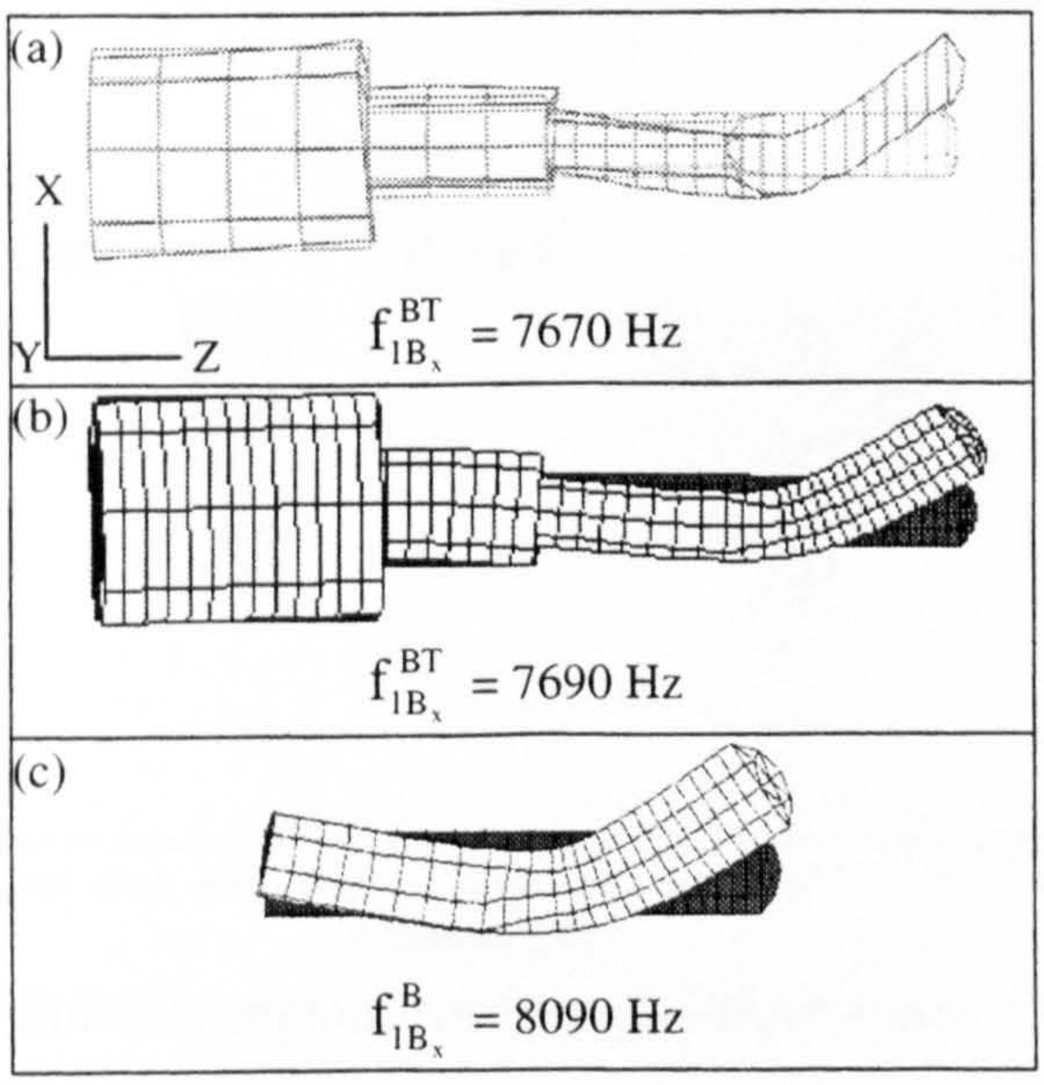

Figure 7.15. (a-b) Measured and predicted 2nd in-plane bending mode of the assembly, (c) Predicted 1st in-plane bending mode of the blade

Another example demonstrating how incomplete FE models lead to misinterpreted mode shapes, is shown in Figure 7.15. Figure 7.15 (a) and (b) illustrate the measured and predicted second in-plane bending mode of the assembly at 7.7 kHz. The blade model alone predicts its first in-plane bending mode at a close frequency (Figure 7.15 (c)), but the two modes are different.

7.4.2.2 Stabiliy regions

It is convenient to identify the regions inside which the system response switches from a single mode to a multi-modal response, in terms of the excitation frequency and the excitation level. Experimentally obtained boundaries for the transition from stable single-mode to unstable multi-modal responses of both combination resonances detected for the transducer-blade system, are given in Figure 7.16. The excitation level versus frequency chart shows two v-shaped zones inside which the combination resonances (secondary responses) participate within the primary response (driven mode). Curve I shows the experimental transition values for the combination resonance detected when the assembly is driven in the second longitudinal mode at 35.3 kHz, and it can be noted that the instability region is relatively narrow. In addition, the excitation threshold at which the system goes unstable is 30 V. On the other hand, the instability region of the second combination resonance, detected when the system is driven at 42.9 kHz, described by Curve II, is wider and has a lower threshold.

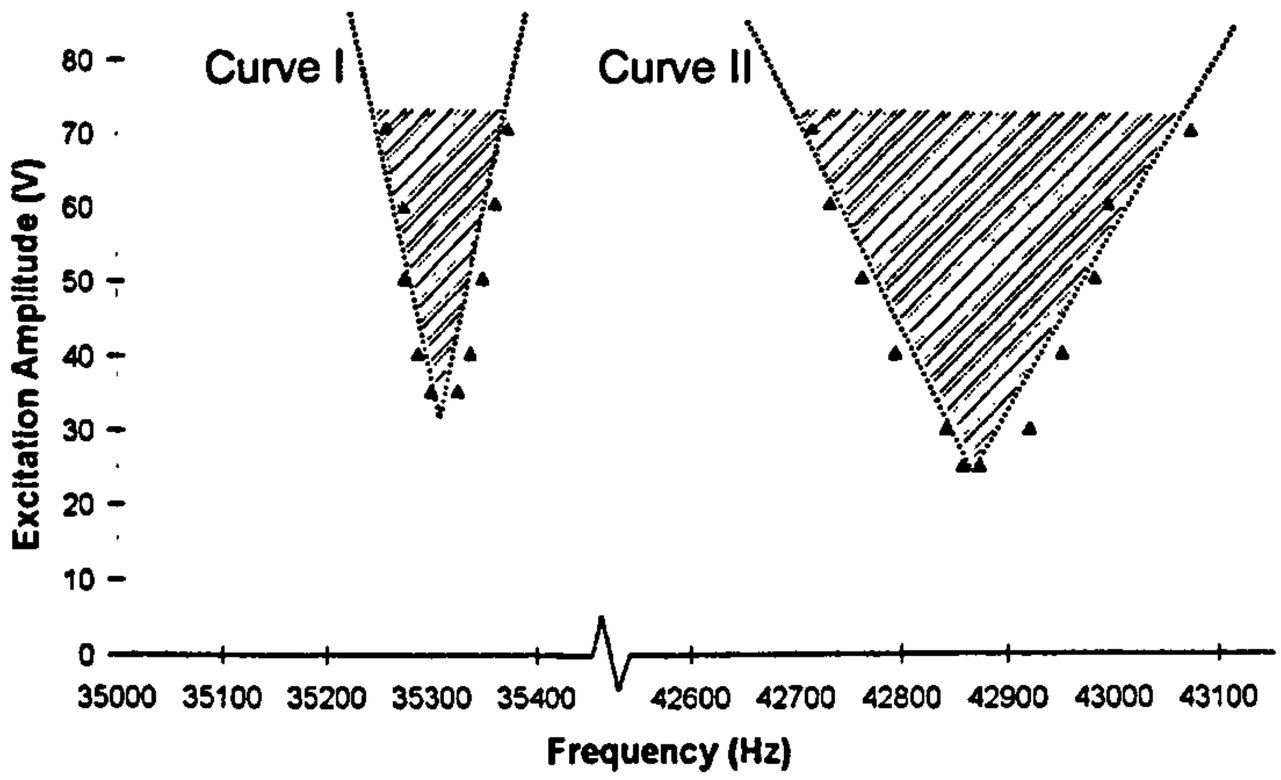

Figure 7.16. Stability regions for the transducer-blade ultrasonic cutting system

The transition curves of the instability regions indicate the degree of coupling between the tuned mode and the internally excited modes. Frequency shifts of the modes involved in a combination resonance are necessary to uncouple the externally excited mode from the internal modes. These frequency shifts depend on the width and threshold of the transition curve. Bigger frequency shifts are required to get rid of a strong modal coupling, characterised by a wider instability zone and lower threshold.

Alteration of the positioning and/or length of the threaded stud connecting the transducer and the blade, constitutes a simple strategy to control the frequencies of the modes involved in a resonance condition. The normal attachment configuration has the threaded stud connecting the blade and the transducer half screwed into the transducer and half into the blade.

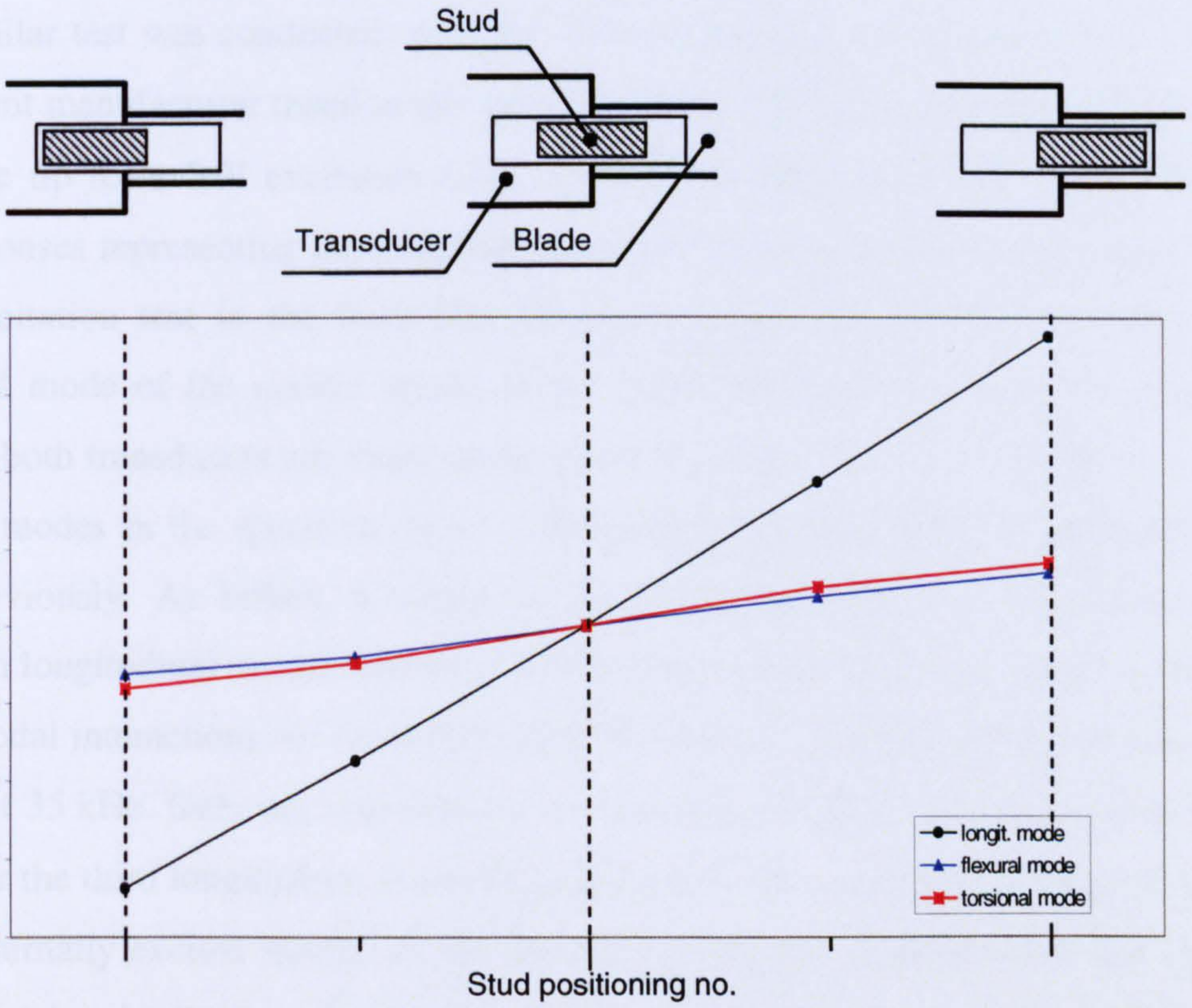

Figure 7.17. Frequency trend of the combination modes due to different stud positioning

A sensitivity analysis is performed of the combination mode frequencies, detected in the operation tuned mode response, to different positions of the threaded stud. Figure

7.17 shows the dependence of the modal frequencies of the first combination resonance on stud position. It is evident that the stud location mainly affects the frequency of the tuned mode, whereas the other modal frequencies prove comparatively insensitive. The largest shift of the tuned mode frequency is detected for the configuration with the threaded stud fully screwed into the blade.

A frequency sweep around the tuned mode frequency, obtained for this attachment configuration, reveals no energy exchange between the driven mode and other modes in the spectrum. Therefore, a detuning strategy based only on connecting stud repositioning results eliminates the modal interaction in the single-blade cutting assembly.

7.4.2.3 Influence of transducers on response characteristics

Finally, to establish whether modal interactions are related to the type of transducer used, a similar test was conducted, with the blade mounted on a transducer supplied by a different manufacturer tuned to the same frequency (35 kHz). The FRF measured at the blade tip for a 5 V excitation level is shown in Figure 7.18 (a). Again three modal responses representing the longitudinal modes of the assembly are detected by random excitation test in the 0-50 kHz frequency range. As expected, the tuned longitudinal mode of the system occurs at the same frequency as in the preceding case, since both transducers are tuned at the same frequency. However, the other two responsive modes in the spectrum occur at different frequencies than for the system studied previously. As before, a sweep of the excitation frequency is performed around each longitudinal modal frequency at increments of the excitation level. In this case, no modal interactions are measured when the system is excited around its tuned frequency at 35 kHz. Only one combination resonance is detected, when the system is excited near the third longitudinal mode frequency at 45 kHz, as shown in Figure 7.18 (b). The internally excited modes are the second out-of-plane bending mode and the tuned second longitudinal mode of the assembly occurring at 10 kHz and 35 kHz, respectively.

Since the cutting system is designed to operate in the longitudinal mode at 35 kHz, the second transducer provides a better excitation source. In general, an ultrasonic tool

that works well when mounted on one transducer, can perform poorly when driven by another.

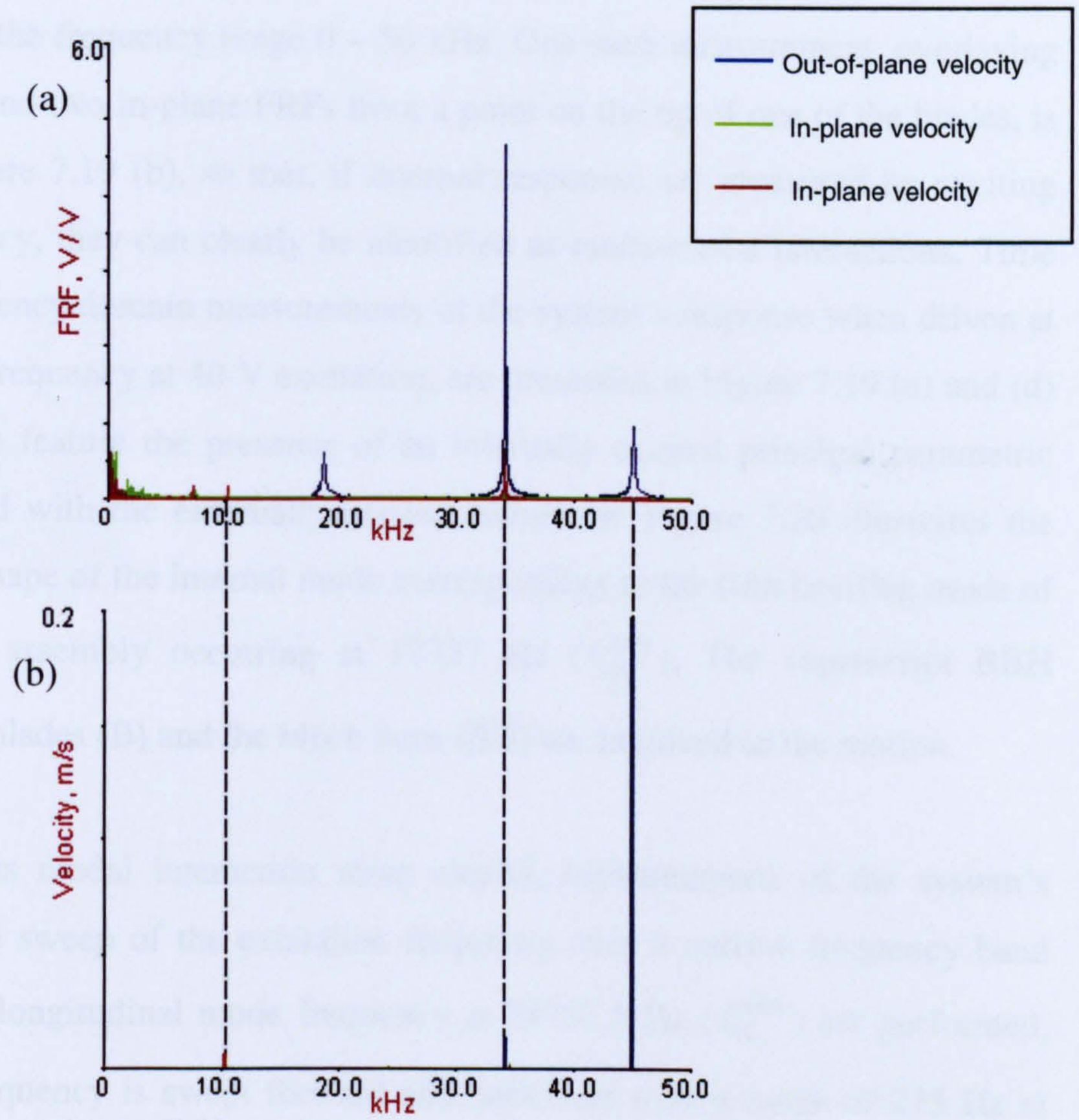

Figure 7.18. (a) FRF from transducer-blade,
(b) combination resonance

7.4.3 Combination resonances in three-blade cutting systems

It has been shown that in ultrasonic systems, energy can leak into bending and torsional modes at frequencies lower than the excitation frequency, as a direct result of tuning and exciting the system in a longitudinal mode of vibration.

In this section, the energy exchange from the operating mode into a modal frequency close to half of the tuned frequency, and excitation of combination resonances consisting of two modal frequencies whose sum is close to the tuned frequency, are characterised for two three-blade cutting systems. The measured energy transfers from the primary responses to the internally excited modes are compared with the theory of simple autoparametric systems discussed in Section 7.3.2.

7.4.3.1 Principal parametric resonance

Figure 7.19 (a) shows the first three-blade cutting system investigated. Initially, an experimental modal analysis is performed in order to identify the modes by random excitation test in the frequency range 0 – 50 kHz. One such measurement, overlaying the out-of-plane and two in-plane FRFs from a point on the tip of one of the blades, is illustrated in Figure 7.19 (b), so that, if internal responses are measured by exciting the tuned frequency, they can clearly be identified as multi-modal interactions. Time domain and frequency domain measurements of the system's response when driven at the tuned modal frequency at 40 V excitation, are presented in Figure 7.19 (c) and (d) respectively. Both feature the presence of an internally excited principal parametric resonance coupled with the externally excited resonance. Figure 7.20 illustrates the measured mode shape of the internal mode corresponding to the fifth bending mode of the block-blades assembly occurring at 17737 Hz ($f_{5B_y}^{BBH}$). The superscript BBH indicates that the blades (B) and the block horn (BH) are involved in the motion.

To investigate this modal interaction more clearly, measurements of the system's response to a sine sweep of the excitation frequency over a narrow frequency band around the tuned longitudinal mode frequency at 34737.5 Hz ($f_{2L_z}^{BBH}$) are performed. The excitation frequency is swept forward and backward over a range of 275 Hz at two different excitation levels. A slow sweep rate and small frequency step (12.5 Hz) are adopted in order to record only steady responses. Figure 7.21 (a) shows how the system responds to an excitation level of 40 V. It is observed that when sweeping the frequency forward initially from 34625 Hz, the system responds only at the excitation frequency (primary response), and no modal interactions are detected. However, when the frequency reaches 34712.5 Hz, the primary response suddenly increases and a large secondary response is also excited (Figure 7.21 (d)). When the excitation frequency is further increased, both responses decrease, reaching a minimum at 34750 Hz.

Continuing the frequency sweep, the responses once more increase up to 34762.5 Hz and then the secondary response disappears, whereas the primary response decreases. Identical response paths are identified through a sweep down of the excitation frequency as shown in the figure. The time responses measured at each frequency step

are in a steady state during the intermodal energy exchange as illustrated in Figure 7.19 (c). The resulting v-shaped curve, due to energy flow from the primary response to the internally excited mode, appears qualitatively similar to the predicted response of the theoretical 2DoF model discussed in Section 7.3.2 and illustrated in Figure 7.4.

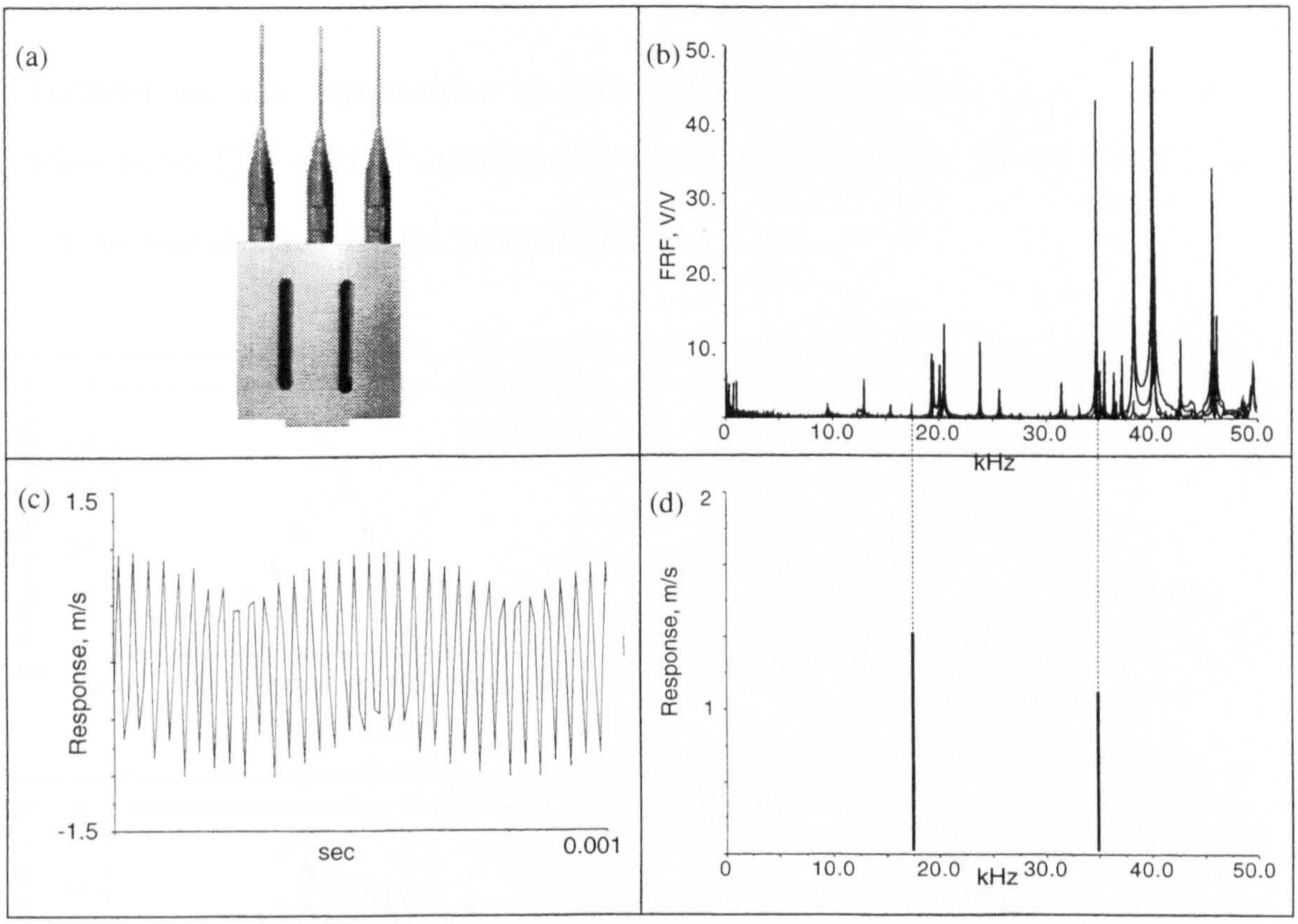

Figure 7.19. (a) Three-bladed cutting head, (b) FRF, (c) time domain response, (d) response spectrum

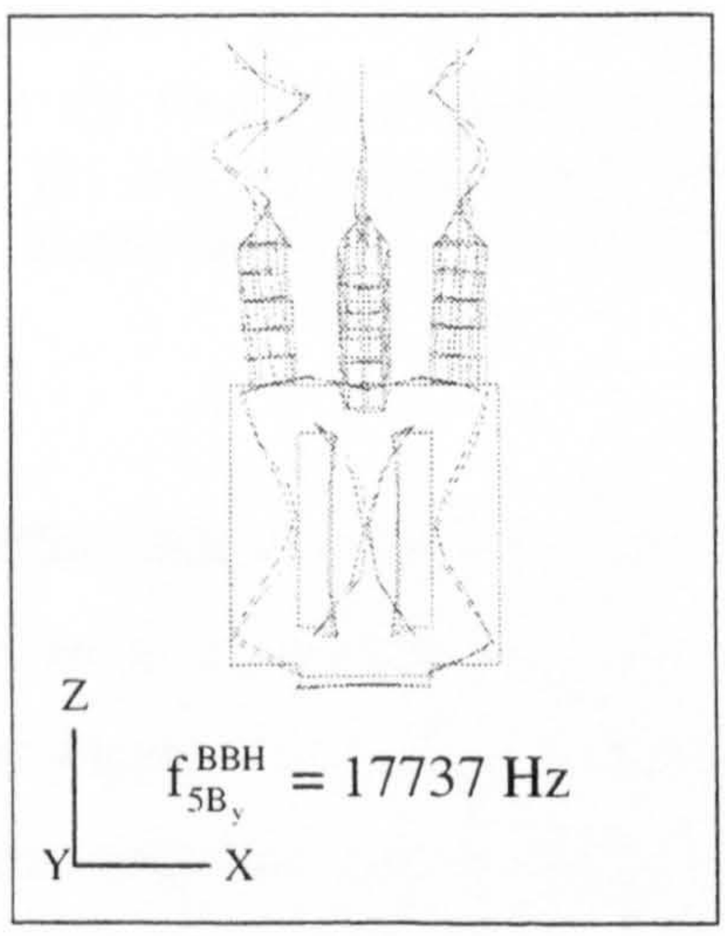

Figure 7.20. Measured modes shape of the indirectly excited fifth bending mode of the assembly

Measurements of the system at an increased excitation level of 80 V show that the primary response curve is independent of the excitation level in the double response region (Figure 7.21 (b) and (c)). The higher excitation level extends the region over which the multiple-response exists (Figure 7.21 (c)), which again agrees with the theoretical analysis of Section 7.3.2.

Furthermore, the asymmetries of the primary response due to the not exact relationship $f_{2L_y}^{BBH} \cong 2 f_{5B_y}^{BBH}$, predicted by the theoretical analysis and shown in Figure 7.5, are also illustrated in the measurements.

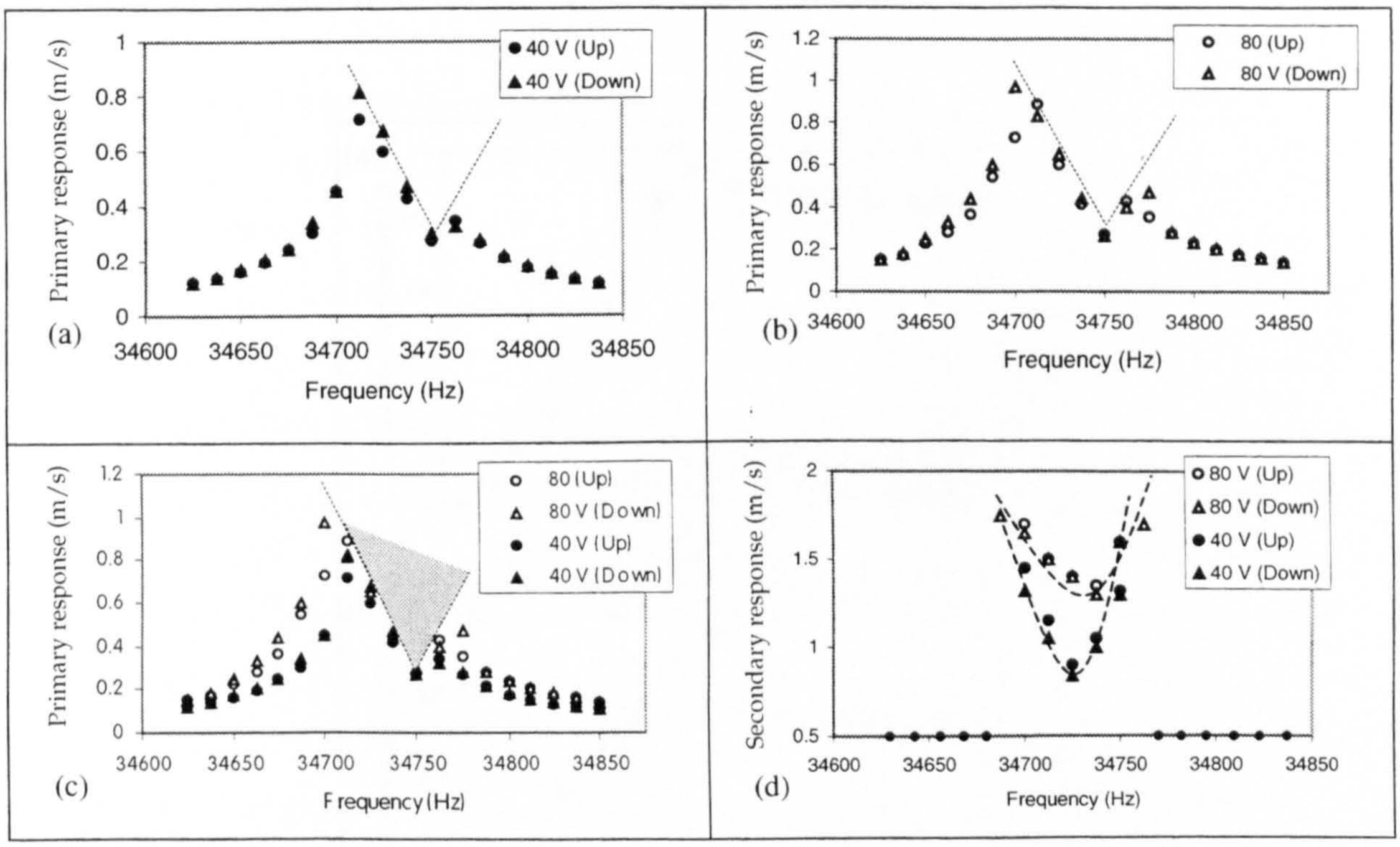

Figure 7.21. Responses for the two mode autoparametric coupling: (a) measured primary response at 40 V, (b) measured primary response at 80 V, (c) measured primary responses at both excitation levels, (d) measured secondary responses at both excitation levels

Figure 7.22 illustrates the effect that varying the excitation level has on the primary response of the system driven at a constant external excitation frequency. In the measurements illustrated in Figure 7.22 (a) the excitation frequency matches the frequency at which the double response is initially detected (34712.5 Hz) during the upward frequency sweep. An excitation frequency corresponding to the frequency of

the minimum nonlinear response (at the bottom of the 'v-shape at 34750 Hz) is adopted for the measurement plotted in Figure 7.22 (b). In both measurements the primary response increases linearly with excitation level up to the threshold (where the secondary response appears). Further increasing the excitation level, the primary response first decreases and then stays constant. This confirms that the primary response of the system is not governed by the excitation level when the modal interaction is underway. From the comparison of Figure 7.22 (a) and (b), it is also evident that the drop in the primary response, associated with the internal excitation of the secondary response, is greater when the system is driven at the minimum nonlinear response frequency. This is not a surprising result since the largest amount of energy extracted from the primary mode occurs at this frequency.

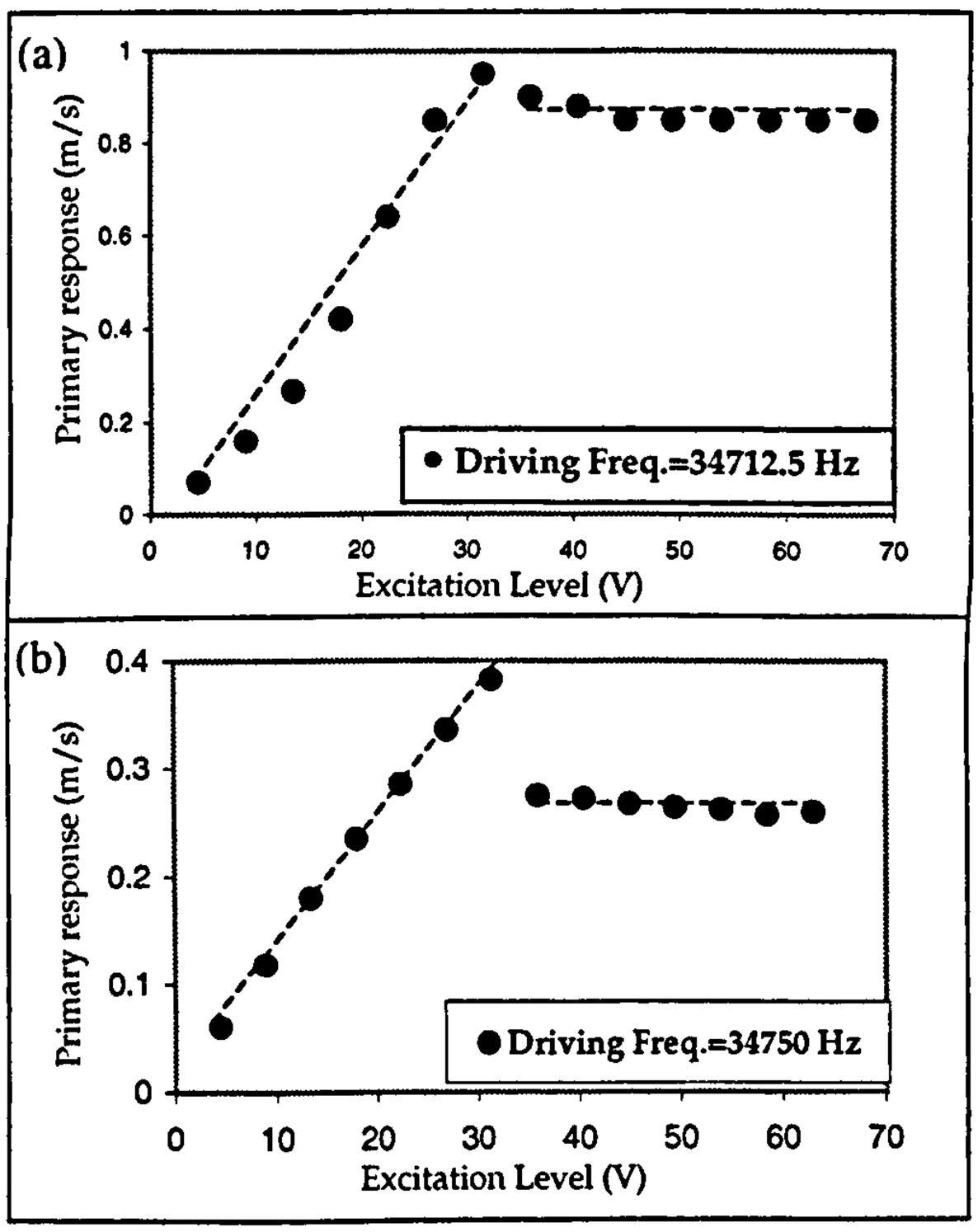

Figure 7.22. Primary responses measured as a function of excitation level

Figure 7.23 shows the secondary system response over the same excitation level range, also for the excitation frequency equal to the minimum nonlinear response frequency. It can be seen that the response of the internally excited mode, above the threshold, increases with excitation level. A response saturation effect, attributable to the inherent nonlinear behaviour of the system, limits the growth at high excitations.

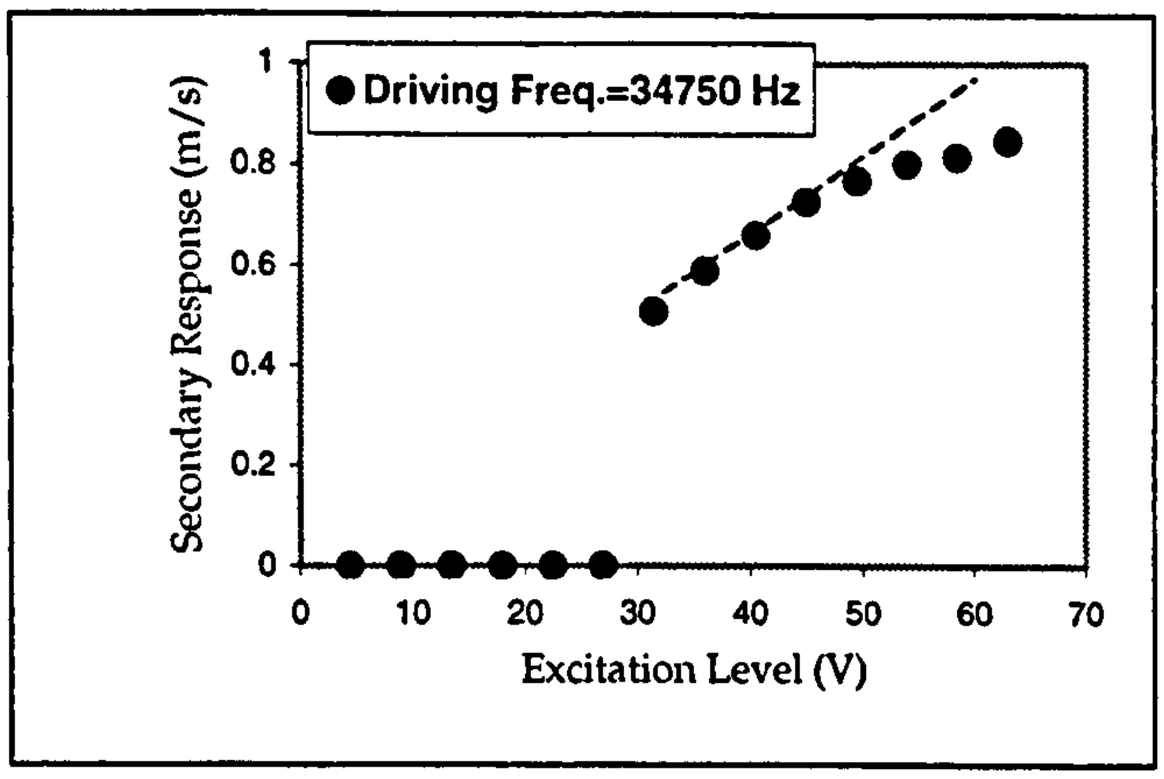

Figure 7.23. Secondary response measured as a function of excitation level

7.4.3.2 Double principal parametric resonance

Theoretical modelling of simple autoparametric systems has predicted that diverse modal interactions can be excited when the external frequency is varied in the vicinity of a modal frequency [84]. In particular it is found that, for certain excitation level thresholds, primary responses are characterised by a number of v-shaped regions each of which indicates a single modal interaction. In Figure 7.24, the primary response of the cutting device is measured through a sweep of the excitation frequency over the same range considered in the previous measurements. However, in this case the sweep is performed at a higher excitation level (100V).

The figure shows two v-regions in two distinct frequency bands of the primary response, indicating that the excitation level threshold for two modal couplings is reached. In this case, the first combination resonance, occurring in the lower frequency v-region of the figure, has a higher excitation level threshold, which is not reached, at the lower excitation levels of Figure 7.21. Hence, this combination is weakly coupled. The second combination corresponds to the same modal coupling detected in the previous measurements at lower excitation levels. This combination is strongly coupled. Both modal interactions feature two internally excited principal parametric resonances coupled with the external mode. The internally excited modes, occurring at 17.3 kHz and 17.35 kHz, are identified in the FRF of the cutting device as shown in Figure 7.25. For measurements carried out at even higher excitation levels, an overlap of the two v-shaped regions over a frequency bandwidth will occur. As a result three modal responses, one external and two internal, would be excited in the response spectrum.

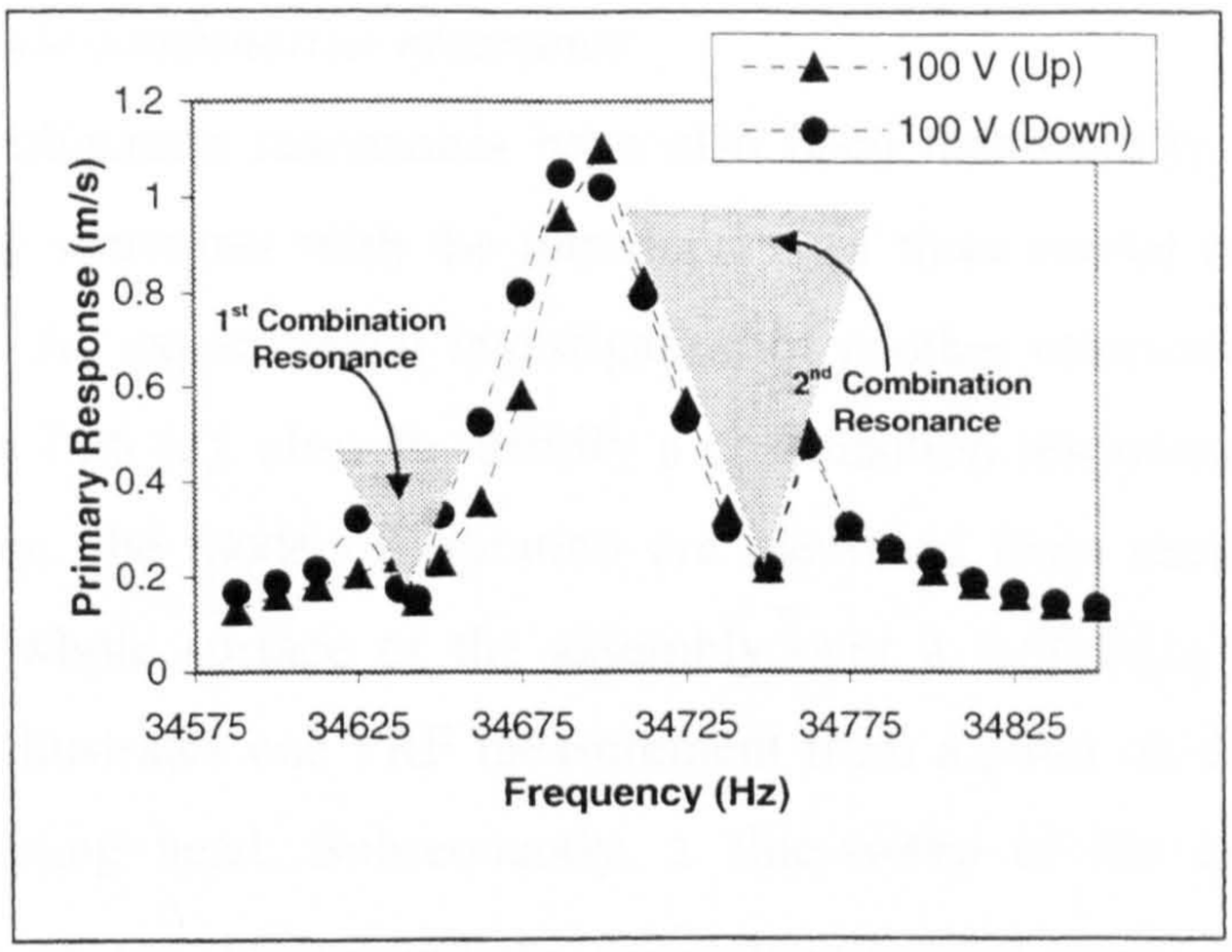

Figure 7.24. Primary response for two internal resonances

Since different modal interactions can be excited at different excitation thresholds, it is important in the experimental assessment of an ultrasonic device to check the response up to the excitation level typical of its operating conditions. From the experimental evidence gathered in this study, it would appear that, for high power ultrasonic systems that incorporate multiple tuned components and particularly high-gain components, if one of the frequency relationships which results in a modal interaction exists, the threshold will lie within the operating excitation level range.

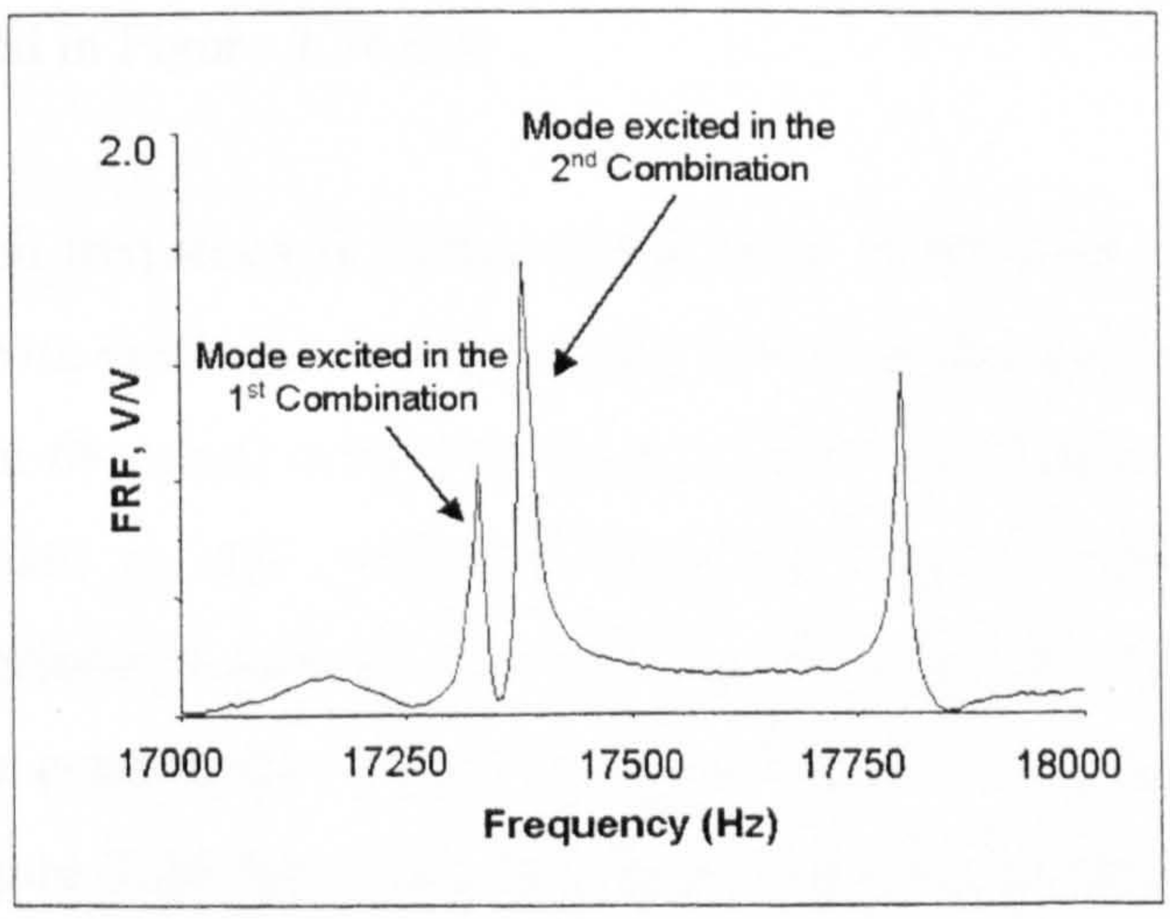

Figure 7.25. Measured FRF in 1 kHz frequency range centred at half of the excitation frequency

7.4.3.3 Three-mode combination resonance

Multi-modal combination resonances have also been theoretically characterised for simple beam-like structures with the introduction of three modal coordinates in the Eq. 7.4 and 7.5. An experimental investigation of another ultrasonic cutting device, shown in Figure 7.26 (a), aims to identify a combination resonance involving three modes. As before, the mode of vibration are identified from measurements of the FRFs from the whole surface of the assembly over a 0-50 kHz frequency range. Figure 7.26 (b) illustrates one FRF measurement from a point on the tip of an outer blade of the cutting head. Subsequently, a sine-sweep of the excitation, over a frequency range of 175 Hz around the tuned longitudinal mode frequency ($f_{2L_y}^{BBH}$ = 34405 Hz), is carried out at an excitation level of 40 V. A slow sweep is performed for frequency increments of 6 Hz. Initially, for the forward sweep, starting from 34325 Hz, the response consists only of a response at the excitation frequency. At 34400 Hz, two responses, in addition to the directly driven response, appear in two lower frequency modes (Figure 7.26 (d)). These modes, corresponding to the second bending mode of the blade (Figure 7.27 (a)) and the fifth bending mode of the assembly (Figure 7.27 (b)), occur at 6 kHz ($f_{2B_y}^{B}$) and 28.4 kHz ($f_{5B_y}^{BBH}$), respectively. Their frequencies satisfy the combination resonance, $f_{2L_z}^{BBH} \cong f_{2B_y}^{B} + f_{5B_y}^{BBH}$. The measured time response at this excitation frequency shows periodicity of the three modes, as illustrated in Figure 7.26 (c).

When the excitation frequency is further swept up to 34406 kHz, the three responses become enriched with sidebands, which rapidly spread across the frequency spectrum, and the response in the tuned mode decreases, as shown in Figure 7.26 (f). The time domain measurement at this excitation frequency step (Figure 7.26 (e)), shows evidence of non-periodic responses. At 34412 Hz, the sidebands disappear leaving the three modes of the combination in the spectrum (Figure 7.26 (h)), and periodicity is re-established (Figure 7.26 (g)). Carrying on the forward frequency sweep, the two internally excited modes disappear, and the primary response decreases.

Figure 7.28 shows the system primary response obtained as function of the excitation frequency. As expected, a v-shaped curve indicting the energy flow from the primary response to the internally excited modes is detected.

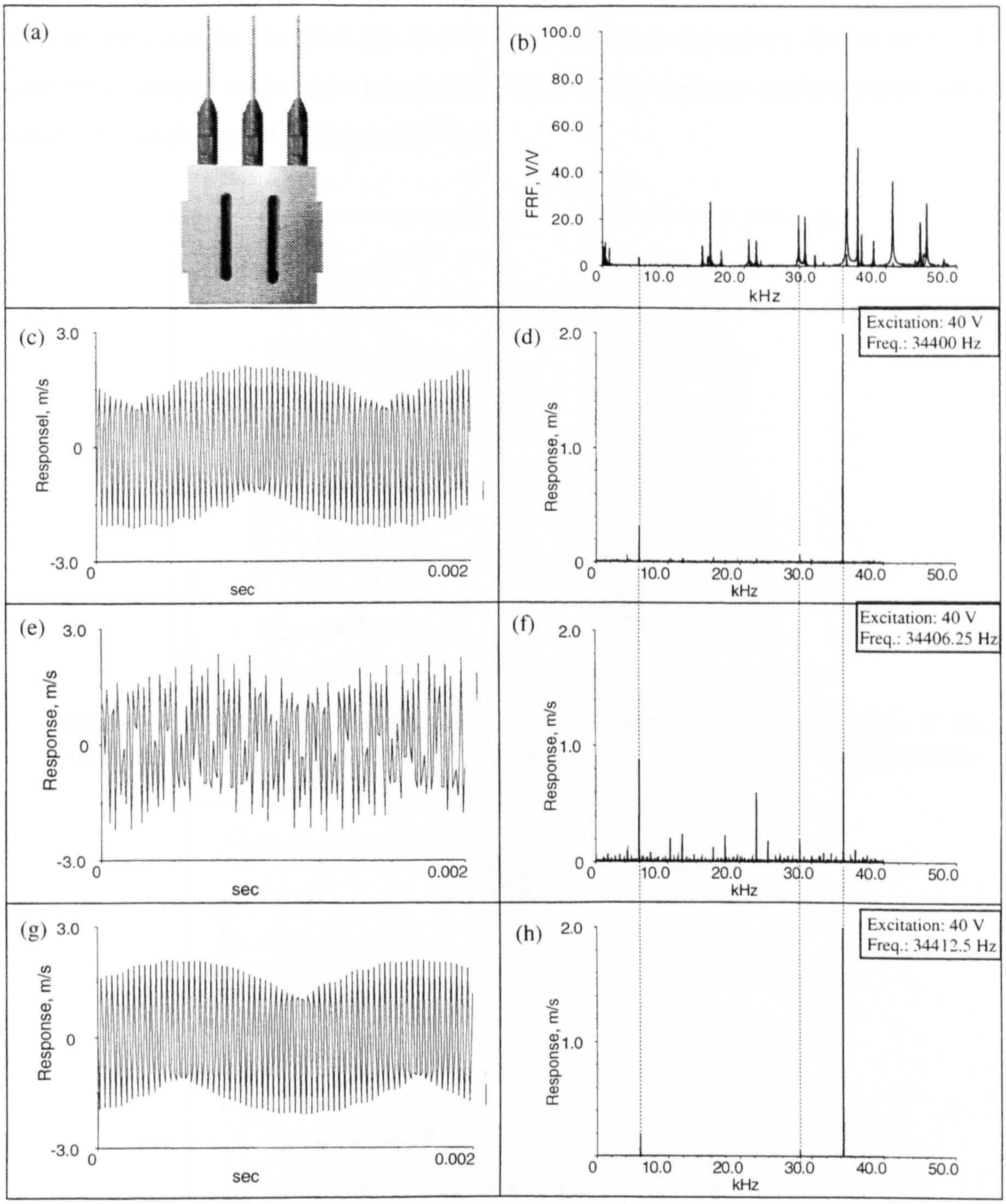

Figure 7.26. (a) Three-blade cutting head, (b) FRF. (c), (e), (g) time domain responses; (d), (f), (h) corresponding response spectra

Subsequently, measurements of the system at an increased excitation level (80 V) are performed. Figure 7.29 illustrates the responses obtained through a slow downward sweep of the excitation frequency carried out in a frequency band around the tuned modal frequency. Responses qualitatively similar to those detected at the lower excitation (40 V) are measured. However, the frequency region over which the system

becomes unstable, triggering off the multi-modal response, proves to be wider. Moreover it can be observed that at 34400 Hz excitation frequency the amplitude of the three excited modes (the tuned mode and the two internal modes) significantly decreases as illustrated in Figure 7.29 (g).

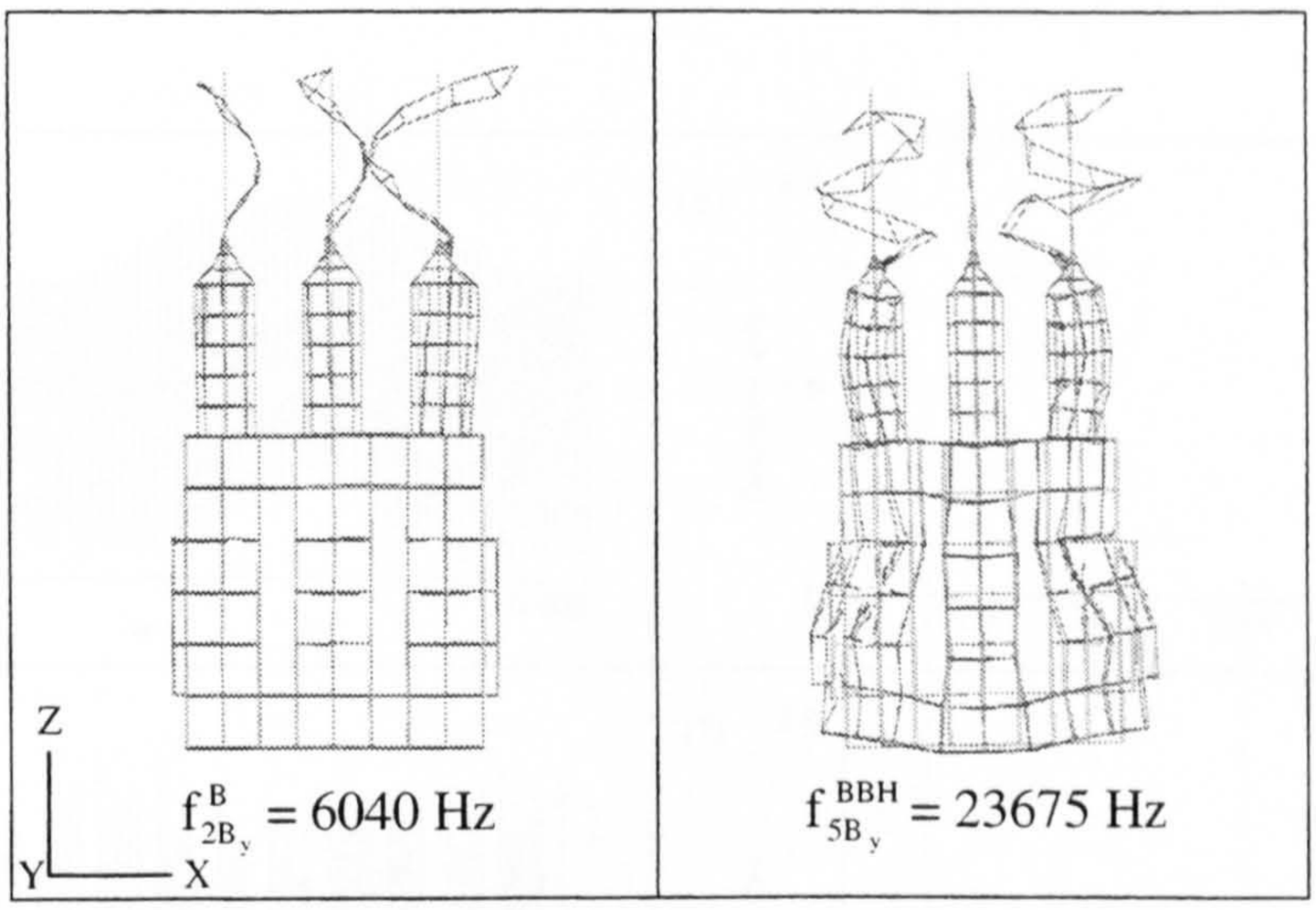

Figure 7.27. Measured modes shapes of the internally excited modes of the combination resonance, (a) blade 2nd bending mode (b) assembly 5th bending mode

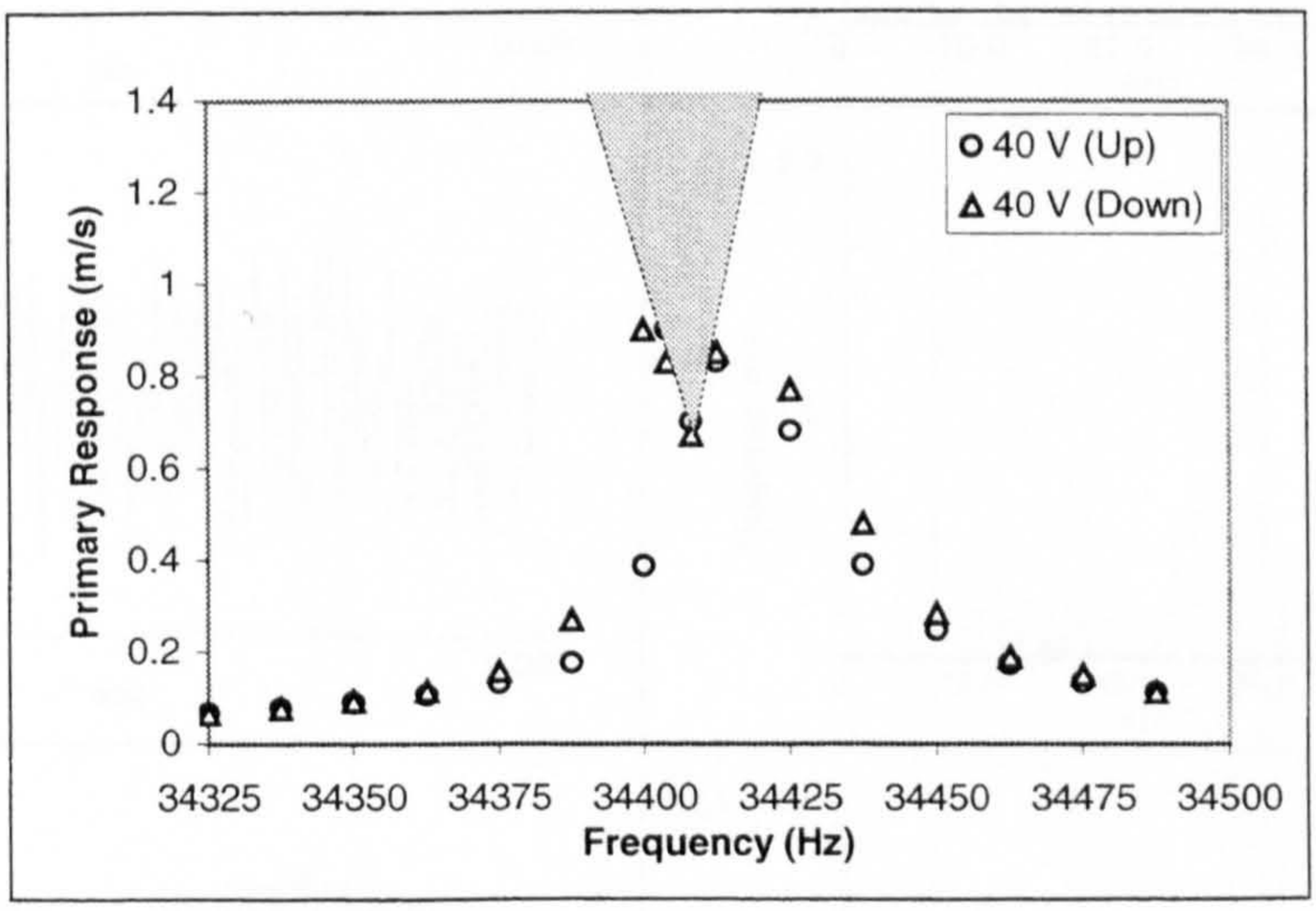

Figure 7.28. Measured primary response for the three-mode combination resonance

Large amounts of energy are fed in other modes as a result of a cascading effect which involves the excitation of other internal resonances. The response spreads across the frequency spectrum. The time domain measurement shown in Figure 7.29 (c) is clearly a non-periodic response, which, alongside the broadband spectrum response of Figure 7.29 (g), shows evidence of a dynamic behaviour typical of chaotic motions.

This modal interaction differs from the one investigated in the previous section, not only in the number of modes involved, but also in the conditions under which the energy flows from the primary to the secondary responses. In fact, interactions between three modes are characterised by non-steady responses, whereas the energy exchange involving two modes is typically steady-state.

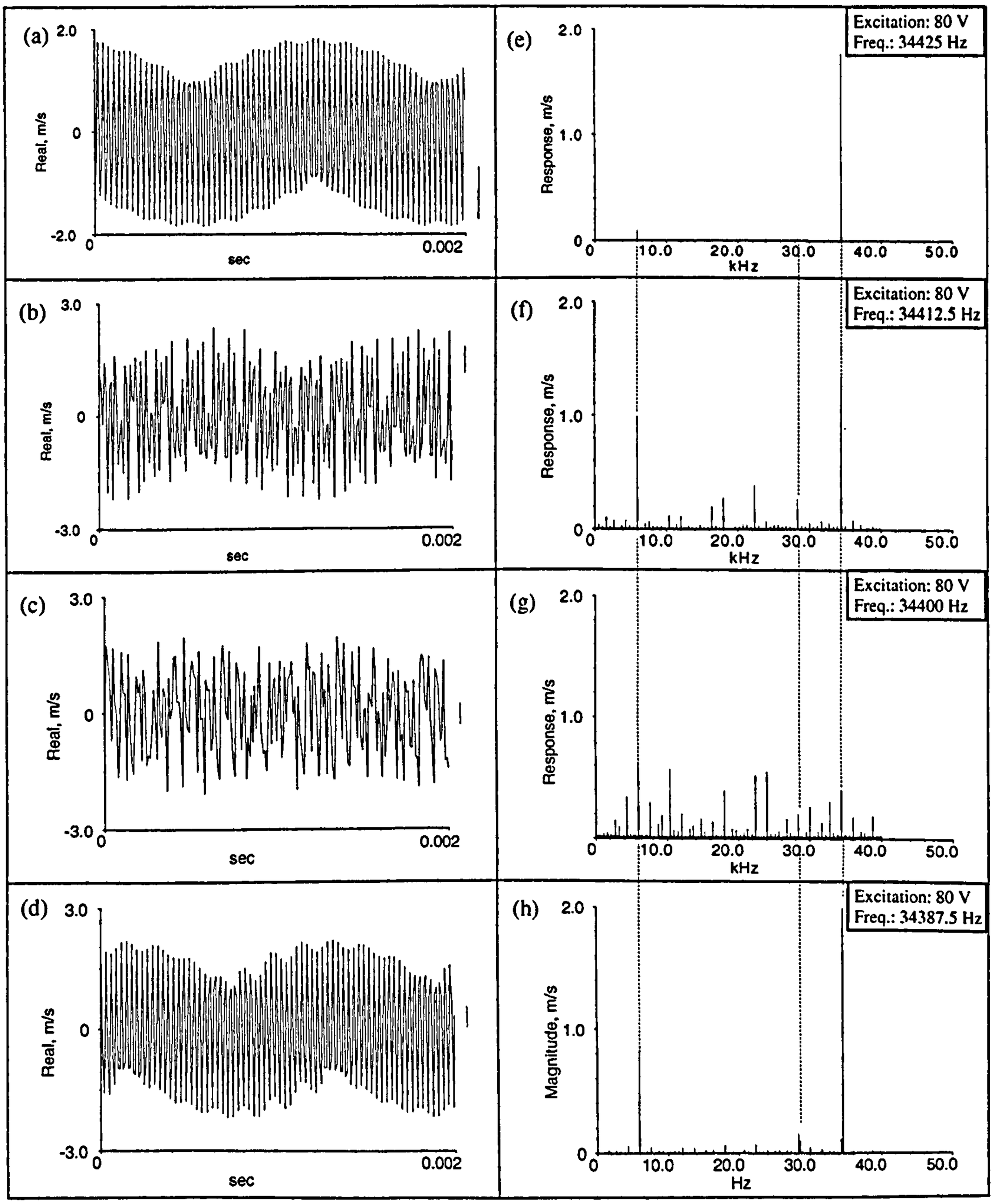

Figure 7.29. (a-d) Time domain responses, (e-f) corresponding response spectra, measured at frequency steps of 12.5 Hz

V-shaped regions indicating energy transfers from the externally driven mode (primary response) to one or more internal modes (secondary response) are more difficult to detect in the systems discussed in Section 7.4.1 and 7.4.2. Single-component assemblies exhibit lower amplitudes of the internal modes compared with the tuned mode amplitude therefore revealing small energy leakages.

7.4.3.4 Stud relocations

Alternative positions of the threaded studs connecting the block horn to the blades are considered in order to provide shifts in the modal frequencies required to eliminate the resonance condition, $f_{2L_z}^{BBH} \cong f_{2B_y}^{B} + f_{5B_y}^{BBH}$. Figure 7.30 shows the frequency dependence of the three modes of the combination resonance on stud location.

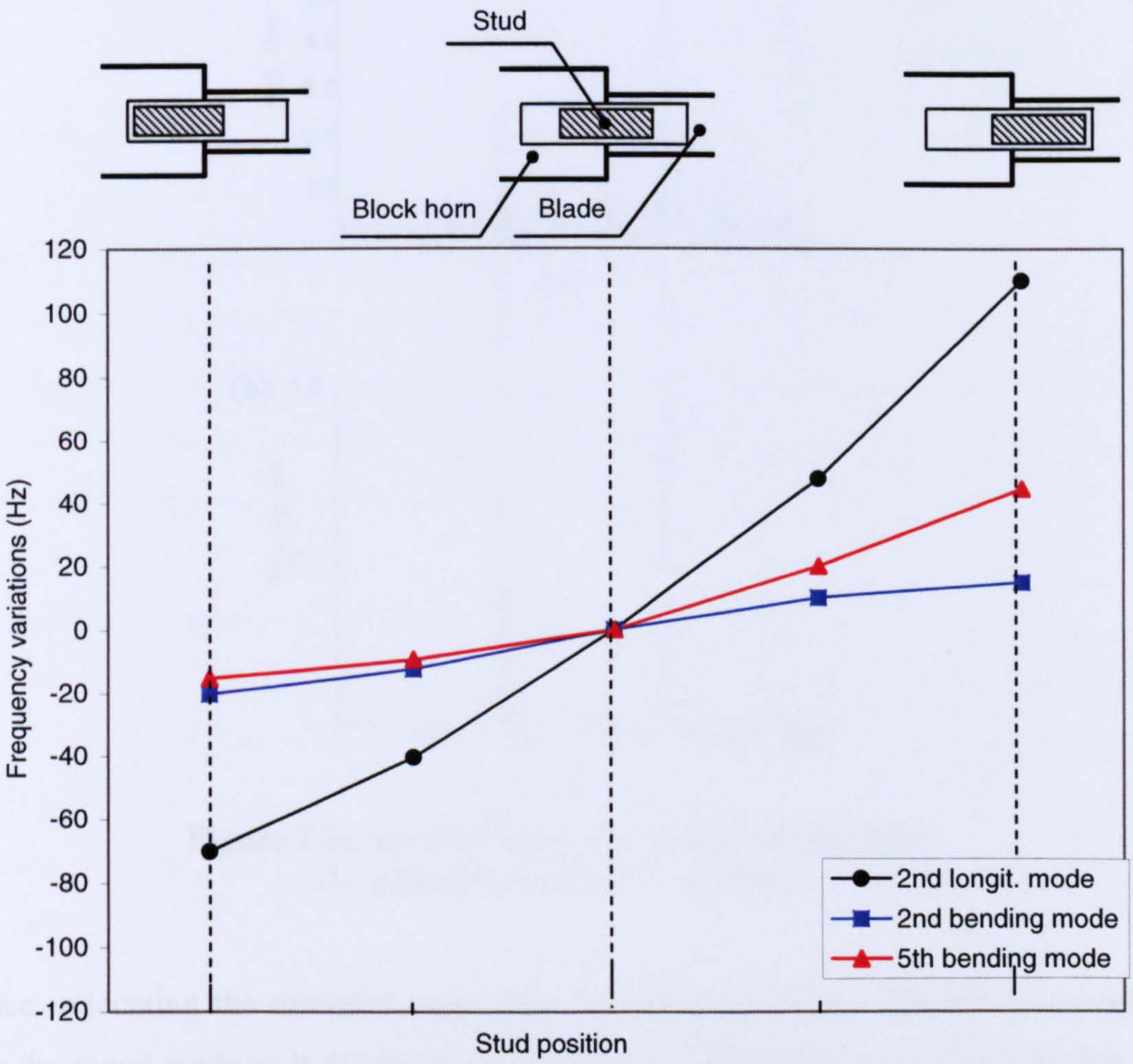

Figure 7.30. Frequency trend of the combination modes due to different stud positioning

The initial attachment configuration has the threaded studs half screwed into the blade and half screwed into the horn. It is evident that the configurations with the studs fully

screwed into the blade bases provide the greatest frequency shift of the tuned mode, whereas the internal frequencies result less sensitive to the alteration. Hence, a slow sweep of the excitation frequency near the tuned mode for this attachment configuration is performed. Up to a 30 V excitation, the response consists only of the longitudinal mode, whereas above it, a response occurring at 17250 Hz, exactly half of the tuned frequency (34500 Hz), appears in the spectrum (Figure 7.31 (b)). The result of shifting the frequencies of the internal modes involved in the original resonance condition is that parametric resonance is excited.

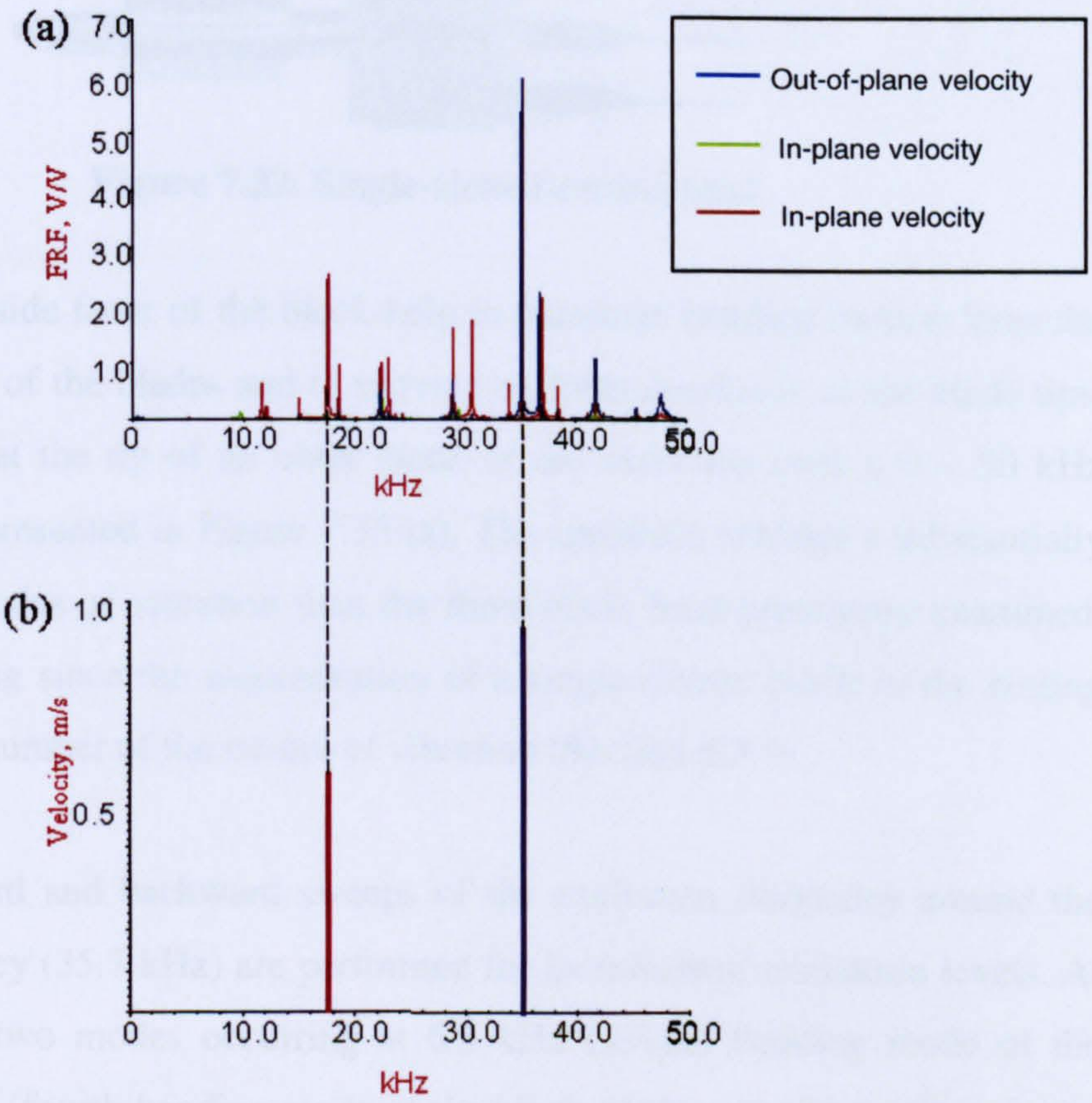

Figure 7.31. (a) FRF from wavelength cutting head;
(b) principal parametric resonance

Hence, relocating the threaded studs does not eliminate modal interactions coupled with the tuned mode as it did for the single blade system (Section 7.4.2.2). In this, in the investigated multi-component assembly, which is characterised by a large number of modes of vibration below the tuned frequency, a slight detuning via stud relocations may eliminate an internal resonance condition. However, the general shifts in modal frequencies can often lead to the excitation of a different modal interaction.

This provides a strong argument for minimising, as far as possible, the number below the tuned mode in multi-component ultrasonic assemblies.

7.4.3.5 Single-slotted block horn

In Figure 7.32, a redesigned multi-blade cutting head is presented, where the half-wavelength single-slotted block horn of Figure 6.18 (b) is attached to three half-wavelength tuned blades.

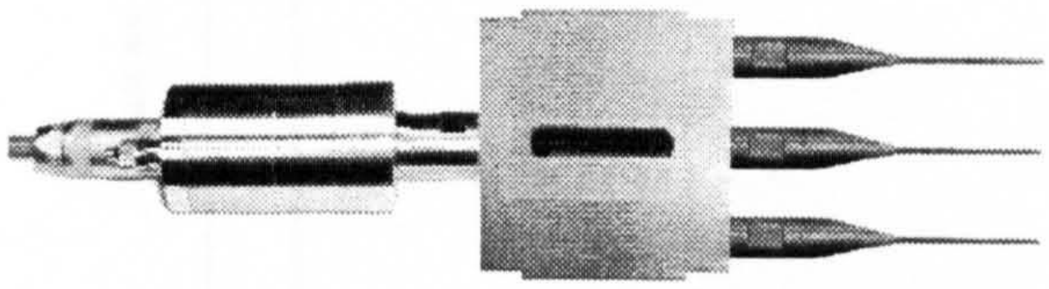

Figure 7.32. Single-slotted cutting head

Castellations at the side faces of the block help to eliminate bending motion from the longitudinal motion of the blades and to provide uniform amplitude at the blade tips. An FRF measured at the tip of an outer blade of the assembly over a 0 – 50 kHz frequency range is presented in Figure 7.33 (a). The spectrum exhibits a substantially lower number of modes of vibration than the three-blade head previously examined. This is not surprising since the incorporation of a single-slotted block in the cutting system reduces the number of the modes of vibration (Section 6.3.1).

Subsequently forward and backward sweeps of the excitation frequency around the tuned mode frequency (35.7 kHz) are performed for incremented excitation levels. At a 50 V excitation, two modes occurring at 6.5 kHz (second bending mode of the blade) and 29.1 kHz (fourth bending mode of the block-blade assembly) appear in the response spectrum, indicating the occurrence of a combination resonance (Figure 7.33 (b)).

Figure 7.34 shows the frequency sensitivity of the modal frequencies of the combination resonance to threaded stud positions. It is evident that the configuration with the studs fully screwed into the block horn provides the greatest shift in the tuned mode frequency.

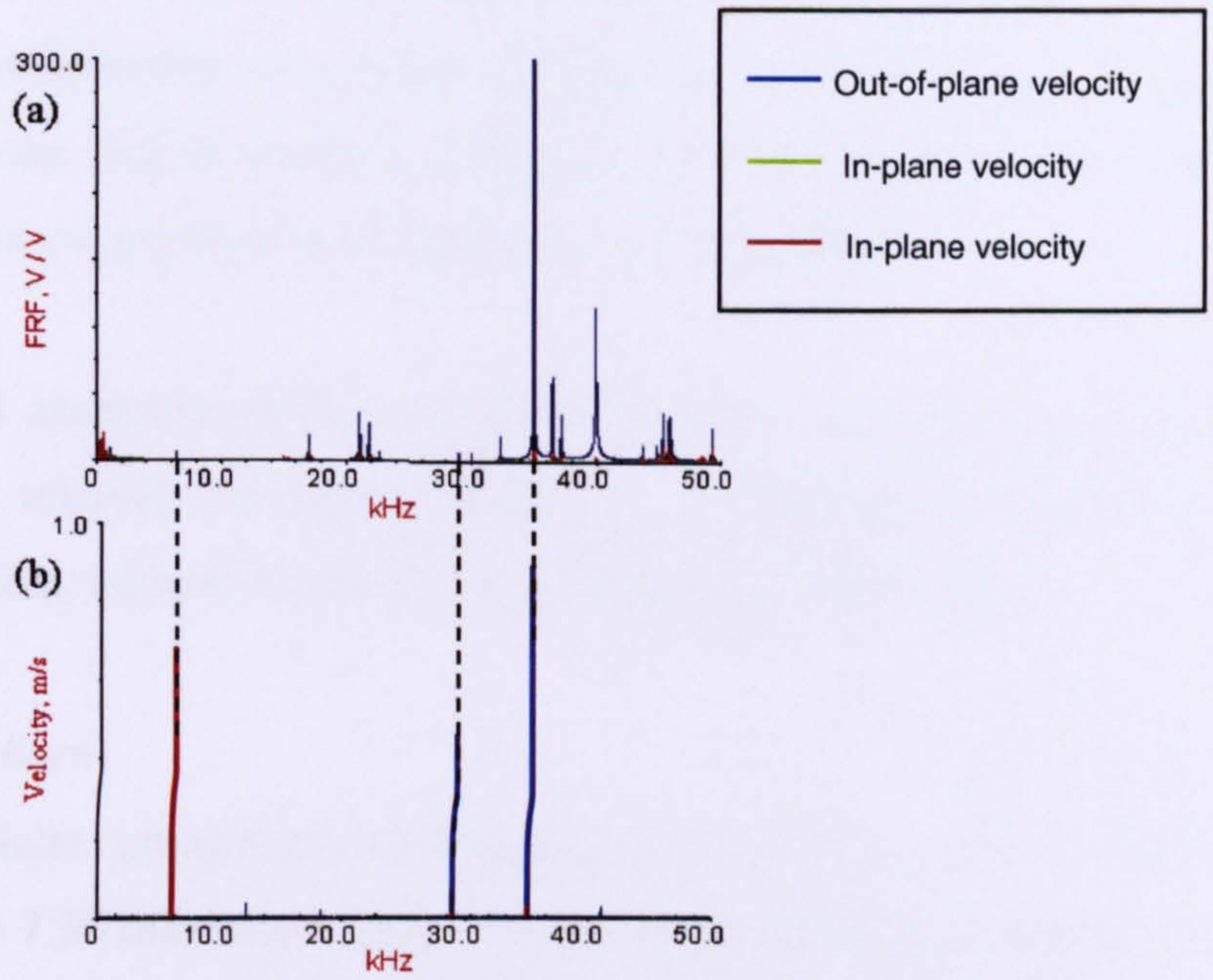

Figure 7.33. (a) FRF from single-slotted cutting head, (b) two-mode combination resonance

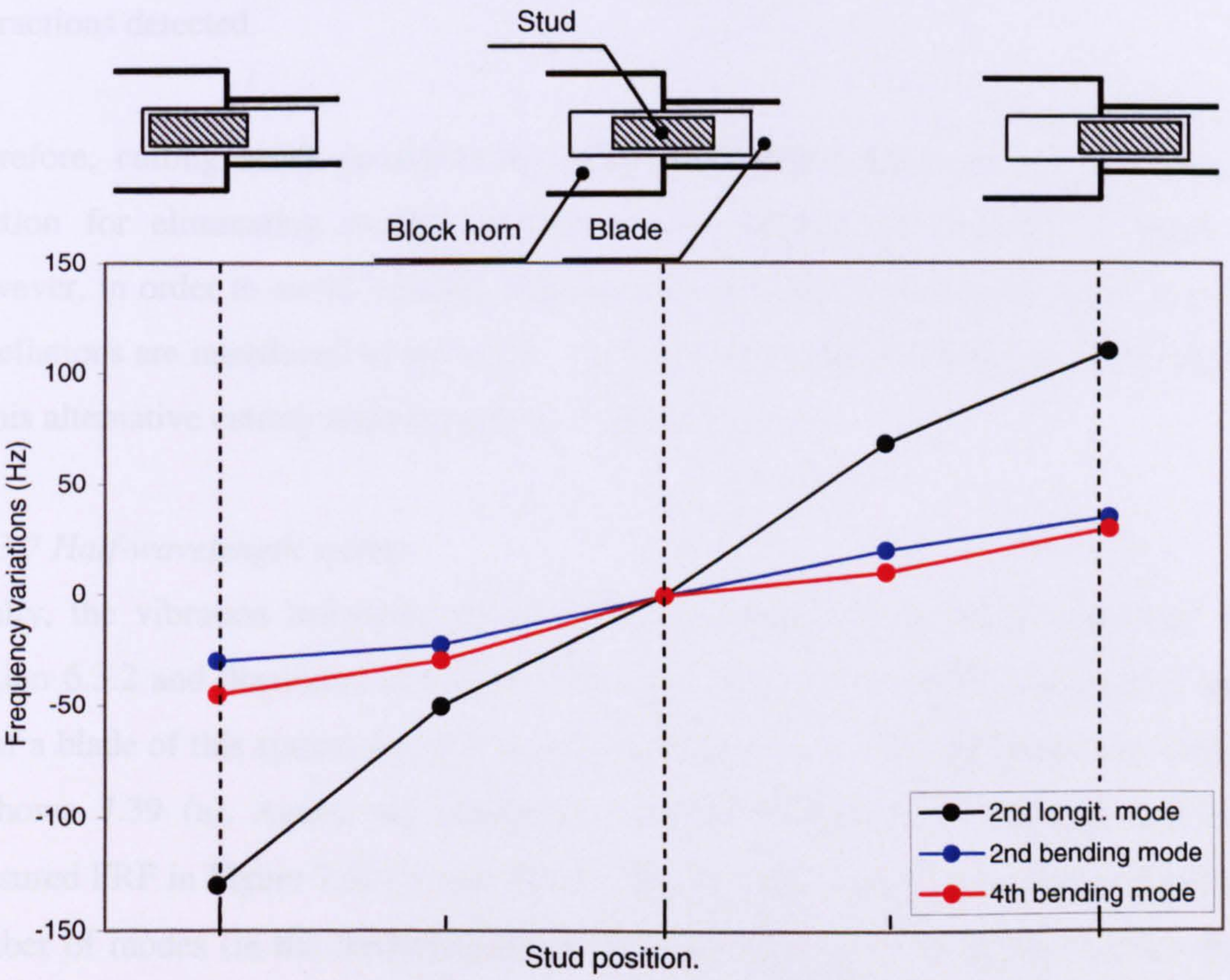

Figure 7.34. Frequency trend of the combination modes due to different stud positioning

Subsequent frequency sweeps of the excitation frequency carried out on the assembly with this attachment configuration are conducted. The excitation level is increased after each frequency sweep, and no modal interaction is detected up to the excitation level required to drive the cutting head at its operating cutting amplitude.

Since this single-slotted assembly exhibits a reduced number of modes, it may be possible to eliminate internal resonance conditions through small geometric modifications of the system, without exciting other combination resonances.

7.4.3.6 No-slotted block horn

In Figure 7.35, a multi-blade cutting head incorporating the solid block horn of Figure 6.18 (c) is shown. Figure 7.36 illustrates the FRF measured at the tip of a blade of this system. The number of modes is less than in the configurations with one or two slots in the block horn. The cutting head is driven in the tuned mode up excitation levels sufficient to excite the required cutting amplitude in the blades with no modal interactions detected.

Therefore, cutting heads incorporating solid block horns represent a valid design solution for eliminating modal interactions by reducing the number of modes. However, in order to avoid bending responses of the outer blades at the tuned mode, castellations are introduced in the block. The predicted mode shape of the tuned mode of this alternative cutting head is shown in Figure 7.37.

7.4.3.7 Half-wavelength system

Finally, the vibration behaviour of the half-wavelength cutting head, described in Section 6.3.2 and illustrated in Figure 7.38, is investigated. An FRF measured at the tip of a blade of this system excited by random test in the 0 – 50 kHz frequency range is shown 7.39 (a). Again, the number of modes is significantly reduced and the measured FRF in Figure 7.39 (a) and the full EMA of the device, have shown that the number of modes (in the frequency range up to 50 kHz) is 50 % fewer than for the double-slotted wave-length system operating at the same nominal driving frequency. The measured response also showed no evidence of inter-modal energy exchanges (Figure 7.39 (b)).

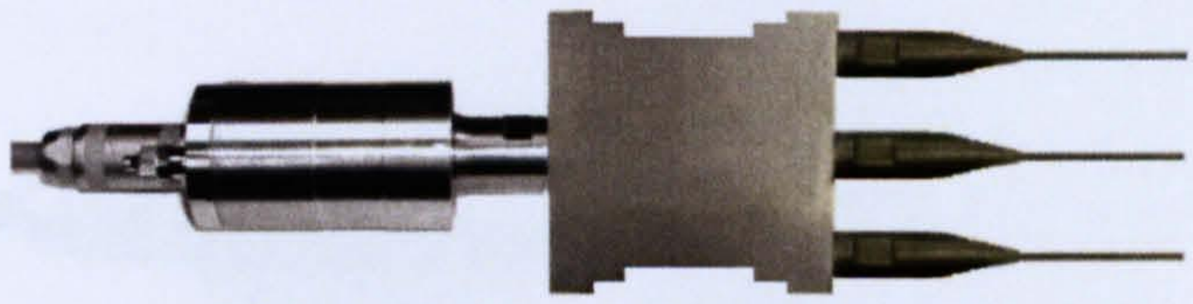

Figure 7.35. Solid block cutting head cutting head

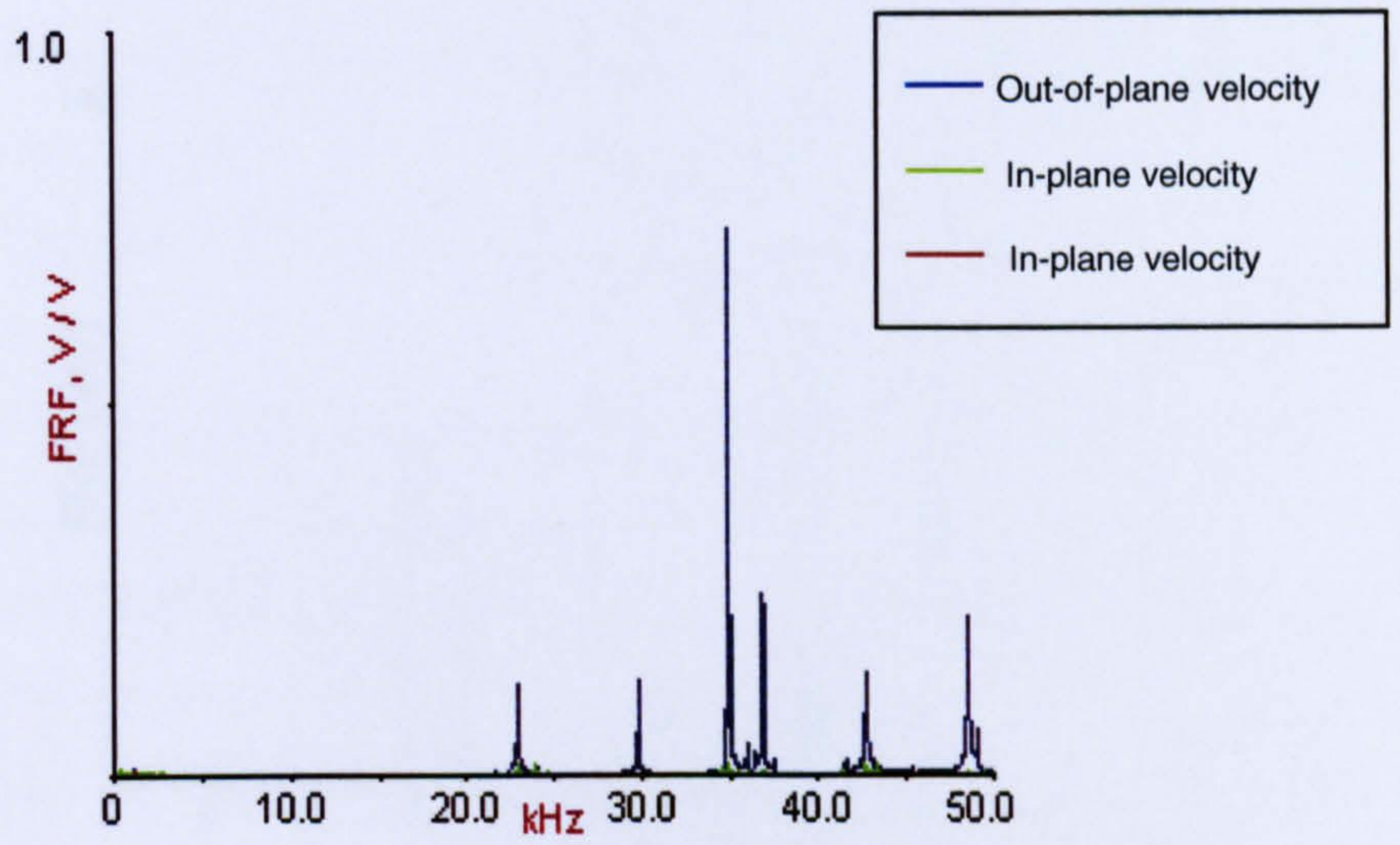

Figure 7.36. FRF from solid block cutting head

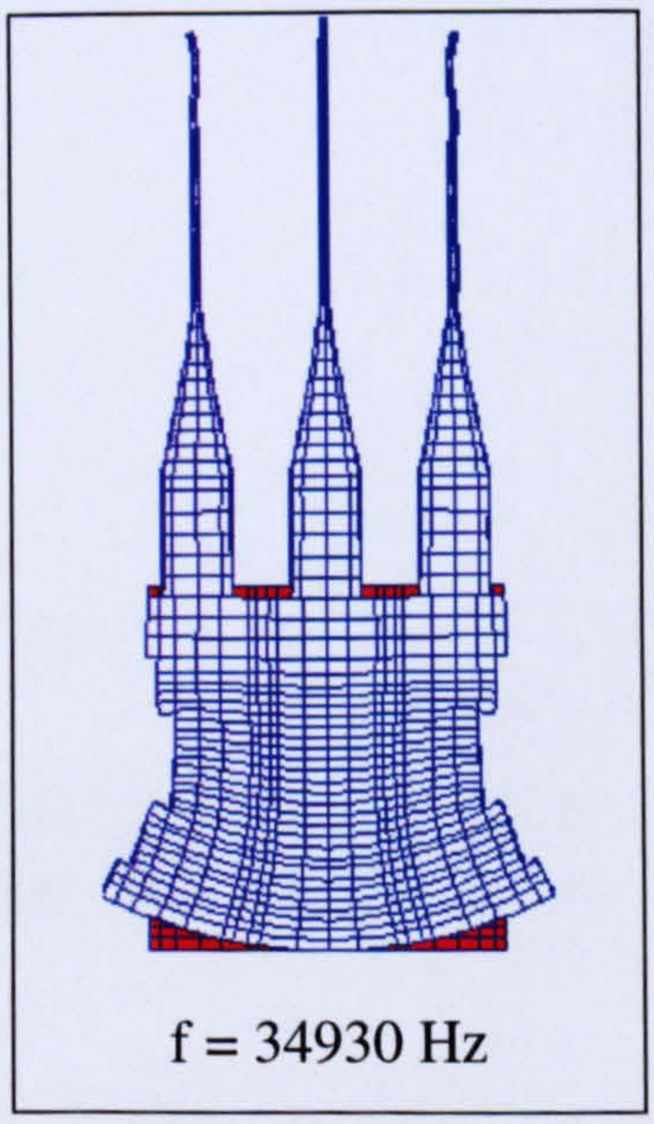

Figure 7.37. Predicted longitudinal mode
of a solid block cutting head with castellations

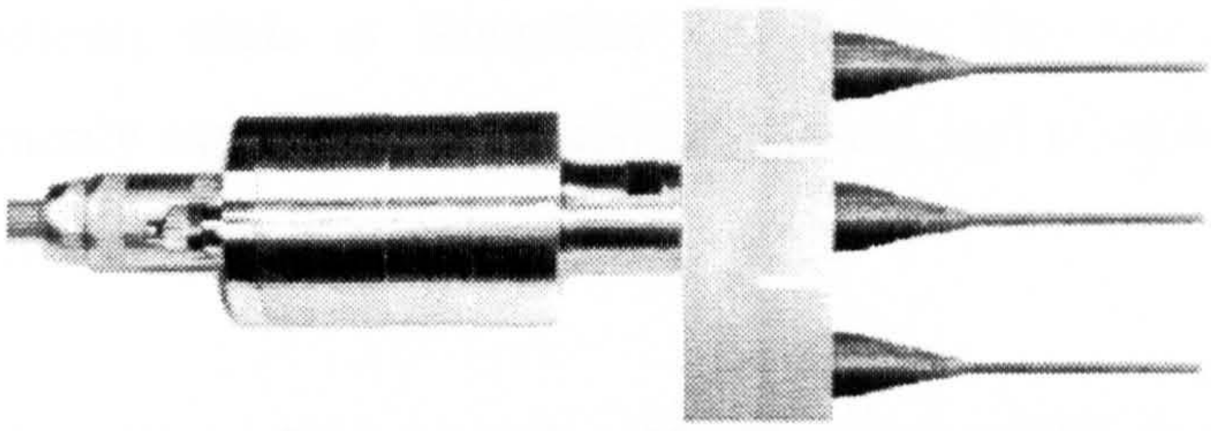

Figure 7.38. Half-wavelength cutting head

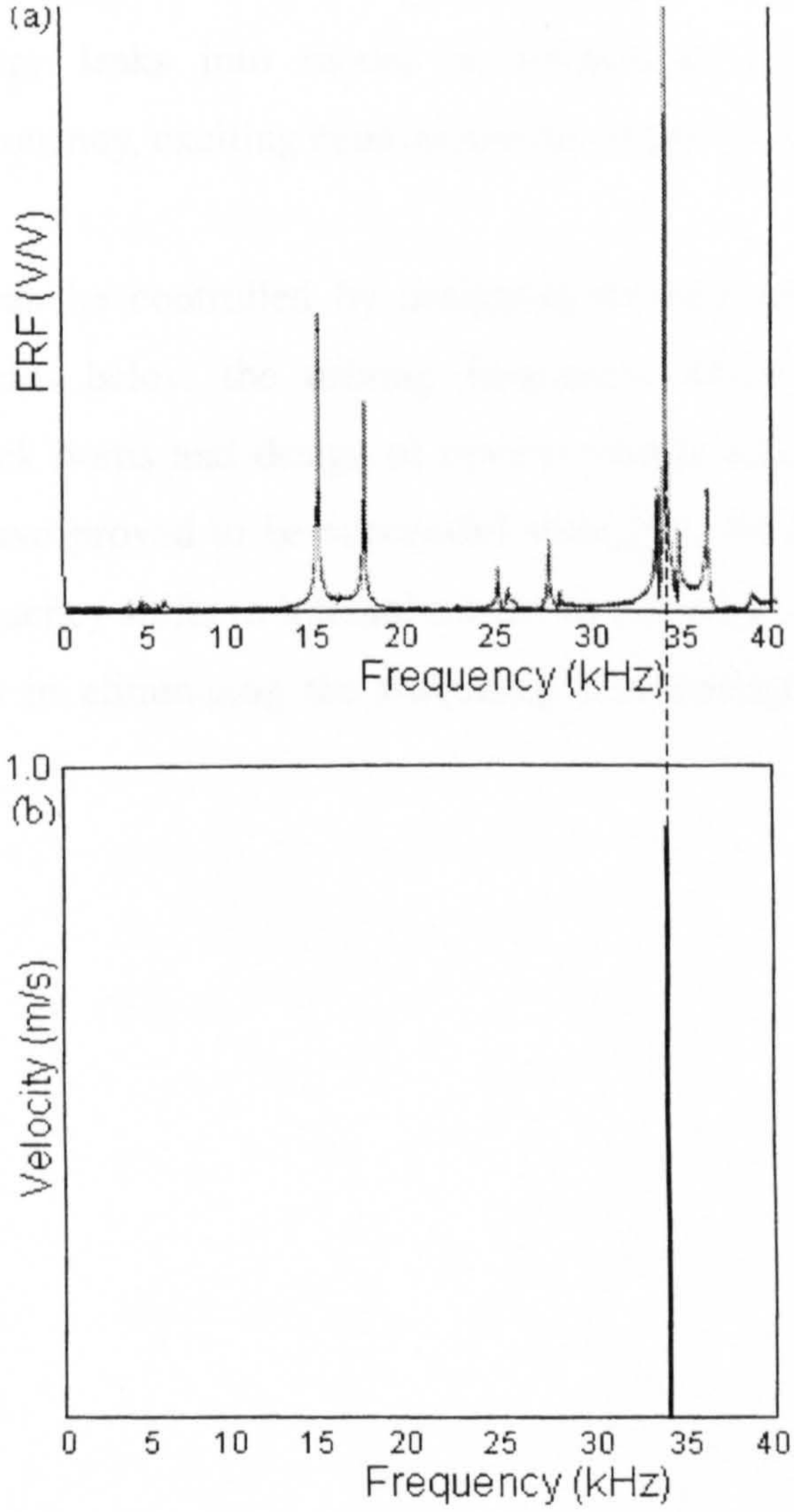

Figure 7.39. (a) FRF from half-wavelength cutting head, (b) external resonance

7.5 Conclusions

The experimental study of the vibration behaviour of single-blade and multi-blade ultrasonic systems demonstrates that modal interactions can be characterised by measuring the responses and referring to mathematical models of simple

autoparametric systems such as beam-like structures. The two and three-mode interactions, commonly identified in ultrasonic devices, excite responses which are clearly qualitatively similar to such theoretical models.

Energy leaks are characterised for a number of different modal interactions, including principal parametric resonances, double principal parametric resonances and three-mode combination resonances. These are typical responses of high power ultrasonic devices, where energy leaks into modes at frequencies lower than the tuned longitudinal mode frequency, exciting bending modes of the system.

Modal interactions can be controlled by designing devices with as few modes as possible at frequencies below the driving frequency, within design constraints. Modifications of block horns and design of devices within a half-wavelength of the driving frequency, have proved to be successful strategies. With a lower number of modes, effecting frequency shifts to internal modes by simple geometry modifications can prove successful in eliminating the frequency relationships that lead to modal interactions.

CHAPTER 8

NONLINEAR RESPONSE CHARACTERISTICS OF ULTRASONIC SYSTEMS

8.1 Introduction

Ultrasonic energy is generated within piezoelectric transducers, which are inherently nonlinear and which are physically coupled to one or more tuned components such as block horns and cutting blades. When transducers are driven at high voltage levels, the nonlinear domain for piezoelectric ceramics is reached [10]. Instabilities appear and the performance of ultrasonic systems is limited by nonlinearities.

Nonlinear behaviour of ultrasonic systems is responsible for resonance frequency shifts, multivalued responses and energy leaks into non-tuned modes, leading to an uncontrollable ultrasonic performance often accompanied by noise and component failures [8]. Although the nonlinear behaviour of piezoelectric stack transducers has been examined in the published literature [10,85,86], the consequences of this behaviour on the performance of high power tooling components have only previously been reported by Lucas et al. [9]. In a study of a multiple bar-horn stack, it was shown that the type of nonlinear response measured at the tuned operating frequency depends on the number of bars in the stack.

The present study builds on this preliminary work [9] to progress to design solutions for ultrasonic devices. The nonlinear dynamic behaviour of the excitation system and the tuned components are characterised. Nonlinearities in the form of harmonic generations, and amplitude saturation and frequency shifts of the tuned mode are measured in two piezoelectric transducers. Subsequently, various transducer-component configurations are examined. Hence, strategies to control and possibly mitigate the inherent nonlinear characteristics of one transducer are discussed through design modifications of the attached components.

8.2 Review of literature

A whole range of nonlinear phenomena such as multiple solutions, amplitude jumps, subharmonic resonance, frequency modulations and chaotic motions have been extensively researched in simple mechanical structures, such as rods and beams, under harmonic excitation.

Cusumano and Moon published a theoretical and experimental study of the dynamics of a thin, cantilevered rod subject to forced vibrations [87]. In a graph plotting the excitation frequency versus the amplitude of the excitation they have observed wedge-shaped regions of instability were the motions of the rod become chaotic. Pai and Nayfeh presented a general nonlinear theory for anisotropic beams undergoing three-dimensional vibrations, in order to find the point of bifurcation [88]. Hence, they studied chaotic motions, modulations and chaotically modulated motions.

Anderson et al. experimentally investigated the vibrations of a cantilevered beam excited at a frequency near the fourth bending-mode frequency for different directions of the applied force [89]. They found that when the excitation was axial, a parametric combination resonance was detected. On the other hand, when the base excitation was applied perpendicular to the axis of the beam and a stationary sweep of the external frequency was carried out, no combinations were measured. Instead the response, consisting only of the fourth bending mode, showed features of a classical softening Duffing's equation, and a jump from a large-amplitude to a small-amplitude response occurred when the frequency was decreased. Moreover a nonplanar chaotic motion of the beam was detected for excitation amplitudes above a threshold value. Bajaj and Johnson applied asymptotic techniques to predict complex dynamical motions in weakly non-linear forced mechanical systems [90]. They showed that the averaged equations of a harmonically excited string possess non-planar constant solutions, which become unstable and give rise to limit cycles, period-doublings, and isolated periodic solutions, as well as chaotic attractors.

8.3 Nonlinear vibrations

Nonlinear behaviour, to some extent, is present in mechanical and structural systems due to inherent sources of nonlinearities existing even in simple systems. Nonlinearities are responsible for a variety of effects which are absent in linear

systems, such as the jump phenomenon, natural frequency shifting, combination resonances, frequency modulations and chaotic motions [83]. Many systems excited in vibration, which exhibit linear behaviour at low levels of excitation, become nonlinear at higher levels of excitation.

Nonlinearities appear in the majority of real systems in one form or another. Nonlinearities can be grouped in two main categories. The first category contains nonlinearities which are not based on a known physical phenomenon (such as damping) but are essentially geometrical in origin. The other group are due to physical characteristics of systems such as nonlinear damping which may be generated by material composition.

A form of nonlinearity of the first group, characterised by the inclusion of a cubic term in the equation of motion of a single DoF system is as follows:

$$\ddot{x} + 2\zeta\dot{x} \pm h x^3 + \omega_0^2 x = A\cos\Omega t \tag{8.1}$$

Such an equation, containing a cubic nonlinearity, linear viscous damping, linear stiffness and a single frequency excitation, is a form of the well-known Duffing equation [91].

Figure 8.1 shows the representative curves for $h = 0$, $h > 0$ and $h < 0$. It is evident that the sign of the cubic term determines the hardening or softening nature of the elastic element. Hence, if the cubic term is positive the frequency response curve bends to the right (the system hardens), and conversely if the cubic term is negative the curve bends to the left (the system softens).

Duffing-type systems frequently display nonlinear jump phenomena and hysteresis effects. The jump phenomenon for a system characterised by a softening response is shown in Figure 8.2. The hysteresis effect is visible in the loop ABCD, obtained from a sweep up and down of the excitation frequency around a system natural frequency. Response transitions from periodic, to amplitude-modulated, to chaotic motions,

through swept-frequency excitation have been theoretically and experimentally observed for simple structures characterised by a form of nonlinear behaviour [87].

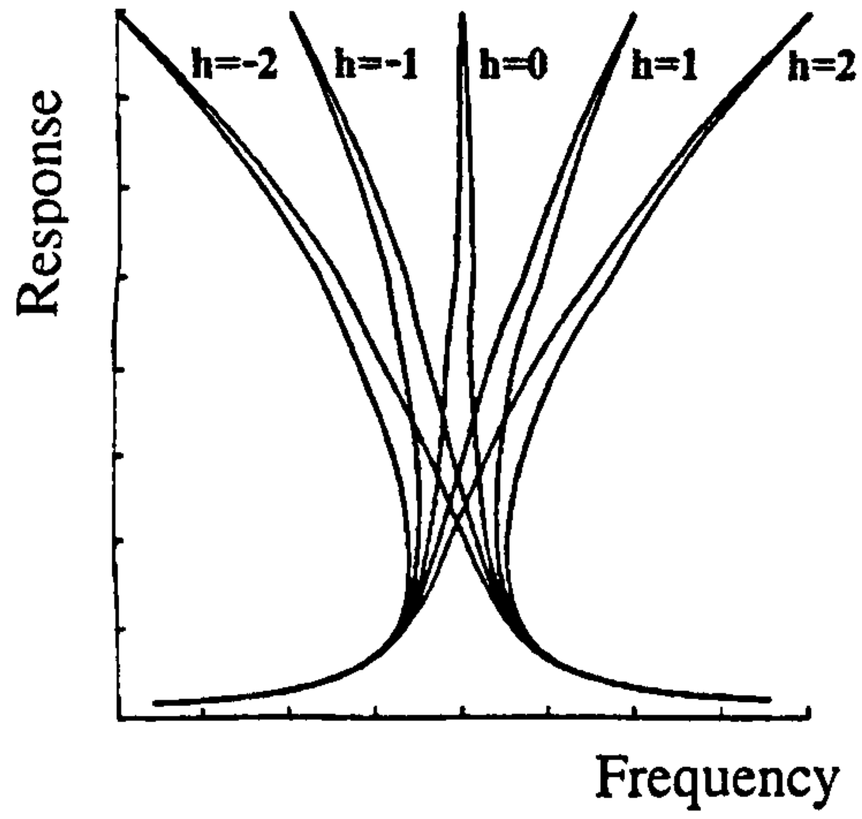

Figure 8.1. Frequency-response curves for different *h* values [72]

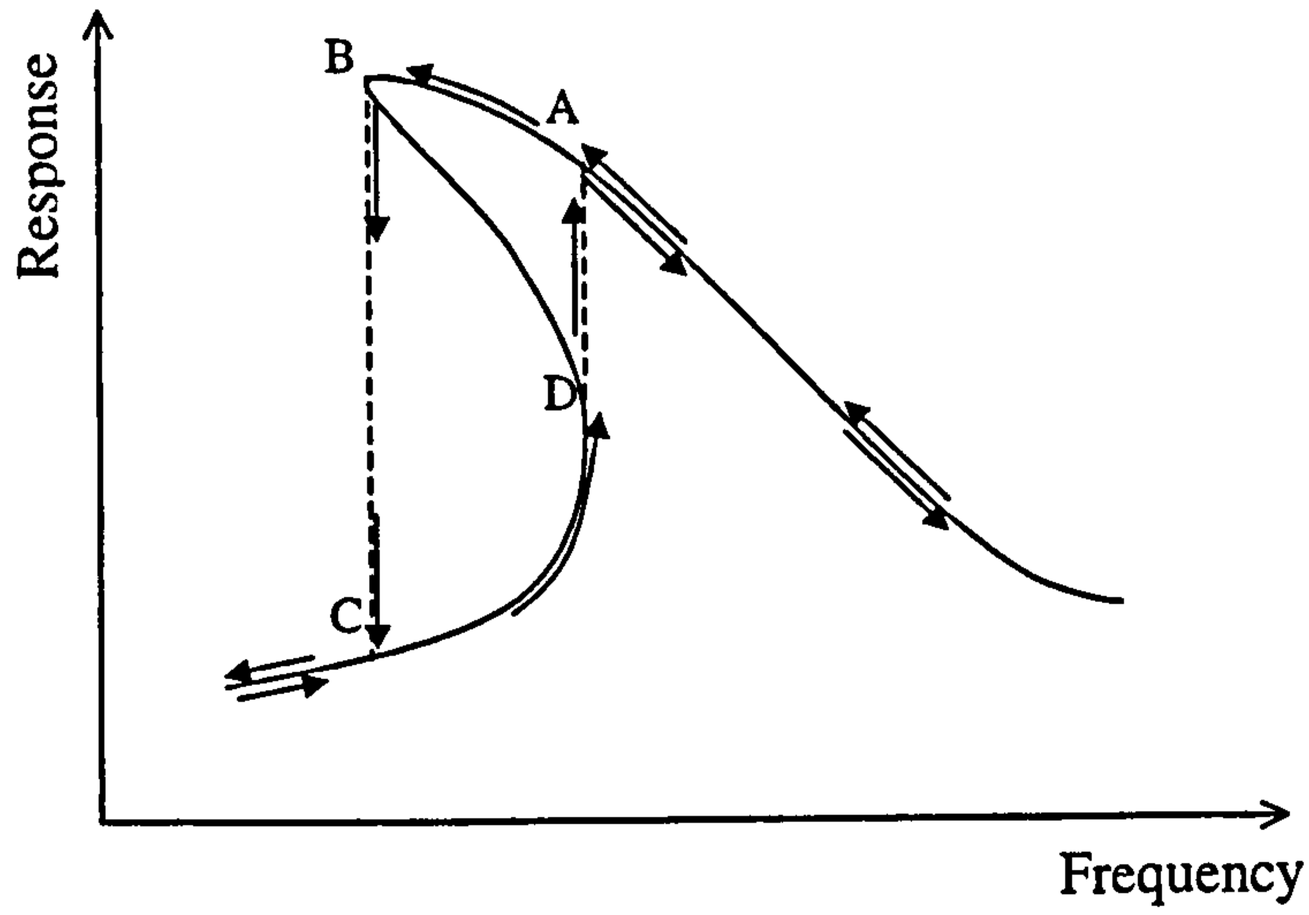

Figure 8.2. Jump phenomenon for softening response characteristic

A typical route to chaos is described by Greene [92] in an experimental and numerical investigation of the nonlinear behaviour of a simple driven diode resonator. The diode resonator circuit is shown in Figure 8.3. When driven at a frequency near the diode's resonant frequency, the circuit exhibits periodic behaviour (Figure 8.4). The harmonic frequency appears at that of the driving force, while a small ultrasubharmonic appears at double of the driving force frequency. Ultrasubharmonic frequencies are found at mf_0/n where n=1 and m= 1,2,3,...,. Figure 8.4 is the time series for the periodic

solution. This display shows that the function of the circuit is similar to a sine wave and therefore periodic.

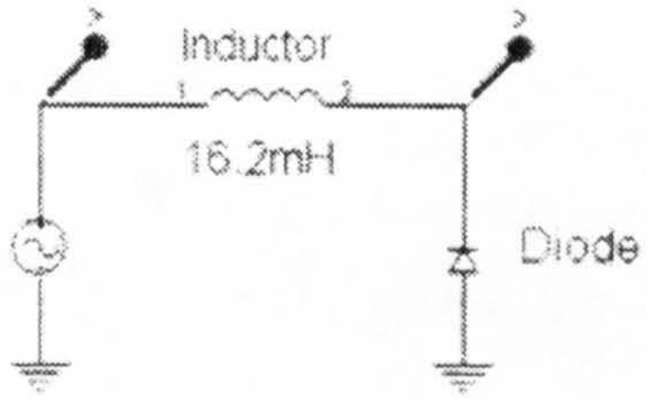

Figure 8.3. Diode resonator circuit [92]

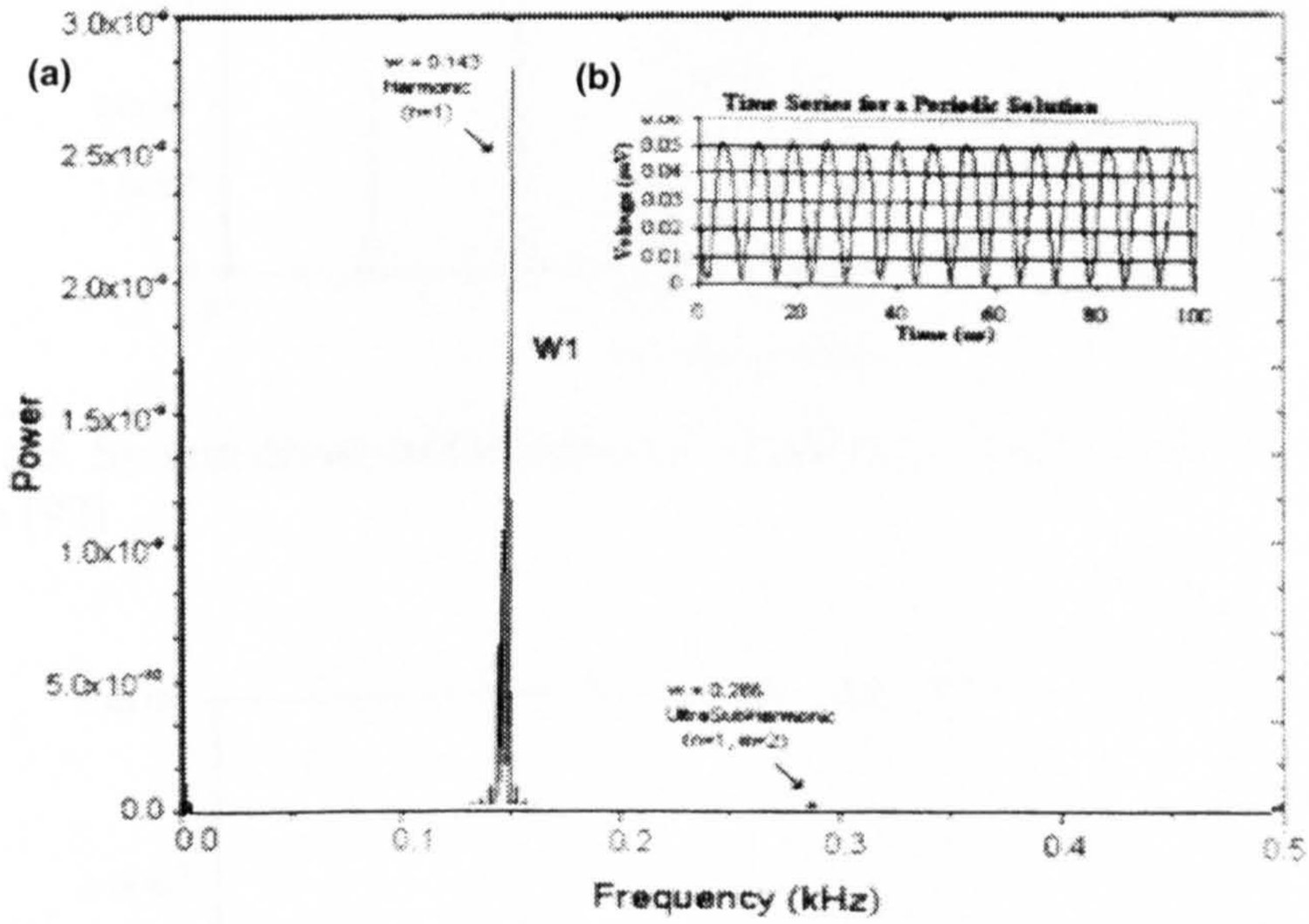

Figure 8.4. System driven at the harmonic frequency at low amplitude. Periodic behaviour [92]

As the driving amplitude is increased, the periodic state becomes unstable. A second frequency appears in the response at a frequency half of the driven resonance, resulting in a period doubling bifurcation (Figure 8.5). This system exhibits the same ultraharmonic frequencies as seen in the periodic solution, but now there are ultrasubharmonic frequencies as well. Ultrasubharmonic frequencies can be found at mf_0/n where n=1,2,4,…, and m= 1,2,3,… Figure 8.5 (b) exhibits the time series graph of the period-2 solution. The two different frequencies are clearly visible in this display. Further increase in the excitation amplitude results in the splitting of the two periods, giving quadrupling, octupling, and finally chaos (Figure 8.6).

These indirectly excited responses differ from the resonance conditions typical of parametric systems as they generally do not correspond to the frequencies of internal modes.

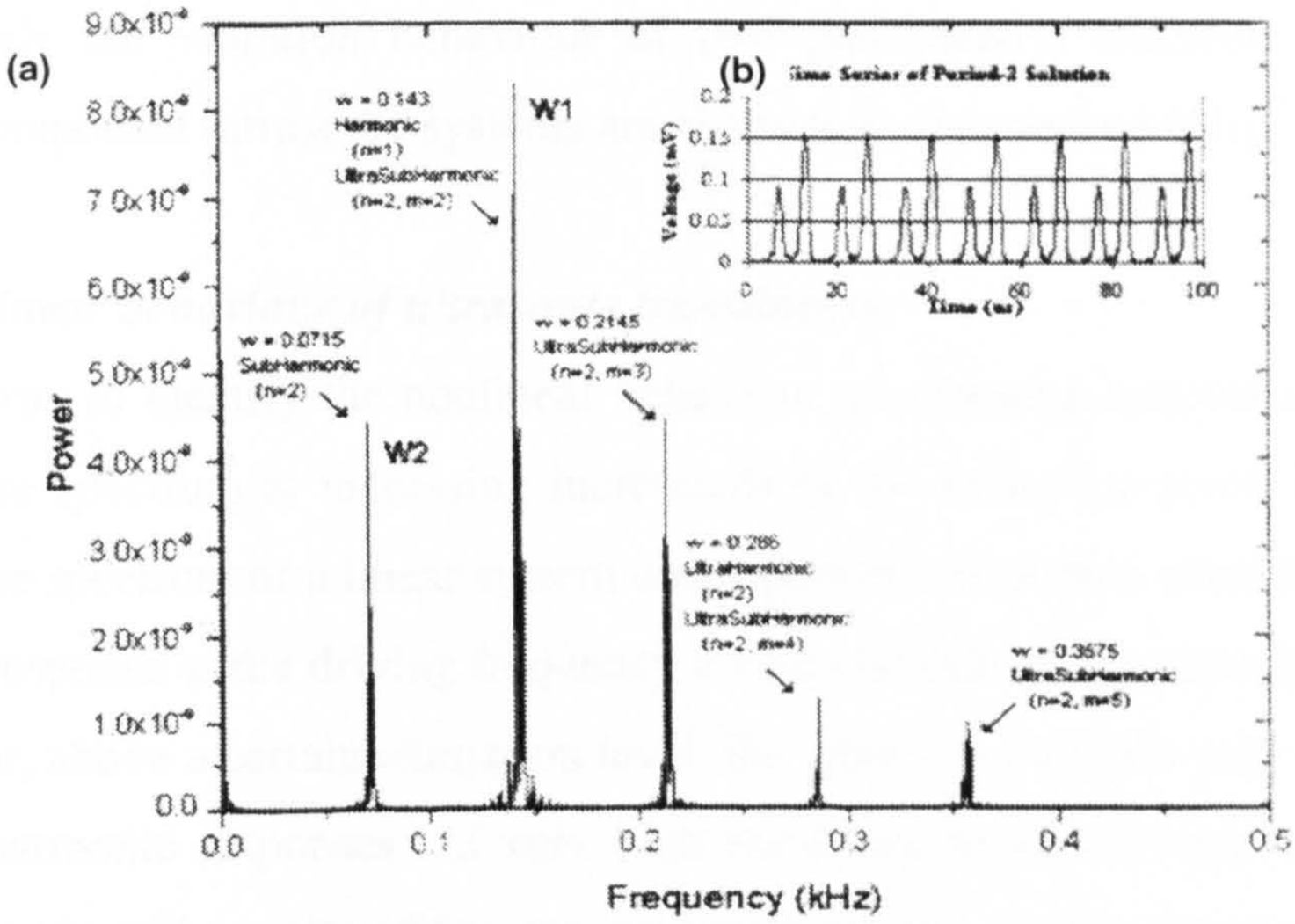

Figure 8.5. System driven at the harmonic frequency at high amplitude. Period-2 solution [92]

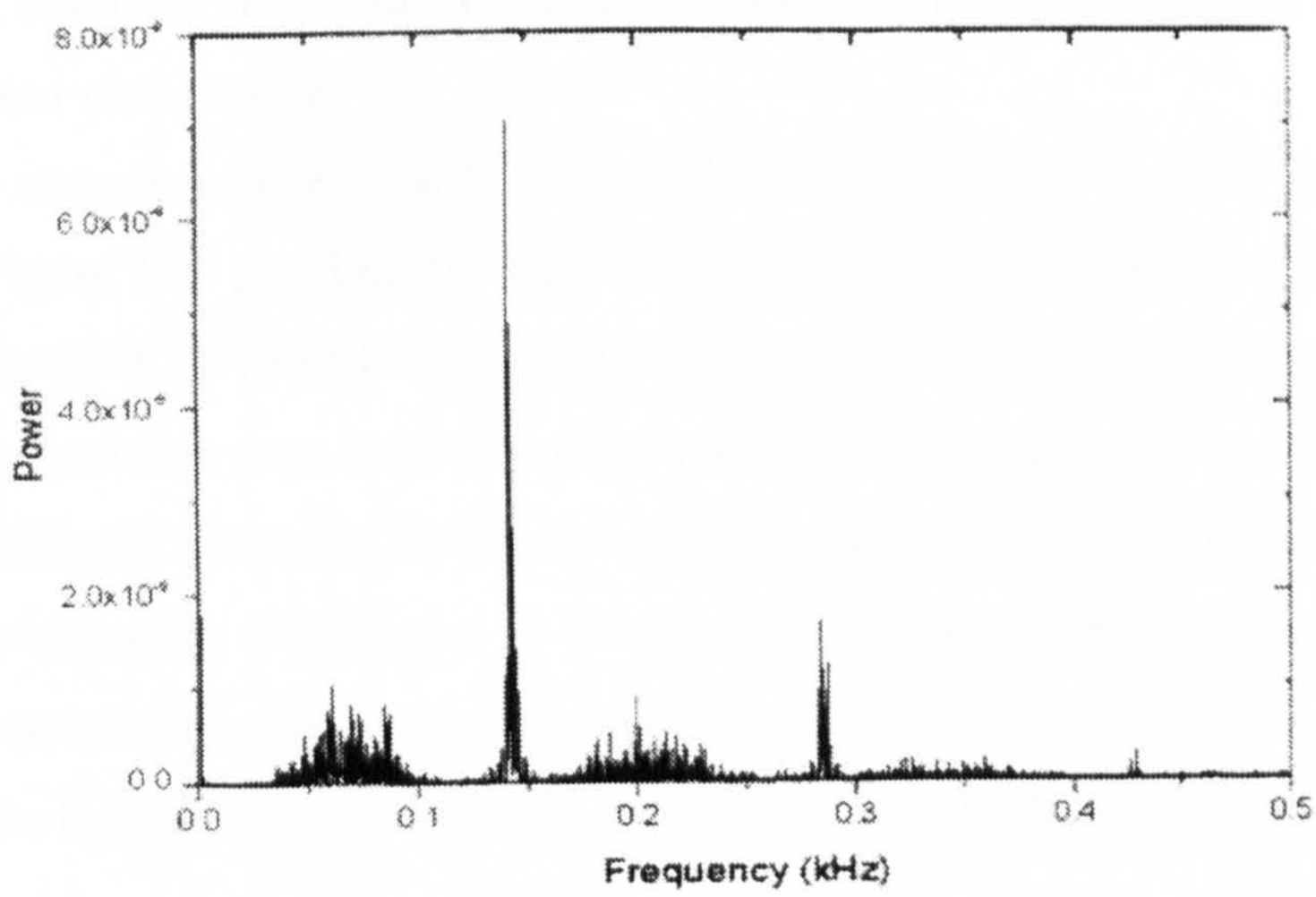

Figure 8.6. System driven at the harmonic frequency of 143 kHz at amplitude 304 mV. Chaotic solution [92]

8.4 Nonlinear vibrations in ultrasonic systems

High power ultrasonic systems, designed to resonate in a tuned mode of vibration at a low ultrasonic frequency, exhibit response characteristics strongly associated with

positive and negative cubic stiffness effects typical of Duffing oscillators. High levels of modal spill-over, such as multivalued responses and complex bifurcatory behaviour, are also detectable in the responses of ultrasonic devices.

In this study the vibration behaviour of two piezoelectric transducers and three multiple-component ultrasonic systems are characterised experimentally.

8.4.1 Nonlinear behaviour of ultrasonic transducers

A simple way to identify the nonlinear behaviour of vibrating systems is to measure the response spectrum at increasing increments of the excitation level. For instance, the response spectrum of a linear system under periodic excitation consists only of the harmonic response at the driving frequency for all excitations. Conversely, if a system is nonlinear, above a certain excitation level, the spectrum enriches with subharmonic and superharmonic responses. At very high excitation levels the responses can also become chaotic with spectra of frequencies replacing the specific response peaks.

The nonlinear response characteristics of two different 35 kHz high power ultrasonic transducers, used for industrial applications, are investigated. Figure 8.7 shows the first transducer under study.

Initially the transducer is driven in the tuned mode frequency at 30 V excitation, as shown in Figure 8.8 (a). The velocity response measured at the transducer tip by means of the 3D LDV, exhibits a period bifurcation. In fact, the response splits into numerous frequencies over the 0 - 50 kHz range, indicating that the nonlinear domain of the piezoelectric ceramics is reached. These indirectly excited frequencies differ from the combination frequencies of parametric and autoparametric systems as they do not necessarily correspond to internal modes. The dots, squares, and triangles marked in the figure indicate three sets of harmonically related frequencies.

Figure 8.7. Transducer 1 [Telsonic Ultrasonics Inc.]

Subsequently the response spectrum of the transducer driven at 50 V excitation is measured, as shown in Figure 8.8 (b). At this excitation level the response spectrum shows a spreading of the responses around certain frequencies in the spectrum, a typical sign of chaotic behaviour.

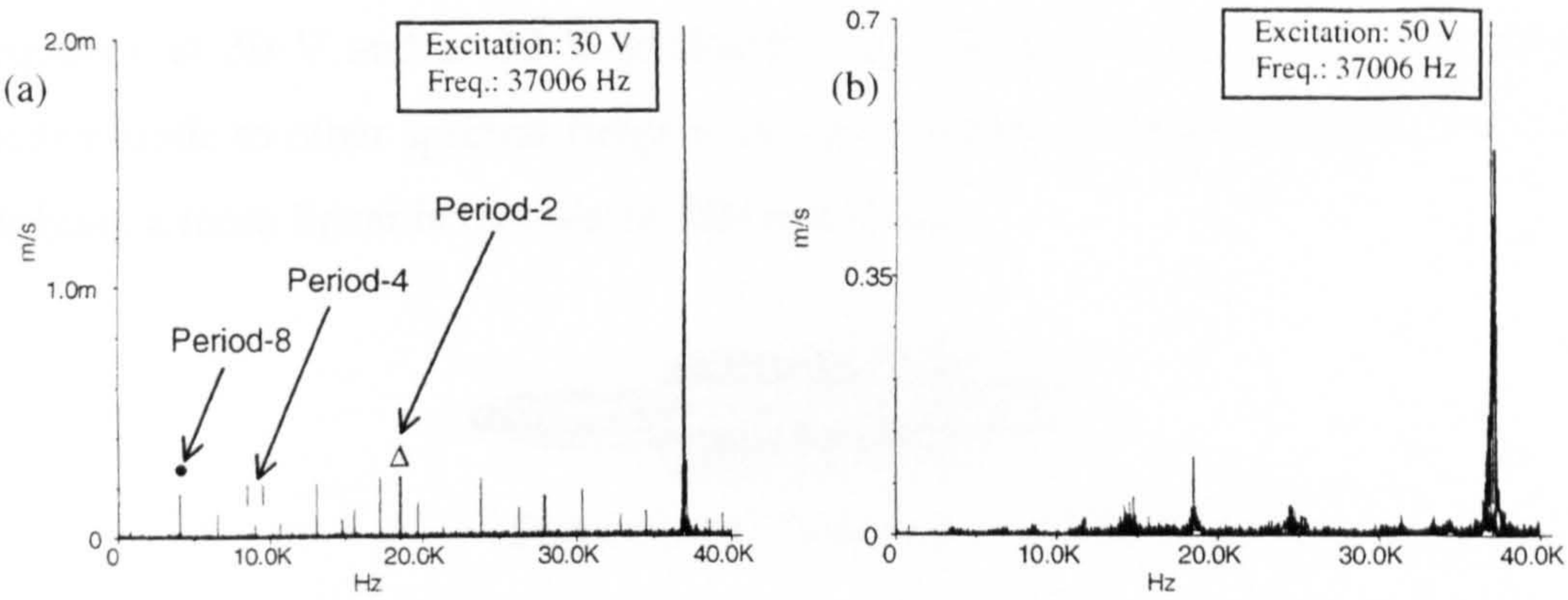

Figure 8.8. Response spectra measured at (a) 30 V, (b) 50 V excitation

Finally, the response of the transducer is measured through a slow forward and backward sweep of the excitation frequency around the tuned frequency. Figure 8.9 illustrates the response measured at 50 V excitation.

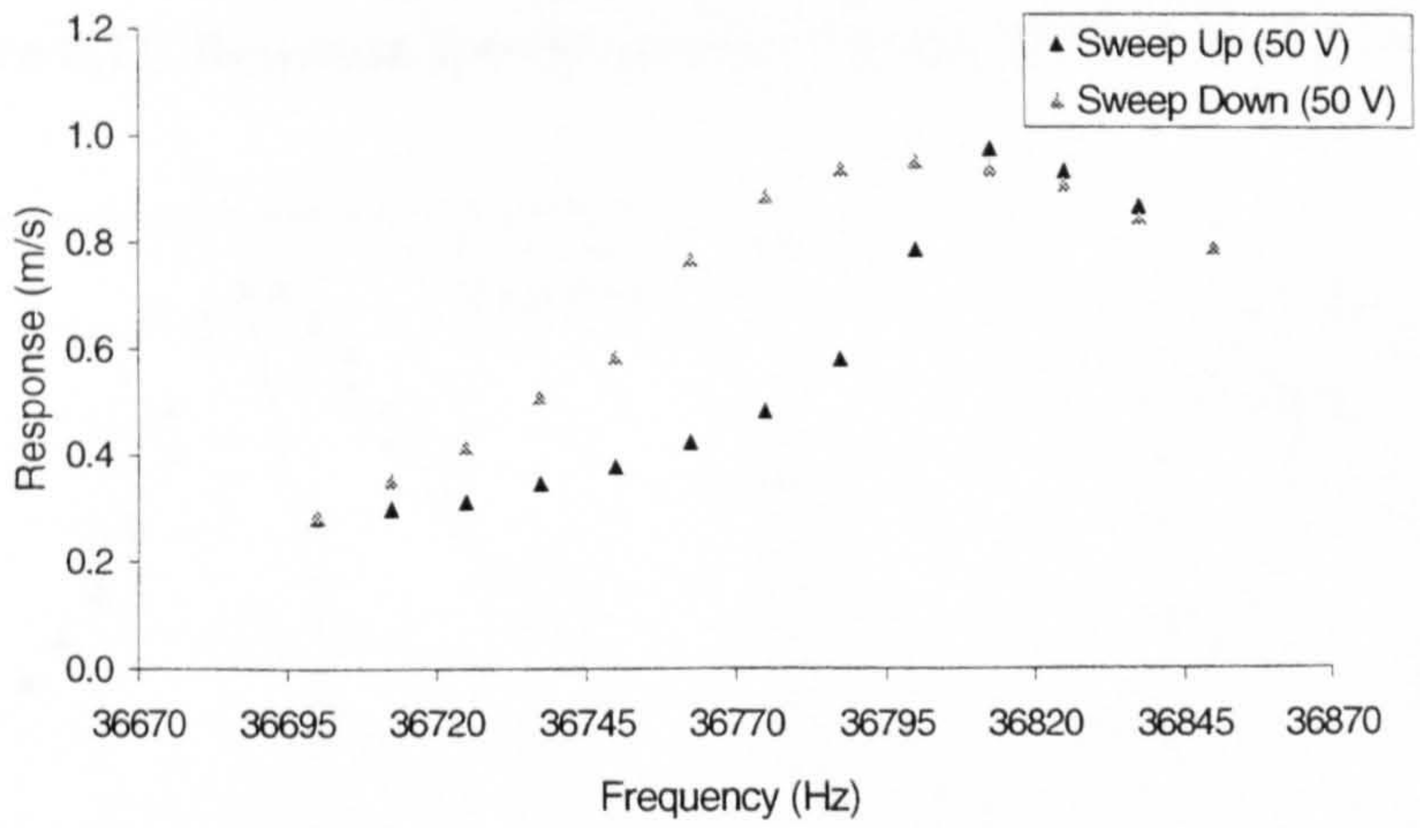

Figure 8.9. Response characterstic of transducer 1 at 50 V excitation level

From this figure two observations can be made. First, the transducer longitudinal resonance exhibits a low Q factor, as a consequence of the response saturation due to the energy spill-over. Second, the responses measured during the frequency sweep up

differ from those ones detected in the sweep down. This is because different mechanisms of energy leakage occur during the frequency sweeps.

The second transducer investigated is illustrated in Figure 8.10. Figure 8.11 (a) and (b) show the measured response spectra of the transducer driven at the tuned mode frequency at 30 V and at 50 V excitation. No energy transfers from the externally excited mode to other spectral frequencies are detected at either excitation levels, thus implying a more linear behaviour of this transducer.

Figure 8.10. Transducer 2 [Martin Walter]

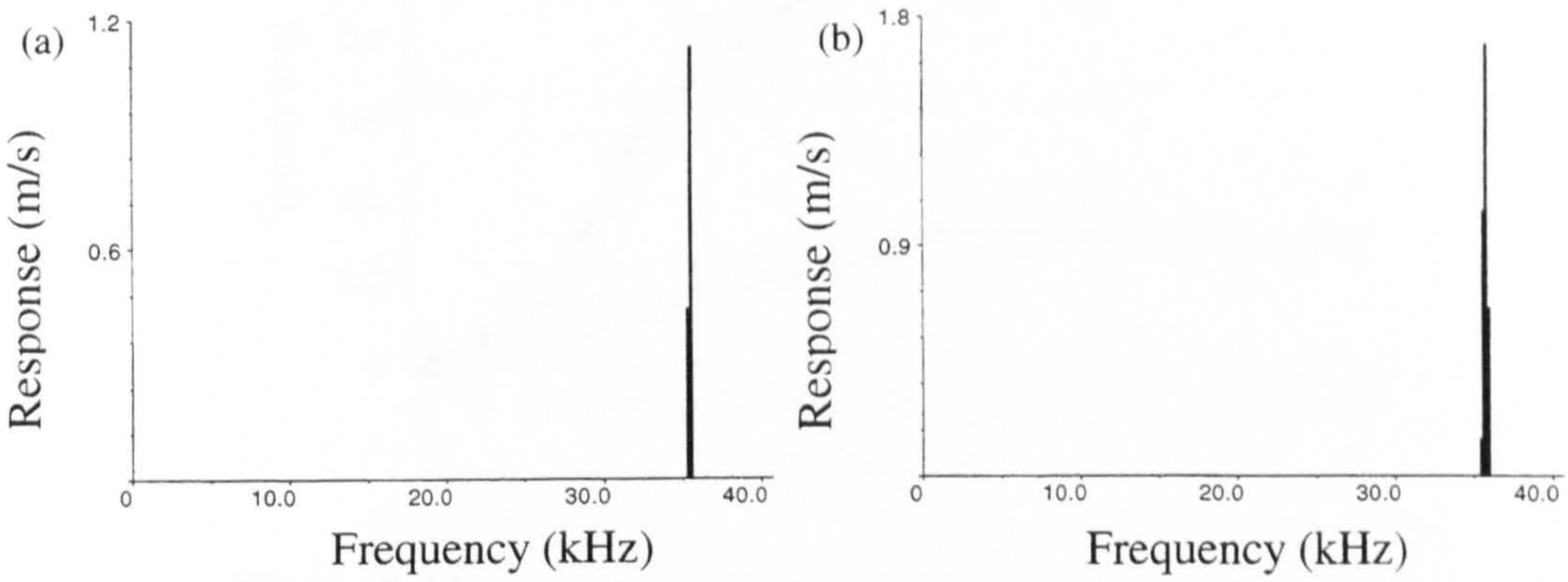

Figure 8.11. Response spectra measured at (a) 30 V, (b) 50 excitation levels

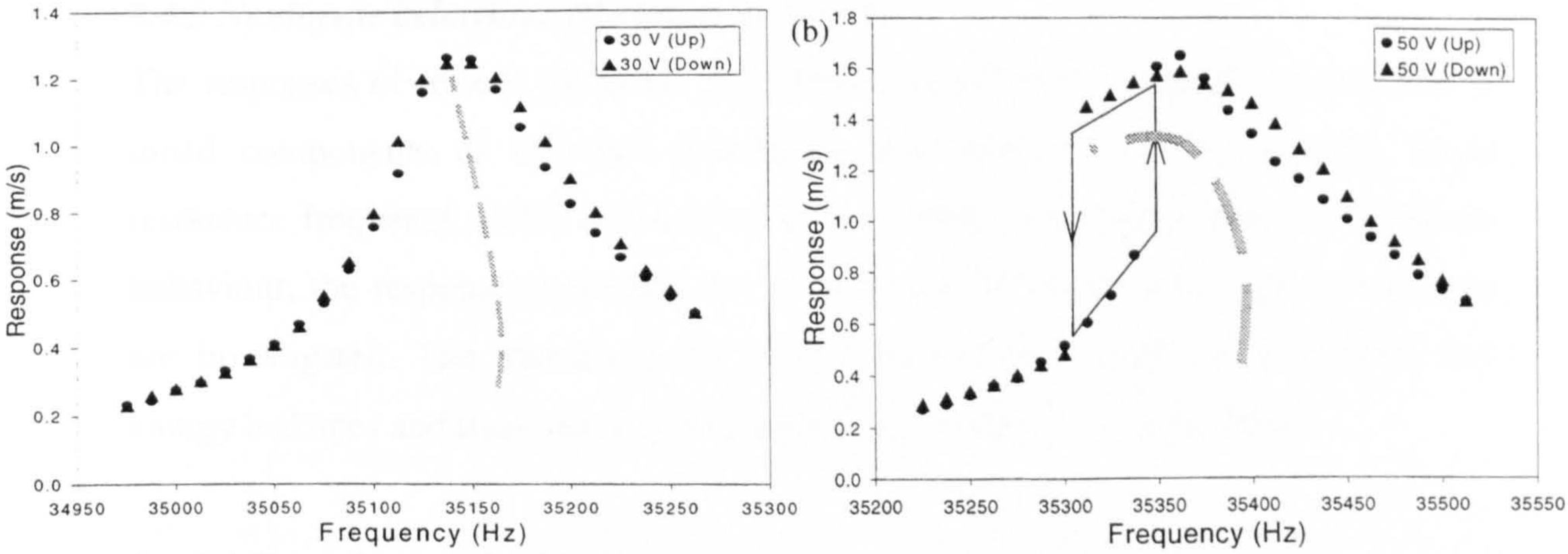

Figure 8.12. Response characterstics of transducer 2 at (a) 30 V, (b) 50 V excitation level

Frequency sweeps at 30 V and 50 V excitation levels, measured around the tuned mode frequency, are shown in Figure 8.12 (a) and (b). A softening characteristic of

the transducer responses, increasing with the excitation level, is evident in the figure. Such asymmetric responses are an indication of nonlinear behaviour. However, the higher Q factor and the absence of bifurcation demonstrate that the second transducer represents a better design for high power ultrasonic applications. The responses of the two transducers, measured over a range of excitation levels, are plotted in Figure 8.13. The measurements show that transducer 2 provides higher velocity response at the output face for all excitation levels. In addition, this transducer exhibits a saturation of response for excitations over 60 V, whereas transducer 1 saturates at 50 V.

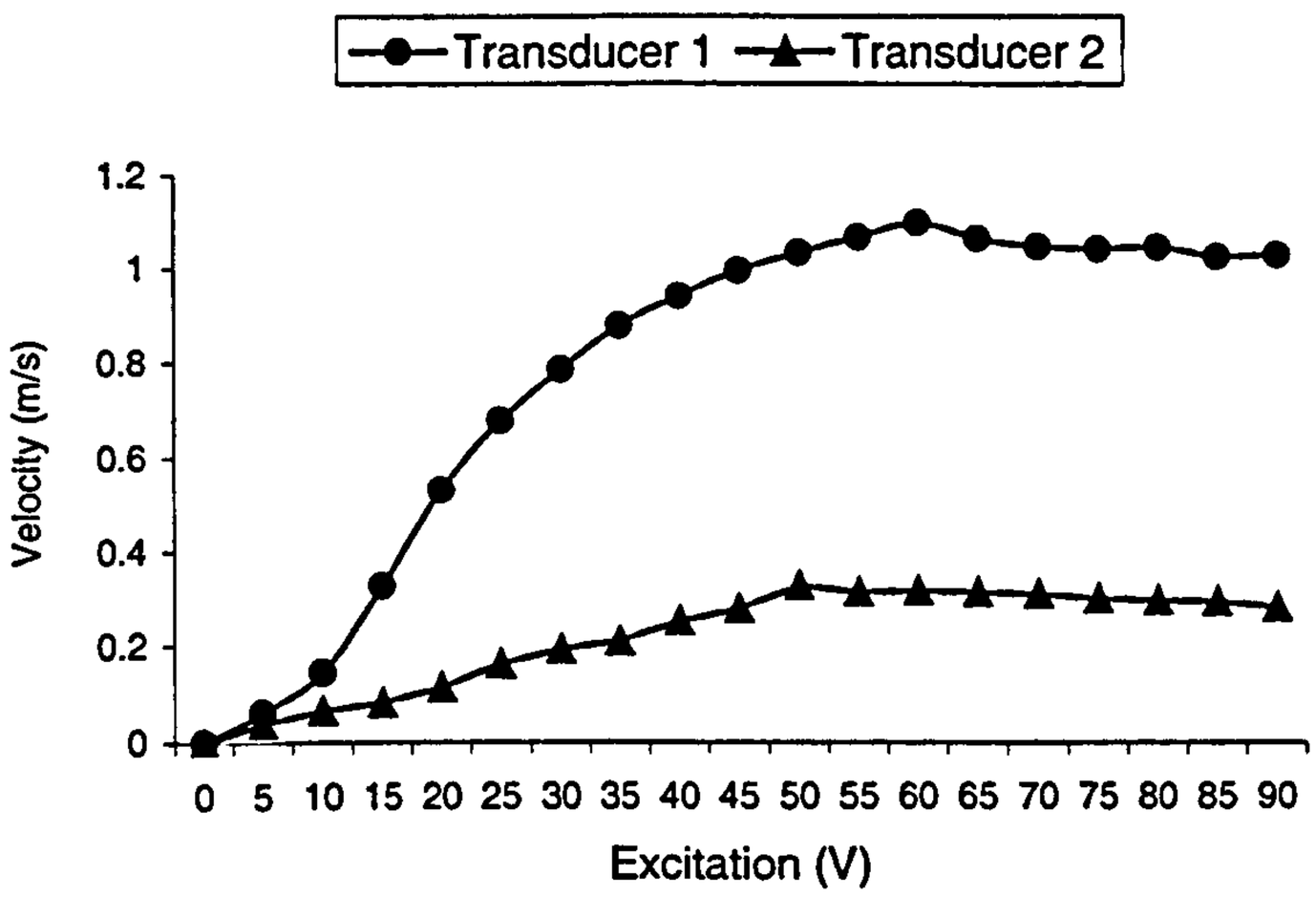

Figure 8.13. Velocity response plotted against excitation level

8.4.2 Nonlinear behaviour of ultrasonic systems

The responses of several ultrasonic assemblies consisting of a transducer attached to tuned components of different geometries and materials are investigated. Since resonance frequency shifts and hysteresis phenomena are typical signs of nonlinear behaviour, the response characteristics of these assemblies driven in the tuned mode are investigated. The transducer shown in Figure 8.10 is used, as it exhibits low energy leakages and therefore a clearly identifiable response characteristic.

8.4.2.1 Transducer-1.5 λ bar horn

Initially, a solid aluminium cylindrical rod, or bar horn, of one and a half-wavelengths at 35 kHz is attached to the transducer as shown in Figure 8.14. The threaded cutting stud is half-screwed into both components. The response characteristic of the assembly measured at 30 V excitation is shown in Figure 8.15 (a). It can be seen that

the response of the assembly exhibits a softening characteristic which is less soft than for the transducer alone (Figure 8.12 (a)). A similar observation applies in the case of 50 V excitation, where the response of the transducer-bar horn exhibits a less soft characteristic than the transducer measured at the same excitation (Figure 8.12 (b)). The implication is that the 1.5 λ bar horn exhibits an inherent hardening characteristic which, combined with the soft response of the transducer, tends to linearise the response of the transducer-bar assembly. A preliminary theoretical investigation has successfully modelled this phenomenon for a 2DoF system consisting of two serially coupled oscillators of opposite nonlinear characteristics [93].

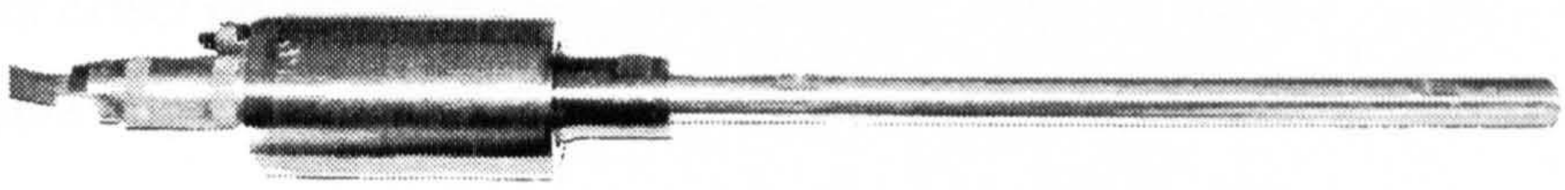

Figure 8.14. 1.5 λ bar horn screwed into transducer

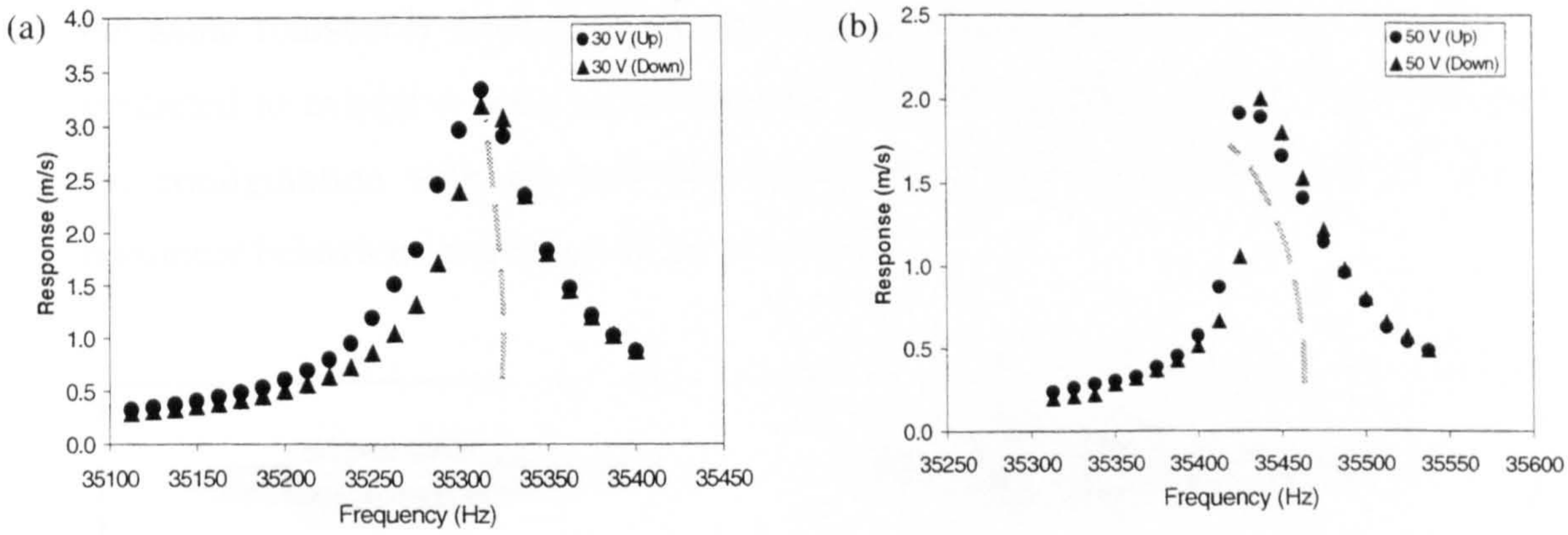

Figure 8.15. Response characteristics of transducer-bar horn assembly at (a) 30 V, (b) 50 V excitation level

The measurements suggest that, for typical industrially relevant equipment, the softening nature of the transducer can be mitigated to a certain extent by the addition of characteristically hardening tuned components. However, a truly linearised response characteristic at the output of the system is not easily achieved. Evidence in the literature demonstrating that beam-like structures exhibit a hardening characteristic [94], tends to support the likelihood that the 1.5 λ bar horn exhibits a hardening nonlinearity. This, in turn temds to linearise the response of the transducer-bar system.

8.4.2.2 Transducer attached to half- and full-wavelength blades

Figure 8.17 (a) and (b) show the response characteristics of the transducer attached to a half-wavelength and a wavelength cutting blade (Figure 8.16 (a) and (b)), respectively. Both blades manufactured from tool steel. At 30 V excitation, the response of the first configuration, exhibits a softer response than the transducer measured alone, as shown in Figure 8.12 (a)). At the same excitation level, the response of the second configuration exhibits an almost linear characteristic (Figure 8.17 (b)). It appears that the half-wavelength blade exhibits an inherent softening characteristic which, combined with the soft response of the transducer, produces a softer nonlinear response. By contrast, the wavelength blade does not have a significant effect on the nonlinear characteristic of the transducer but tends to linearise the response slightly.

An observation regarding the strain levels reached in these two single-blade and transducer configurations can explain the differences in the measured responses. For the same transducer excitation, the wavelength blade, due to its tapered profile, is predicted to exhibit a lower strain than the half-wavelength blade. It is possible that the configuration with the half-wavelength blade reaches the threshold of elastic nonlinear behaviour at a lower excitation [95].

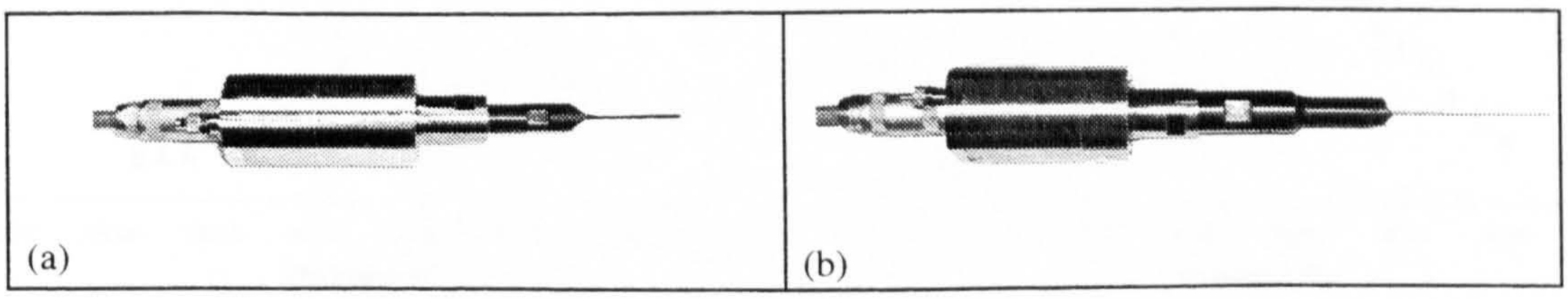

Figure 8.16. Transducer-blade assemblies: (a) transducer and half-wavelength blade, (b) Transducer and wavelength blade

8.4.2.3 Influence of joint tightness on system nonlinearity

The effect of tightness of the joint connecting two components, on the response characteristic is investigated. The threaded stud between the transducer and the bar horn in Figure 8.14 is tightened at two different torque levels. Figure 8.18 shows that, for the same excitation (50 V), a more linear response is achieved for the configuration with higher torque (Figure 8.18 (a)) than for that with lower-torque (Figure 8.18 (b)). These measurements find analogies with recent studies carried out

on NDE of imperfect interfaces and adhesive bonds [96]. In fact, it has emerged that imperfect interfaces, resembling a low torque joint, exhibit much stronger nonlinearities than do bulk materials or well-bonded interfaces, resembling a high torque joint.

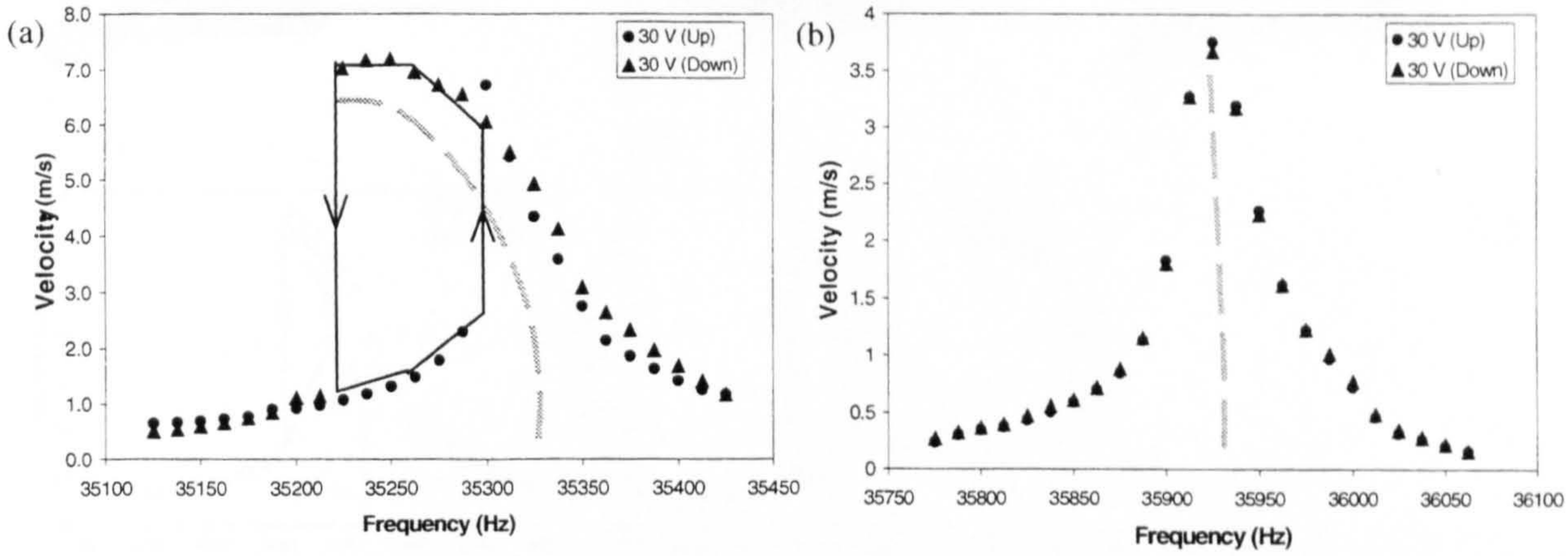

Figure 8.17. Responses of an industrial ultrasonic transducer and (a) 0.5 λ and (b) λ blades at 30 V excitation level

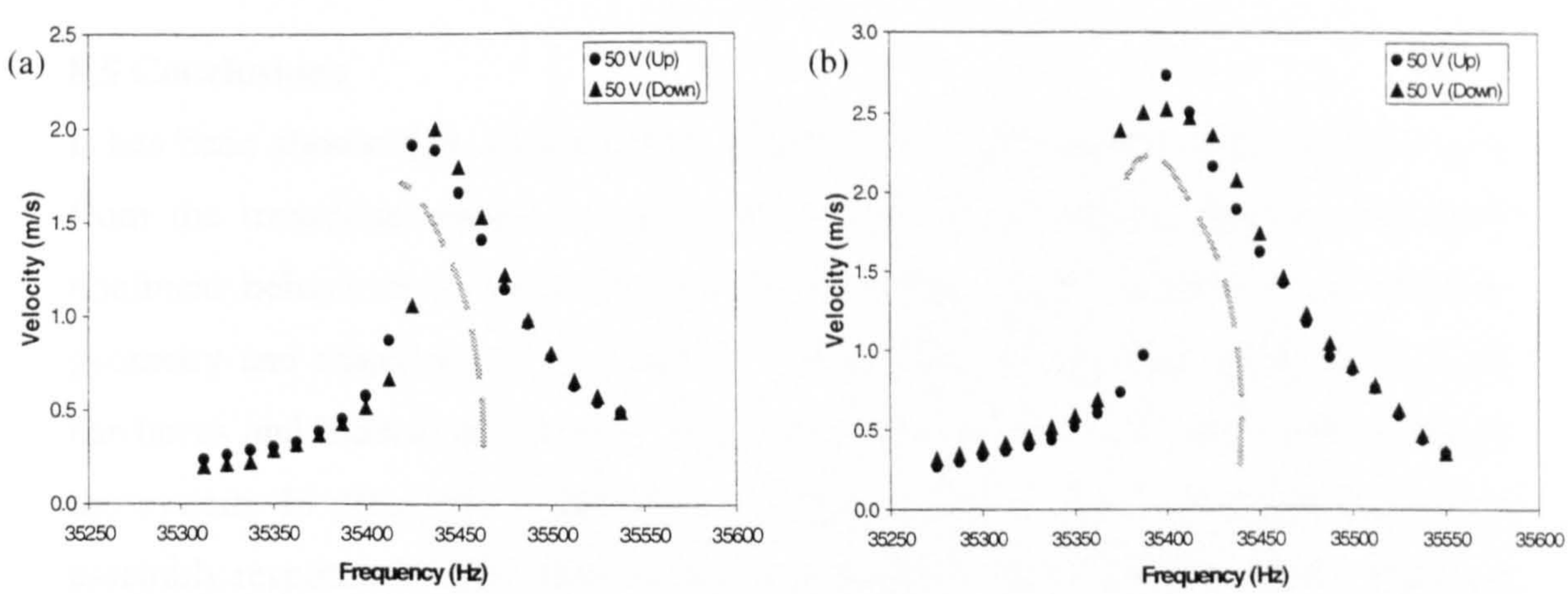

Figure 8.18. Effects of joint tightness on the response: (a) high torque joint, (b) low torque joint

8.4.2.4 Influence of positioning of stud on system nonlinearity

The nonlinear characteristics of an assembly can also be varied by means of the axial positioning of the stud within the joint. Figure 8.19 shows three different configurations for the position of the threaded stud. When the stud is fully-fitted into the transducer-base (Figure 8.19 (a)) the narrowest nonlinear region is exhibited in the response measured at the blade tip. When the stud is fully-fitted into the blade-base

(Figure 8.19 (c)), the nonlinear response region is widest. This configuration exhibits the softest response.

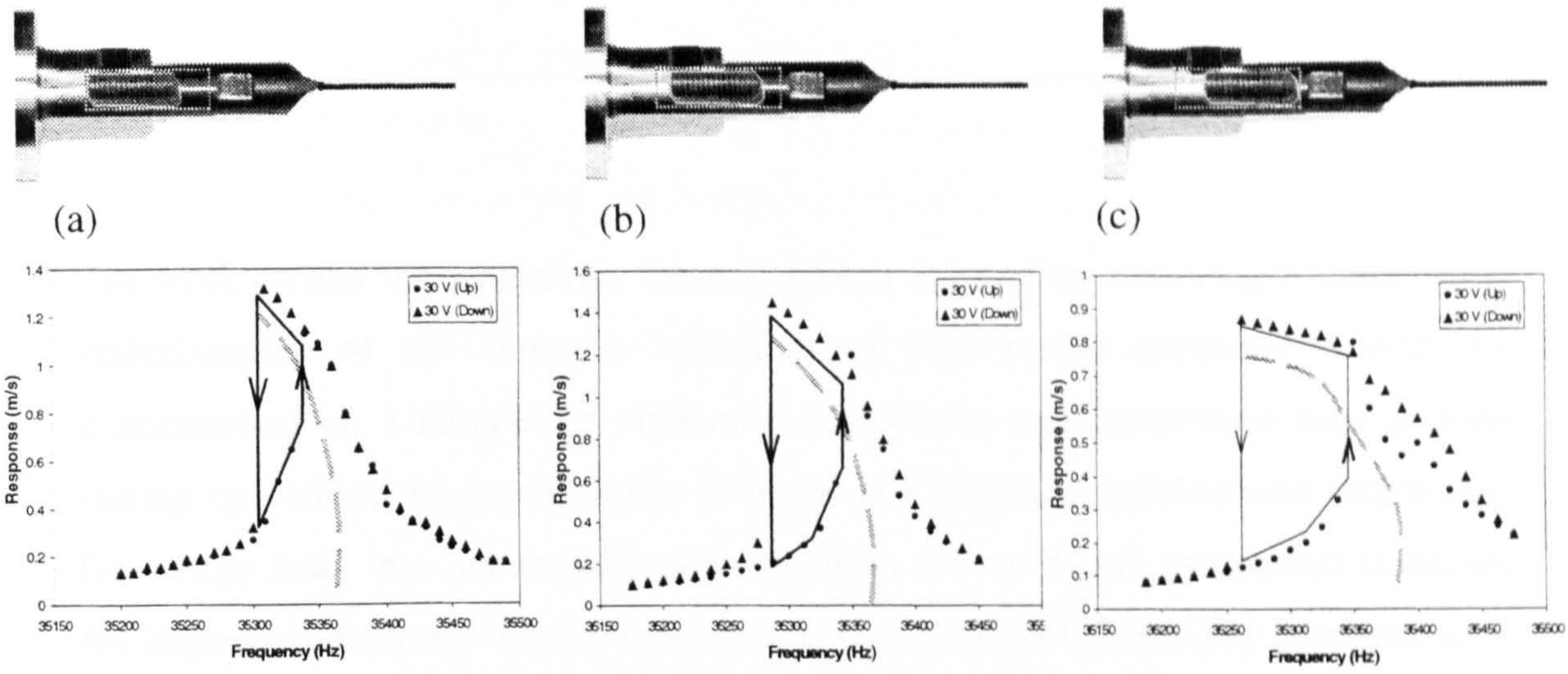

Figure 8.19. Different stud configurations: (a) Stud fully-fitted into the transducer-base, (b) Stud half-fitted into the blade-base, and (c) Stud fully-fitted into the blade-base

8.5 Conclusions

It has been shown that nonlinearities in high power ultrasonic systems mainly stem from the transducer behaviour. A practical method for influencing the inherently nonlinear behaviour of the transducer, by attaching tuned components of different geometry and materials, is proposed. It is found that some tuned components (long bar horns and blades) are capable of reducing the effect of the nonlinearities within the system. In other cases, including a half-wavelength blade, the blade-transducer assembly response is softer than that of the transducer alone. In addition, the tightness of the joints and the configuration of the threaded stud connection prove crucial in the control of nonlinearities.

Therefore, a manipulation of the nonlinear characteristics of ultrasonic assemblies may be achieved by opportune component design and joint configurations without the need for exclusively modifying the transducer response characteristic. On the other hand, the softening characteristic of an ultrasonic transducer is an inherent characteristic of piezo-ceramic elements, and therefore difficult to adjust.

CHAPTER 9

CONCLUSIONS

The work carried out within this thesis has been focused on achieving a fundamental understanding of the vibration behaviour of high power ultrasonic devices by concentrating on a number of ultrasonic components and assemblies used in food cutting operations. Characterisation of linear and nonlinear mechanisms responsible for energy leaks into non-tuned modes has been achieved, and subsequent strategies for improved ultrasonic device design have been proposed. Many key advances have been made during the research and these innovations and developments are summarised in the following sections.

9.1 Reducing component failures by design

Most ultrasonic tools and devices are designed with amplitude gain, allowing high vibration amplitudes at the working surface. The tuned components' profiles are stepped or shaped to provide the required gain, but the maximum stress then occurs at the steepest section reduction, which in turn becomes a common failure location. Finite element analysis has been successfully used to model a wide range of component geometries, predicting that, for the same gain, the highest stressed components are those where the longitudinal mode node is at or closest to the highest stress location. For the study of ultrasonic cutting blades, requiring a gain factor of six to eight, blade failures were significantly reduced by judicious repositioning of the node away from the failure location by blade reshaping. For example, a reduction in stress of 45% was achieved for a blade design which located the node further into the thickest blade section.

It was found that for multi-component systems, failures are often caused by bending responses in the longitudinal mode. For these systems, stress reduction requires a dual approach. First, node repositioning is achieved by detuning the different attached components while maintaining the overall system tuned frequency. This again allows

nodes to be located away from highest stress locations. Second, the use of block horns as intermediate components in multi-component systems required a new approach to block horn design. Block horns are widely used in ultrasonic systems, as working tools or as intermediate components linking the transducer-booster system to the working tools. In multi-component systems, block horns allow several working tools (such as cutting blades) to be driven by one transducer. Standard block horn design rules exist, which are based on satisfying two performance criteria: tuned mode frequency isolation from non-tuned mode frequencies and vibration amplitude uniformity on the working surface. These two criteria cause conflict in the design as the first is more easily achieved if the number of modes is small, whereas the second is achieved by slotting configurations which hugely increase the number of modes.

A new approach to block horn design has been proposed which concentrates on eliminating bending responses in the attached components, reducing stress and improving reliability. For a three-blade cutting system, the study has characterised the effects of slotting configurations, the use of fine slots and block castellations in terms of the vibration response of the three blades, which should be in-phase, of equal amplitude, and purely longitudinal. The design procedure also concentrates on reducing the number of modes and improving tuned mode isolation. This is also critical in controlling the effects of energy leakage mechanisms associated with nonlinear vibration behaviour and therefore the new block horn designs have also been crucial in reducing the adverse effects of nonlinear behaviour.

9.2 Linear modal coupling

For reliable operation of ultrasonic components and assemblies, the frequency of the operating mode has to be isolated from close modal frequencies which can result in non-tuned modes participating in the response at the operating frequency via modal coupling, or can cause mode switching to occur during operation. Operating mode isolation can be achieved by FEA, where models are validated by accurate EMA using 1D LDV. However, the experimental validation of numerical data has not always been satisfactory using conventional normal-to-surface response measurements, therefore, improvements in the detection of modal responses are required.

In this investigation vibration velocity measurements were carried out using a 3D LDV, which allows both in-plane and out-of-plane responses to be characterised, and which resulted in accurate identification of modes and significant improvement in data correlation. The combination of FE modelling and 3D LDV response measurements has enabled a greater depth of understanding of vibration behaviour of ultrasonic systems and components to be gained.

In particular, two ultrasonic applications dominated by the behaviour of block horns have been discussed: the first involving a block horn acting as a tuned working tool; the second a block horn used to transmit vibration to three cutting blades. Due to the multi-slotted profile of the block horns numerous modes with similar characteristics, differentiated by spatial phase variations between adjacent columns, appeared in the response spectra, with some of them coupling with the tuned mode. The use of the 3D LDV was crucial for the identification of these coupling modes and for the measurement of their responses. This information was vital for the redesign stage as it allowed unresponsive modes to be neglected in the sensitivity analysis stage.

9.3 Characterisation of system nonlinearities

Characterising the nonlinear behaviour of multi-component systems has relied on first obtaining an accurate description of the system's modes and modal frequencies. The use of a 3D laser vibrometer and finite element models has been critical in this exercise. The number of modes is high and many of the system's bending modes are difficult to detect when the excitation can only be adequately provided by a longitudinal mode transducer. The modal analysis is conducted at low power, where the system responses are linear. Energy leakage into non-tuned modes is detected by adjusting the power to the transducer until responses are detected at known modal frequencies.

In particular, energy exchanges from the operating mode into a modal frequency close to half of the tuned frequency, and excitation of combination resonances consisting of two modal frequencies whose sum is close to the tuned frequency, were detected in single- and multi-component devices. The measured energy transfers from the primary responses to the internally excited modes (secondary responses) were shown to be qualitatively similar to the theoretical descriptions of autoparametric systems. In

particular it was observed that, once the nonlinear threshold is reached, the primary response becomes independent of the excitation level, but the secondary response increases with it. Also, response transitions from periodic, to amplitude-modulated, to chaotic motions, have been experimentally observed inside the frequency regions of instability.

It was shown that predicting and controlling the dynamic response of high power ultrasonic cutting devices is more easily realised if there are a small number of modes at frequencies below the driving frequency, because modal interactions are a result of energy leaks into lower modes of vibration. If the number of modes is small, there are reduced opportunities to couple the longitudinal resonance with bending modes and reduced opportunities for the required special relationships between the modal frequencies to exist. Hence modifications of block horns and design of devices within a half-wavelength of the driving frequency, have proved to be successful strategies for eliminating the frequency relationships that lead to modal interactions.

The nonlinear response characteristics of systems were also determined. Ultrasonic transducers are inherently nonlinear at high power and tend to exhibit a cubic softening characteristic, with a jump phenomenon typical of a Duffing oscillator. To find a practical design solution to the effects of nonlinear responses, it was first necessary to measure the linear regime and nonlinear response at a range of input voltages to the transducer. The effect on this response of attaching different tuned components was assessed, as well as the attachment method. It was found that some tuned components, including some wavelength blades and block horns, tended to reduce the softening response when attached to the transducer and result in the system increasing its linear threshold, and operating with a near linear response. In other cases, including half-wavelength blades, the blade-transducer system response was softer than the transducer alone, had a lower linear threshold and wider instability region. A bank of information on the nonlinear characteristics of transducers, bar horns, and blades had been obtained, providing valuable data for understanding serially-coupled multi-component system configurations which assist the control of the nonlinear response in the design of ultrasonic devices. Additionally, the width of the instability region could be manipulated by altering the tightness of joints and by altering the position of the stud between attached components.

It has always been understood in the high power ultrasonics community that careful assembly of system components is critical for good system performance. There have been many "rules of thumb" applied, concerned with stud sizes, stud position and torque requirements for joining components, although there are inconsistencies between manufacturers recommendations.

The work carried out in this project has clarified this issue providing a fundamental understanding of the nonlinear phenomena which have considerably limited the development of ultrasonic technology.

9.4 Design of ultrasonic system components for preferential modal characteristics

The design of multi-component ultrasonic devices relies on the combined knowledge of reducing stress in high gain components, block horn design for a reduced number of modes and reduced coupling of bending motions, modal interactions resulting in combination resonances, and the manipulation of nonlinear responses from an understanding of the hard and soft characteristics of the interacting components. Despite the seemingly complex nature of the system dynamics, many practically realisable solutions are possible. For the example of the three-blade cutting device, finite element models are used initially to design a new system, serially coupling components with appropriate hard and soft characteristics to mitigate the effects of the transducer nonlinearity.

Low stress and high gain blade profiles are modelled to accommodate the required cutting depth and other geometry restrictions. The number of modes is constrained by adopting a reduced slotting design for the block horn with appropriate castellations for a wavelength device, or by incorporating elements of the block and blades within a single half-wavelength device. Mode combinations where, for instance, the sum of two modal frequencies is approximately equal to the tuned frequency, are identified and eliminated by geometry modifications via a sensitivity analysis. The resulting cutting heads benefit from comparably low stress, parallel and purely longitudinal blade responses, low modal density, reduced nonlinearity at high power and elimination of combination resonances. Although all modal interactions are not

eliminated, their threshold of activation is raised such that the cutting heads can run at higher power without their effects being detected.

9.5 New ultrasonic cutting heads

A range of new three-bladed cutting heads has been designed and manufactured. By pulling together the various analytical and experimental strands of the project, the new cutting heads have lower stress, no bending responses in the blades, a much cleaner spectrum than any other multi-component systems, a high threshold for combination resonances, and are assembled and shaped for minimising nonlinearity. Additionally, it was possible to design several different block horn and blade combinations that satisfied these requirements. All have been successfully tested in the laboratory. This research has resulted in new knowledge about the dynamic response of high power ultrasonic systems and has provided insights into resolving the problems associated with nonlinear dynamic phenomena in the design of multi-component tuned systems.

CHAPTER 10

RECOMMENDATIONS FOR FUTURE WORK

The work proposed in this thesis can be expanded to include the following tasks:

- The current work provides design strategies to control the inherent nonlinear behaviour of ultrasonic cutting systems resonating longitudinally. In particular, a design approach focused on reducing the number of modes is demonstrated to improve the performance of three-blade cutting systems. The same approach could be extended to ultrasonic devices designed for other applications such as welding tools and medical devices, and also to those operating in other modes of vibrations, such as radial, bending and/or torsional. Hence, more numerical and experimental work needs to be conducted to verify the applicability of this design strategy to a variety of ultrasonic systems characterised by enriched modal activity.

- Theoretical models of simple parametric systems [84] have shown that the threshold and the width of the regions inside which combination resonances involving multi-modal responses appear, depend on the amount of damping inherent in the vibrating systems. Hence, ultrasonic devices manufactured from alternative materials exhibiting higher structural damping, should be considered in order to push the thresholds of the instability regions above the nominal operating amplitudes.

- It has been shown that the softening response characteristic of a piezoelectric transducer can be influenced by the attached component/s. In particular, experiments have proved that attaching high gain blades further increases the saturation effect detected in the transducer response. The high stress levels and strain conditions associated with the longitudinal vibration of these blade

types are, in fact, beyond the linear range of the constituting materials. The design and testing of ultrasonic block horn-blades assemblies in which the required amplitude gain is distributed between the components is recommended in order to limit the contribution of the amplitude saturation effect to the inherent nonlinear transducer.

REFERENCES

[1] M. Lucas, G. Graham, and A.C. Smith, "Enhanced vibration control of an ultrasonic cutting process", Ultrasonics, vol. 34, 1996, pp. 205-211.

[2] A. Smith, A. Nurse, G. Graham, M. Lucas, "Ultrasonic cutting-a fracture mechanics model", Ultrasonics, vol. 34, 1996, pp. 197-203.

[3] K. Adachi, S. Ueha, "Modal vibration control of large ultrasonic tools with the Use of Wave-Trapped Horns", Journal of Acoustic Society of America, vol. 87, 1, 1990, pp. 208-214.

[4] K. O`Shea, "Enhanced vibration control of ultrasonic tooling using finite element analysis", ASME Vibration analysis - Analytical and computational, DE-37, 1991, pp. 259-265.

[5] M. Lucas, G. Graham, J.N. Petzing, "Modal analysis of tuned longitudinal mode ultrasonic bar horns", Proc. ISMA21, Leuven, September 1996, pp. 893-901.

[6] M. Lucas, A.C. Smith, "Redesign of ultrasonic block horns for improved Vibration Performance", Trans. ASME JVA, vol. 119, Part 3, 1997, pp. 410-414.

[7] G. Graham, J.N. Petzing, M. Lucas, "Modal analysis of ultrasonic block horns by ESPI", Ultrasonics, vol. 37, Part 2, 1999, pp. 205-211.

[8] G. Graham, M. Lucas, "Off-resonances system behaviour in multi-component ultrasonic tools", BSSM Conference, Sheffield, 1995, pp. 49-51.

[9] M. Lucas, J.N. Petzing, G. Graham, "Experimental characterisation of nonlinear vibration in ultrasonic tools", Proc. 11th Int. Conf. on Experimental Mechanics, Oxford, (UK), 1998, pp. 945-949.

[10] N. Aurelle, D. Guyomar, C. Richard, P. Gonnard, L. Eyraud, "Nonlinear behaviour of an ultrasonic transducer", Ultrasonics, 34, 1996, pp. 187-191.

[11] K. F. Graff, "A history of ultrasonics," Chapter 1 of "Physical Acoustics," Vol. 15, Mason and Thurston, editors, Academic press, 1981.

[12] L.G. Merkulov, "Theory of ultrasonic concentrators", Soviet Physical Acoustics, vol. 3, 1957, pp. 230-238.

[13] L.G. Merkulov, A.V. Kharitonov, "Theory and analysis of sectional concentrators", Soviet Physical Acoustics, vol. 5, 1959, pp. 183-190.

[14] D. Ensminger, "Solid cone in longitudinal half-wave resonance", Journal of the Acoustical Society of America, vol. 32, no. 2, 1959, pp. 194-196.

[15] E.A. Neppiras, "Very high energy ultrasonics", British Journal of Applied Physics, vol. 11, April 1960, pp. 143-150.

[16] P.L.L.M. Derks, "The design of ultrasonic resonators with wide output cross-sections", Eindhoven University of Technology, PhD thesis. 1984.

[17] J. Dhar, A. Davidson, F. Martinez, S. Barr, I. Desai, S. Nakai, "Ultrasonication, lyophilization, freezing and storage effects on fat loss during mechanical infusion of expressed human milk" Journal of Food Science, vol. 60, 2 , 1995, pp. 375-377.

[18] F.W. Jansen, T. Timbos- Kemper, J.B. Trimbos, "Ultrasonic scalpel in laparoscopic gynaecological surgery: an observational study in 354 cases", Gynaecological endoscopy, vol. 11, issue 1, February 2002, pp.47.

[19] L. Bjorno, "Forty years of nonlinear ultrasound", Ultrasonics, vol. 40, 2002, pp. 11-17.

[20] E. Eisner "Design of sonic amplitude transformers for high magnification", Journal of the acoustical society of America, Vol. 35, no. 9, 1963, pp. 1367-1377.

[21] E. Eisner, J.S. Seager, "A longitudinally resonant stub for vibrations of large amplitude", Ultrasonics, vol. 3, April 1965, pp. 88-98.

[22] E.A. Neppiras, "What is ultrasonic machining?", Metalworking production, August 17th, 1956, pp. 1283-1288.

[23] E.A. Neppiras, "The mechanism of ultrasonic cutting", Metalworking Production, August 24th, 1956, pp. 1333-1336.

[24] E.A. Neppiras, "How fast will ultrasonic drills cut (i)",Metalworking Production, August 31st, 1956, pp. 1377-1382.

[25] E.A. Neppiras, "How fast will ultrasonic drills cut (ii)", Metalworking Production, September 7th, 1956, pp. 1420-1424.

[26] E.A. Neppiras, "Tools and transformers for ultrasonic drilling", Metalworking Production, September 14th, 1956, pp. 1464-1468.

[27] E.A. Neppiras, "How accurate can ultrasonic drill be?", Metalworking Production, September 28th, 1956, pp. 1554-1560.

[28] E.A. Neppiras, "Special ultrasonic drilling techniques", Metalworking Production, October 5th, 1956, pp. 1599-1604.

[29] Editorial, "Ultrasonic drilling with a diamond impregnated probe", Ultrasonics, vol. 2, 1964, pp. 1-5.

[30] Editorial, "New Russian cutting machines", Ultrasonics, vol. 2, 1964, pp.148-149.

[31] V.F. Kazantsev, L.D. Rosenberg, "The mechanism of ultrasonic cutting", ultrasonics, vol. 3, 1965, pp. 166-174.

[32] P. Legge, "Machining without abrasive slurry", Ultrasonics, 1966, vol.4, pp. 157-162.

[33] E.H. Smith, "Optimization of the machining process and overall system concepts", CIRP annals, 1971, pp. 385

[34] J. Devine, "Ultrasonically assisted metal removal", SAMPE Quarterly, April 1979, pp. 1-6.

[35] M.A. Mooreland, D.O. Moore, "Versatile performance of ultrasonic machining", Ceramic Bulletin, vol. 67, no. 6, 1988, pp.1045-1047.

[36] V.K. Astashev, "Effect of ultrasonic vibration of a single-point tool on the process of cutting", Journal of machinery manufacture and reliability, no. 3, 1992, pp. 65-70.

[37] V.K. Astashev, V.I. Babitsky, "Ultrasonic cutting as a nonlinear (vibro-impact) process", Ultrasonics, vol. 36, 1998, pp. 89-96.

[38] A. Shoh, "Welding of thermoplastics by ultrasound", Ultrasonics, September 1976, pp. 209-217.

[39] L.D. Rozenberg, "Sources of high-intensity ultrasound", vol.2, Plenum Press, New York, 1969, pp.212.

[40] J. Tsujino, T. Ueoka "Ultrasonic multi-spot continuous welding of metal plate specimens using a two-vibration-system welding equipment", ultrasonics, 1996, vol. 34, pp. 229-233.

[41] J. Tsujino, T. Ueoka, Hasegawa, Y. Fujita, T. Shiraki, T Okada, T. Tamura, "New methods of ultrasonic welding of metal and plastic materials", ultrasonics, 1996, vol. 34, pp. 177-185.

[42] J. Tsujino, T. Ueoka, T. Kashino, F. Sugahara, "Transverse and torsional complex vibration systems for ultrasonic seam welding of metal plates", ultrasonics, 2000, vol. 38, pp. 67-71.

[43] J. Tsujino, M. Hongoh, R. Tanaka, R. Onoguchi, T. Ueoka, "Ultrasonic plastic welding using fundamental and higher resonance frequencies", ultrasonics, 2002, vol. 40, pp. 375-378.

[44] J. Tsujino, K. Hasegawa, "Ultrasonic wire bonding using high frequency 330, 600 kHz and complex vibration 190 kHz welding systems" ultrasonics, 1996, vol. 34, pp. 223-228.

[45] J. Tsujino, H. Yoshihara, K. Kamimoto, Y. Osada, "High frequency longitudinal -transverse complex vibration systems for ultrasonic wire bonding", IEEE ultrasonics symposium, 1997, pp. 849-854.

[46] J. Tsujino, H. Yoshihara, K. Kamimoto, Y. Osada, "Welding characteristics and temperature rise of high frequency and complex vibration ultrasonic wire bonding", ultrasonics, 1998, vol. 36, pp. 59-65.

[47] J. Tsujino, H. Yoshihara, T. Sano, S. Ihara, "High-frequency ultrasonic wire-bonding systems", ultrasonics, 2000, vol. 38, pp. 77-80.

[48] S. Ueha, Recent advances of high power ultrasonic applications- A focus on actuators",Plenary lecture, International ultrasonics, Granada, 2003.

[49] M. Jakubowski, "Ultrasonic horn design: Translating an art into sound principles", Electromechanical design, April 1972, pp. 30-37.

[50] G. Amza, D. Drimer, "The design and construction of solid concentrators for ultrasonic energy", Ultrasonics, September 1976, pp. 223-226.

[51] K. Adachi, S. Ueha, E. Mori, "Modal vibration analysis of ultrasonic plastic welding tools using the finite element method", Proceedings of Ultrasonic International (Butterworths, London), 1986, pp. 727-732.

[52] M.C. Shellabear, J.R. Tyrer, "Three dimensional vibration analysis using electronic speckle pattern interferometry (ESPI)", International conf – Laser technology in industry, Porto, June 1988, SPI v952.

[53] M. Lucas, G.M. Chapman, "Vibration analysis at ultrasonic frequencies", Proc. 12th biennial ASME conf. on mechanical vibration and noise, Montreal, 1989, pp. 235-240.

[54] G.M. Chapman, M. Lucas, "Frequency analysis of an ultrasonically excited thick cylinder", International journal of mechanical sciences, vol. 32, part 3, 1990, pp. 205-214.

[55] M. Lucas, A.C. Smith, "The design of large ultrasonic resonators", Proceedings of the 10th International Conference on Experimental Mechanics, Lisbon (Portugal), 1994, pp. 625-630.

[56] A. Smith, M. Lucas, "Closing the loop on ultrasonic tool design", Proc. 5th international conference on recent advances in structural dynamics, Southampton, 1994, pp. 243-252.

[57] M. Lucas, "Vibration sensitivity in the design of ultrasonic forming dies", Ultrasonics, vol. 34, 1996, pp. 35-41.

[58] M. Lucas, G.M. Chapman, "Design of ultrasonically assisted radial dies by validated finite element methods", Proc. Ultrasonics International, 1993, pp. 707-710.

[59] M.J.R. Young, C.E. Winsper, D.H. Sansome, "Radial mode vibrators for oscillatory metal forming", Applied acoustics, 1970.

[60] L.D. Rozenberg, "Sources of high power ultrasound", vol. 2, Plenum Press, New York (1969).

[61] L. Shuyu, "Study of sandwiched piezoelectric ultrasonic torsional transducer", Ultrasonics, vol. 32, no. 6, 1994, pp. 461-465.

[62] L. Shuyu, "Study on multifrequency Langevin ultrasonic transducer", Ultrasonics, vol.33, no. 6, 1995, pp. 445-448.

[63] L. Shuyu, "Study on the longitudinal-torsional composite mode exponential ultrasonic horns", Ultrasonics, vol. 34, 1996, pp. 757-762.

[64] G. Zhou, Y. Zhang, B. Zhang, "The complex-mode vibration of ultrasonic vibration systems", Ultrasonics, vol. 40, 2002, pp. 907-911.

[65] J. Tsujino, T. Uchida, K. Yamano, T. Iwamoto, T. Ueoka, "Ultrasonic plastic welding using two 27 kHz complex vibration systems", IEEE ultrasonics symposium, 1997, pp. 855-860.

[66] J. Tsujino, T. Ueoka, K. Otoda, A. Fujimi, "One-dimensional longitudinal-torsional vibration converter with multiple diagonally slitted parts", Ultrasonics, vol. 38, 2000, pp. 72-76.

[67] J. Tsujino, T. Sano, H. Ogata, S. Tanaka, Y Harada, "Complex vibration welding systems with large area welding tips", Ultrasonics, vol. 40, 2002, pp. 361-364.

[68] B.J. Schwarz, M.H. Richardson, "Experimental modal analysis", Vibrant Technology inc., CSI reliability week, Orlando, FL, October 1999, pp.1-12.

[69] P. Avitabile, "Experimental modal analysis- A simple non-mathematical presentation", Sound and Vibration, January, 2001, pp. 1-11.

[70] D.J. Ewins, "Modal testing: theory, practice and application", Research studies press ltd., Baldock, England, *2000*.

[71] D. Formenti, M.H. Richardson, "Global curve fitting of frequency response measurements using the rational fraction polynomial method", 3rd international modal analysis conference, Orlando, FL, January 1985.

[72] A.H. Nayfeh, "Perturbation methods", Wiley, New York, 1973.

[73] M.R.M. Crespo da Silva, "On the whirling of a base-excited cantilever beam", Journal of Acoustic. Society of America, vol.67, part 2, February 1980, pp. 704-707.

[74] J. Dugundji, V. Mukhopadhyay, "Lateral bending-torsion vibrations of a thin beam under parametric excitation", Journal of applied mechanics, vol. 40, September 1973, pp. 693-698.

[75] A. H. Nayfeh, D. T. Mook, "Nonlinear Oscillations", Wiley-Interscience, New York, 1979.

[76] A.H. Nayfeh, B. Balachandran, "Modal interactions in dynamical and structural systems" Applied mechanics review, vol. 42, no 11, part 2, November 1989, pp. S175-S201.

[77] A.D.S. Barr, "Some developments in parametric stability and nonlinear vibration", Proc. Int. Conf. On Recent Advances in Structural Dynamics, Southampton, UK, 1980, pp. 545-567.

[78] M.P. Cartmell, J.W. Roberts, "Simultaneous combination resonances in a parametrically excited cantilever beam", Strain, August 1987, pp. 117-126.

[79] D.I.M. Forehand and M.P. Cartmell, "On the derivation of the equations of motion for a parametrically excited cantilever beam" Journal of Sound and Vibration, vol. 245, part 1, 2001, pp. 165-177.

[80] A.G. Haddow and S.M. Hasan, "Nonlinear oscillation of a flexible cantilever: experimental results", Proc. of the second conference on non-linear vibrations, stability, and dynamics of structures and mechanisms, Blacksburg, VA, June 1988.

[81] T.D. Burton, M. Kolowith, "Nonlinear resonances and chaotic motion in a flexible parametrically excited beam", Proceedings of the second conference on non-linear vibrations, stability, and dynamic structures and mechanisms, Blacksburg, VA, 1988.

[82] T.J. Anderson, B. Balachandran, A.H. Nayfeh, "Observations of nonlinear interactions in a flexible cantilever beam", Proc. AIAA, 92-2332, 1992, pp. 1678-1685.

[83] S. A. Nayfeh, A. H. Nayfeh, "Energy transfer from high- to low-frequency modes in a flexible structure via modulation", Journal of Vibration and Acoustics 116, 1994, pp.203-207.

[84] M.P. Cartmell, "Introduction to linear, parametric and nonlinear vibrations", Chapman Hall, UK, 1990.

[85] K. Yamamoto, A. Kokubo, K. Sakai, K. Takagi, "Nonlinear piezoelectricity in PZT ceramics for generating ultrasonic phase conjugate waves", Ultrasonics, vol. 38, 2000, pp. 830-833.

[86] M. Ohno, B. R. Tittman, A. Kokubo, K. Takagi, "Incident-angle dependence of the phase conjugate reflectivity by nonlinear piezoelectric interaction in PZT ceramics", Ultrasonics, vol. 39, 2001, pp. 425-428.

[87] J.P. Cusumano, F.C. Moon, "Low dimensional behaviour in chaotic nonplanar motions of a forced elastic rod: Experiment and theory", Nonlinear dynamics in engineering systems IUTAM symposium, Stuttgart (Germany), 1989, 59-65.

[88] P.F. Pai, A.H. Nayfeh, "Non-linear non-planar parametric response of an inextensional beam", International Journal of non-linear mechanics, vol. 24, pp. 139-158.

[89] T.J. Anderson, B. Balachandran, A.H. Nayfeh, "Investigation of multi-mode interactions in a continuous structure", Proc. 62nd Shock and Vibration, symposium, Springfield, USA, October 1991, pp. 112-119.

[90] A.K. Bajaj, J.M. Johnson, "Asymptotic techniques and complex dynamics in weakly non-linear forced mechanical systems", International Journal of non-linear meachanics, vol. 25,2/3,1990, pp. 211-226.

[91] G. Duffing, "Erzwungene schwingungen bei veranderlicher eigenfrequenz", Vieweg: Braunschweig, 1918.

[92] C. Greene, C. Chiang, "Period doubling route to chaos" Davidson College, North Carolina 28036, 2000.

[93] F. C. N. Lim, "A preliminary investigation into the effects of nonlinear response modification within couple oscillators", University of Glasgow, PhD thesis 2003.

[94] G. Chakraborty, A.K. Mallik, H. Hatwal, "Normal modes and near-resonances response of beams with non-linear effects", Journal of sound and vibration, 210(1),1998, pp. 19-36.

[95] R.A. Guyer, P.A. Johnson, "Nonlinear mesoscopic elasticity: evidence for a new class of materials", Physics Today, April 1999, pp. 30-36.

[96] S. Hirsekorn, "Nonlinear transfer of ultrasound by adhesive joints – a theoretical description", ultrasonics, vol. 39, 2001, pp. 57-68.

APPENDIX: PUBLICATIONS

Journal papers

[1] CARDONI, A., LUCAS, M., "Enhanced vibration performance of ultrasonic block horns", *Ultrasonics*, Vol. 40, 2002, pp 365-369.

[2] CARDONI, A., LUCAS, M., "A novel multiple blade ultrasonic cutting device", 2003, *Ultrasonics*, in press, 2003.

[3] LUCAS, M., PETZING, J.N., CARDONI, A., SMITH, L.J., "Design and characterisation of ultrasonic cutting tools", *Annals of CIRP*, 50/1, pp 149-152, 2001.

[4] LIM, F.C.N., CARTMELL, M.P., CARDONI, A., LUCAS, M., "A preliminary investigation into optimising the response of vibrating systems used for ultrasonic cutting", *Journal of Sound and Vibration*, in press, 2003.

[5] LUCAS, M., CARDONI, A., CARTMELL, M.P., LIM, F.C.N., "Effects of modal interactions on vibration performance in ultrasonic cutting", *Annals of CIRP*, 52/1, pp. 193-196, 2003.

[6] CARTMELL, M.P., LIM, F.C.N., CARDONI, A., LUCAS, M., "Optimisation of the vibrational response of ultrasonic cutting systems", *Journal of Applied Mathematics*, under review, 2003.

Conference papers

[7] CARDONI, A., LUCAS, M., CARTMELL, M.P., LIM, F., "Characterising modal interactions in an ultrasonic cutting system", *Forum Acusticum*, Seville (Spain), paper ULT-02-003-IP, September 2002.

[8] CARDONI, A., LUCAS, M., "Strategies for reducing stress in ultrasonic cutting systems", *BSSM International Conference on Advances in Experimental Mechanics*, Stratford (UK), pp 101-104, August 2002.

[9] LUCAS, M., CARDONI, "Experimental and computational modelling of vibration performance of ultrasonic tools for manufacturing applications", *32nd Ultrasonics Industries Association Symposium*, New York (USA), October 2002.

[10] CARTMELL, M.P., LIM, F.C.N., CARDONI, A., LUCAS, M., "Optimisation of the vibrational response of ultrasonic cutting systems", *IMA Conference*, Southampton (UK), June 2003.

[11] CARDONI, A., LUCAS, M., "Design of ultrasonic block horns by finite element models", *18th International CAPE Conference*, Edinburgh (UK), March 2003.

[12] CARDONI, A., LUCAS, M., CARTMELL, M.P., LIM, F.C.N., "Nonlinear and parametric vibrations in an ultrasonic cutting system", *MPSVA conference*, Glasgow (UK), September 2003.

[13] LUCAS, M., CARDONI, A., CARTMELL, M.P., LIM, F.C.N., "Controlling the effects of modal interactions in ultrasonic cutting devices", *World Congress on Ultrasonics*, Paris (France), September 2003.

[14] CARDONI, A., LUCAS, M., "Characterising energy exchanges from high- to low-frequency modes in ultrasonic cutting systems", *33rd Ultrasonics Industries Association Symposium*, Indianapolis (USA), September 2003.